MODELLING OF NEWTONIAN AND POWER LAW FLUID FLOW PAST MULTI-PARTICLE ASSEMBLAGES BY FINITE ELEMENT METHOD

by

ANIL KUMAR JAISWAL

DEPARTMENT OF MECHANICAL ENGINEERING

INDIAN INSTITUTE OF TECHNOLOGY, KANPUR

SEPTEMBER, 1990

MODELLING OF NEWTONIAN AND POWER LAW FLUID FLOW PAST MULTI-PARTICLE ASSEMBLAGES BY FINITE ELEMENT METHOD

A Thesis Submitted
in Partial Fulfilment of the Requirements
for the Degree of
DOCTOR OF PHILOSOPHY

by
ANIL KUMAR JAISWAL

to the
DEPARTMENT OF MECHANICAL ENGINEERING
INDIAN INSTITUTE OF TECHNOLOGY, KANPUR
SEPTEMBER, 1990

4/9/90

CERTIFICATE

It is certified that the work contained in the thesis entitled, **MODELLING OF NEWTONIAN AND POWER LAW FLUID FLOW PAST MULTI-PARTICLE ASSEMBLAGES BY FINITE ELEMENT METHOD**, by Anil Kumar Jaiswal, has been carried out under our supervision and this work has not been submitted elsewhere for a degree.

(R. P. Chhabra)
Chemical Engineering Dept.
Indian Institute of Technology
Kanpur 208 016, INDIA

(T. Sundararajan)
Mechanical Engineering Dept.
Indian Institute of Technology
Kanpur 208 016, INDIA

September, 1990

SYNOPSIS

Viscous flow of Newtonian and non-Newtonian fluids past an assemblage of particles represents an idealisation of processes occurring in diverse engineering applications such as ground water hydrology, polymer processing, biotechnology and numerous particle separation techniques. Despite their overwhelming importance, the progress in the modelling of transfer processes in these systems has been rather slow. This is so partly due to the formidable difficulties encountered in describing the interparticle interactions satisfactorily and mathematical complexities arising due to non-linear governing equations The currently available theoretical studies concentrate mainly on evaluation of macroscopic quantities such as drag coefficients and Sherwood number. Detailed studies corresponding to intermediate Reynolds number flows are scarce for both Newtonian and non-Newtonian fluids. In fact, even for creeping flow of non-Newtonian fluids, the detailed flow field solutions have not been reported in open literature.

In present work, comprehensive theoretical results on the detailed structure of the flow field, namely, pressure and shear stress distribution, angular and radial velocity profiles, streamline patterns as well as the macroscopic parameters such as drag coefficients have been obtained over a wide range of bed voidage, Reynolds number and rheological behaviour of the fluid The major contribution lies in providing physical insight for the observed drag behaviour based on the detailed flow field structure prevailing around the particle.

In Chapter I, the basic features of flow past a multi-particle assemblage are introduced and the scope of this study is outlined In Chapter II, the methodologies available for modelling interparticle interactions are reviewed and the pertinent literature is critically examined. Among the various approaches, the capillary and cell models are discussed at length. The serious limitations of the capillary model (apart from its strengths) are highlighted and the relative advantage of the cell model is brought forth The central concepts of the cell model regarding the division of the particle assemblage into several unit cells each housing a single particle and the subsequent analysis of flow through the assemblage in terms of flow within a typical cell are described. The widely accepted free-surface and zero-vorticity cell models are elaborately discussed

In Chapter III, the application of free surface cell model to the steady flow of a Generalized Newtonian fluid past an assemblage of spherical particles is presented. The Generalized Newtonian fluid description provides a convenient representation of Newtonian and power-law type non-Newtonian fluids through a single rheological equation. The non-dimensional continuity and momentum equations in conjunction with appropriate boundary conditions have been solved by the FEM procedure based on the Galerkin's weighted residual approach. The discretization of the flow domain has been done using eight-noded quadrilateral elements. The nodal equations for velocity components and pressure have been derived respectively from the application of the residue principle to the momentum and continuity equations On the boundary, however, the nodal equations are obtained by the

direct implementation of the boundary conditions The resulting system of non-linear algebraic equations are solved iteratively using the FRONTAL technique

In Chapter IV, the validity and accuracy of the numerical scheme are examined. Comparison of present results with the analytical solution of Happel for the creeping flow of a Newtonian fluid shows a perfect agreement of drag coefficients (pressure, friction and total), surface stresses and the velocity and pressure field solutions. For intermediate Reynolds number flow of Newtonian fluid through a dense assemblage, the drag results of present study are in excellent agreement with the perturbation results of El-Kaissy and Homsy At higher voidage, the Reynolds number upto which agreement exists decreases For the creeping flow of a power law fluid, fair agreement is observed between the drag predictions of present work and the upper and lower bounds available in the literature in the range of power law index, $1 \geq n \geq 0.5$. Experimentation with the radial step size and grid pattern indicates that the number of elements in radial direction required for accurate prediction increases with voidage; also, for dilute assemblages, a grid with exponential size variation is found to be far superior to a uniform mesh Convergence of drag coefficients requires less iterations than those needed for the convergence of velocity and pressure solutions. The rate of convergence is reduced when the voidage and power law index are decreased, while the Reynolds number has no appreciable effect.

In Chapter V, Newtonian flow results are presented over a wide range of voidage and Reynolds number. For dense assemblages,many creeping flow features such as inverse

proportionality between drag coefficients and Re, symmetric surface shear stress profiles, etc. are displayed even at intermediate Reynolds number. The critical Reynolds number upto which the creeping flow solution is valid depends on the voidage (ϵ). At low voidages, pressure drag dominates over friction drag ($C_{DP} > C_{DF}$) and the reverse is true at high voidages The switch over between C_{DP} and C_{DF} takes place around $\epsilon = 0.7$. Comparison of present results with the experimental correlation of Ergun for packed beds shows that the free surface cell model is accurate for $Re < 10$ and for higher Reynolds number (Re), the zero vorticity model predictions are slightly better, although both models diverge from Ergun's correlation as Re increases For fluidization best correspondence between the predictions of widely accepted Richardson and Zaki correlation and the present results is observed at $Re = 20.0$.

In Chapter VI, the drag and the detailed flow results for a power law fluid are presented. For creeping flow, the pressure and friction drag coefficients vary as a power function of the average Newtonian surface shear rate for the range of power law index, $1 \geq n \geq 0.5$. With respect to voidage, the pressure drag dominates over the friction drag for dense assemblages and vice versa for dilute assemblages. For $0.3 \leq \epsilon \leq 0.9$, the ratio C_{DP}/C_{DF} decreases as n is decreased, while an exactly opposite trend is observed for voidage close to single sphere limit. The surface shear stress and pressure profiles become increasingly flat as the degree of non-Newtonian behaviour increases; this trend is more evident at low voidage. The flattening of the surface shear stress is caused by the simultaneous decrease in the

fluid viscosity and the increase in the shear rate adjacent to the particle The variation of surface viscosity with angle is seen to be prominent only near the axis The effects of power law index and voidage at intermediate Reynolds number flows are essentially similar to those of creeping flow. The inertial effects on drag are noticeable only for high Re, high voidage and low values of n. The surface shear stress and pressure profiles are, however, significantly affected, shear stress becomes increasingly asymmetric about the mid-plane and the pressure approaches the potential flow pressure profile. Finally, present theoretical predictions have been substantiated by performing detailed comparisons with appropriate experimental data available in the literature for packed beds, fluidized beds and single particle falling through a fluid under the action of gravity

ACKNOWLEDGEMENTS

I wish to express my deep sense of gratitude to Dr. T. Sundararajan and Dr. R.P. Chhabra for suggesting this problem and for their valuable guidance and encouragement at every stage of this work. Innumerable discussions with them reinforced with constructive criticism have greatly contributed to the technical merit of the work.

I am indebted to the administration of R.I T. Jamshedpur, for sponsoring me under Quality Improvement Programme of Govt. of India to pursue higher study at IIT Kanpur.

I would like to express my gratitude to Prof. M.M. Oberai and Dr. N.N. Kishore, Dept. of Mechanical Engineering, IIT Kanpur for providing adequate physical and computational facility to accomplish this work smoothly.

I am grateful to Prof. B. Sahay, Coordinator, CAD Project, IIT Kanpur for allowing access to the computational facility available in CAD centre.

It is my pleasure to extend my very special thanks to Dr. Surendra Prasad for his invaluable help in countless occasions beginning with my first week in this Institute. Sincere thanks are due to Capt. Bijoy Jha for providing help during the preparation of this thesis.

Last but not the least, I am thankful to my wife Pratibha and our daughters Priti and Tanya for their patience and understanding during the entire course of this study. To them I dedicate this thesis.

A. K. Jaiswal
4/9/90

CONTENTS

LIST OF FIGURES

LIST OF TABLES

NOMENCLATURE

A	Constant appearing in Eqns. (2.1) and (2.2)
c	Boundary surface of the solution domain
C_D, C_{DP}, C_{DF}	Total drag, pressure drag and friction drag coefficients
C_{Dst}	Stokes' drag coefficient (= 24/Re)
d_p	Particle diameter
dl	Differential length of a boundary curve lying in the half plane which contains the flow axis
e	Index denoting a typical element
e	Shear rate in viscometric flow
$\hat{e}_x$, $\hat{e}_y$	Unit vectors in X and Y directions
E	Number of elements in the computational domain
E_s	Number of elements lying adjacent to the particle surface
f	Fanning's friction factor (= $\frac{\Delta P}{L} \frac{d_p}{2\rho U_\infty^2}$)
f_{bk}	Blake-Kozeny friction factor (= $\frac{\Delta P}{L} \frac{\epsilon^3}{1-\epsilon} \frac{d_p}{\rho U_\infty^2}$)
f_g	Gravitational force vector
F_x	Right hand side vector for the X-momentum equations of the FEM formulation
F_y	Right hand side vector for Y-momentum equations of the FEM formulation
i, j, k	Indices denoting nodes
I_1, I_2, I_3	First, second and third invariants of deformation

K	Consistency factor for Power law type fluid
K_1	Factor arising in friction factor expression of equation (6 6)
l	Total number of X-velocity or Y-velocity unknowns
L	Length across the particulate bed
m	Total number of pressure unknowns
M	Bilinear shape functions used for pressure interpolation in an element
n	Power law index
$\underset{\sim}{n}$	Unit vector in the normal direction to a surface
N	Quadratic shape functions used for velocity interpolation
p	Pressure
r	Spherical radial coordinate
R_c	Radius of spherical cell
R_p	Radius of the spherical particle
Re	Reynolds number based on partial diameter ($\equiv \frac{\rho U_\infty^{2-n} d_p^n}{K}$)
Re_o	Reynolds number based on free settling velocity ($\equiv \frac{\rho U_o^{2-n} d_p^n}{K}$)
Re_r	Reynolds number based on particle radius ($\equiv \frac{\rho U_\infty^{2-n} R_P^n}{K}$)
Re_{bk}	Modified Reynolds number occuring in equation (2.1) and (2.2)
Re'_{bk}	Modified Reynolds number for power law fluids defined in equation (6.6)
U_∞	Superficial velocity of flow through the bed
U_o	Free settling velocity of a single particle
V	Velocity vector

V_r, V_θ Radial and angular velocity components in spherical coordinate system

V_x, V_y Axial and Radial velocity components in cylindrical coordinate system

x Coordinate along the flow axis measured from the particle centre (within a cell)

y Radial coordinate in cylindrical system

Y Drag correction factor ($= \frac{C_D\ Re}{24}$)

Y_U Upper bound on drag (in table 4.7)

Y_L Lower bound ot drag (in table 4 7)

Greek Letters

β Coefficient in equation (3 4)

δ Radial gap between the particle and the cell surface ($\delta = R_c^{*} - 1$)

Δr, $\Delta\theta$ Grid step size in radial and angular direction

$\underset{\approx}{\Delta}$ Rate of deformation tensor

Δ_{rr}, $\Delta_{\theta\theta}$, $\Delta_{r\theta}$, $\Delta_{\phi\phi}$ Components of rate of deformation tensor

ϵ Cell voidage ($= 1 - R_c^{-3}$)

η Viscosity function

η_c Cross viscosity appearing in equation (3 4)

θ Spherical polar angle

μ Newtonian viscosity

μ_c A factor defined in equation (6.6)

ξ_1, ξ_2 Local coordinates of a quadrilateral element

ρ Fluid density

ρ_p Particle density

$\underset{\approx}{\sigma}$ Total stress tensor

$\underset{\approx}{\tau}$	Deviatoric stress tensor
ϕ	Azimuthal angle
ψ	Stream function, factor appearing in equation (6.6)
Ω	Computational domain

Subscripts

C	At the cell boundary
i, j, k	Pertain to nodal quantities for the i-th, j-th and k-th nodes respectively
r, θ	Components in r, θ (spherical) directions
x, y	Components in x, y (cylindrical) directions
$\underline{\ }$	Vector quantity
$\approx$	Tensorial quantity
s	At the surface

Superscripts

e	Pertaining to a typical element e
T	Transpose
$\bar{\ }$	Variable corresponding to previous iteration, for surface stress scaled by ρU_∞^2
'	For surface stress scaled by $(\eta\ U_\infty/R_p)$
*	Dimensionless quantity

CHAPTER I

INTRODUCTION

1.1 MULTI-PARTICLE SYSTEMS AND THEIR APPLICATIONS

Fluid flow through an assemblage of particles has received wide research attention both theoretically as well as experimentally due to its importance in several engineering disciplines. The flow configurations involving multi-particle assemblages can be classified in many ways based on factors such as the proportion of solid to fluid and the relative motion between the solid and fluid phase, etc. Depending upon the relative proportion of solid to fluid, these are defined as concentrated or dilute particle assemblages. In practical applications, three broad classifications can be identified according to the direction of motion of the particle assemblage in relation to that of the fluid flow, namely, sedimentation, packed bed and fluidization. In certain other applications where the specific surface of the solid matrix is very high and pores comprising the void space are relatively narrow, the system may be termed as a porous medium. Each of these configurations of multi-particle assemblages is of considerable practical significance

The flow of fluids through packed beds is an operation encountered in various engineering applications. Common examples concerning single phase flow are:

(a) Filtration of industrial suspensions, water treatment through sand filters, etc.

(b) Mixing by means of flow through a porous bed in order to equalize temperature, velocity field or composition in the fluid.

(c) Flow through a porous bed in underground hydraulics.

The process of sedimentation is commonly employed in chemical and petroleum industries as a way of separating particles from fluid or separating particles of different sizes. Examples of such separations include dewatering of coal slurries, clarification of waste water, removal of sugar crystals from syrup and the processing of drilling and mining fluids containing rocks and mineral particles of different sizes. The separation of different particles by sedimentation is also the basis of some laboratory techniques for determining the distribution of particle sizes in particulate dispersion.

The process of fluidization of solid particles by a liquid which was considered to be just a scientific curiosity, is rapidly becoming more and more important from industrial point of view. New processes involving liquid-fluidized beds are being developed in areas such as hydrometallurgy, food processing, biochemical technology, water treatment, etc. The operations involved may include crystallization, lixivation, ion exchange, adsorption, enzyme catalysis or cell culturing.

Innumerable efforts have been made to analyse the Newtonian flow through multi-particle assemblages and detailed reviews are available in several monographs. The classic treatise by Happel and Brenner (1965) outlines a rational approach to analyse the

fluid particle dynamics based on principles of fluid mechanics.

In the last three decades, wide interest has been evinced in the study of non-Newtonian fluid flow in multi-particle systems, as it constitutes an important part of many industrial processes. Typical examples include flow of oil through porous rocks, polymer flooding in tertiary oil recovery operations, filtration of polymer solutions and slurries, ore-processing, catalytic polymerization in hydroxydation process, waste water treatment and ion exchange beds which are used to recover metals like uranium from slurries and sludges before their disposal. Microbial masses are also highly non-Newtonian fluids and in several processes in bio-technology these are prepared in fixed bed reactors. Besides, many industrial processes involving non-Newtonian fluids are carried out in packed and fluidized beds to improve the heat and mass transfer rates. In view of these overwhelming practical applications cited above numerous studies have been reported on this subject. Reviews of published literature in the area of non-Newtonian flow through packed beds and porous media have been presented by Savins (1969), Kemblowski and Michniewicz (1979), Kumar et al. (1981), etc. It is appropriate to mention here that the motion of particles in non-Newtonian fluid is significantly different from its Newtonian counterpart, since non-Newtonian fluids exhibit a wide spectrum of rheological complexities including shear dependent viscosity, visco-elasticity, time dependency, coupling of rheological behaviour with flow geometry etc. Therefore, analysing the non-Newtonian flow is a much more complex and challenging task than that for the Newtonian system

1.2 GENERAL TRENDS OF RESEARCH ON FLOW PAST A MULTI-PARTICLE ASSEMBLAGE:

Despite the wide spread occurrence and pragmatic importance of multi-particle fluid flow systems, the progress made towards the modelling of transport phenomena associated with these systems has been rather slow and inadequate, especially for non-Newtonian media. The available literature on this subject is inundated with a great number of experimental and semi-theoretical correlations. Beginning with the celebrated work of Darcy (1856), numerous experimental and theoretical studies have been attempted to determine the characteristics of fluid flow through packed beds in general and pressure drop across the bed in particular. Similarly, the chief objective of research studies on sedimentation and fluidization processes has been the evaluation of the settling velocity/fluidization velocity for various concentrations of solid particles. However, in all these studies, the detailed flow field around a typical particle in the assemblage is very scarcely reported beyond the creeping flow regime, even for Newtonian fluid flow. For non-Newtonian media, detailed flow field results have not been obtained so far even for creeping flow regime. There is a strong need to fill in the existing lacuna on the details of fluid particle interaction for both Newtonian and non-Newtonian media.

In order to model the multi-particle effects on flow through a bed of particles, two approaches have been commonly adopted, namely (a) Capillary tube bundle model and (b) unit cell model. A few other approaches such as the continuum model and the submerged object model have also been in use albeit to a lesser extent. The

main obstacle to be overcome while modelling such flow problems is that of providing a satisfactory treatment of the particle-particle interactions Each of the available models in the literature accounts for the multi-particle effects in a different manner and there are advantages and disadvantages associated with each approach.

In "Capillary tube" bundle model, the interstitial space between the particles is visualised as a bundle of capillaries, whose lengths and diameters are such that it presents the same resistance to fluid flow as the actual interstices in the real multi-particle system. The starting point for the modelling is the well known Hagen-Poiseuille equation (or its equivalent for Non-Newtonian flow) in conjunction with the concept of hydraulic radius. The success of this model with Newtonian fluids has led to its extension to non-Newtonian flow by using a suitable rheological equation to represent fluid behaviour. However, the success of this approach in both Newtonian and non-Newtonian systems has been somewhat surprising because it presents an over simplified picture of the real flow configuration and the concept of "mean hydraulic radius" has little theoretical justification.

In cell model, each particle, (assumed to be uniformly-spaced in the assemblage) is enveloped by a hypothetical fluid cell which represents the inter-particle interactions. The radius of the envelope is such that the voidage of each cell is equal to the statistically-averaged overall voidage of the assemblage. In the free surface cell model proposed by Happel (1958), the shear stress and the mass flux vanish on the cell surface. In a similar model independently proposed by Kuwabara (1959), zero vorticity is

prescribed on the cell surface Several investigators have pointed out the conceptual difficulties arising in the zero-vorticity model due to prescription of vorticity at the cell surface. The free surface cell model has been successfully applied to predict the pressure drop incurred during the flow of Newtonian and purely viscous type non-Newtonian fluids through fixed beds. It has also been employed with success in the analysis of the relative motion between a swarm of gas bubbles and a Newtonian or non-Newtonian continuous phase. However, all the aforementioned applications are limited to the creeping flow regime only. Very little theoretical work has been reported regarding the suitability of free surface cell model outside the creeping flow regime.

1.3 SCOPE OF PRESENT WORK

It appears from a close scrutiny of the existing literature that not only very little is known about the flow of shear thinning fluids through particle assemblages, but most of the earlier investigators have concentrated mainly on the overall macroscopic behaviour. No insight has been provided as to the causes of the observed macroscopic trends and no efforts have been made to relate these trends with the structure of the flow field prevailing around a typical particle in an assemblage In fact, beyond the creeping flow regime even macroscopic quantities such as drag coefficients, rate of hindered settling etc. are not known. Bearing in mind that momentum transport serves as a precursor to the modelling of heat and mass transport, it is felt that there is a need to launch a systematic study of the detailed flow field structure (Pressure, velocity, streamlines and stress

profiles) over a wide range of physical, kinematic and rheological conditions The data accrued from such a study would facilitate the meaningful interpretation of experimental results and empirical correlations concerning heat, mass and momentum transport. For instance, the answer to the question such as when and why viscous drag becomes dominant over the pressure drag can come only from the knowledge of detailed flow field around a particle The influence of various factors such as voidage, non-Newtonian behaviour index and Reynolds number on important macroscopic quantities such as drag coefficients, fluidization velocity or settling velocity of suspension can be elucidated. Moreover, the flow configuration of a multi-particle assemblage provides an opportunity to examine the applicability of various constitutive relations containing parameters determined entirely from viscometric flow. However, it deserves to be mentioned at this stage that the results accomplished through such a theoretical study are likely to show some deviations from reality for the following reasons.

1) Idealisations and approximations in modelling the hydrodynamic interactions between particles.
2) Uncertainty concerning the applicability of the rheological constitutive equation which has been developed from viscometric flow data.
3) Variance in the experimental data of different investigators arising primarily from the improper characterization of non-Newtonian fluid behaviour.

With regards to Newtonian fluid flow also, it is evident that very little is known about the usefulness and applicability of the

cell model approach in general and of free surface cell model in particular, to the intermediate Reynolds number regime. In view of the wider acceptance of Happel's cell model in a large variety of problems, an improved understanding in this direction is desired.

In the present study, comprehensive numerical results for steady flow of both Newtonian and non-Newtonian (Power law type) fluid flow relative to an assemblage of spherical particles have been obtained, by the use of the free surface cell model. The intermediate Reynolds number regime has been analysed for the Newtonian fluid, while the creeping as well as intermediate Reynolds number flow regimes have been considered for the power law type shear thinning fluid. Detailed flow field results have been presented and the influence of the flow field structure around the particle on macroscopic quantities of interest such as drag force have been elucidated. A wide range of physical, kinematic and rheological conditions have been considered and the effects of problem parameters upon both microscopic and macroscopic flow quantities are discussed in detail.

CHAPTER II

LITERATURE SURVEY

A brief literature survey comprising a general overview of flow past multi-particle assemblages and a detailed discussion on modelling methodologies in particular, is presented here. Keeping in view the vastness of the subject, only pertinent literature has been referred to and discussed.

2.1 OVERVIEW OF GENERAL RESEARCH ACTIVITY ON FLOW THROUGH MULTI-PARTICLE SYSTEMS:

Ever since the pioneering work of Darcy (1856) the characteristics of fluid flow through packed beds and the determination of pressure drop across the bed have been the subject of numerous experimental and theoretical studies. The large number of variables involved makes exact treatment of the problem exceedingly difficult. In most of the available pressure drop correlations, the following factors have been considered: fractional void volume, type of fluid flow, particle shape, roughness, size distribution and manner of packing, etc. The effects of side walls and the bed support have also been reported. However, the theoretical treatments are usually confined to the simplest system involving uniformly sized spherical particles without wall and end effects. The findings of such studies pertaining to Newtonian fluid flow have been summarized in several excellent monographs on the topic (Carman, 1956; Scheidegger,

1960; Collins, 1961; Bear, 1972, Dullien, 1979; Greenkorn, 1983; etc.) Reviews of literature that has evolved in the area of non-Newtonian flow through packed beds and porous media have been presented by Savins (1969), Kemblowski and Michniewicz (1979), Kumar et al. (1981), etc

Research on the sedimentation process has been mainly concerned with the characteristics of the particle settling velocity. Theoretical and experimental analyses relating the particle settling velocity to the concentration of solids have been developed in the dilute limit (Burgers, 1941, 1942; Batchelor, 1972; Davis and Birdsell, 1988) The intermediate and high concentration regimes are more important in practice but less amenable to rigorous theoretical analysis. They have been investigated experimentally by Richardson and Zaki, 1954a; Garside and Al-Dibouni, 1977; Moritomi et al., 1986; etc. These authors have developed reliable empirical correlations for predicting the settling velocity in a container with closed bottom, as a function of solid concentration. Amongst the numerous equations available, the correlation of Richardson and Zaki (1954) has been most widely adopted due to its simplicity. A comprehensive review of recent advances in the area of sedimentation was presented by Davis and Acrivos (1985). A comparative study of several models for gravity-driven sedimentation of bi-disperse and Tri-disperse concentrated suspensions was recently reported by Al-Naffa and Selim (1989).

Similar to the sedimentation process, the numerous practical applications of fluidization have stimulated theoretical and

experimental investigations (Joshi, 1983; Richardson, 1971) on this subject. Correlations giving the relationship between the sedimentation velocity and particulate concentration (Richardson and Zaki, 1954; Garside and Al-Dibouni, 1977, Moritomi et al., 1986) have been found to be applicable to the fluidization process also, with the replacement of settling velocity by fluidization velocity. Most of the previous work concerning the modelling of these aspects of fluidized beds has been summarized by several authors (Leva, 1957; Kunni and Levenspiel, 1969, Couderc, 1986).

Research on the hydrodynamics of non-Newtonian fluid particle systems has been focussed hitherto chiefly on packed beds. Even, the two most important design parameters for a fluidized bed, namely, fluidization velocity and bed expansion characteristics (Yu et al., 1968; Mishra et al , 1975; Kumar and Upadhayay, 1981; Tonini et al., 1981; Machac et al., 1986) have received very little attention and more importantly the emerging picture is rather incoherent. Similarly, although many suspensions of particles have been known to exhibit non-Newtonian behaviour, investigations of sedimentation in non-Newtonian fluid media (Balkrishna et al., 1971; Allen and Uhlherr, 1989) are limited The only theoretical study concerning the influence of non-Newtonian behaviour on sedimentation velocity of particles is that of Kawase and Ulbrecht (1981c). It was found in this study that pseudo-plasticity decreases the sedimentation velocity and its reduction is pronounced at large voidage. A vast gap still continues to exist in the understanding of the hydrodynamics of non-Newtonian flow through a multi-particle assemblage.

2.2 MODELLING TECHNIQUES

Modelling the fluid flow past an assemblage of particles has remained a formidable task, because of the large number of factors involved such as the nature of fluid, fractional void volume, hydrodynamic interaction between neighbouring particles, wall and end effects, etc The difficulty encountered in isolating the influence of each variable has marred the achievement of a clear understanding of the problem. However, innumerable efforts have gone into analysing the various aspects of multiparticle fluid flow systems

Some of the popular approaches employed in the modelling of viscous fluid flow past an assemblage of particles are the Darcy's law approach, The Geometric Pore model approach, the Submerged Object approach, Continuum approach and the Cell model approach. The last two approaches, namely, the continuum and the cell models, are completely theoretical in the sense that they employ only the basic principles of fluid dynamics to account for the hydrodynamic interaction between particles. Rest of the models, on the other hand, are based fully or partially upon empirical reasoning.

Considerable efforts expended in analysing the non-Newtonian fluid flow through multi-particle systems involve an extension of the modelling techniques which were found successful for Newtonian fluids, with the incorporation of an appropriate constitutive equation to describe the non-Newtonian fluid behaviour. Detailed survey of the relevant literature shows that the effect of shear thinning (or pseudo-plasticity) on pressure drop and drag

coefficient has received considerable attention in these studies. There are only a few cases (Marshall and Metzner, 1967; Park, 1972, Machac and Dolejes, 1982) where the effects of viscoelasticity have been accounted for, during the interpretation and correlation of results. However, a completely satisfactory picture has not yet emerged.

With regard to the modelling technique for non-Newtonian flow through particle-assemblages, three approaches have been generally adopted, namely, the geometric pore model, the Darcy's law approach and the cell model approach. Among other available approaches, the elegant dimensional analysis of Slattery (1967) for visco-elastic fluids and the correlation procedure by Hassell and Bondi (1965) are noteworthy. Savins (1969) in his excellent review paper on this subject, has also suggested a method using the capillary model-hydraulic radius concept which does not involve any rheological equation.

2.2.1 Geometric Pore Model

A geometric pore model which has been extensively used to idealize the flow through the packed bed is the "Capillary tube bundle" approximation In capillary model, the space between particles is represented in terms of a bundle of tortuous capillaries, the length and diameter of which is determined such that the same resistance to flow is offered as the actual interstices of the multi-particle system. The starting point for this model is the Hagen-Poiseuille equation. The most well-known representations of this class of models are due to Blake, Blake-Kozeny, Kozeny-Carman and Ergun. In Blake's model, the bed

is envisaged as a bundle of straight tubes of complicated cross-section The Blake-Kozeny model portrays the bed or porous medium as a bundle of tangled tubes with an effective length greater than the actual length of the bed by a tortuosity factor In the Kozeny-Carman model, the effect of tortuosity on the mean velocity of flow is also considered by taking the mean velocity as the product of Dupuit (1863) velocity and the tortuosity factor. According to this model, the final expression for the modified friction factor, f_{bk}, in terms of the modified Reynolds number, Re_{bk} takes the simple form

$$f_{bk} = \frac{A}{Re_{bk}} \qquad (2\ 1)$$

The Kozeny-Carman model may be considered to provide a more accurate representation of flow through the bed, comprising of tortuous tubes.

All the above discussed capillary models are applicable for laminar flow regime only. The correlation for pressure drop through a fixed bed in turbulent flow regime was first developed by Burke and Plummer (1928). Subsequently, Ergun (1952) combined this correlation with that of Kozeny-Carman to provide a single expression valid for the entire flow range. The Ergun equation which essentially considers the total pressure drop as the sum of viscous and inertial pressure losses through the bed is expressed in the form,

$$f_{bk} = \frac{A}{Re_{bk}} + 1.75 \qquad (2.2)$$

The success of capillary models for Newtonian fluid flows has led to their extension to non-Newtonian flows also by many

investigators The earliest attempts in this direction were made by Christopher and Middleman (1965), who used the power law fluid model; and Sadowski and Bird (1965), who in a parallel treatment, used the Ellis fluid model to study the creeping flow. These authors related the flow rate and pressure drop by suitably modifying the Blake-Kozeny equation. Since then, numerous investigators have followed suit and studied a wide variety of fluid models (Gaitonde and Middleman, 1967; Kemblowski and Mertl, 1974, Brea et al. 1976; Kumar and Upadhyay, 1981; Kozicki and Tiu, 1988). Most of these studies are restricted to the creeping flow regime, save those of Brea et al. (1976) and Hanna et al. (1977) who obtained equations covering the laminar as well as turbulent flow regimes. Srinivas and Chhabra (1990) recently made exhaustive comparisons of the predictability of methods available in literature for the prediction of pressure loss during the flow of non-Newtonian fluids through packed beds. In this study, they used their own experimental data and those of others' available in literature (Sadowski and Bird, 1965; Park et al., 1975). The range of power law index covered in this study was 0.38 to 1.0 and the fixed bed porosity varied from 0.369 to 0.447. It was concluded that almost all the correlations overpredict the value of pressure drop for a given flow condition. The correlation proposed by Dharmadhikari and Kale (1985) was found to provide the closest agreement amongst all the results examined.

Despite the popular use of capillary models and numerous experimental results available in literature, there is still no agreement on the value of the constant A occurring in the

Kozeny-Carman equation. For Newtonian fluids, the values suggested range from 115 to 200, but the most commonly used are the values of 180 and 150 as determined by Carman (1937) and Ergun (1952) respectively Kemblowski and Michniewicz (1979) have re-analyzed most of the experimental data in literature and suggested a value of 180 for Newtonian and 150 for power law fluids. However, based on their own analysis, they have suggested a value of 180 for power law fluids, which was subsequently confirmed also for the flow of Carreau fluids (Kemblowski and Michniewicz, 1981). Apart from the afore-mentioned inconsistency, the capillary models have been criticized by several investigators (Barnea and Mednick, 1978; Molerus, 1980) for the following reasons·

(a) The tube bundle model represents an over-simplification of the real porous medium and the concept of mean hydraulic radius has little theoretical justification for laminar flow in a non-circular channel. Sheffield and Metzner (1976) and many others found the capillary model to be conceptually weak in that it does not take into account the converging-diverging nature of flow path and the inter-connection between pores. In case of non-Newtonian fluids this deficiency appears to be more serious because the viscoelastic effects are manifested in a converging-diverging flow path.

(b) In laminar tube flow the inertial effects are observed only with the onset of turbulence beyond a critical Reynolds number. In the case of flow through particle assemblages,

due to frequent deflection of fluid flow, inertial effects begin to dominate long before the onset of turbulance. In this regard, the pipe flow similarity with the flow in a packed bed does not exist

(c) Durst et al (1987) have pointed out that the pressure drop of porous media flow is only to a small extent due to the shear force term which is usually employed in the capillary model. For more correct derivations, additional terms have to be taken into account since the flow field is subjected to both shear and elongational strain.

In order to partly obviate some of these deficiencies, complex pore models have been proposed (Batra et al., 1970 Dullien, 1975; Scheidegger, 1974; Payatakes and Neira, 1977; Sheffield and Metzner, 1976; Deiber and Schowalter, 1979; Kanellopoulos, 1985). Although such more sophisticated pore models may be useful in accounting for some of the second order effects, they do not offer any measurable improvement (Cohen and Metzner, 1981) concerning the prediction of reltionships between the pressure drop and the flow rate. Therefore, classical capillary models continue to remain popular for describing flow through packed beds.

2.2.2 Darcy's Model

Most of the available analytical work on transport processes through porous media are based on Darcy's law. This law was established in 1856 by Darcy empirically, and since then has been verified experimentally by numerous investigators for Newtonian fluid motion in porous media at low flow rates. It states that

for an isothermal fluid moving with a slow steady velocity V under a pressure gradient $\frac{dP}{dx}$, through a homogeneous and isotropic porous bed

$$V = - \frac{C}{\eta} \frac{dP}{dx} \qquad (2\ 3)$$

where, η is the fluid viscosity and C is an empirical constant called the permeability of the medium. Originally, the Darcy's law was established to obtain the average or apparent flow rates of fluids through porous media in one-dimensional flows Later researchers, assuming the fluid velocity to be a continuous function of space coordinates, have given Darcy's law for two or three dimensional flow fields. The extension of Darcy's law to multi-dimensional flow including the body force term is expressed as,

$$V = \frac{C}{\eta} [- \nabla p + f_g] \qquad (2.4)$$

where, f_g is the body force vector given by the weight of the fluid per unit volume. It is to be noted, however, that the Darcy's law is established empirically and it can not be derived analytically by performing the momentum balance on a small element of porous medium. It is merely a constitutive relation which does not yield much information about the permeability of the porous medium. The drawbacks of Darcy's law are that it does not satisfy the no-slip boundary conditions on impermeable side walls confining the porous medium and also it becomes inapplicable if the permeability of the porous medium is high. In these cases, due consideration needs to be given to factors such as inertial effects in the fluid. Later generalizations of the Darcy's law

have focussed attention on some of these factors.

The inclusion of viscous shear stress terms in the flow equations and the consideration of a velocity field which satisfies no-slip at impermeable walls, have been proposed by Brinkman (1947). This is the so called Brinkman's extension, which accounts for the flow resistance due to the fluid viscosity itself. Yamamoto and Iwamura (1976) proposed a flow model in which the effects of inertia are taken into account via convection terms in the momentum equations Obviously, this is an important correction which has to be considered at higher flow rates through the porous medium Yet another approach to handle the inertial effects was proposed by Forchheimer (1901), which approximately accounts for the pressure loss due to flow separation in the pores, by the inclusion of an additional term in the flow equations. With all these extensions, the flow models for porous media situations have more or less the same general structure as that of the Navier-Stokes equations for free fluid flows. It is to be mentioned that despite these developments most of the studies available at present on porous medium applications, especially for non-Newtonian fluid flow, do not consider a generalized Darcy's law.

The Darcy's model has also been extended to non-Newtonian flows with the help of suitable rheological equations. This approach has been adopted by Kozicki et al. (1967, 1973), Gregory and Griskey (1967), Al-Farris (1989), and some others for a variety of fluid models.

2.2.3 Submerged Object Approach

The capillary and Darcy models are reported to fail at higher voidage and the experimental facts are better described by the submerged object models in this range These models are also known as discrete particle models, as they involve the determination of pressure drop across the bed from the expression for drag on a single particle immersed in the fluid, by assuming simple drag force additivity. Hydrodynamic interactions of neighbouring particles which affect the drag force on each individual particle, are not taken into account. The only indirect effect of neighbouring particles that is taken into account is the decrease in the average cross-sectional area available for fluid flow.

At a very early stage, Burke and Plummer (1928) had proposed a discrete particle model which regards each particle in the assemblage as being enveloped by a separate boundary layer. This approach was later expanded by Ranz (1952). Subsequently many other variations (Gauvin and Katta, 1973; Foscolo et al., 1983, Barnea and Mizrahi, 1973; Barnea and Mednick, 1978; Zimmels, 1988) of the submerged object model have been reported. The method of determining the drag force on a typical particle in the assemblage differs from one model to another; however, the common feature of all the submerged object models is the concept of simple drag force additivity.

The submerged object models are comparatively less popular than the capillary models and cell models, since they do not incorporate the particle to particle interaction directly.

However, analyses of non-Newtonian multiparticle systems based on the model are not available in the literature.

2.2.4 Continuum Approach

In the continuum model, the hydrodynamic forces and torques exerted on the particle by the fluid are computed by taking into account all particle-particle and particle-fluid interactions and then solving this complicated problem in the bounded region. One of the earliest exact solutions accounting for particle interactions in this way is that of Stimson and Jeffery (1926). They solved the problem of slow motion of two equal-sized spheres parallel to their line of centres. For the same problem Cooley and O'Neill (1969) gave a more comprehensive set of results for the cases in which spheres may be of unequal sizes. An exact solution for the two spheres problem has been possible primarily because of the use of separation of variables technique in bispherical coordinates. For a larger collection of spheres, or for a pair of non-spherical particles, it is not possible to find a suitable coordinate system for this purpose. It is then necessary to seek an approximate solution to the problem using a systematic scheme of successive iterations, whereby the boundary value problem may be solved in principle to a degree of accuracy by considering boundary conditions associated with one particle at a time. Such schemes are provided by the "method of reflections" (Smoluchowski, 1972) or the pairwise additive interaction model (Kim and Russel, 1985).

The major difficulty in modelling the multi-particle interaction by this model arises in summing the contribution of

different particles on the test particle. The analysis is complicated by the fact that in a system containing a large number of particles, the resulting sums or integrals are often divergent. One of the earliest attempts to overcome this difficulty was made by Hasimoto (1959), who obtained spatially periodic (Fourier series) fundamental solutions to the Stokes equation of motion for viscous flow past a periodic array of spheres This approach was later employed by Zick and Homsy (1982) and modified by Sangani and Acrivas (1982) to investigate slow flow past an array of spheres. Amongst the several other methods available (Hinch, 1977) to handle the divergent nature of sums of all contributions on the test particles, the renormalization technique (Batchelor, 1972; O'Brien, 1979; Feuillebois, 1984; Kim and Russel, 1985) has been widely used.

In summary, though it has been possible in principle, to formulate continuum models for most multi-particle flow problems, the solutions are generally too complicated to be useful or sometimes are even impossible to obtain. In general, the applicability of this model has so far been limited to dilute multiparticle systems and low Reynolds number flows of Newtonian fluids. Investigations of non-Newtonian fluid flows past an assemblage of particles using continuum approach is hardly available in literature.

2.2.5 Cell Model

Amongst the various models to describe the hydrodynamic interactions between the particles of a multi-particle system, the cell model has received extensive attention, probably because of

the relative ease with which significant results can be obtained. In its formulation, the difficult many body problem is replaced by a simple and conceptually more amenable situation involving one particle. Wall, entry and exit effects are usually neglected. It is then of great application in concentrated assemblages, where the effects of container walls will not be important. The assembly of particles in the fluid is usually assumed to be uniform and each sphere is fixed in space The interaction of a particular sphere with its neighbours is modelled by considering a hypothetical fluid envelope around that sphere such that the fractional void volume in the cell is identical to that of the entire assemblage. The two most extensively used cell models are the Happel's free surface model (1958) and the Kuwabara's zero vorticity cell model (1959). However, many other cell models have also been reported in the literature.

A somewhat similar model for study of the velocity of steady fall of spherical particles through a fluid medium was employed by Cunnigham (1910), who assumed that each particle in a cloud would be effectively limited to motion within a concentric mass of fluid. However, he assumed that the boundary of the outside fluid envelope was solid; this corresponded in someway to the surfaces of the surrounding spheres present in the cloud. As commented by Happel (1958), in this model the size of the spherical envelope must be fixed by some additional considerations.

Uchida (1949) proposed a model for viscous flow through packed beds. He assumed that the bed is divided into numerous centres and the particle is placed in the centre of each cube.

The boundary value problem of satisfying the appropriate boundary conditions simultaneously on spherical and cubical surfaces proved intractable and consequently, Uchida simplified it. The prediction of Uchida for the pressure drop through the cubic assemblage of particles does not agree well with experimental results of Happel and Epstein (1954) and the fixed bed data represented by Kozeny-Carman equation (Carman, 1937).

Richardson and Zaki (1954b) developed a semi-theoretical cell model for sedimenting spherical particles. The particles in the suspension were arrayed in a hexagonal pattern in horizontal planes. Two models were proposed In the first, the vertical layers had the same spacing as that between the particles in the horizontal plane and in the second, the vertical spacing was such that adjacent horizontal layers of spheres were in contact. In order to simplify the boundary conditions, it was assumed that each particle was surrounded by a cylinder of fluid with the same cross sectional area as the hexagonal prism. The appropriate boundary conditions for symmetric flow with respect to adjacent particles and zero vorticity at the particle surface, were prescribed for the system and solutions were obtained. In the development, the theoretical treatment was not rigorous and many simplifying assumptions were made. The predictions of sedimentation velocity from this analysis for the two configurations were found not to be applicable to a dilute concentration of particles, although configuration II gives better agreement of the two with the experimental data of Richardson and Zaki (1954a) in the intermediate particle concentration range.

The deviations may be attributed partly to the over-simplification of the pressure gradient and partly to the questionable assumptions (Jean and Fan, 1989) regarding the angles between the stream lines and the vertical axis.

Kawaguti (1958) proposed a "cylindrical cell model" to estimate the sedimentation velocity of uniform spheres in the Stokes flow regime. The drag force on a particle exerted by the fluid in a cylindrical cell was evaluated, based on viscous flow of a fluid past a sphere in a frictionless circular pipe of infinite length Since Faxen's procedure (Faxen, 1923) was used to approximate the velocity profile for such a flow, the result is valid only for a relatively dilute particle concentration. Furthermore, the relationship between the particle concentration and the ratio of the particle diameter to the radius of the imaginary pipe, is based on the effective projected area of the pipe and particle rather than the volume, an assumption whose validity is rather questionable.

Happel (1958) proposed a "spherical" cell model similar to that of Cunnigham (1910), and attempted to predict the bed expansion (or sedimentation velocity in a sedimentation process) and the pressure drops at low Reynolds numbers for fluidized and fixed beds respectively. The only difference in Happel's cell model compared to that of Cunnigham (1910) is that zero shear stress is prescribed at the outer spherical fluid envelope. This assumption is probably more reasonable than that of zero fluid velocity on the outer sphere adopted by Cunnigham. The specification of zero shear stress boundary condition is motivated

by the reasoning that the cells are of non-interacting type, thereby requiring no energy exchange with the surroundings. The entire disturbance due to each particle is thus confined to the cell of the fluid with which it is associated Within the bounded region of the cell, the Navier-Stokes equations after omitting the inertia terms, describe the fluid motion. The Happel cell model, also known as the free surface cell model, has been successful in predicting the pressure drop and hindered settling characteristics of concentrated ($0.3 \leq \epsilon \leq 0.6$) systems of spheres. It reduces to Stokes law as a limiting case at infinite dilution, but fails to predict the hindered settling behaviour of dilute suspensions. For the fluidization or sedimentation cases, it shows poor agreement with the experimental data of Steinour (1944), Virschoor (1951), Richardson and Zaki (1954a) and Hanratty and Bandukwala (1957), but shows reasonable agreement with the data of Adler (1958). It is important to recognise that the type of flow distributor used in the experiment exerts a significant influence on the flow field (Jean and Fan, 1989).

Theoretical predictions based on the Happel's model agree well with the experimental data for heat and mass transfer in multiparticle systems in the creeping flow region (Pfeffer, 1964; Pfeffer and Happel, 1964). The Happel's analysis for solid particles has been extended to analyse swarms of drops and bubbles in the presence or absence of surfactant impurities (Gal-or and Waslo, 1968). Subsequently, Yaron and Gal-or (1971, 1972) used the hydrodynamic solution of Gal-or and Waslo (1968) to investigate heat and mass transfer processes from side-distributed

drops, bubbles or solid particles and later on to calculate the effective viscosity of concentrated suspensions and emulsions.

Another spherical cell model was proposed by Kuwabara (1959), who used a zero vorticity assumption instead of the zero shear stress assumption on the outer spherical envelope in otherwise identical flow conditions. He calculated the drag in the creeping flow regime by integrating the dissipation energy function. Several authors (Happel and Brenner, 1965; El-Kaissy and Homsy, 1973) have criticized the zero vorticity spherical cell model for the inconsistency arising due to the fact that shear stress does not vanish at the outer surface; this is tantamount to the exchange of energy between neighboring cells, which violates the basic promise regarding the non-interacting nature of cells. Also, the zero vorticity cell model results in larger energy dissipation within the fluid envelope as compared to the free surface cell model of Happel (1958); the increased dissipation presumably is due to the additional work done by the stresses existing at the outer fluid envelope. As a consequence, Kuwabara's solution yields a stronger concentration dependance of the drag on a typical particle, experienced by uniformily distributed spheres in viscous flow at low Reynolds number.

Most of the applications of cell models in describing the transport processes in multi-particle assemblages have been limited to creeping flow conditions. Very little work has been reported outside the creeping flow regime. Leclair and Hamielec (1968) solved the complete Navier-Stokes equations for the zero vorticity cell model using the finite difference method and

reported the values of drag coefficient as a function of bed voidage and Reynolds number, encompassing wide range of conditions ($0.408 \leq \epsilon \leq 0.9$; $1 \leq Re \leq 500$). It is not at all clear whether the choice of zero vorticity cell model was based on its merit or simply because of its ease in implementation for vorticity-stream function approach. In an attempt to explore the extent to which the spherical cell models may be extended to higher Reynolds numbers, El-Kaissy and Homsy (1973) carried out a regular perturbation analysis for both free surface and zero vorticity cell models and have provided analytical expressions for the friction factor as a function of bed voidage ($0.3 \leq \epsilon \leq 0.6$) and Reynolds number. However, the perturbation scheme has limited applicability beyond the creeping flow regime in the sense that as the interparticle distance increases (i.e. the voidage increases), the maximum value of Reynolds number upto which their analysis is valid decreases Based on the comparison between theory and available experimental data, El-Kaissy and Homsy found that the free surface cell model yields consistently better results than the zero vorticity cell model. However, for $Re > 20$, both models show appreciable departures from experimental measurements.

Nishimura and Ishii (1980a,b) employed the free surface cell model together with the Karman-Pohlhausen integral method to examine the momentum and mass transfer boundary layers in particle assemblages at high Reynolds numbers. Using fourth order polynomial expansions these authors reported extensive results on the variation of friction factor and Sherwood number as functions of bed voidage and Reynolds number and claimed their results to be

applicable in the range $10 \leq Re \leq 10^5$. Intuitively, it is unlikely that the boundary layer approximation will be valid at values of Reynolds number as low as 10. Another somewhat unusual feature of their study is that the form drag is shown to be independent of the value of Reynolds number; also their results in the limit of voidage approaching unity differs from the value of drag coefficient available in literature by a factor of 2 or more. In a subsequent paper Fukuchi and Ishii (1982) employed a 5th degree polynomial and re-investigated the same problem However, qualitatively similar results have been reported in this study also

In addition to the aforementioned widely used cell models, many other cell models have been reported but their applicability has been examined only for a narrow range of applications. Gunn and Malik (1966) proposed a model for fluidized beds and sedimenting systems based upon arrays of particles where periodic conditions are established throughout the flow field. This model postulates the enclosing boundary to be frictionless; therefore, the total pressure drop across the cell can be equated to particle drag. As the mathematical difficulty of solving the equations subject to the boundary condition was formidable, Gunn and Malik (1966) presented only some general properties of solution in conjunction with the experimental results.

Like the sphere-in-sphere configuration of spherical cell models, sphere-in-cylinder configuration leading to what is commonly called as "cylindrical cell model" have been proposed by several investigators. Such models were earlier proposed by

Happel and Ast (1960), Kawaguti (1958) and Wakiya (1953). The Happel and Ast model was developed to represent the process of sedimentation The key concept in this model is the postulate of zero shear at the cylinder walls Within the bounded region, the Stokes equation for viscous flow was solved by using the method of Haberman to obtain the drag on the particle. It is important to add here that all these cell models apply in creeping flow regime only Recently, a cylindrical cell model for the hydrodynamics of particle assemblages at intermediate Reynolds number was reported by Tal and Sirignano (1982). These authors suggested that their model can be applied to study transport process in fluidized and packed beds as well as in predicting the rheological properties of suspensions.

The success of Happel's free surface cell models (1958) in the Newtonian case has led to its natural extension to non-Newtonian fluids. For instance, Mohan and Raghuraman (1976a, 1976b) extended its applicability to power law and Ellis model type fluids to calculate the drag coefficient Later on, an analogous treatment for the Carreau model fluids was presented by Chhabra and Raghuraman (1984). Qualitatively, for power law type fluids the analysis of Mohan and Raghuraman (1976a) predicts an increase in the value of drag coefficient above its Newtonian value, whereas, if a fluid model containing a zero shear viscosity is used to depict the shear thinning behaviour, a reduction in the drag is predicted below the Newtonian value (Mohan and Raghuraman, 1976b; Chhabra and Raghuraman, 1984). It needs to be emphasised here that there is no inconsistency in this Whether the drag is

augmented or suppressed with reference to the corresponding Newtonian value is only a matter of how the Reynolds number is defined However, a notable feature of all these analyses (which are approximate only) is that the two bounds diverge with the increasing degree of shear thinning characteristics In the absence of any definitive information, the use of arithmetic average of two bounds has been generally suggested. In another study, Kawase and Ulbrecht (1981a) linearised the governing equations using the approach earlier developed by Hirose and Moo Young (1969) and obtained a closed form analytical expression for the total drag force experienced by a particle assemblage in relative motion with respect to power law liquids This analysis also predicts an increase in the drag force over its Newtonian value. Owing to the approximate nature of their treatment and associated assumptions, the results of Kawase and Ulbrecht (1981a) are likely to be applicable only for mild to moderate shearthinning fluids through multi-particle assemblages. The only other study of the flow of shear thinning fluids through multi-particle assemblages is that of Hua and Ishii (1981). In this study, high Reynolds number flow of power law liquids through particle assemblage was simulated by employing the assumption of boundary layer flow in Happel's free surface cell model.

A close scrutiny of the above cited literature reveals that results are limited on the detailed flow field structure around a typical particle in an assemblage and explanations for the observed drag phenomena are still wanting, except for the creeping flow of Newtonian fluids. The performance of the Happel cell

model in the intermediate Reynolds number regime is also to be ascertained As already described at the end of Chapter-I, it is the intent of the present study to analyse some of these aspects in detail

CHAPTER III

MATHEMATICAL MODELLING

The flow of a generalized Newtonian fluid relative to an assemblage of spherical particles has been considered. Modelling of such multiparticle fluid flow systems rests upon the application of the principles of conservation of mass and momentum, in conjunction with a constitutive equation for the rheological behaviour of the fluid and a model for the representation of the hydrodynamic interactions between the particles, wall effects and end effects. The choice of a Generalized Newtonian fluid facilitates the use of the same formulation for both Newtonian as well as inelastic viscous non-Newtonian fluids. However, before embarking upon the actual formulation of the problem, it is instructive and desirable to present a terse discussion of the rheological equation of state for a non-Newtonian fluid.

3.1 RHEOLOGICAL EQUATION OF STATE

One of the simplest forms for the constitutive relationship between the stress tensor and the rate of deformation tensor at a point in a fluid is the Newton's law of viscosity. For an incompressible fluid, the stress tensor can be written as

$$\underset{\approx}{\sigma} = - P\underset{\approx}{\delta} + \eta\underset{\approx}{\Delta} \qquad (3.1)$$

where the rate of deformation tensor is given by

$$\underset{\approx}{\Delta} = \underset{\sim}{\nabla V} + (\underset{\sim}{\nabla V})^{T} \qquad (3.2)$$

For a Newtonian fluid, the viscosity depends only on temperature and pressure, and the fluids obeying equations (3.1) and (3.2) with a viscosity variation described by $\eta = \eta(p, T)$ are called Newtonian fluids All gases and low molecular weight liquids are known to display Newtonian behaviour.

It is well known that structurally complex fluids such as polymer melts and their solutions, suspensions and emulsions, etc. exhibit complex rheological behaviour which can not be described by the Newton's law of viscosity and hence these fluids are accordingly called non-Newtonian fluids. From an engineering view point, perhaps the most important non-Newtonian effect is the shear rate dependence of viscosity. Most non-Newtonian fluids display shearthinning or pseudo-plastic behaviour, that is, their apparent viscosity decreases with increasing shear rate. Other non-Newtonian effects include the existence of unequal normal stresses in steady shear flow and complex transient response in unsteady shear flow. Some examples of the former are the "Weissenberg effect" (Bird, Armstrong and Hassager, 1977) in which a macromolecular fluid climbs a rotating rod; the "hole pressure error" inherent in pressure transducers that are not flush mounted (Higashitani and Pritchard, 1972; Higashitani and Lodge, 1975) and the reversal of the direction of secondary flow when a disc rotates a liquid in a beaker. Unsteadyy state responses, on the other hand, are mainly observed in dynamic testing, stress relaxation, creep, recoil (Ferry, 1970) and in the other time

dependent experiments such as the start up of a shear flow, etc.

All the examples cited above are confined to shearing flows. Additional non-Newtonian effects which are encountered in non-shearing flows are the die-swell (Lodge, 1964); development of a toroidal vortex in the inlet flow to a die (Tordella, 1957; Gieskus, 1968; Metzner, Uebler and Chan Man Fong, 1968); the bizarre "Kaye Phenomenon", where a falling stream of polymer solution impinging on the puddle of the same fluid "bounces back" from the liquid surface (Lodge, 1964). Bird et al. (1977) have presented all excellent discussion of many of these pohenomena in their classic treatise.

In order to describe these non-Newtonian effects quantitatively Eqn. (3.1) must be replaced by an appropriate rheological equation of state. The earliest attempts involved simple adhoc empiricism to describe some very limited class of such flows. In this catagory the models of "Generalised Newtonian fluid and the "Linear viscoelastic fluid" were developed to describe shearthinning behaviour and the transient phenomena in small scale deformations, respectively Further, attempts were made to devise empirical "non-linear viscoelastic models" that could describe and interrelate, at least qualitatively, a wide variety of phenomena. Finally more complex integral expansions of basic memory functions were evolved which provide a better perspective of the aforementioned effects. However, it is also appropriate to add here that failures encountered in many careful numerical studies in recent years, have raised questions about the utility of some of these (Rallison and Hinch, 1988) constitutive

equations for describing the viscoelastic effects. Since the present work is concerned with the hydrodynamics of generalised Newtonian fluids (GNF) in multiparticle assemblages, it is appropriate to present a brief discussion on the rheological behaviour of this class of fluids.

3.2 GENERALISED NEWTONIAN FLUIDS

The general expression used to describe the behaviour of a time independent isotropic fluid is given by

$$\underset{\approx}{\sigma} = -p\underset{\approx}{\delta} + \underset{\approx}{\tau} \tag{3.3}$$

$$\underset{\approx}{\tau} = \beta\underset{\approx}{\Delta} + \eta\underset{\approx}{\Delta} + \eta_c \, (\underset{\approx}{\Delta}.\underset{\approx}{\Delta}) \tag{3.4}$$

where η is the "non-Newtonian viscosity", η_c is the "cross viscosity" and τ is the deviatoric stress tensor; β, η and η_c are functions of the three principal invariants of the rate of deformation tensor, $\underset{\approx}{\Delta}$. The fluids obeying Eqn. (3.4) are known as Reiner-Rivlin fluids. The absence of time derivatives in the above equation is tantamount to excluding viscoelastic phenomena from the theoretical consideration. For incompressible fluids both β and the first invariant are identically zero, and therefore, eqn. (3.4) reduces to

$$\underset{\approx}{\tau} = \eta\underset{\approx}{\Delta} + \eta_c \, (\underset{\approx}{\Delta}.\underset{\approx}{\Delta}) \tag{3.5}$$

where $\eta = \eta\,(I_2, I_3)$; and I_2 and I_3, the second and third invariants of the rate of deformation tensor are given by the expressions

$$I_2 = \underset{\approx}{\Delta} : \underset{\approx}{\Delta} \tag{3.6}$$

$$I_3 = \det \underset{\approx}{\Delta} \tag{3.7}$$

Several investigators have questioned the usefulness of the

Reiner-Rivlin equation on the grounds that the available experimental evidence does not support the existance of non-vanishing normal stress coefficient η_c without appreciable viscoelasticity. However, it is possible to derive the constitutive equations for a purely viscous (inelastic), incompressible fluid by considering β and η_c as zero in eqn (3.4) and η being a function of only the second invariant of the rate of deformation tensor. Thus,

$$\underset{\approx}{\tau} = \eta \underset{\approx}{\Delta} \tag{3.8}$$

where $$\eta = \eta (I_2) \tag{3.9}$$

Reiner called eqn. (3.8) as the Generalised Newtonian fluid model and it reduces to the Newtonian case for a constant value of η. The form of eqn. (3.9) has received further support from the fact that the third invariant of the rate of deformation tensor is identically zero for viscometric flows and it is considered to be unimportant in other flow situations as well (Slattery and Bird, 1961; Tanner, 1966). Hence, eqn. (3.9) represents a good approximation suitable for engineering applications.

Based on experimental measurements conducted for viscometric flows, the functional dependence of the appareent viscosity η on I_2 has been portrayed by a variety of empirical formulations. Consequently, there is no scarcity of such equations in the literature and these have been summarized by Bird (1965, 1976) and Skelland (1969), among others.

3.2.1 The Newtonian Model

For a Newtonian fluid

$$\eta = \text{constant} = \mu \tag{3 10}$$

where μ is the Newtonian viscosity. Hence,

$$\underset{\approx}{\tau} = \mu \underset{\approx}{\Delta} \qquad (3\ 11)$$

and in steady one dimensional shear flow

$$\tau = \mu\ e \qquad (3\ 12)$$

where e is the shear rate

3.2.2 The Power-Law Model

According to this model, the apparant viscosity is given by

$$\eta = K \left(\frac{I_2}{2} \right)^{\frac{n-1}{2}} \qquad (3\ 13)$$

where n is the power law flow behaviour index and K is the consistency factor, which are determined using shear stress-shear rate data For steady one dimensional shear flow, Eqn. (3 13) can be re-written as

$$\tau = K\ e^n \qquad (3.14)$$

The apparant viscosity is defined from Eqn (3.14) as

$$\eta = K\ |\ e\ |^{n-1} \qquad (3.15)$$

Eqn. (3.15) is probably "the most criticized, most maligned and yet most widely used equation in all of the rheology" (Schowalter, 1978). The main virtue of the power law model is its simplicity, as the extent of shear thinning behaviour is simply characterised by the value of n. When n is unity, Eqn (3.15) reduces to the standard Newtonian fluid with a viscosity K. When n < 1, the viscosity decreases with increasing shear rate (pseudoplastic or shearthinning behaviour); and for n > 1 the viscosity increases with increasing shear rate (dilatant or shear thickening behaviour). Most fluids tend to exhibit power law behaviour over a

range of shear rates. One of the severe drawbacks of the power law model is that it fails to predict a constant viscosity in the zero shear rate region. Numerous models containing more than two parameters are available, which overcome some of the drawbacks of the power law model. These have been covered adequately in several references e.g see Bird (1965), Skelland (1967), Darby (1967), Bird et al. (1977), etc. However, it must be borne in mind that the introduction of each parameter in the rheological equation of state also makes the solutions of hydrodynamic problems increasingly difficult (Matsuhisa and Bird, 1965) The two such models which have found widespread use in approximating shear stress-shear rate behaviour of a range of several substances are the Ellis and the Carreau models Several workers have employed these models for investigting the behaviour of non-Newtonian fluid particle systems (Mohan and Raghuraman, 1976b; Chhabra and Raghuraman, 1984; Kemblowski and Michniewicz, 1981; Gummalam, Narayan and Chhabra, 1988; Bush and Phan-thien, 1984). However, there is no question that in majority of the experimental and theoretical investigations pertaining to viscous flow past an assemblage of particles, power law model has been employed. In the present study also, the power law type Generalised Newtonian fluid model has been selected for describing the fluid behaviour. However, the problem formulation itself has been made general so as to be applicable to other kinds of Generalised Newtonian fluids with minor modifications.

3.3 PARTICLE-PARTICLE INTERACTION

Various approaches adopted to model the hydrodynamic interactions between the particles have been discussed in Chapter II. Though in principle, it is possible to formulate continuum models for multiparticle systems, the solutions of these models are generally too complicated to be useful In contrast to this, the cell models have been extensively used in modelling the multi-particle assemblages and indeed have yielded significant results. As discussed in the previous chapter, the free surface cell model has gained wide acceptance in predicting the pressure drop through packed beds (Mohan and Raghuraman, 1976a; Kawase and Ulbrecht, 1981; Nishimura and Ishii, 1980a,b; Chhabra and Raghuraman, 1984), settling characteristics of concentrated suspensions (Kawase and Ulbrect, 1983; Prasad et al , 1990) and rise and fall of drops and bubbles (Gal-Or and Waslo, 1968; Bhavraju et al., 1978; Jarzebski and Malinowski, 1986; Gummalam et al , 1988) in Newtonian as well as in non-Newtonian media. Hence, this model is employed to describe the particle-particle interactions in the present work.

The free surface cell model envisions the particle assemblage to consist of a number of identical unit cells, each of which contains a particle placed inside a fluid envelope such that the voidage of the cell is equal to the statistically averaged overall voidage of the assemblage. The cells are of non-interacting type and therefore, one unit cell represents the complete assemblage, neglecting the wall and end effects.

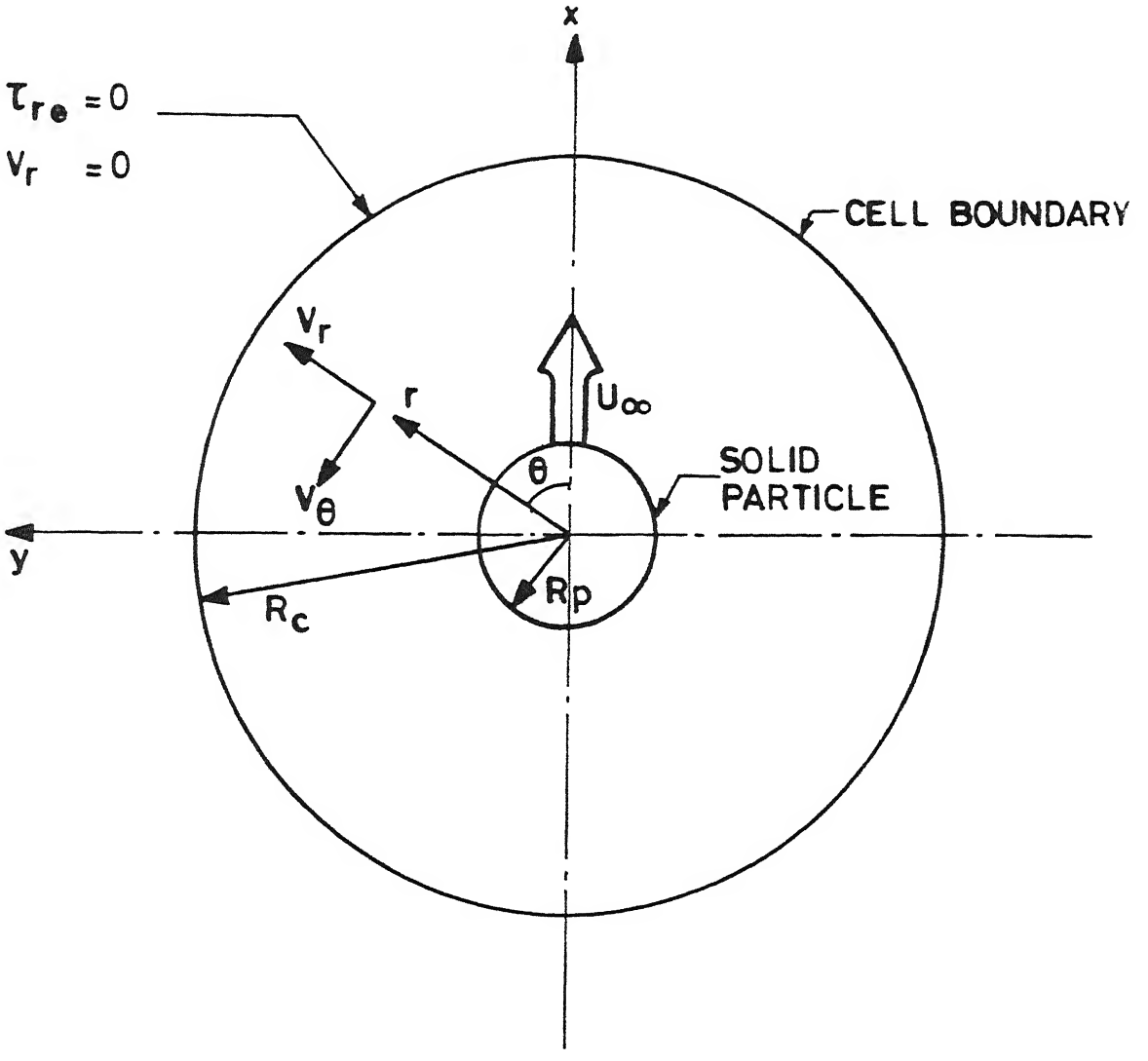

Fig 3 1: Schematic representation of the flow configuration (Happel Cell).

3.4 PROBLEM STATEMENT AND FORMULATION

The steady, linear motion of a uniformly spaced assemblage of rigid spherical particles through an incompressible, inelastic, viscous fluid has been considered. The rheological behaviour of the fluid is modelled using the power law equation (Eqn 3 13), with Newtonian fluid as a special case (n = 1) Each particle of radius R_p in the assemblage, is isolated from the rest of the particles by defining a cell boundary of radius R_c concentric with the particle. The flow around a typical particle in its cell is the flow configuration analysed The schematic representation of the flow configuration (unit cell) along with the coordinate system (r, θ, ϕ) is shown in Fig. 3 1. Axisymmetry is assumed to prevail within the cell about the direction of particle motion. The solid sphere moves in the positive X-direction with a velocity, U_∞ As stipulated by the free surface cell model, the radial velocity and the tangential stresses vanish on the fluid cell surface.

The continuity and momentum equations for a variable viscosity system in conservative term can be expressed as

$$\nabla \cdot V = 0 \qquad (3.16)$$

$$\rho V \cdot \nabla V = - \nabla p + \nabla (\eta (\nabla V + \nabla V^T)) \qquad (3.17)$$

where p is the non-gravitational pressure, V is the velocity vector; ρ and η are liquid density and apparent viscosity respectively. The constitutive equation for the rheological behaviour of a power law type fluid is expressed as

$$\tau_{ij} = K \left(\frac{I_2}{2} \right)^{\frac{n-1}{2}} \Delta_{ij} \qquad (3.18)$$

where

$$\Delta_{ij} = V_{i,j} + V_{j,i}$$

and

$$I_2 = \sum_i \sum_j \Delta_{ij} \Delta_{ji} = \Delta_{rr}^2 + \Delta_{\theta\theta}^2 + \Delta_{\phi\phi}^2 + 2\,\Delta_{r\theta}^2 \qquad (3.19)$$

For the free surface cell model, the appropriate boundary conditions on the particle surface ($r = R_p$) in the spherical polar coordinates are:

At $r = R_p$

$$V_r = U_\infty \cos\theta \qquad (3.20a)$$

$$V_\theta = -U_\infty \sin\theta \qquad (3.20b)$$

At the cell surface, $r = R_c$

$$V_r = 0 \qquad (3.20c)$$

$$\tau_{r\theta} = \eta \frac{\partial}{\partial r} \left(\frac{V_\theta}{v} \right) = 0 \qquad (3.20d)$$

The radius of the fluid cell, R_c, and the voidage of the assemblage ϵ are related by the expression

$$R_c = R_p (1 - \epsilon)^{-1/3} \qquad (3.21)$$

The variables in the above equations are non-dimensionalised as

$$V^* = \frac{V}{U_\infty}, \quad \nabla^* = R_p \nabla, \quad P^* = \frac{P}{\rho U_\infty^2}$$

$$\eta^* = \frac{\eta}{K \left(\frac{U_\infty}{R_p} \right)^{n-1}}, \quad r^* = \frac{r}{R_p}, \quad \Delta_{ij}^* = \frac{\Delta_{ij}}{\left(\frac{U_\infty}{R_p} \right)}$$

$$I_2^* = \frac{I_2}{\left(\frac{U_\infty}{R_P}\right)^2}, \quad \tau^* = \frac{\tau}{K\left(\frac{U_\infty}{R_P}\right)^n} \tag{3.22}$$

Using these non-dimensionalised variables, Eqns. (3.16) to (3 21) are rewritten in their dimensionless form as

$$\nabla^* \; V^* = 0 \tag{3 23}$$

$$V^* . \nabla^* \; V^* = - \nabla^* \; p^* + \frac{1}{Re_r} \nabla^* \left\{ \eta^* \left(\nabla^* \; V^* + \nabla^* \; V^{*T} \right) \right\} \tag{3 24}$$

with

$$Re_r = \frac{\rho \; U_\infty \; R_P}{K\left(\frac{U_\infty}{R_P}\right)^{n-1}} \tag{3 25}$$

and

$$\eta^* = \left(\frac{I_2^*}{2} \right)^{\frac{n-1}{2}} \tag{3.26}$$

At $r^* = 1$

$$V_r^* = \text{Cos } \theta \tag{3.27a}$$

$$V_\theta^* = - \text{Sin } \theta \tag{3.27b}$$

At $r^* = R_c^*$ (i.e R_c/R_P)

$$V_r^* = 0 \tag{3.27c}$$

$$\tau_{r\theta}^* = 0 \tag{3.27d}$$

The solutions of Eqns. (3.23) and (3.24) for the boundary conditions stated in Eqns. (3.27) represent the detailed flow field (u, p, v) around a particle in the assemblage.

The dimensionless drag coefficient defined as

$$C_D = F_D / \left(\frac{1}{2} \rho \; \pi \; R_P^2 \; U_\infty^2 \right)$$

may be obtained by integrating the viscous and the pressure forces over the sphere surface The pressure drag coefficient is obtained as

$$C_{DP} = -4 \int_{\theta=0}^{\theta=\pi} P^* \Big|_{r^*=1} \sin\theta \cos\theta \, d\theta \qquad (3\ 28)$$

The friction drag coefficient is obtained by integrating the normal and tangential components of the viscous stress tensor as·

$$C_{DF} = \frac{4}{Re_r} \int_{\theta=0}^{\theta=\pi} \eta^* \left\{ 2 \frac{\partial V_r^*}{\partial r^*} \cos\theta - \frac{\partial V_\theta^*}{\partial r^*} \sin\theta + \frac{V_\theta^*}{r^*} \sin\theta - \frac{1}{r^*} \frac{\partial V_r^*}{\partial \theta} \sin\theta \right\} \Big|_{r^*=1} \sin\theta \, d\theta \qquad (3.29)$$

The total drag coefficient is simply the sum of pressure drag coefficient and the friction drag coefficient, given by the expression

$$C_D = C_{DP} + C_{DF} \qquad (3.30)$$

3.5 SOLUTION METHODOLOGIES

An exact solution of these equations of motion has so far been obtained only for creeping flow of Newtonian fluids (See Appendix-I). However, analytical solutions are not possible for non-Newtonian fluids even under creeping flow condition, owing to the non-linear form of the rheological equation of state (Eqns. 2.13 or 2.14). Therefore, existing analyses of the problem pertain to varying degrees of approximation. Two distinct approaches have been used in seeking approximate solutions to this class of problems.

(i) For the steady, creeping flow of incompressible Generalized Newtonian fluids, variational principles have been extensively used This approach yields upper and lower bounds on the integrated quantities such as drag coefficients and does not provide any insight into the physical features of the flow field Furthermore, in this approach, either the equation of continuity (upper bound) or the momentum equation (lower bound) is satisfied It has also been shown that this technique yields true bounds only in the cae of Newtonian and power law fluids (Slattery, 1972) An important feature of such analysis is that the two bounds diverge increasingly as the extent of non-Newtonian behaviour increases Excellent discussions on the variational principle approach (with special reference to its applications to fluid mechanical problems) have been given by Powlowski (1954), Bird (1960), Johnson (1960,61) and Leonov (1988) Similar applications of this technique to non-Newtonian fluid-particle systems have been illustrated by numerous workers (e g see Bird, 1960, Yoshioka and Adachi, 1971, 1973, Slattery, 1972, Wasserman and Slattery, 1964; Hopke and Slattery, 1970, Mohan, 1974, Chhabra et al , 1980; Mohan and Raghuraman, 1976a,b, Chhabra and Raghuraman, 1984, Jarzebski and Malinowski, 1986; Gummalam and Chhabra, 1987; Leonov, 1988; Prasad et al , 1990)

(ii) The second class of solutions rests on the linearizion of the non-linear viscous terms in the momentum equations for creeping flow conditions. The essence of this approach lies in approximating the second invariant of the rate of deformation tensor by the corresponding Newtonian value, and this together

with some other assumptions, allows a closed form solution to be obtained. Perhaps Hirose and Moo-Young (1969) were the first to employ this approach to obtain a closed form expression for drag coefficient of a bubble moving in a power law fluid Since then, it has been extended to encompass swarms of bubbles in power law and Bingham plastic fluids (Bhavraju et al., 1978), single as well as assemblage of solid spheres moving in power law liquids (Acharya et al., 1976; Kawase and Ulbrecht, 1981a, b). Owing to the nature of the simplifications made in this approach, one would intuitively expect the results to be applicable for weakly non-Newtonian conditions only.

Beyond creeping flow conditions, no approximate solutions are possible even for Newtonian fluid. Numerical Methods (Leclair and Hamielec, 1968), perturbation analysis (El-Kaissy and Homsy, 1973) and boundary layer approximations (Nishimura and Ishii, 1980a,b) have been employed to analyse Newtonian fluid flow through multi-particle systems at intermediate and high Reynolds numbers. For non-Newtonian liquids the application of numerical methods such as finite difference, finite element and boundary element method has been limited to the creeping flow past a single sphere. These methods have not been extended to multi-particle systems. There is a paucity of full scale numerical results for free surface cell model in the intermediate Reynolds number regime particularly for non-Newtonian flow. An approximate solution was obtained (Kawase and Ulbrecht, 1981a; Hua and Ishii, 1981) by using the Happel's free surface cell model in conjunction with

boundary layer theory for flow of power law fluid past an assemblage of spheres.

In most of the available numerical studies on fluid flow through particle assemblages stream function-vorticity approach of finite difference technique has been extensively used (Leclair and Hamielec, 1968; Hamielec et al., 1967; Tiefenbruck and Leal, 1982, Sundararajan and Ayyaswamy, 1984). Over the past two decades the finite element method (FEM) has emerged as a very effective method for solving a wide range of flow problems (Gallaghar et al , 1978, Baker, 1985). The creeping motion of a single sphere in Newtonian and non-Newtonian media has been analysed with the help of the finite element method (Crochet, 1982; Gu and Tanner, 1985) and the boundary element method (Bush and Phan-thien, 1984). In fact, for simulating low Reynolds number flows, the FEM solution procedures offer several attractive features over the conventional numerical techniques. These include, easy handling of stress boundary conditions, incorporation of complex viscosity variation in the fluid, convenient application to complex geometry and the development of general codes for a variety of flow problems. Furthermore, the incorporation of primitive variables (u, p, v) approach in these studies is definitely more convenient and advantageous than the stream function-vorticity formulation. It is well known that for the solution of the vorticity transport equation which constitutes an elliptic boundary value problem, a linear combination of vorticity and its normal derivative is required to be specified on a closed boundary. In general, vorticity is not known *a priori* along the boundry. Moreover,

owing to the variable viscosity of non-Newtonian fluids, the transformation of the equations of motion into the classical equation for the convective diffusion of the vorticity is very cumbersome. Besides, the pressure recovery process from the stream function-vorticity solutions is susceptible to large numerical errors (Crochet, 1984) as it involves the evaluation of higher order derivatives of stream function and their integrtion along the particle surface. It is, therefore, not at all surprising that the primitive variable approach of the finite element method for solving flow problems has found widespread use. The penalty function approach (Bercovier and Engleman, 1979) has also been applied with great success to the solution of Navier-Stokes equations for incompressible Newtonian fluid flow In this approach, the pressure variable is eliminated and only velocity components are solved which results in considerable savings in computing time However, in the case of non-Newtonian fluid flow, the penalty approach has not been found very useful (Bernstein et al., 1981; Nakazawa et al., 1982). In this study therefore, the primitive variable formulation of the flow equations has been adopted. In the following section, construction of a finite element scheme based on such a formulation is elaborated.

3.6 FEM FORMULATION

The finite element method is a numerical procedure for solving physical problems governed by a set of differential equations or a variational principle. It has two characteristics that distinguish it from the other numerical procedures.

(a) It utilizes an integeral formulation to generate a system of algebraic equations, and

(b) Continuous piecewise smooth interpolation functions are used for approximating the unknowns.

Amongst the various mathematical theories, the variational principle has been (and continues to be) the most popular basis of forming a finite element approximation. However, for many problems in fluid mechanics, variational principles do not exist. This is so because in the Eulerian frame of reference, the expression for conservation of momentum is explicitly non-linear In such cases, the weighted residual approach offers a more powerful tool for constructing the integral formulation Here, the residue of each governing conservation equation is itself not set equal to zero every where but its integeral with respect to a selected weighting function is required to vanish (Finlayson, 1972). Several approximation techniques based on this approach are available such as the collocation method, the Galerkin method, the least square method etc. The Galerkin's weighted residual technique is by far the most versatile and popular method (Baker, 1973; Popinski and Baker, 1976; Barrett and Elliott, 1982; Engleman and Sani, 1986) and is also more suitable for elliptic operator problems.

In present work, the Galerkin's weighted residual approach has been used to construct a finite element scheme to solve the governing equations. At the outset, it is worthwhile to recognize that owing to the axisymmetry in ϕ direction, it is much more convenient to numerically solve the equations of motion along with

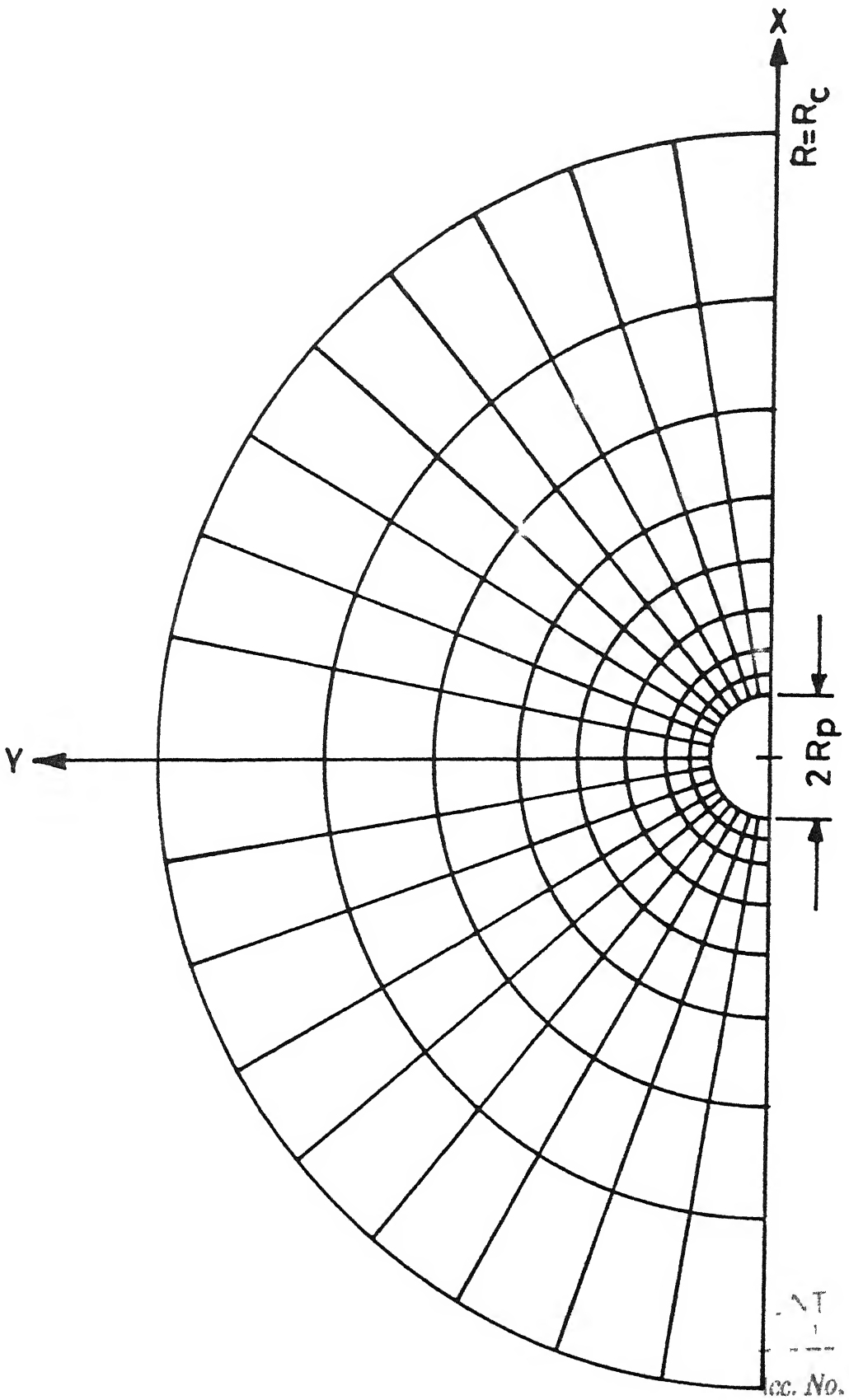

Fig 3 2 Typical spatial discretization of flow domain (ε = 0 999) utilising quadrilateral elements with exponential step size in radial direction

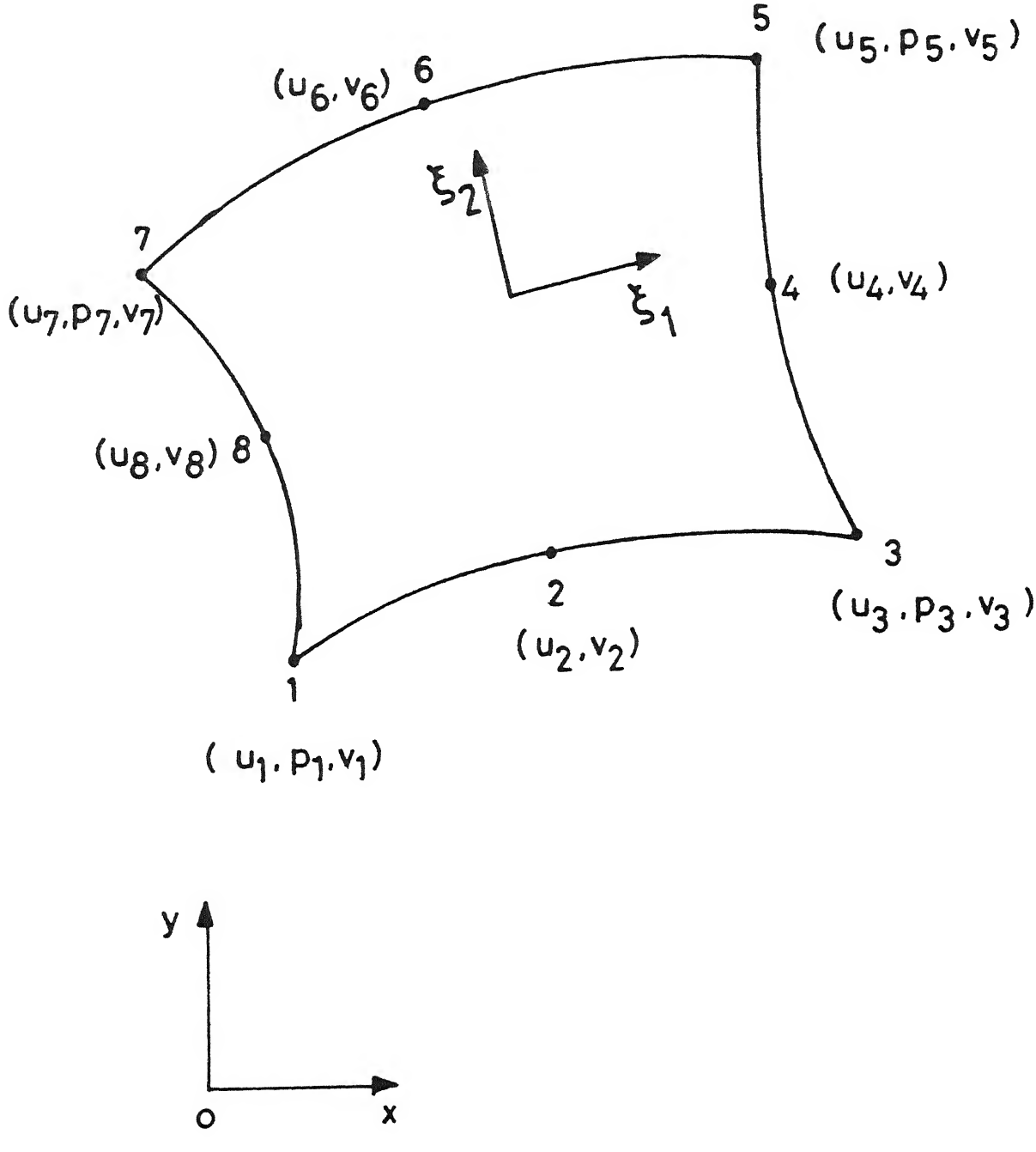

Fig 3.3 Parabolic eight noded element showing typical node numbering and local coordinate system.

the associated boundary conditions (which have been presented in Section 3 3 in spherical poloar coordinates) in a cylindrical coordinate frame (y, ϕ, x) shown in Fig 3 1 Indeed, the FEM formulation is considerably simplified due to the asixymmetry in ϕ direction and has a form which is only slightly different from a 2-D formulation.

The spatial discretization of the flow domain (Fig. 3.2) has been done using 8-noded quadrilateral elements (Fig 3.3) of the serendipity type containing one node at each corner and one at the midpoint of each side. The variation of V_x, V_y and p over each element is defined as

$$V_x = \sum_{i=1}^{i=8} N_i V_{xi}, \quad V_y = \sum_{i=1}^{i=8} N_i V_{yi}, \quad p = \sum_{i=1}^{i=8} M_i p_i, \qquad (3.31)$$

where V_{xi}, V_{yi} and p_i are the nodal values of the variables. Also N_i and M_i are the interpolation functions (shape functions) for velocity and pressure respectively. Since V_x and V_y have a similar range of variation and satisfy similar equations, same shape functions have been used for both V_x and V_y. One of the problems usually encountered in solving the Navier-Stokes equations by the finite element method has been the occurrence of spurious pressure fluctuations for certain choices of elements (Taylor and Hood, 1974; Olson and Tuann, 1976; Jackson and Cliffe, 1980; Sani, 1980). The "mixed interpolation" method obviates this difficulty, though one can not say that the problem has been fully understood (Rae, 1982). It is now a standard practice (Taylor and Hughes, 1984) to approximate the variation of pressure by shape functions of one order lower than those used for velocity. The

pressure in the present scheme is interpolated by means of a bilinear polynomial, whereas the velocity components are approximated by serendipity shape functions giving an approximation of P^2-C^0 type These features are implemented by using the same element geometry, where all the eight nodes are associated with velocities but only corner nodes involve pressure. The various options available for the choice of the elemental shapes and the shape functions have been adequately discussed by Crochet et al. (1984).

Dropping the asterisk for convenience from the non-dimensional eqns. (3.23) to (3.27), the weighted residual statement for the governing equations of continuity and momentum in X and Y directions, may be written as

$$\iiint_{\Omega} M_i \, (\nabla . V) \; y \; dy \; dx \; d\phi, \quad i = 1, \ldots, m \tag{3.32}$$

$$\iiint_{\Omega} N_i \, \hat{e}_x . \left[V . \nabla V + \nabla p - \frac{1}{Re_r} \nabla . \left\{ \eta \, (\nabla V + \nabla V^T) \right\} \right] y \; dy \; dx \; d\phi$$

$$= [0], \; i = 1, \ldots l \tag{3.33}$$

$$\iiint_{\Omega} N_i \, \hat{e}_y . \left[V . \nabla V + \nabla p - \frac{1}{Re_r} \nabla . \left\{ \eta \, (\nabla V + \nabla V^T) \right\} \right] y \; dy \; dx \; d\phi$$

$$= [0], \quad i = 1, \ldots l \tag{3.34}$$

where Ω refers to the solution domain, m is the total number of pressure unknowns and l is the total number of velocity unknowns. It is interesting to note that even though the pressure gradient forms a part of the momentum equations, yet there is no obvious equation for obtaining the pressure variables. Therefore, pressure is evaluated only indirectly through the continuity

equation in the sense that when the correct pressure field is substituted into the momentum equations, the resulting velocity field satisfies the continuity equation One approach to avoid spurious oscillations due to the non-satisfaction of continuity equation is to make the pressure field explicitly compatible with the continuity equation

The choice of the shape functions M_i and N_i as weighting functions for minimising the residue of the continuity and momentum equations respectively, can be shown to yield a diagonally dominant system of matrix equations in viscosity-dominated situations as encountered in the applications involving particle assemblages. However, for convection-dominated situations, upwind weighting functions (in Petrov-Galerkin method) which give more weightage for residue in the downstream direction as compared to that in the upstream direction have also been proposed. In the present work, since Reynolds number is not very high (Re < 100) the above choice of weighting functions is considered to be adequate and justified.

Invoking the Green's theorem, the second order terms in the momentum equations can be reduced leading to what is commonly called as the weak form of weighted residual statement, as given below:

$$\iiint_{\Omega} N_i \, (V . \nabla V + \nabla p) + \nabla N_i . \frac{\eta}{Re_r} (\nabla V + \nabla V^T)) \; y \; dy \; dx \; d\phi$$

$$- \oint_c \underset{\sim}{n} . \frac{\eta}{Re_r} N_i \, (\nabla V + \nabla V^T)) \; y \; dl \; d\phi = [0] \qquad (3.35)$$

where n is the outward normal at a point on the boundary surface c of the domain Ω Substituting the approximation for V_x, V_y and p

from Eqn. (3.31) in Eqns. (3.32) to (3.35), the final form of weighted residual statements for continuity equation and momentum equations turn out to be

$$\sum_{e=1}^{e=E} \left[\iiint_{\Omega^e} M_i \left\{ \frac{\partial N_j}{\partial x} \right\} y \, dy \, dx \, d\phi \right] \left[V_{xj} \right] + \left[\iiint_{\Omega^e} M_i \left\{ \frac{\partial N_j}{\partial y} + \frac{N_j}{y} \right\} y \, dy \, dx \, d\phi \right] \left[V_{yj} \right] = [0] \tag{3.36}$$

$$\begin{aligned} \sum_{e=1}^{e=E} \Bigg[\iiint_{\Omega^e} \Bigg\{ \Bigg(\sum_{k=1}^{8} N_k \bar{V}_{xk} \Bigg) N_i \frac{\partial N_j}{\partial x} + \Bigg(\sum_{k=1}^{8} N_k \bar{V}_{yk} \Bigg) N_i \frac{\partial N_j}{\partial y} \\ + \frac{2\eta}{Re_r} \frac{\partial N_i}{\partial x} \frac{\partial N_j}{\partial x} + \frac{\eta}{Re_r} \frac{\partial N_i}{\partial y} \frac{\partial N_j}{\partial y} \Bigg\} y \, dy \, dx \, d\phi \Bigg] \left[V_{xj} \right] \\ + \left[\iiint_{\Omega^e} \frac{\eta}{Re_r} \frac{\partial N_i}{\partial y} \frac{\partial N_j}{\partial x} y \, dy \, dx \, d\phi \right] \left[V_{yj} \right] \\ + \left[\iiint_{\Omega^e} N_i \frac{\partial M_j}{\partial x} y \, dy \, dx \, d\phi \right] \left[P_j \right] = [F_{x,i}] \end{aligned} \tag{3.37}$$

$$\begin{aligned} \sum_{e=1}^{e=E} \Bigg[\iiint_{\Omega^e} \Bigg\{ \Bigg(\sum_{k=1}^{8} N_k \bar{V}_{xk} \Bigg) N_i \frac{\partial N_j}{\partial x} + \Bigg(\sum_{k=1}^{8} N_k \bar{V}_{yk} \Bigg) N_i \frac{\partial N_j}{\partial y} \\ + \frac{\eta}{Re_r} \frac{\partial N_i}{\partial x} \frac{\partial N_j}{\partial x} + \frac{2\eta}{Re_r} \frac{\partial N_i}{\partial y} \frac{\partial N_j}{\partial y} \Bigg\} y \, dy \, dx \, d\phi \Bigg] \left[V_{yj} \right] \\ + \left[\iiint_{\Omega^e} \frac{\eta}{Re_r} \frac{\partial N_i}{\partial x} \frac{\partial N_j}{\partial y} y \, dy \, dx \, d\phi \right] \left[V_{xj} \right] \\ + \left[\iiint_{\Omega^e} N_i \frac{\partial M_j}{\partial y} y \, dy \, dx \, d\phi \right] \left[P_j \right] = [F_{y,i}] \end{aligned} \tag{3.38}$$

In above equations, the terms $F_{x,i}$ and $F_{y,i}$ on R.H.S. are the force contributions from the deviatoric stress on the cell boundary. However, in the present work, there is no need to

evaluate these forces since, a simpler method has been adopted (which is described subsequently) for incorporating the cell boundary conditions of the free surface cell model

Equations (3.37) and (3.38) exhibit strong non-linear behaviour both due to the presence of the inertial terms and the shear dependent viscosity. To facilitate the ease of obtaining a solution, these non-linear terms have been quasilinearised, by evaluating them on the basis of the solution corresponding to the previous iteration. For the sake of clarity, the use of the previous iteration solution is indicated with an overbar (e.g. $\bar{V}_{xk}$ and $\bar{V}_{yk}$) wherever it occurs explicitly The elemental integrals in the Equations (3.36) to (3.38) have been numerically evaluated using Gauss Legendre quadrature with 3 x 3 sample points Thus, the system of the non-linear integral equations is reduced to a system of non-linear algebraic equations. In matrix form, for an element, these equations can be expressed as

$$[K]\ \{\phi_1\} = \{F\} \qquad (3.39)$$

where [K] is a 20 x 20 coefficient matrix, $\{\phi_1\}$ is the vector containing all the nodal unknowns e.g u_j, p_j and v_j and {F} is the right hand side vector also known as flux vector. Non-zero values of the components of flux vector arise only for elements lying on the boundary as the contributions for the interior elements mutually cancel each other.

Before discussing the assemblage of these elemental coefficient matrices into a Global Coefficient matrix, the evaluation of the non-Newtonian viscosity and the method of implementing the free surface cell boundary conditions is

presented in the following section.

3.7 Evaluation of Non-Newtonian Viscosity

The non-dimensional viscosity for a power law fluid is given by

$$\eta = \left(\frac{I_2}{2} \right)^{\frac{n-1}{2}}$$

where I_2, the second invariant of the rate of deformation tensor in cylindrical coordinate system (y, ϕ, x) with axisymmetry prevailing in ϕ direction, can be expressed as:

$$I_2 = \left\{ \left[\left(\frac{2\partial V_y}{\partial y} \right)^2 + \left(\frac{2V_y}{y} \right)^2 + \left(\frac{2\partial V_x}{\partial x} \right)^2 \right] + 2 \left(\frac{\partial V_y}{\partial y} + \frac{\partial V_x}{\partial x} \right)^2 \right\} \tag{3.40}$$

The viscosity is determined at the Gauss points for evaluating the integrals in equations (3.36) and (3.37) for any interior element The velocities V_x and V_y as well as the global coordinates x and y at the Gauss points are determined using the interpolation formulae

$$V_x = \sum_{k=1}^{8} N_k \bar{V}_{xk}, \quad V_y = \sum_{k=1}^{8} N_k \bar{V}_{yk}, \tag{3.41a}$$

$$x = \sum_{k=1}^{8} N_k x_k, \quad y = \sum_{k=1}^{8} N_k x_k, \tag{3.41b}$$

Here $\bar{V}_{xk}$ and $\bar{V}_{yk}$ represent the velocity components at the nodal points obtained from the previous iteration. While determining the shear stress and the viscous drag on the particle surface, the viscosity is evaluated at three gauss points located on the side of element which lies on the particle surface.

For the determination of the second invariant (I_2) and also other terms contained in equations (3.36) to (3.38), the first

order derivatives of shape functions with respect to the global coordinates (x, y) are needed. These are obtained as follows:

$$\begin{Bmatrix} \frac{\partial N_k}{\partial \xi_1} \\ \\ \frac{\partial N_k}{\partial \xi_2} \end{Bmatrix} = \begin{bmatrix} \frac{\partial x}{\partial \xi_1} & \frac{\partial y}{\partial \xi_1} \\ \\ \frac{\partial x}{\partial \xi_2} & \frac{\partial y}{\partial \xi_2} \end{bmatrix} \begin{Bmatrix} \frac{\partial N_k}{\partial x} \\ \\ \frac{\partial N_k}{\partial y} \end{Bmatrix} = [J] \begin{Bmatrix} \frac{\partial N_k}{\partial x} \\ \\ \frac{\partial N_k}{\partial y} \end{Bmatrix} \tag{3.42}$$

Alternatively,

$$\begin{Bmatrix} \frac{\partial N_k}{\partial x} \\ \\ \frac{\partial N_k}{\partial y} \end{Bmatrix} = [J]^{-1} \begin{Bmatrix} \frac{\partial N_k}{\partial \xi_1} \\ \\ \frac{\partial N_k}{\partial \xi_2} \end{Bmatrix} \tag{3 43}$$

where J is referred to as the Jacobian of transformation and ξ_1, ξ_2 are the local curvilinear coordinates of an element. The Jacobian matrix can be evaluated explicitly by substituting the variations of x and y from equation (3.41b) into the definition of [J]. Thus,

$$[J] = \begin{bmatrix} \sum_{k=1}^{k=8} \frac{\partial N_k}{\partial \xi_1} x_k & \sum_{k=1}^{k=8} \frac{\partial N_k}{\partial \xi_1} y_k \\ \\ \sum_{k=1}^{k=8} \frac{\partial N_k}{\partial \xi_2} x_k & \sum_{k=1}^{k=8} \frac{\partial N_k}{\partial \xi_2} y_k \end{bmatrix} \tag{3.44}$$

3.8 Implementation of Boundary Conditions:

The non-dimensional boundary conditions for the free surface cell model in cylindrical coordinate system are written (without asterisk) as

$$\text{at } (x^2 + y^2)^{1/2} = 1 \ , \ V_x = 1, \quad V_y = 0 \tag{3 45a}$$

$$\text{at } (x^2 + y^2)^{1/2} = \frac{R_\infty}{R_p} \ ; \ V_r = V_x \cos\theta + V_y \sin\theta = 0 \tag{3.45b}$$

$$\tau_{r\theta} = \eta\left\{\left(\frac{\partial V_y}{\partial r} - \frac{V_y}{r}\right)\right\} \cos\theta - \eta\left\{\left(\frac{\partial V_x}{\partial r} - \frac{V_x}{r}\right)\right\} \sin\theta = 0 \tag{3 45c}$$

where V_r is the normal velocity and $\tau_{r\theta}$ is the shear stress on the cell surface It is appropriate to add here that while applying the stress boundary condition at the cell surface, it is convenient to apply it in polar spherical coordinate system. Thus only V_r and V_θ have been transformed into cylindrical velocities, V_x and V_y while applying the cell boundary conditions. Since one of the local coordinates (ξ_1 or ξ_2 depending on respective side of the element) coincides with the radial direction, the first order derivative in this direction can easily be converted into first order derivative with respect to the local coordinate system

Substituting the elementwise interpolation of V_x and V_y for each element lying adjacent to the cell boundary, the zero shear stress boundary condition i.e. Eqn (3 45c) becomes

$$\sum_{j=1}^{8} \left[\cos\theta \left(\frac{2}{\Delta r} \frac{\partial N_j}{\partial \xi_1} - \frac{N_j}{R_c} \right)\right] \left[V_{yj}\right] - \left[\sin\theta \left(\frac{2}{\Delta r} \frac{\partial N_j}{\partial \xi_1} - \frac{N_j}{R_c} \right)\right] \left[V_{xj}\right] = \left[0\right] \tag{3.46a}$$

where ξ_1 has been taken to lie in the radial direction (r), with no loss of generality The zero normal velocity at the cell boundary can be written in the form

$$V_{xj} \cos\theta + V_{yj} \sin\theta = 0 \qquad (3\ 46b)$$

where j is the number of each node which lies on the cell boundary. For nodes lying on the cell boundary, Equations (3.46a) and (3 46b) replace the respective momentum equations at these nodes For the nodes on the particle surface the essential boundary conditions of the form

$$V_{xj} = 1.0, \quad V_{yj} = 0.0 \qquad (3.47)$$

are applied.

3.9 GLOBAL MATRIX AND SOLUTION TECHNIQUE

After the formation of an elemental coefficient matrix [K] and the associated right hand side vector {F} in Eqn. (3.39), further logical steps in arriving at the final solution are:

(a) Assemblage of elemental matrix into a Global matrix.

(b) Suitable matrix operations to obtain the detailed flow field solution.

The method adopted for solving the assembled matrix equations has a significant bearing on the computer storage requirement and execution time. When a large set of equations are to be solved, a simple matrix inversion technique will be very cumbersome and expensive due to large computer core memory requirement. In such conditions the direct elimination FRONTAL SOLUTION METHOD has proved to be very effective for solving positive definite matrices. The size of the Global matrix in present problem is of

the order of 1000 x 1000 and therefore, the choice of FRONTAL method as a matrix solver becomes inevitable.

The FRONTAL method, originally developed by Irons (1970) has been based on direct Gaussian elimination for solving symmetric matrices where the leading diagonal is always used as the pivot. For unsymmetric matrices which are encountered in a wide range of problems in engineering fluid mechanics, the most suitable pivot is not necessarily on the leading diagonal and FRONTAL solution routines exist for off diagonal pivoting (Hood, 1976). These, however, tend to be more time consuming and therefore, for the solution of non-symmetric matrices, in the present work only diagonal pivoting has been employed. The philosophy and operation of a FRONTAL method has been covered at length by Taylor and Hughes (1981). The method excellently manages the core memory requirement by writing the fully assembled nodal equations on to the disc memory as soon as contributions from all the elements which surround that node are added. The assembled equations are reduced by Gaussian elimination before being written on tape. After all equations have been completed, the back substitution process of unknowns is performed by recalling the equations in reverse order from tape. Thus, since assembled equations are never stored in core memory, the FRONTAL method drastically reduces the size of memory to perform all the required matrix operations.

The non-linearities of the Eqns. (3 37) and (3.38) earlier mentioned necessitate an iterative type of solution procedure. It was found that under some circumstances, the solutions have to be

under-relaxed between two successive iterations to increase the stability of the numerical results. The computational work reported herein was performed on DEC 1090 and ND 560 systems The CPU time taken for a typical iteratior using 18 x 8 Mesh varied from 3 to 4 minutes

3.10 POST PROCESSING OF RESULTS

After obtaining converged flow field solutions, the results are processed further to evaluate various quantities of interest such as the dimensionless stresses at the particle surface, the drag coefficients (C_{DP}, C_{DF} and C_D) and the dimensionless stream function value at each node. For the sake of convenience in presentation, two sets of dimensionless stresses are defined using the expressions

$$\bar{\tau} = \tau/\rho U_\infty^2 \; ; \quad \bar{p} = p/\rho U_\infty^2 \qquad (3\ 48a)$$

and, $$\tau' = \tau/\left(\frac{\eta U_\infty}{R_p}\right); \quad p' = p/\left(\frac{\eta U_\infty}{R_p}\right) \qquad (3.48b)$$

The use of $\bar{\tau}$ and $\bar{p}$ is advantageous for power law fluids, since the scaling quantity used in their definition is independent of the power law index n. On the other hand, τ' and p' are useful for Newtonian fluids with constant viscosity, since both τ' and p' will be of the order of 1 for the range of Reynolds numbers considered in the present study. In terms of the numerically predicted flow field quantities V_x^*, V_y^* and p^*, the dimensionless stresses are given as·

$$\bar{p} = \frac{p'}{Re_r} = p^* \qquad (3.49a)$$

$$\bar{\tau} = \frac{\tau'}{Re_r} = \frac{8}{Re_r} \left\{ \eta^* \frac{\partial V_\theta^*}{\partial r^*} \right\} \Big|_{r=1} \qquad (3.49b)$$

The velocity gradient $\frac{\partial V_\theta^*}{\partial r^*}$ in eqn. (3.49b) can, in turn, be represented as

$$\frac{\partial V_\theta^*}{\partial r^*} = \frac{1}{\Delta r^*} \frac{\partial}{\partial \xi_1} (- V_x^* \sin\theta + V_y^* \cos\theta)$$

$$= \frac{1}{\Delta r^*} \sum_{j=1}^{8} \frac{\partial N_j}{\partial \xi_1} (- V_{xj}^* \sin\theta + V_{yj}^* \cos\theta) \qquad (3.50)$$

where, Δr^* is the dimensionless radial step and ξ_1 is the local coordinate in the radial direction. The summation in Eqn. (3.50) is carried over all the nodes of the element of which the surface node under consideration forms a part.

The drag coefficients C_{DP} and C_{DF} can be evaluated by integrating equations (3.28) and (3.29), via 3-point Gauss-Legendre quadrature method along the boundary curves of elements which lie on the particle surface. Thus, eqns. (3.28 and 3.29) can be rewritten as:

$$C_{DP} = - 4 \sum_{e=1}^{e=E_s} \int_{\Omega^e} \sum_{i=1}^{4} M_i P_i^* \sin\theta \cos\theta \, d\theta \qquad (3.51a)$$

$$C_{DF} = \frac{8}{Re} \sum_{e=1}^{e=E_s} \int_{\Omega^e} \sum_{i=1}^{8} \eta^* \left\{ 2 \frac{\partial N_i}{\partial X^*} V_{xi}^* \cos\theta + \frac{\partial N_i}{\partial Y^*} V_{xi}^* \sin\theta \right.$$

$$\left. + \frac{\partial N_i}{\partial X^*} V_{yi}^* \sin\theta \right\} \sin\theta \, d\theta \qquad (3.51b)$$

where the subscript Ω^e signifies integration over the boundary of

a typical surface element Ω^e and the summation is carried out for all the elements lying adjacent to the particle, with E_s denoting the total number of such elements.

For the sake of plotting the streamlines, dimensionless Stream function (ψ) values have been calculated at each node by integrating the expression

$$V_r = - \frac{1}{r^2 \sin \theta} \frac{\partial \psi}{\partial \theta} \qquad (3\ 52)$$

with respect to angle θ at a constant r The stream-function on the axis ($\theta = 0$) is assigned the value zero and marching is done in the θ direction from $\theta = 0$ to $\theta = \pi$ in steps of $\Delta\theta$ at a constant r, using the FEM grid for the problem. This procedure is repeated for each value of r ranging from r = 1 to $r = R_c^*$ in steps of Δr^*, to obtain the stream function values for the whole domain.

CHAPTER IV

VALIDATION OF NUMERICAL SCHEME

In order to establish the correctness of the numerical scheme employed in the present work, the drag coefficients and the detailed flow field solutions have been compared with existing analytical and numerical results in literature. In addition to these comparative studies, the effects of various numerical parameters, namely, the radial step size, the grid pattern and the initial guess profiles, etc., on the accuracy and rate of convergence of the predicted results have also been investigated.

4.1 NEWTONIAN FLUID FLOW PAST MULTI-PARTICLE ASSEMBLAGES

Numerical results using FEM have been obtained for Newtonian as well as non-Newtonian fluid flows relative to multi-particle assemblages at low and intermediate Reynolds number regimes. However, a detailed bench mark comparison is possible only for the creeping flow of a Newtonian fluid, for which an analytical solution using Stoke's stream function was earlier provided by Happel (1958). The drag coefficients evaluated for any other flow situation using Happel cell model is based on certain approximations and linearization techniques. In Table 4.1, a comparison between the analytical results reported by Happel (1958) and the present numerical results for the creeping flow of Newtonian fluids past an assemblage of particles is presented. Though the analytical expression for the total drag coefficient

Table 4.1 Comparison of analytical and present numerical results on drag coefficients for Newtonian flow (Re = 0.001).

		Drag Coefficients-Analytical			Drag Coefficients-Present numerical method		
ε	r_c	C_{DP}	C_{DF}	C_D	C_{DP}	C_{DF}	C_D
0.3	1.1261	0.4335×10^{7}	0.1210×10^{7}	0.5545×10^{7}	0.4333×10^{7}	0.1210×10^{7}	0.5543×10^{7}
0.4	1.1854	0.1440×10^{7}	0.6088×10^{6}	0.2048×10^{7}	0.1438×10^{7}	0.6086×10^{6}	0.2047×10^{7}
0.5	1.2596	0.5681×10^{6}	0.3440×10^{6}	0.9121×10^{6}	0.5673×10^{6}	0.3438×10^{6}	0.9111×10^{6}
0.6	1.3568	0.2477×10^{6}	0.2073×10^{6}	0.4550×10^{6}	0.2469×10^{6}	0.2068×10^{6}	0.4537×10^{6}
0.7	1.4932	0.1147×10^{6}	0.1290×10^{6}	0.2437×10^{6}	0.1144×10^{6}	0.1289×10^{6}	0.2433×10^{6}
0.8	1.7091	0.5509×10^{5}	0.8052×10^{5}	0.1356×10^{6}	0.5495×10^{5}	0.8045×10^{5}	0.1354×10^{6}
0.9	2.1528	0.2669×10^{5}	0.4807×10^{5}	0.7476×10^{5}	0.2643×10^{5}	0.4803×10^{5}	0.7446×10^{5}
0.99	4.6345	0.1175×10^{5}	0.2349×10^{5}	0.3524×10^{5}	0.1170×10^{5}	0.2387×10^{5}	0.3557×10^{5}
9999	21.4771	0.86007×10^{4}	0.1720×10^{5}	0.2580×10^{5}	0.8225×10^{4}	0.1784×10^{5}	0.2607×10^{5}

has been explicitly provided by Happel, the correspc ding expressions for friction and pressure drag coefficients are, however, not available in open literature and hence are included in Appendix I An examination of Table 4.1 shows that the individual contributions (i e. friction and pressure drag coefficients) as well as the values of total drag coefficients obtained herein are in complete agreement with the analytical results over the entire range of values of voidage the maximum deviation observed between the two values is of the order of 1.3% for the highest value of voidage (ϵ = 0.9999) used here In view of this, it is therefore safe to conclude that the correspondence between the analytical results and present numerical results is excellent.

In Tables 4 2 and 4.3, a comparison between the analytically and numerically obtained surface pressure and shear stress values for creeping flow are presented at different angular positions for two voidages (ϵ = 0.4 and 0.9). These two voidages typically represent concentrated (ϵ = 0.4) and dilute (ϵ = 0.9) assemblage of particles. It is evident that there is an excellent agreement between the analytical and numerical predictions of surface shear stress at all angular positions. For surface pressure, it is observed that although there is almost total agreement between the numerical and analytical results (Maximum deviation < 1%) over a wide range of angular positions ($20^{\circ} \leq \theta \leq 180^{\circ}$), there exists a narrow zone in the front region ($0^{\circ} \leq \theta \leq 20^{\circ}$) over which the two results show a higher deviation (maximum about 10%). The reason for this could be that the pressure in this narrow zone is much smaller than the highest pressure occurring in the computational

Table 4.2 Comparison of Analytical and Numerical Results - Non dimensional surface pressure, $P_s/(\eta U_\infty/R_p)$ and shear stress $\tau_s/(\eta U_\infty/R_p)$.
ϵ = 0 4, Re = 0 001 n = 1

Angular position θ°	P_s		τ_s	
	Analytical	Numerical	Analytical	Numerical
0	0.0	0 0	0 0	0 0
10	$-0\ 8199\times10^{4}$	$-0\ 888\times10^{4}$	$-0\ 198\times10^{5}$	0.200×10^{5}
20	$-0\ 3255\times10^{5}$	-0.331×10^{5}	0.390×10^{5}	0.391×10^{5}
30	-0.723×10^{5}	-0.728×10^{5}	0.570×10^{5}	0.568×10^{5}
40	$-0\ 1262\times10^{6}$	-0.127×10^{6}	$0\ 733\times10^{5}$	0.730×10^{5}
50	$-0\ 1928\times10^{6}$	-0.193×10^{6}	0.874×10^{5}	0.870×10^{5}
60	$-0\ 2699\times10^{6}$	-0.270×10^{6}	0.988×10^{5}	$0\ 984\times10^{5}$
70	$-0\ 3551\times10^{6}$	-0.355×10^{6}	0.107×10^{6}	0.106×10^{6}
80	-0.446×10^{6}	-0.446×10^{6}	0.1124×10^{6}	0.111×10^{6}
90	-0.5398×10^{6}	-0.539×10^{6}	0.1141×10^{6}	0.113×10^{6}
100	-0.6335×10^{6}	-0.633×10^{6}	0.1124×10^{6}	$0\ 1118\times10^{6}$
110	-0.7244×10^{6}	-0.724×10^{6}	0.1072×10^{6}	0.1068×10^{6}
120	-0.8097×10^{6}	-0.809×10^{6}	0.9885×10^{5}	0.984×10^{5}
130	-0.8868×10^{6}	-0.886×10^{6}	$0\ 8743\times10^{5}$	0.870×10^{5}
140	-0.9533×10^{6}	-0.952×10^{6}	$0\ 7337\times10^{5}$	0.730×10^{5}
150	-0.1007×10^{7}	-0.101×10^{7}	0.5707×10^{5}	0.568×10^{5}
160	-0.1047×10^{7}	-0.105×10^{7}	0.3903×10^{5}	0.390×10^{5}
170	-0.1071×10^{7}	$-0\ 107\times10^{7}$	0.1982×10^{5}	0.200×10^{5}
180	-0.1079×10^{7}	-0.108×10^{7}	0.0	0.0

Table 4 3: Comparison of Analytical and Numerical Results - Non dimensional surface pressure, $P_s/(\eta U_\infty/R_p)$ and shear stress $\tau_s/(\eta U_\infty/R_p)$
$\epsilon = 0.9$; Re = 0.001 n = 1

Angular position θ^0	P_s		τ_s	
	Analytical	Numerical	Analytical	Numerical
0	0.0	0 0	0 0	0 0
10	$-0\ 1520\times10^{4}$	-0.139×10^{4}	0.1565×10^{4}	0.1564×10^{4}
20	$-0\ 6035\times10^{4}$	-0.588×10^{4}	0.3082×10^{4}	0.3080×10^{4}
30	$-0\ 1340\times10^{4}$	-0.132×10^{4}	0.4506×10^{4}	0.4500×10^{4}
40	-0.2341×10^{4}	$-0\ 232\times10^{4}$	0.5793×10^{4}	0.5780×10^{4}
50	-0.3575×10^{4}	$-0\ 356\times10^{4}$	0.6904×10^{4}	0.6880×10^{4}
60	-0.5004×10^{4}	$-0\ 499\times10^{4}$	0.7805×10^{4}	0.7780×10^{4}
70	-0.6585×10^{4}	$-0\ 657\times10^{4}$	0.8469×10^{4}	0.8440×10^{4}
80	-0.8270×10^{4}	-0.825×10^{4}	0.8876×10^{4}	0.8860×10^{4}
90	-0.1000×10^{5}	$-0\ 999\times10^{4}$	0.9013×10^{4}	$0\ 8980\times10^{4}$
100	-0.1174×10^{5}	-0.117×10^{5}	$0\ 8876\times10^{4}$	0.8860×10^{4}
110	-0.1342×10^{5}	-0.134×10^{5}	0.8469×10^{4}	0.8440×10^{4}
120	-0.1501×10^{5}	-0.150×10^{5}	$0\ 7805\times10^{4}$	$0\ 7780\times10^{4}$
130	-0.1643×10^{5}	-0.164×10^{5}	0.6904×10^{4}	$0\ 6880\times10^{4}$
140	-0.1767×10^{5}	-0.177×10^{5}	0.5793×10^{4}	0.5780×10^{4}
150	-0.1867×10^{5}	-0.187×10^{5}	0.4506×10^{4}	0.4500×10^{4}
160	-0.1941×10^{5}	$0\ 194\times10^{5}$	0.3082×10^{4}	0.3080×10^{4}
170	-0.1986×10^{5}	$-0\ 198\times10^{5}$	0.1565×10^{4}	0.1564×10^{4}
180	-0.2001×10^{5}	$-0\ 2000\times10^{5}$	0.0	0.0

domain. It is a well known problem to the numerical analyst that during the simultaneous solution of the (u, p, v) variables, the smallest values of pressure undergo wild fluctuations. In order to obviate this difficulty of spurious pressure oscillations, one of the commonly adopted procedures is to exempt the lower values of pressure from the convergence test. In the present work also, a cut-off value for pressure was prescribed below which the convergence test was not applied It is believed that the higher deviation between the analytical and numerical results for $0^{\circ} \leq \theta \leq 20^{\circ}$, arises from the occurrence of pressure oscillations in that region. However, the pressure drag coefficient remains uneffected by these oscillations because it is an integrated quantity on which the contribution due to very low values of pressure is insignificantly small. Notwithstanding these aspects, it is readily recognized that the analytical and numerical values of surface stresses are in excellent overall agreement

The validity of the numerical results has been finally ascertained by comparing the numerically computed radial velocity and angular velocity values against the corresponding analytical values in Tables 4.4 and 4.5 Table 4 4 corresponds to a dense assemblage of particles (ϵ = 0.4), whereas Table 4.5 contains the results for a dilute assemblage (ϵ = 0.9). The velocity values have been compared at several radial positions Excellent agreement between the analytical and numerical results is evident from the Tables.

In view of the above discussed comparisons between the present results and the analytical results of Happel (1958), the credibility of the numerical scheme adopted and the validity of

Table 4.4 Comparison of analytical and numerical results - non-dimensional radial velocity and angular velocity.
ϵ = 0.4, Re = 0.001, n = 1

r	Analytical $\theta = 30^{o}$		Numerical $\theta = 30^{o}$		Analytical $\theta = 60^{o}$		Numerical $\theta = 60^{o}$		Anal $\theta = 90^{o}$	Numer $\theta = 90^{o}$
	V_r	V_θ	V_r	V_θ	V_r	V_θ	V_r	V_θ	V_θ	V_θ
1.00	0.866	-0.500	0.8660	-0 500	0.500	-0.8660	0.500	-0.8660	-1 00	-1.00
1.023	0.841	0.1154	0.8416	0.1113	0.486	0 1999	0 4859	0.1915	0.2309	0 2210
1.046	0.775	0.6219	0.7742	0.6271	0.448	1.077	0.4476	1.0838	1 2439	1.2511
1.070	0.679	1.066	0.6792	1.065	0.392	1.8466	0.3921	1.8256	2 132	2.1077
1 093	0.550	1.407	0.5605	1.4020	0.324	2.437	0.3236	2 4257	2.814	2 8006
1 116	0.427	1.638	0.4279	1.6732	0.247	2.838	0.2470	2.8953	3.277	3 3429
1.139	0.286	1.873	0.2863	1.8733	0.165	3.244	0.1653	3.2418	3.7469	3 7429
1.162	0.142	2.007	0 1426	2.0077	0.0821	3.476	0 0823	3.4746	4 0146	4 0117
1.185	0.0	2.074	0.0000	2.0796	0.00	3 593	0 00	3 5991	4 1498	4 1555

Table 4 5. Comparison of Analytical and Numerical Results - Non-dimensional radial velocity and angular velocity.
$\in$ = 0.9, Re = 0.001, n = 1.0

r	Analytical $\theta = 30^{o}$		Numerical $\theta = 30^{o}$		Analytical $\theta = 60^{o}$		Numerical $\theta = 60^{o}$		Anal. $\theta = 90^{o}$	Numer. $\theta = 90^{o}$
	V_r	V_θ	V_r	V_θ	V_r	V_θ	V_r	V_θ	V_θ	V_θ
1.00	0.8660	-0.500	0.8660	-0.500	0.500	-0.8660	0.500	-0.8660	-1.00	-1.00
1.049	0.8572	-0.3973	0.8577	-0.3972	0.494	-0.6881	0 4952	-0.6881	-0.7946	-0.7945
1.101	0.8342	-0.3036	0.8345	-0.3044	0 4816	-0 5258	0.4818	-0 5272	-0.6072	-0.6088
1 211	0 7551	-0.1441	0.7551	-0 1439	0 4359	-0.2495	0 4360	-0 2193	-0.2882	-0.2878
1.271	0 7029	-0.0743	0.7032	-0.0747	0.4058	-0.1288	0.4060	-0.1294	-0 1487	-0.1495
1 399	0 5834	0.0451	0 5839	0.0447	0.3368	0.07813	0 3371	0 0774	0.0902	0 0894
1.467	0.5182	0.0960	0.5193	0.0961	0.2297	0.1663	0.2998	0 1664	0 1920	0.1921
1 615	0.3848	0.1843	0.3855	0.1841	0.2222	0 3192	0.2226	0 3189	0.3686	0.3682
1.777	0.2511	0.2567	0 2512	0.2548	0.1450	0 4446	0.1450	0.4412	0 5134	0.5095
1.956	0.1212	0.3097	0.1215	0.3098	0.070	0.5365	0 0701	0 5366	0.6195	0.6196
2.153	0 00	0.3504	0.00	0.3504	0.00	0 6069	0 000	0 6070	0.7008	0 7008

results obtained from it, are firmly established atleast for creeping Newtonian fluid flow. In contrast to this, the validity of the numerical results for the intermediate Reynolds number regime cannot be made in an equally firm manner. The reason for this is that an exact solution for flow past a multi-particle assemblage has not been obtained till date due to the non-linearity associated with the inertial terms. Furthermore, very little theoretical work has been reported on the modelling of fluid flow and heat and mass transport processes occurring in multi-particle assemblages outside the creeping flow conditions using the Happel's free surface cell model. El-Kaissy and Homsy (1973) extended Happel's free surface cell model beyond creeping flow regime by carrying out a regular perturbation analysis. They provided analytical expressions for the friction factor as a function of the bed voidage ($0.3 \leq \epsilon \leq 0.6$) and Reynolds number. The comparison of present numerical results with those of El-Kaissy and Homsy is shown in Table 4.6. The relation between the total drag coefficient and the friction factor for flow through a fixed bed may be established in following way. The Blake-Kozeny friction factor is expressed as

$$f_{bk} = \frac{\Delta p}{L} \frac{\epsilon^3}{(1-\epsilon)} \frac{d_p}{\rho U_\infty^2} \qquad (4.1)$$

Furthermore, by a force balance on the cell, it can be shown that

$$\frac{\Delta p}{L} = \frac{F_D}{4/3\ \pi\ R_c^{\ 3}} \qquad (4.2)$$

Therefore,

$$f_{bk} = \frac{F_D}{4/3\ \pi\ R_c^{\ 3}} \frac{\epsilon^3}{(1-\epsilon)} \frac{d_p}{\rho U_\infty^2} \qquad (4.3)$$

Table 4.6 Comparison of present numerical results with the analysis of El-Kaissy and Homsy, and the predictions of Ergun's equation.

ϵ	Re	f_{bk} (present)	f_{bk} (El-Kaissy & Homsy)	f_{bk} (Ergun)
0.3	1.0	112 289	111 336	106.755
0.4	1.0	98 30	98 0507	91.75
0.5	1 0	85 47	85.3051	76 50
0.3	5.0	22 4295	22 2676	22.75
0.4	5 0	19.66	19.623	19.75
0.5	5 0	17.10	17.08	16 75
0 3	10 0	11.2350	11.134	12 25
0.4	10.0	9 83	9.832	10 75
0.5	10 0	8.558	8.581	9.25
0.3	20.0	5.60	5.568	7.000
0 4	20.0	4 927	4.9567	6.250
0.5	20.0	4 2944	4.3681	5 500
0.3	50.0	2.2567	2 2307	3.85
0.4	50.0	1 99	2.0968	3.55
0.5	50.0	1.7563	1 9638	3.25
0.3	100.0	1.1487	1.1213	2.80
0.4	100.0	1.0363	1 2521	2.67
0.5	100.0	0.9260	1.3681	2.50

f_{bk} (present) $= \frac{3}{4} C_d \epsilon^3$

Expressing Drag force F_D in terms of drag coefficient and on further simplification, equation (4 3) reduces to

$$f_{bk} = \frac{3}{4} C_d \epsilon^3 \qquad (4.4)$$

An examination of Table 4.6 clearly shows that good correspondence exists between the two sets of results upto Re = 50; the maximum divergence between the two sets of results is of the order of 11% for the case of ϵ = 0.5 and Re = 50, whereas the two values differ only by 2% or so for the case of ϵ = 0.3 and Re = 100. This trend is consistent with the findings of El-Kaissy and Homsy (1973) who asserted that the upper limit of Re upto which their analysis is applicable decreases with the increasing value of voidage.

Other theoretical results on the flow of Newtonian fluids through packed beds at intermediate Reynolds number which are based on the Happel's free surface cell model, have been due to Nishimura and Ishii (1980a,b). Using boundary layer assumptions, they reported extensive results on friction factor and Sherwood number as functions of bed voidage and Reynolds number and claimed their results to be applicable in the range, $10 \leq Re \leq 10^5$. Intuitively, it is highly unlikely that the boundary layer flow approximation will be valid at values of Reynolds number as low as 10. Several unusual features of their results have already been discussed in Chapter II. It is for these reasons that a comparison of present results with those of Nishimura and Ishii (1980a,b) has not been made.

Table 4.7 Comparison of variational and present numerical results on drag coefficients for power law fluids (Re = 0.001).

ε	n = 0.9				n = 0.8				n = 0.6			
	Y_u	Y_L	$C_D = \frac{12(Y_u+Y_L)}{Re}$	C_D (Present)	Y_u	Y_L	$C_D = \frac{12(Y_u+Y_L)}{Re}$	C_D (Present)	Y_u	Y_L	$C_D = \frac{12(Y_u+Y_L)}{Re}$	C_D (Present)
0.4	56.18	56.04	0.1346×10^{7}	0.1324×10^{7}	37.06	37.0	0.8887×10^{6}	0.8522×10^{6}	16.08	15.92	0.3840×10^{6}	0.3463×10^{6}
0.5	26.61	26.48	0.6370×10^{6}	0.6269×10^{6}	18.67	18.5	0.4460×10^{6}	0.4292×10^{6}	9.17	9.11	0.2193×10^{6}	0.1966×10^{6}
0.7	7.94	7.91	0.1902×10^{6}	0.1875×10^{6}	6.22	6.21	0.1491×10^{6}	0.1437×10^{6}	3.81	3.78	0.9108×10^{6}	0.8106×10^{5}
0.9	2.75	2.75	0.6600×10^{5}	0.6549×10^{5}	2.44	2.43	0.5844×10^{5}	0.5749×10^{5}	1.9	1.88	0.4536×10^{5}	0.4232×10^{5}
0.99	1.47	1.47	0.3528×10^{5}	0.3573×10^{5}	1.47	1.46	0.3516×10^{5}	0.3561×10^{5}	1.45	1.39	0.3408×10^{5}	0.3415×10^{5}

4.2 NON-NEWTONIAN FLUID FLOW PAST MULTI-PARTICLE ASSEMBLAGES

The utility of the present numerical scheme in dealing with the creeping flow of power law fluids past multi-particle assemblage has also been examined. In Table 4.7, the present results are compared with the approximate upper and lower bounds on drag coefficient reported by Mohan and Raghuraman (1976a). It is seen that a reasonable correspondence exists between the two sets of results obtained using entirely different techniques It is generally recognized that the divergence between the upper and lower bounds increases as the degree of non-Newtonian behaviour increases, i.e., as the value of flow behaviour index (n) decreases. Besides, the variational approach is tantamount to either satisfying the equation of continuity (upper bound) or the momentum equation (lower bound) only. Notwithstanding these aspects of the variational analysis, the agreement between the two sets of results is regarded to be satisfactory and acceptable, albeit the present results are believed to be more accurate especially in the lower range of n.

To the best of our knowledge, there have been only two theoretical studies relating to the flow of power law liquids through particle assemblages outside the creeping flow regime (Reynolds number greater than unity) where, the free-surface cell model has been employed to represent the inter-particle interactions. The boundary layer approximation has been used by Hua and Ishii (1981) and Kawase and Ulbrecht (1981b) to solve the governing equations for the high Reynolds number flow of power law liquids. The values of drag coefficients have been obtained in the Reynolds number range of 10 to 1000. The validity of the

boundary layer approximation appears to be questionable in this flow configuration especially in dense assemblages Moreover, the theoretical results reported by Hua and Ishii (1981) do not reduce to the expected behaviour for a single sphere as the bed voidage approaches unity It is to be mentioned at this stage that in the present study the upper reynolds number has been confined to the value of 20. Therefore, the numerical results were not compared with the approximate results of Hua and Ishii (1981) or Kawase and Ulbrecht (1981b).

4.3 EFFECT OF NUMERICAL PARAMETERS ON COMPUTED RESULTS

The effects of various numerical parameters, namely, the radial step size, grid pattern and initial guess values on the computed values of drag coefficient and the rate of convergence of the solution have been investigated. These are described in the ensuing sections.

(a) Radial Step Size:

In Table 4.8, drag results are presented for two different meshes which consist of 18 elements in the angular direction and 8 or 4 elements in the radial direction. The grid spacing is uniform in both radial and angular directions for these meshes. The values of drag coefficient obtained using these grids are compared with the analytical results under creeping flow conditions, for a range of values of bed voidage. It is readily seen from the results in Table 4.8 that upto about $\epsilon \leq 0.5$, the two grids give virtually identical results. Only for the values of voidage greater than 0.5, the use of a finer grid such as 18 x 8 mesh appears necessary. Further refinement of the mesh using 18 x 16 elements resulted in virtually no change in the values of

Table 4 9 Performance of uniform grid vs exponential grid at different voidages (Re = 0.00).

ε	n	C_D (available in literature)	C_D (present)	
			Uniform grid (18x8)	Exponential grid (18x8)
0 9999	1 0	$0.25802 \times 10^{5+}$	$0\ 1560 \times 10^{5}$	0.2607×10^{5}
0.99	1 0	$0.35520 \times 10^{5+}$	0.3430×10^{5}	$0\ 3557 \times 10^{5}$
0 99	0 8	$0.3510 \times 10^{5=}$	$0\ 3403 \times 10^{5}$	$0\ 3561 \times 10^{5}$
0 99	0 6	$0.34080 \times 10^{5=}$	$0\ 3230 \times 10^{5}$	0.3415×10^{5}
0.99	0 4	--	0.2831×10^{5}	0.3058×10^{5}
0.99	0 2	--	0.2311×10^{5}	0.2449×10^{5}
0.9	1 0	$0.7476 \times 10^{5+}$	0.7446×10^{5}	0.7483×10^{5}
0.9	0 8	$0.5844 \times 10^{5=}$	$0\ 5718 \times 10^{5}$	0.5749×10^{5}
0.9	0.6	$0.45360 \times 10^{5=}$	0.4209×10^{5}	0.4232×10^{5}

\+ Happel (1958)

= Mohan and Raghuraman (1976a)

drag coefficients presented in the table 4.2. It is thus safe to conclude that the 18 x 8 mesh is adequate from accuracy view point and computationally economical in creeping flow conditions for 0.3 $\leq \epsilon \leq$ 0.9. Indeed, the computational time increases by a factor of 6-7 for the 18 x 16 mesh as compared to that of the 18 x 8 mesh.

(b) Need for an Exponential Grid for Dilute Beds:

A comparative study of a uniform grid and an exponential grid has been carried out to demarcate the ranges of their applicability. In creeping flow regime, typical results on drag coefficient obtained using the aforementioned two grids are presented in table 4.9 for Newtonian and power law type fluids and for a range of values of ϵ. For the sake of comparison, analytical results of Happel (1958) for Newtonian fluids and approximate results of Mohan and Raghuraman (1976a) for non-Newtonian fluids are also included in this table. Intuitively, one would expect the two grids to yield comparable results for low values of voidage. An inspection of Table 4.9 suggests that the exponential grid consistently yields better results than those obtained using the uniform grid under all conditions examined here. However, the results from the two grids show noticeable differences only for dilute systems (ϵ > 0.9). For instance, in the case of ϵ = 0.9, the two results are almost identical for both Newtonian and power law liquids, with the maximum divergence between the two being only 0.54% in the case of n = 0.6. As expected, the performance of the uniform grid deteriorates rapidly with the increasing value of voidage. For example, at ϵ = 0.9999, the uniform grid provides a very coarse

discretization of the domain adjacent to the particle surface and gives highly inaccurate results. The use of an exponential grid, on the other hand, leads to results which are accurate to within 1.2% of the corresponding analytical results for Newtonian fluids. Similar observations can be made for power law fluids also From the aforementioned discussion, it is evident that for $\epsilon \geq 0.9$, an exponential grid system is preferable in order to obtain sufficiently accurate results, as compared to a finer uniform mesh which will be prohibitively expensive.

(c) **Effect of Physical and Numerical Factors on Rate of Convergence of Solution:**

For iterative solutions of highly nonlinear equations (such as those of the present study), an important criterion for judging the scheme efficiency is the rate of convergence of the solution. Usually two criteria, namely, a pointwise convergence for velocity and pressure fields, and an overall convergence for the integrated quantity such as drag coefficient are applied. Though the pointwise convergence is desirable at every node in the flow domain, it must be used with a little bit of caution, and no extra efforts should be expended in achieving convergence for small values of velocity and pressure which are known to undergo wild fluctuations during simultaneous solution. Therefore, cut-off values for pressure and velocity were specified as 5% of the maximum velocity and 7% of the maximum pressure; no attempt was made to meet the pointwise convergence criteria below these values The results were assumed to have converged if the difference in the value of a variable at any nodal point for two successive iterations was less than 0.5%. this criterion was

sufficient to ensure the convergence upto four significant digits in most cases except for a few pressure values Drag force was assumed to have converged when no change in the first three digits was detected for three to four consecutive iterations.

Generally speaking, the number of iterations required to achieve the pre-determined level of convergence for primitive flow variables (u,p.v) and for drag depends upon the complex interactions between physical factors such as voidage, Reynolds number and power law index and the numerical parameters such as initial values, relaxation factor, etc. Consequently, each run is different from the other in some way, and indeed it is very difficult to draw specific conclusions on this aspect. Some typical cases are listed in Table 4.10 and based on the information given here, the following observations can be made:

(i) For a given value of Reynolds number and voidage, the number of iterations to achieve the desired level of pointwise and overall convergence increases with increasing non-Newtonian behaviour This finding is in accordance with the observations made by Gu and Tanner (1985).

(ii) For given values of ϵ and n, the number of iterations is virtually unaffected by the value of Reynolds number in the range employed here; similarly, for fixed values of n and Re, the effect of voidage on the rate of convergence is insignificant, although there is a weak tendency for the number of iterations to increase with decrease in ϵ.

(iii) In the packed bed range (ϵ = 0 3 - 0.5) and for highly non-Newtonian fluids (n = 0.2 and 0.4), the drag coefficient was found to converge between 15 and 20

Table 4.10 Influence of various physical and numerical parameters on rate of convergence.

Sl. No.	ϵ	n	Re	Initial guess solution	Relaxation factor	Iterations for u-p-v convergence	Iterations for C_D convergenc
1	0.99	0.8	0.001	Trivial	1.0	7	3-4
2	0.99	0.2	0.001	Solution for ϵ = 0.99, n = 0.4, Re= 0.001	1.0/0.7	11	7
3	0.99	1.0	1	Trivial	1.0	5	3
4	0.99	0.8	1	Trivial	1.0	7	4
5	0.99	0.6	1	Solution for ϵ = 0.99, n = 0.8, Re= 1	1.0	8	5
6	0.99	0.4	1	Solution for ϵ = 0.99, n = 0.6, Re= 1	1.0/0.7	10	6
7	0.99	0.2	1	Solution for ϵ = 0.99, n = 0.4, Re= 1	1.0/0.7	8	5
8	0.9	0.8	0.001	Trivial	1.0	6	4
9	0.9	0.8	1	Trivial	1.0	6	4
10	0.9	0.2	1	Solution for ϵ = 0.9, n = 0.4, Re= 1	1.0/0.7	22+	17
11	0.9	0.8	10	Trivial	1.0	7	5
12	0.9	0.2	10	Solution for ϵ = 0.9, n = 0.4, Re= 10	1.0/0.7/0.5	25+	20
13	0.5	0.8	1	Trivial	1.0	7	4
14	0.5	0.8	20	Trivial	1.0	4	3

15	0.3	0.2	1	Output solution for ε = 0.3, n = 0.4, Re= 1	1.0/0.7/0.5	23+	17
16	0.3	0.8	10	Trivial	1.0	6	4
17	0.3	0.2	10	Output solution for ε = 0.3, n = 0.4, Re= 10	1.0/0.7/0.5	35+	31+
18	0.4	1.0	10	Trivial	1.0	2	2
19	0.4	1.0	10	Trivial	0.5	5	3
20	0.9999	0.8	10	Trivial	1.0	6	4
21	0.9999	0.8	20	Trivial	1.0	8	4
22	0.9999	0.2	20	Output solution for ε = 0.9999, n = 0.4, Re= 20	1.0/0.7	13	8

+ Results did not converge upto desired level.

iterations whereas the pointwise convergence of (u,p,v) required about 20 to 30 iterations However, in some cases, even with these many iterations convergence could not be achieved In general, the desired drag convergence was achieved in about half the number of iterations as those required for the pointwise convergence of velocity and pressure fields

(iv) For mild to moderate degrees of non-Newtonian behaviour ($0.6 \leq n \leq 1$), the initial guess of a trivial solution for pressure and velocity variables led to faster rate of convergence than that by using the solution for the case having same kinematic (Re) and physical conditions ($\in$) but a slightly different value of the power law index (n).

CHAPTER V

RESULTS AND DISCUSSION - NEWTONIAN FLOW PAST MULTI-PARTICLE ASSEMBLAGE

In this chapter, results predicted by the free surface cell model for steady Newtonian flow past a multi-particle system are presented. Pressure, friction and total drag coefficients, the variation of angular and radial velocity components, surface pressure and shear stress distributions and streamline plots have been obtained for a wide range of kinematic and physical conditions covering $0.001 \leq Re \leq 100$, $0.3 \leq \epsilon \leq 0.9$. While the above range of voidage represents the complete spectrum of multi-particle flow situations including fixed, fluidized and distended beds, the performance of the free surface cell model in the case of approach to a single translating sphere has been investigated by using the very high voidage value of $\epsilon = 0.9999$. The numerical results presented herein have been validated by means of comparison with the appropriate theoretical and experimental results for packed beds, fluidized beds and single spheres, available in the literature. The range of applicability of the free surface cell model has been identified, and its performance has been contrasted with that of its rival, the zero-vorticity cell model. Typical streamline patterns are presented to elucidate the salient features of the flow field.

5.1 EFFECTS OF VOIDAGE AND REYNOLDS NUMBER ON DRAG COEFFICIENTS

The complete set of drag results obtained in this study are summarized in Table 5.1. The dependence of the total, pressure and friction drag coefficients on voidage and Reynolds number is shown in Figures 5.1 to 5 3 for representative parametric values.

For a given voidage, the drag coefficients (pressure, friction and total) decrease with Reynolds number. The fact that all the three quantities have the slope of -1 on log-log coordinates over some Reynold number range indicates that they are all proportional to 1/Re in that range. Such behaviour is the characteristic of viscosity-dominated flows Indeed, an examination of the Happel's analytical solution (discussed in Appendix I) reveals that the inverse proportionality between the drag coefficients and the Reynolds number is essentially a creeping flow feature. Therefore, it appears that for flow through multi-particle assemblages the viscous effects remain important even in the intermediate Reynolds number range (upto about Re ~ 30 - 40). However, beyond a critical value of Reynolds number, the drag results begin to veer away from C_D Re = constant behaviour. The critical value of Reynolds number appears to be a function of voidage. For instance, with ϵ = 0.9, this transition seems to occur at about Re ~ 10-15, and it takes place at higher values of Reynolds number for lower value of voidage. In order to understand these trends, it must be recognised that the inertial and viscous forces in multi-particle systems are functions of voidage. Therefore, the particle Reynolds number

Table 5.1: Summary of drag (pressure, friction and total) coefficients for Newtonian fluid flow past an assemblage of particles.

Re	C_{DP}	C_{DF}	C_D
$\epsilon = 0.3$			
0.001	0.4337×10^{7}	0.1210×10^{7}	0.5543×10^{7}
0.1	0.4333×10^{5}	$0\ 1210 \times 10^{5}$	0.5543×10^{5}
1.0	0.4333×10^{4}	$0\ 1210 \times 10^{4}$	0.5543×10^{4}
5.0	0.8646×10^{3}	0.2418×10^{3}	0.1106×10^{4}
10.0	0.4333×10^{3}	0.1211×10^{3}	0.5544×10^{3}
20.0	0.2167×10^{3}	0.6051×10^{2}	0.2769×10^{3}
50.0	0.8701×10^{2}	0.2436×10^{2}	0.1114×10^{3}
100.0	0.4427×10^{2}	0.1242×10^{2}	0.5669×10^{2}
$\epsilon = 0.4$			
0.001	0.1438×10^{7}	0.6085×10^{6}	0.2047×10^{7}
0.1	0.1438×10^{5}	0.6085×10^{4}	0.2047×10^{5}
1.0	0.1438×10^{4}	0.6086×10^{3}	0.2047×10^{4}
5.0	0.2876×10^{3}	0.1217×10^{3}	$0\ 4094 \times 10^{3}$
10.0	0.1439×10^{3}	0.6091×10^{2}	0.2048×10^{3}
20.0	0.7203×10^{2}	0.3055×10^{2}	0.1026×10^{3}
50.0	0.2907×10^{2}	0.1245×10^{2}	0.4152×10^{2}
100.0	0.1495×10^{2}	0.6595×10	0.2151×10^{2}

$\epsilon = 0.5$

0.001	0.5673×10^{6}	0.3438×10^{6}	0.9111×10^{6}
0.1	0.5673×10^{4}	0.3438×10^{4}	0.9111×10^{4}
1.0	0.5673×10^{3}	0.3438×10^{3}	0.9111×10^{3}
5.0	0.1135×10^{3}	0.6880×10^{2}	0.1823×10^{3}
10.0	0.5677×10^{2}	0.3455×10^{2}	0.9122×10^{2}
20.0	0.2845×10^{2}	0.1732×10^{2}	0.4577×10^{2}
50.0	0.1155×10^{2}	0.7178×10	0.1872×10^{2}
100.0	0.5992×10	0.3887×10	0.9875×10

$\epsilon = 0.7$

0.001	0.1144×10^{6}	0.1289×10^{6}	0.2433×10^{6}
0.1	0.1144×10^{4}	0.1289×10^{4}	0.2433×10^{4}
1.0	0.1144×10^{3}	0.1290×10^{3}	0.2433×10^{3}
5.0	0.2288×10^{2}	0.2584×10^{2}	0.4872×10^{2}
10.0	0.1146×10^{2}	0.1299×10^{2}	0.2455×10^{2}
20.0	0.5768×10	0.6656×10	0.1242×10^{2}
50.0	0.2536×10	0.2937×10	0.5293×10
100.0	0.1214×10	0.1665×10	0.2883×10

$\epsilon = 0.9$

0 001	0.2643×10^{5}	0.4803×10^{5}	0.7446×10^{5}
0 1	0.2643×10^{3}	0.4803×10^{3}	0.7446×10^{3}
1.0	0.2643×10^{2}	0.4805×10^{2}	0.7448×10^{2}
5.0	0.5291×10	0.9709×10	0.1500×10^{2}
10.0	0.2652×10	0.5000×10	0.7653×10
20.0	0.1337×10	$0\ 2745 \times 10$	0.4081×10
50.0	0.5452	0.1504×10	0.2049×10
100.0	0.2495	0.8787	$0\ 1128 \times 10$

$\epsilon = 0.9999$

0.001	0.8225×10^{4}	0.1784×10^{5}	0.2607×10^{5}
0.1	0.8214×10^{2}	0.1787×10^{3}	0.2608×10^{3}
1.0	0.8273×10	0.1801×10^{2}	0.2628×10^{2}
5.0	0.1887×10	0.4261×10	0.6148×10
10.0	0.1198×10	0.2811×10	0.4009×10
20.0	0.8491	0.2017×10	0.2866×10
50.0	0.6196	$0\ 1338 \times 10$	0.1958×10
100.0	0.5123	0.8813	0.1394×10

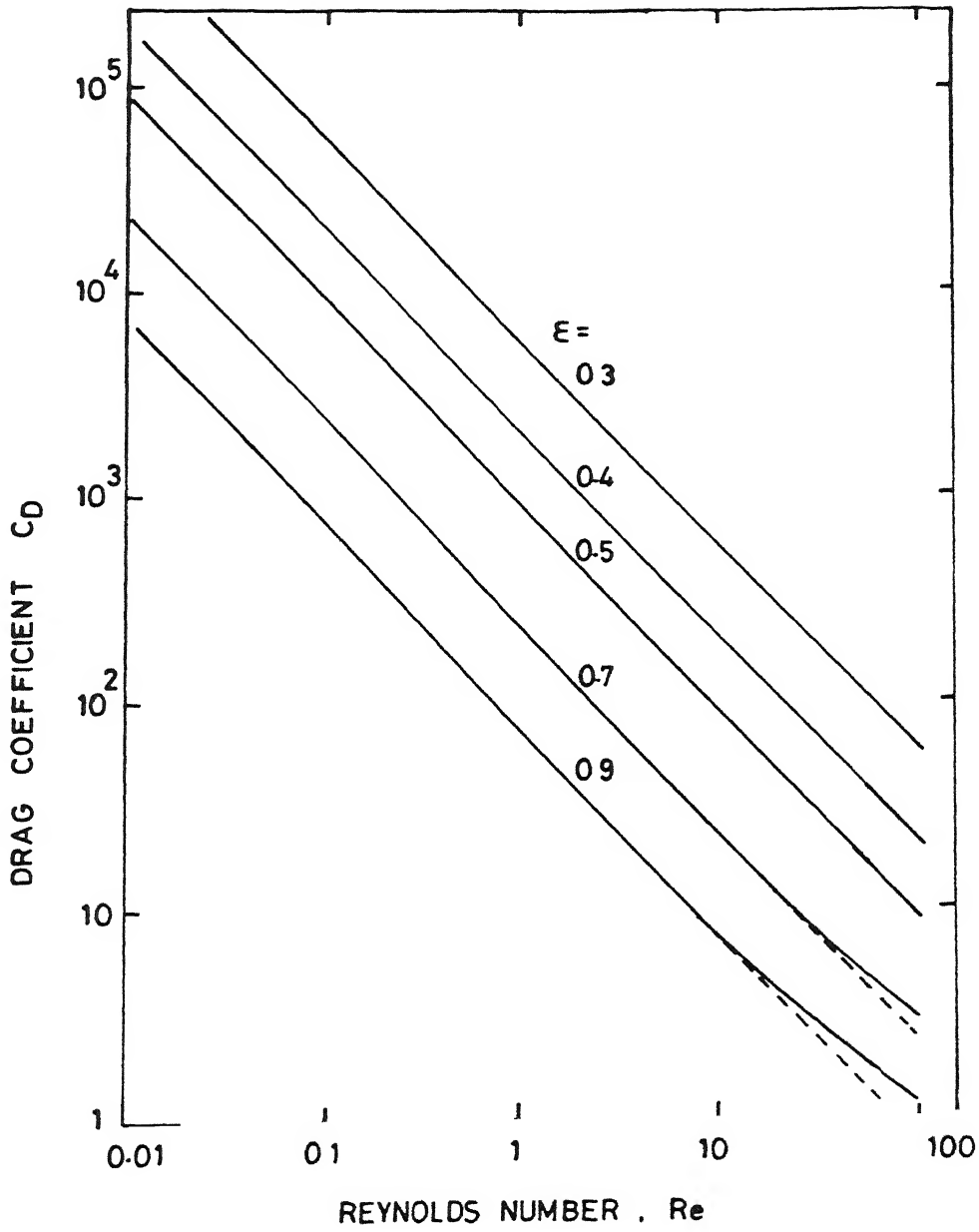

Fig. 5.1 Dependence of total drag coefficient on Reynolds number and bed voidage

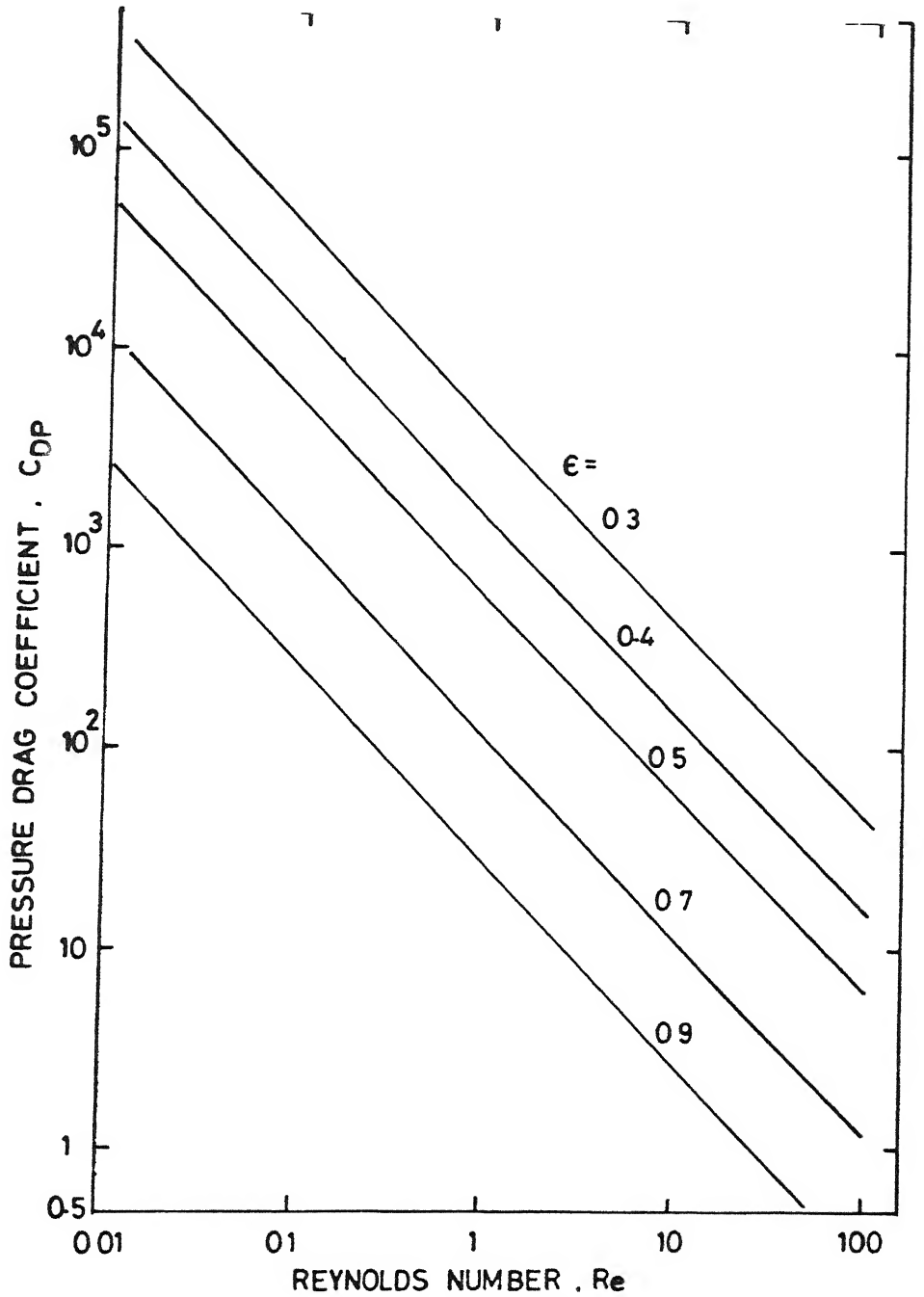

Fig. 5.2 Dependence of pressure drag coefficient on Reynolds number and bed voidage.

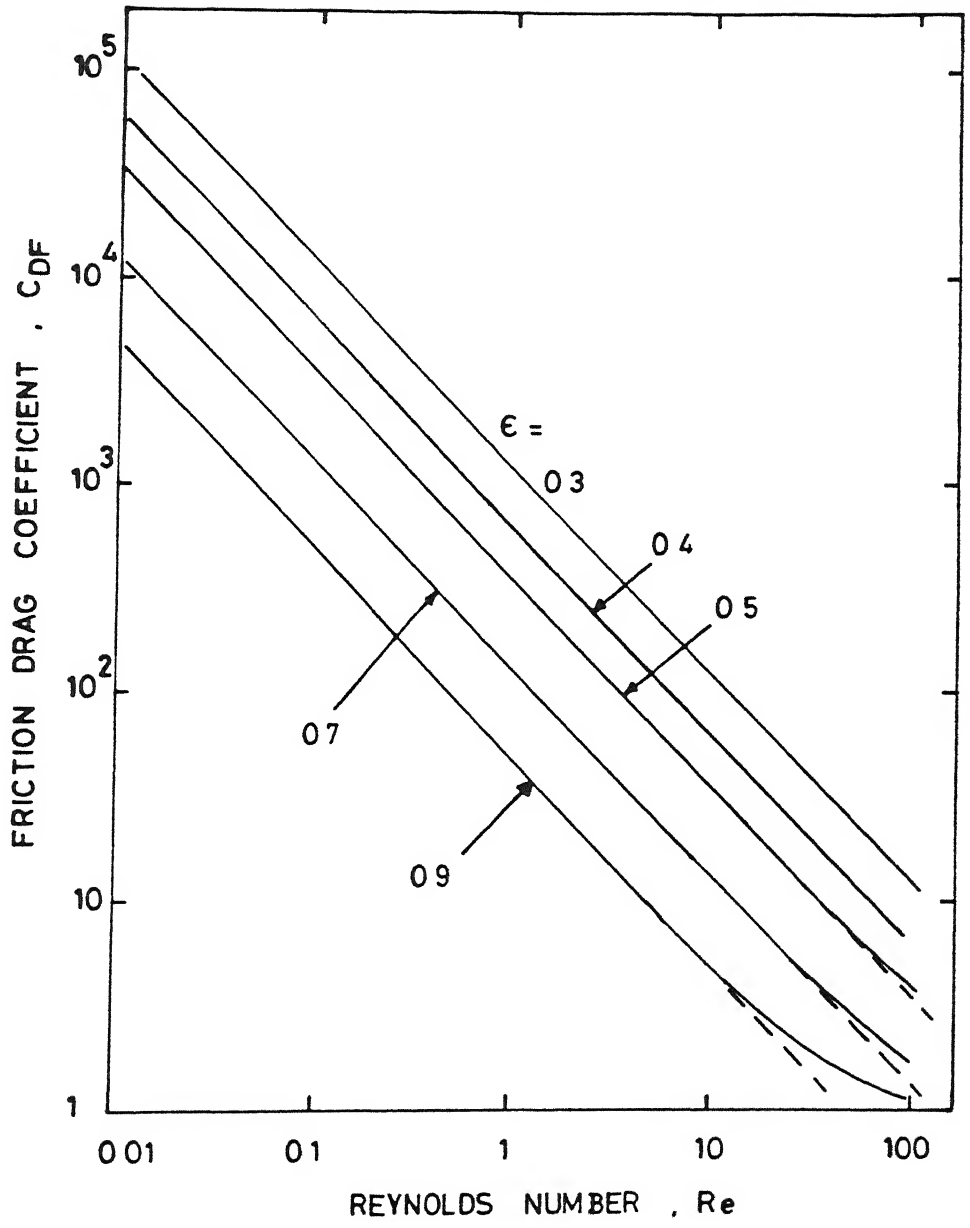

Fig. 5.3 Dependence of Friction drag coefficient on Reynolds number and bed voidage.

which has been defined without incorporating the effect of voidage, does not represent the true ratio of inertial and viscous forces in a dense or moderately dilute assemblage of particles. It is only in the case of extremely dilute assemblages (i.e. approaching the limit of a single sphere) that particle Reynolds number represents the actual ratio of inertial and viscous forces. The predominance of viscous force for highly dense assemblages can be attributed to narrow pore spacing available for flow.

At higher Reynolds numbers the C_D versus Re curve becomes less steep. This is consistent with the well-known trend for flow around single sphere, wherein the slope of C_D vs. Re curve decreases in magnitude at higher Reynolds number due to inertial effects, until C_D becomes nearly a constant in the turbulent flow regime The curious feature, however, is that the decrease in the slope of the C_D curve is largely contributed by the viscous drag as shown in Fig. 5.3.

Figures 5.1 - 5.3 also indicate that for a given Reynolds number, the drag coefficients decrease in magnitude as the voidage increases. The explanations for this observation are readily found if one considers the fact that the available flow area reduces when voidage is lowered. In addition to this, the flow undergoes expansion and contraction more number of times due to the larger solid concentration These factors combined together increase the pressure drop and the viscous losses. It is to be mentioned here that for steady flow situation, where inertial forces are not dominant, the pressure forces are locally balanced by the viscous force.

An interesting feature, not reported or mentioned in the literature hitherto can be clearly seen when the two individual components of the drag coefficients are plotted together as shown in Figure 5.4 An inspection of this figure suggests that at low values of voidage (ϵ = 0.4), the total drag coefficient draws a major contribution from pressure drag. However, as the voidage increases, the contribution of friction drag gradually increases and becomes nearly equal to the pressure drag at ϵ = 0.65 or so, and finally it dominates over the pressure drag (ϵ = 0.9) The above discussed trend implies that the contribution of pressure and viscous drag to the total drag is a function of bed voidage. An order of magnitude analysis (see Appendix-II) shows that pressure and viscous forces vary respectively as $O(1/\delta^3)$ and $O(1/\delta^2)$, where δ is the radial gap between the particle and the cell surface. It is expected that the pressure and friction drag coefficients, which are integrated quantities arising from the surface stresses should show atleast qualitatively a similar dependence on δ. It can be proved from such an order of magnitude estimates that

$$\frac{C_{DP}}{C_{DF}} > 1 \qquad \text{for dense assemblage (i.e. small } \delta)$$

and

$$\frac{C_{DP}}{C_{DF}} < 1 \qquad \text{for dilute assemblage (i.e. large } \delta).$$

Finally, it is of interest to add here that the present numerical results are at variance with some of the theoretical predictions reported by other researchers. For instance,

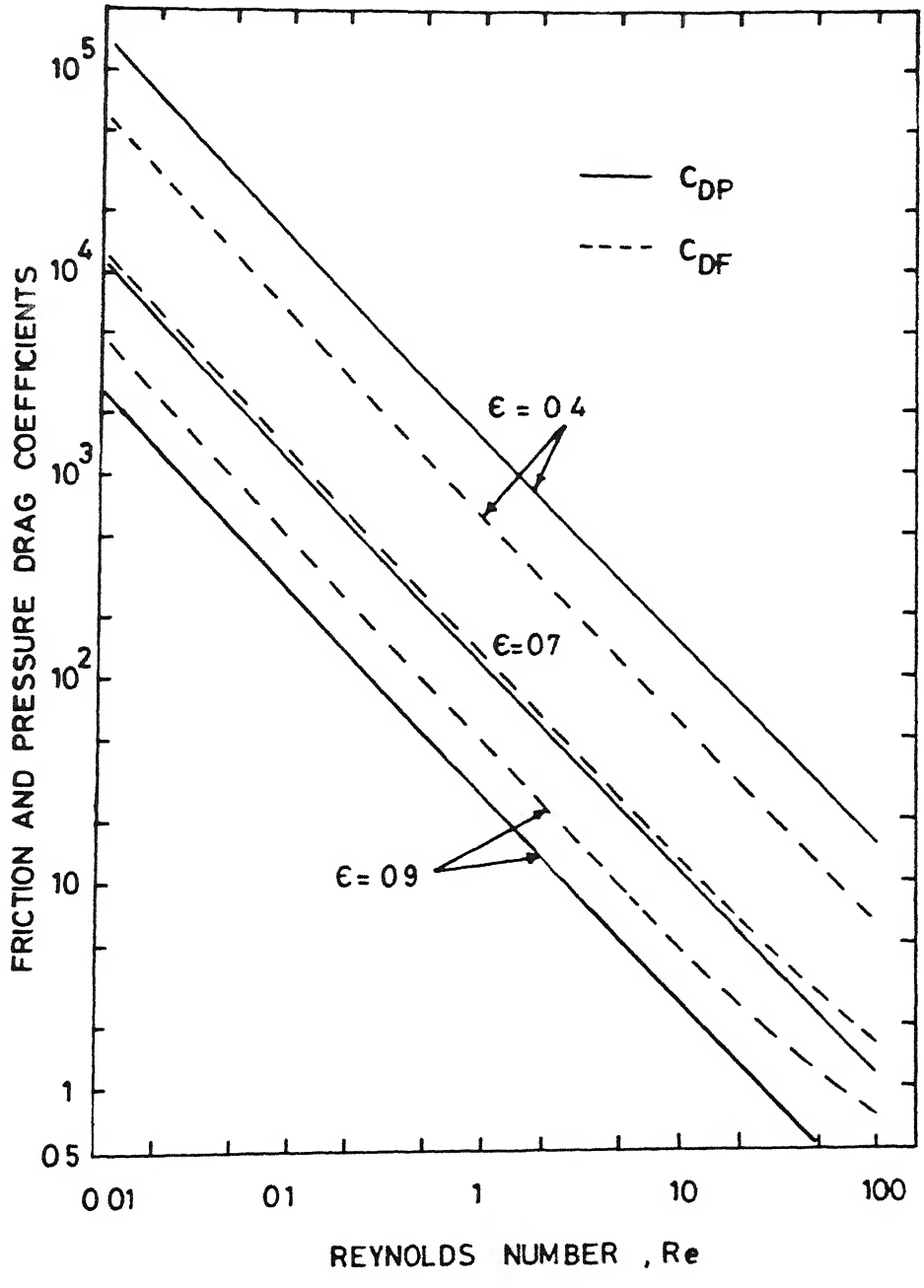

Fig. 5.4 Effect of Reynolds number and bed voidage on relative magnitudes of pressure and friction drag coefficients.

Nishimura and Ishii (1980a) asserted that the pressure drag coefficient, C_{DP} is independent of the value of Reynolds number for Re > 10 for all values of voidage in the range $0.1 \leq \epsilon \leq 0.3$. The observation is not in conformity with the present numerical results.

In another study Leclair and Hamielec (1968) found that the ratio, $\frac{C_{DP}}{C_{DF}}$ increases with increasing Reynolds number, after the initial range in which it remains constant The present numerical results do not display that trend For a given value of bed voidage, $\frac{C_{DP}}{C_{DF}}$ remains constant initially upto a certain value of Re and then starts decreasing with Re. It must be borne in mind, that the earlier authors have not explained their results physically, whereas, the present results are found to be physically consistent with the order of magnitude estimates.

5.2 SURFACE PRESSURE AND SHEAR STRESS DISTRIBUTION

It is intuitively expected that the study of pressure and surface shear stress distribution over the sphere surface will facilitate further rationalization of some of the phenomena discussed in previous section. The surface values of both pressure and shear stress have been re-normalized with respect to a characteristic viscous stress ($\eta\ U_\infty/R_p$) and are shown in Figures 5.5 to 5.16, for various combinations of parametric values to elucidate the effects of voidage (ϵ) and Reynolds number. From the results shown in these figures, the following observations can be made:

(i) At creeping flow (Re = 0.001), the numerically predicted

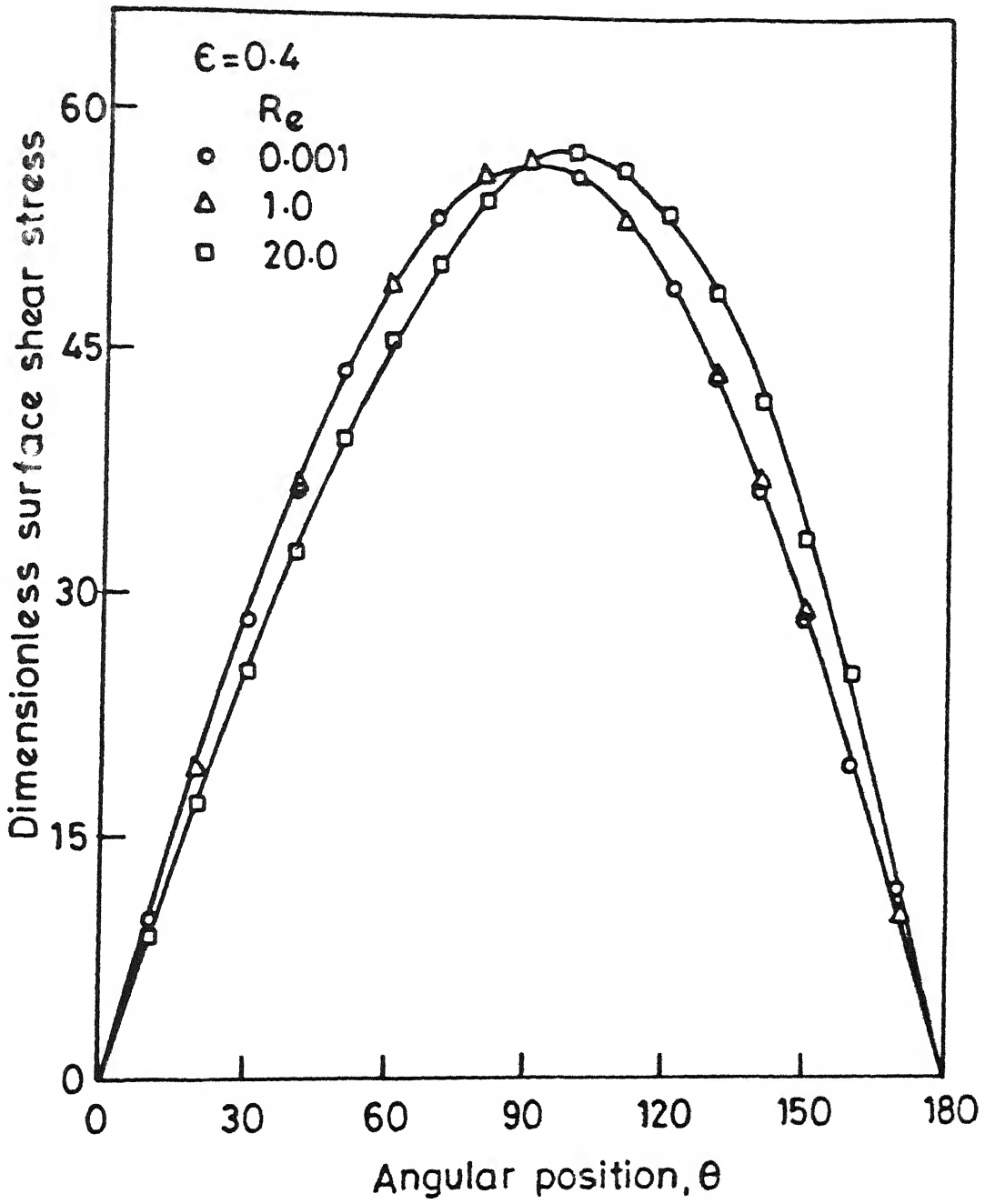

Fig. 5.5 Effect of Reynolds number, on the variation of nondimensional surface shear stress $\tau_s/(\eta \ U_\infty/R_p)$ with angular position, for $\epsilon = 0.4$.

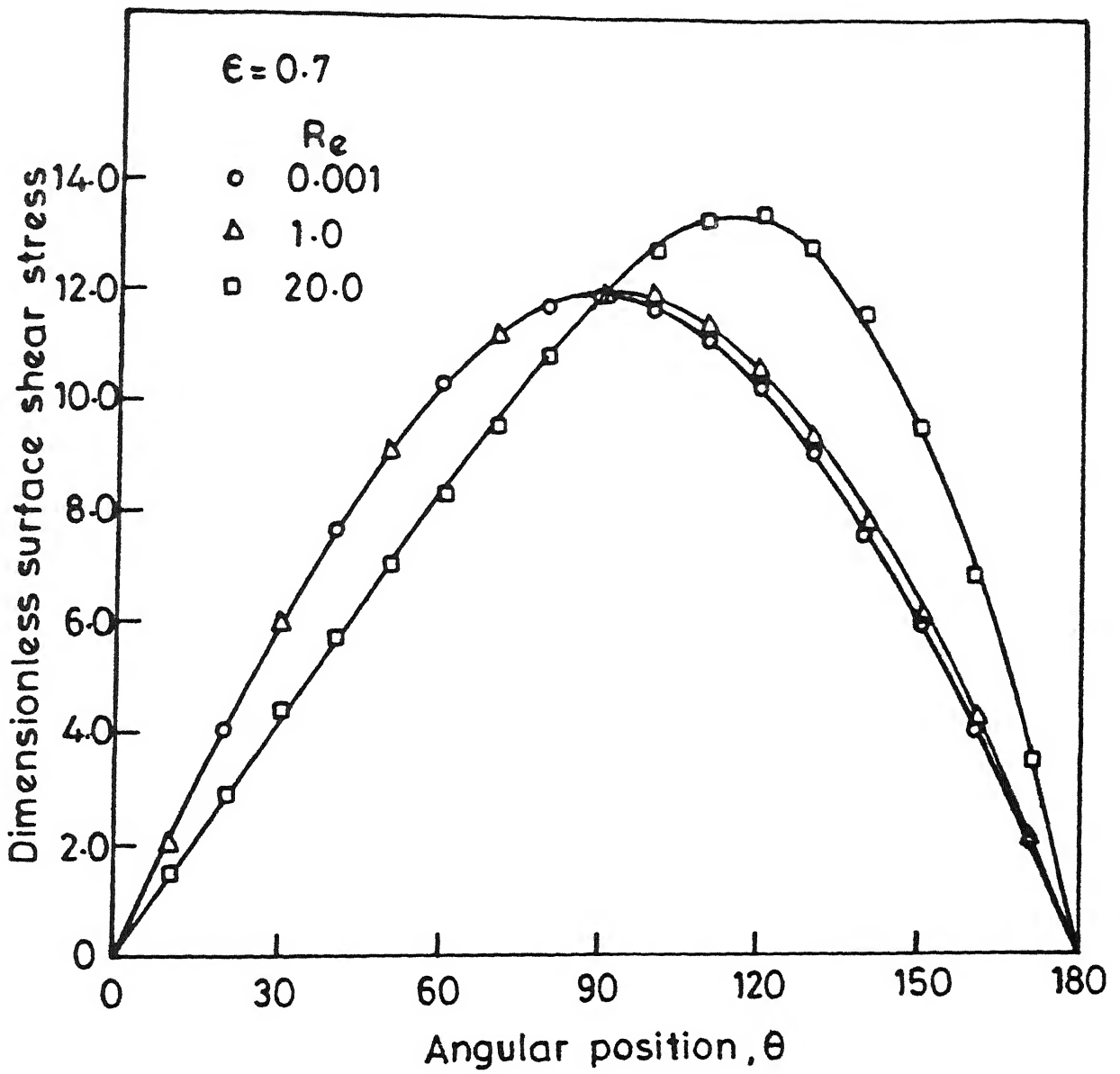

Fig. 5.6 Effect of Reynolds number, on the variation of nondimensional surface shear stress $\tau_s/(\eta\ U_\infty/R_p)$ with angular position, for ϵ = 0.7.

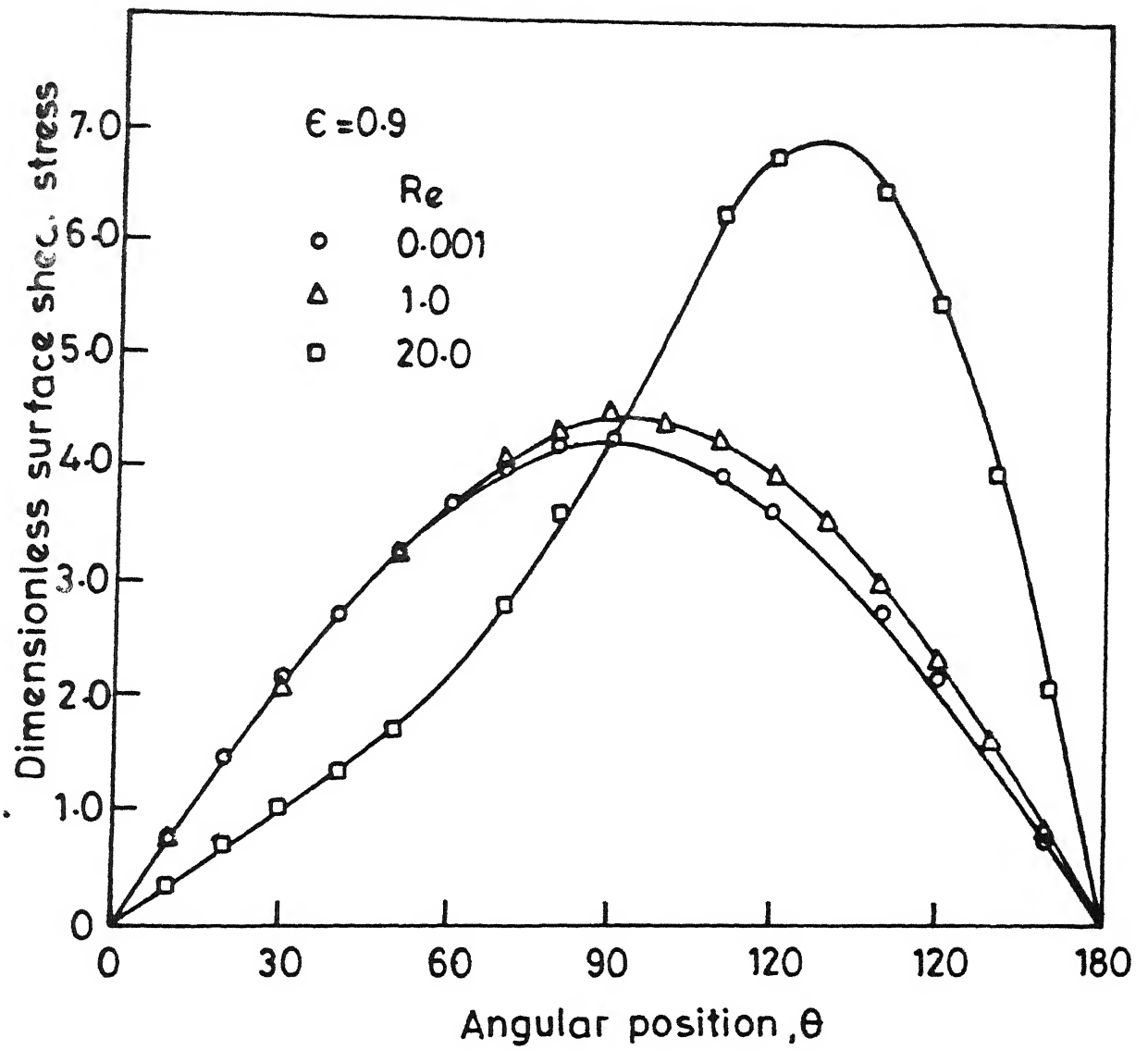

Fig 5.7 Effect of Reynolds number, on the variation of nondimensional surface shear stress $\tau_s/(\eta\ U_\infty/R_p)$ with angular position, for ϵ = 0.9.

surface shear stress varies sinusoidally with angle at all voidages, in conformity with the Happel's analytical solution Moreover, the shear stress exhibits only marginal deviation from the creeping flow results even upto the Reynolds number of 20 at a low voidage (ϵ = 0.4). This is a consequence of large contact area existing between the solid and the fluid phases when ϵ is small At higher voidages (ϵ = 0.7 and ϵ = 0.9) however, there is noticeable divergence from the creeping flow results even at Re = 1 0. In the intermediate Reynolds number regime, the surface shear stress distribution is asymmetric about the mid plane ($\theta = \pi/2$) with increasing skewedness as the bed voidage increases. The maximum shear stress shifts towards the rear region ($90^{\circ} < \theta < 180^{\circ}$) for such a situation. This is believed to be resulting from fluid inertia, which causes the fluid to move with nearly the particle-velocity in front of it. It is evident from Figures (5.5 - 5.7) that in the range $0.001 \leq Re \leq 20$ and $0.4 \leq \epsilon \leq 0\ 9$, the voidage has a stronger influence on the dimensionless shear stress than the Reynolds number. The weak effect of Reynolds number is explained in terms of the fact that for the multiparticle flow situation, the role of inertial force is minor even upto Re = 20. As regards voidage, the claim that shear stress varies approximately as $O(1/\delta^2)$ is supported by trends shown in Figures.

(ii) The pressure profiles (Figures 5.8 - 5 10) vary according to the cosine of the angle at low Reynolds number (Re < 1)

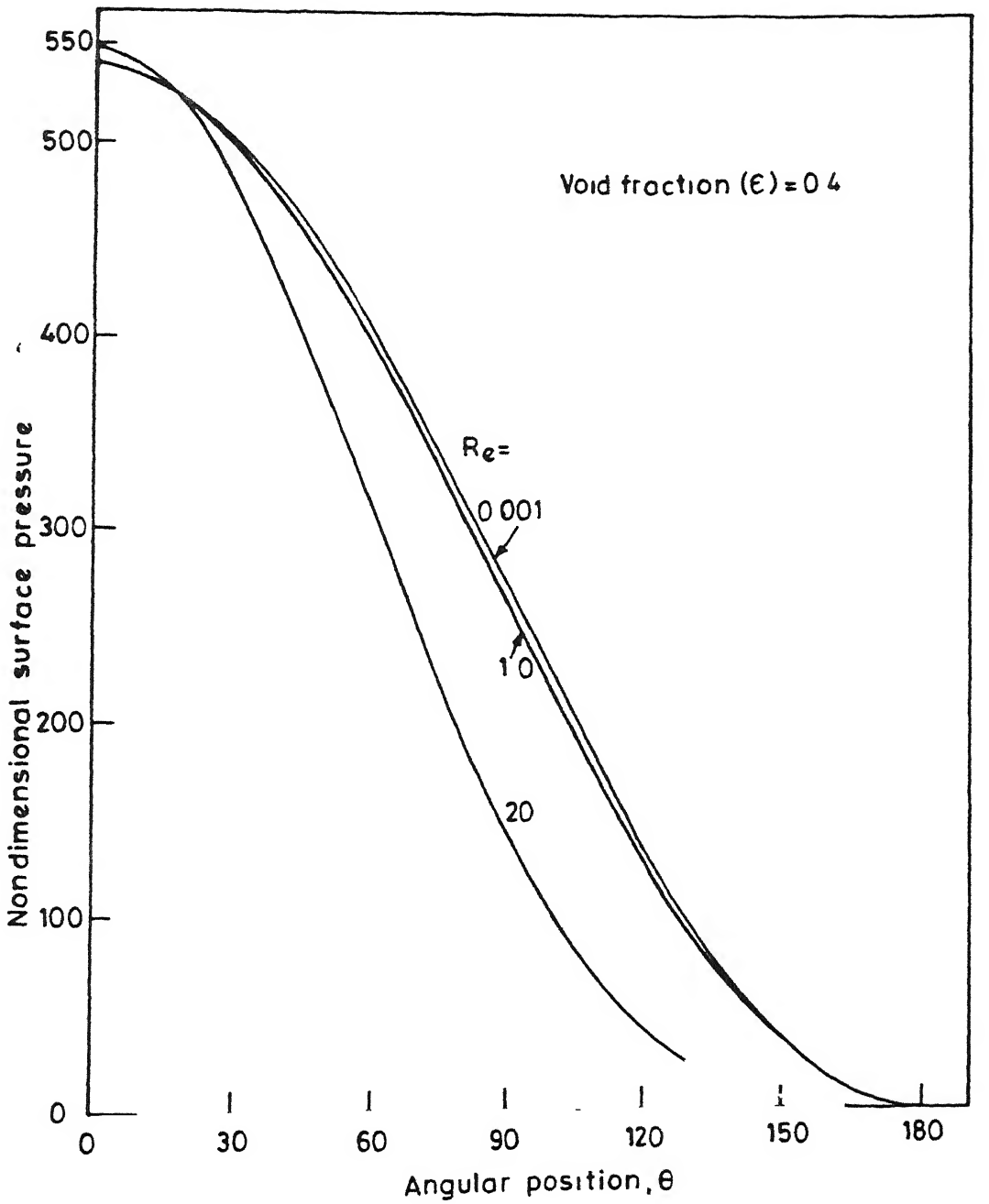

Fig. 5.8 Effect of Reynolds number, on the variation of nondimensional surface pressure $p_s/(\eta\ U_\infty/R_p)$ with angular position, for ϵ = 0 4.

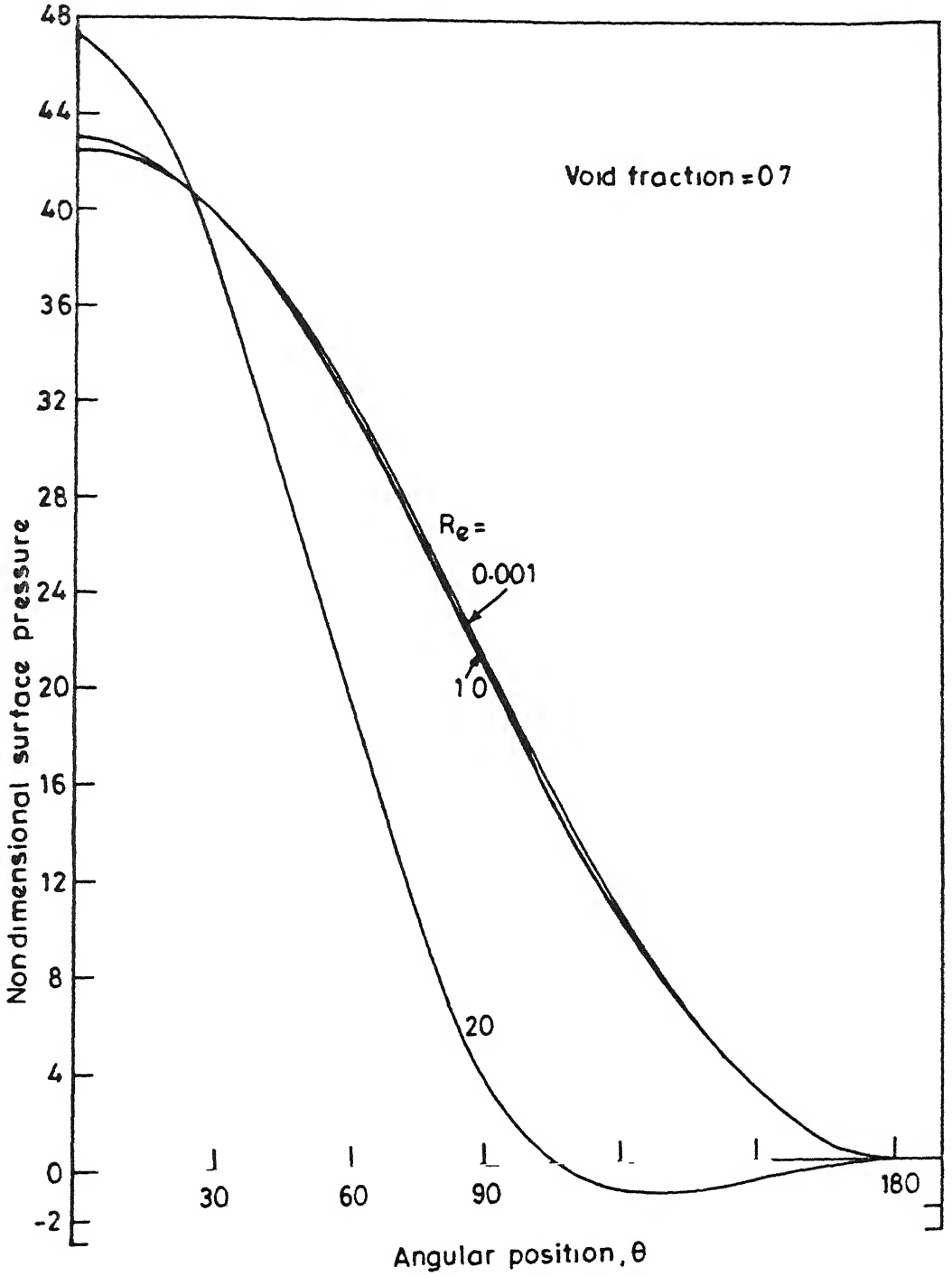

ig 5.9 Effect of Reynolds number, on the variation of nondimensional surface pressure $p_s/(\eta\ U_\infty/R_p)$ with angular position, for ϵ = 0.7.

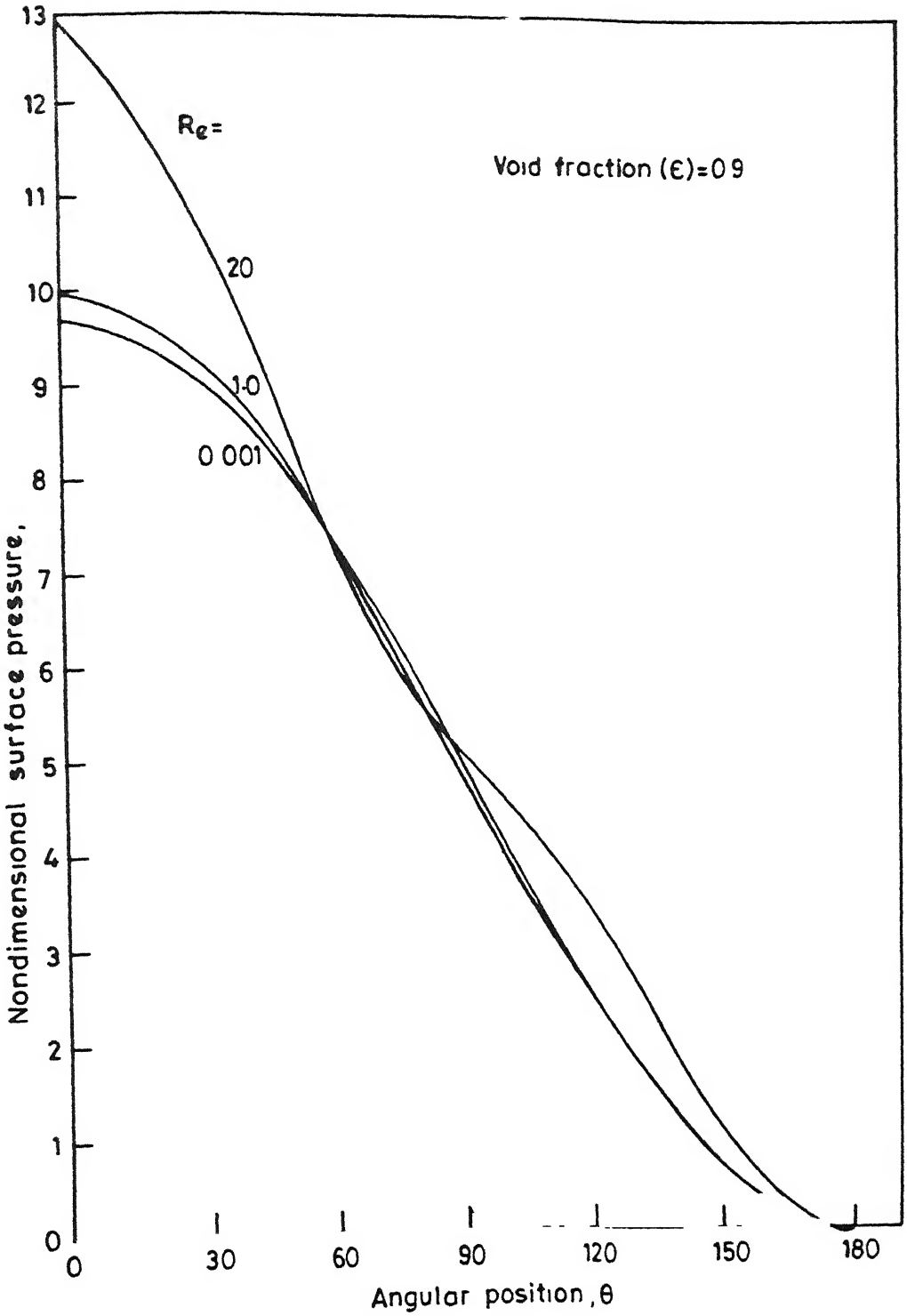

Fig. 5.10 Effect of Reynolds number, on the variation of surface pressure $p_s/(\eta\ U_\infty/R_p)$ with angular position, for ϵ = 0.9.

for all voidages considered here. This is in accordance with the analytical results of Happel. However, unlike the surface shear stress profile, the surface pressure at intermediate Reynolds number range exhibits larger deviation from creeping flow results even for low voidages. Thus, it appears that the inertial effects more directly influence the pressure than the shear stress At higher voidages, the veering away of the surface pressure variation from corresponding creeping flow pressure profile is even more obvious This is hardly surprising because pressure is more sensitive to changes in voidage thar the shear stress, in accordance with the order of magnitude estimates discussed earlier in connection with the pressure and friction drag coefficients. Indeed, for Re = 20, when the voidage is changed from ϵ = 0.4 to 0.9, the maximum shear stress reduces only by a factor of 7 or 8, while the stagnation pressure reduces by a factor of 50.

(iii) The relative magnitudes of the surface pressure and the surface shear stress at three representative voidages (ϵ = 0.4, 0.7 and 0 9) and two Reynolds numbers (Re = 0.001 and 20) are shown in Figures 5.11 to 5.16. It is observed that at low voidage (ϵ = 0.4), the dimensionless pressure variation over almost the whole particle surface is much larger in magnitude than that of the dimensionless shear, save for a small part of the surface in the rear of the sphere. As the voidage increases, the trend reverses, i.e., the front half of the sphere is dominated by pressure

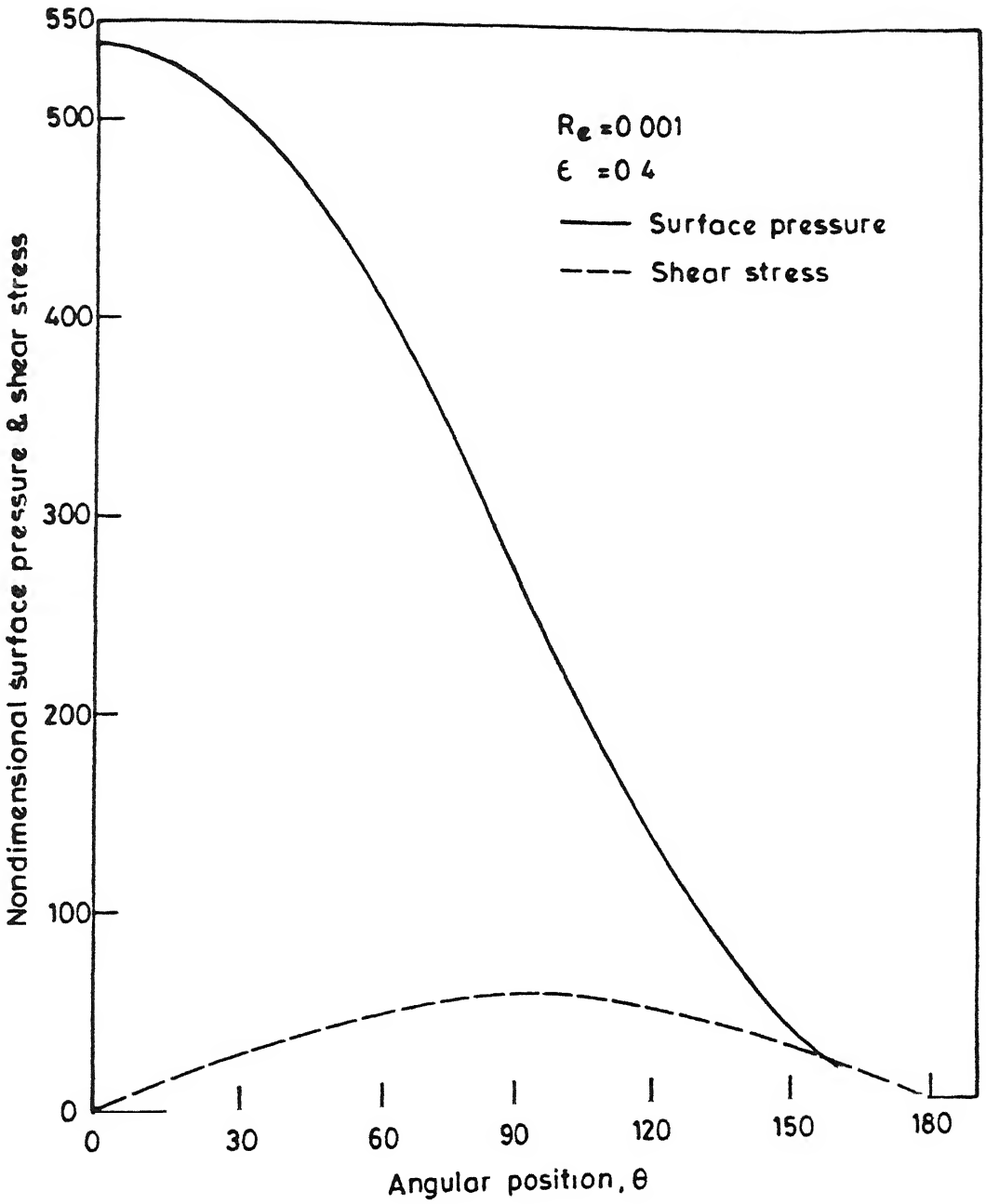

Fig. 5.11 Relative magnitudes of nondimensional surface pressure $p_s/(\eta\ U_\infty/R_p)$ and shear stress $\tau_s/(\eta\ U_\infty/R_p)$, for $\epsilon = 0.4$ and Re = 0.001.

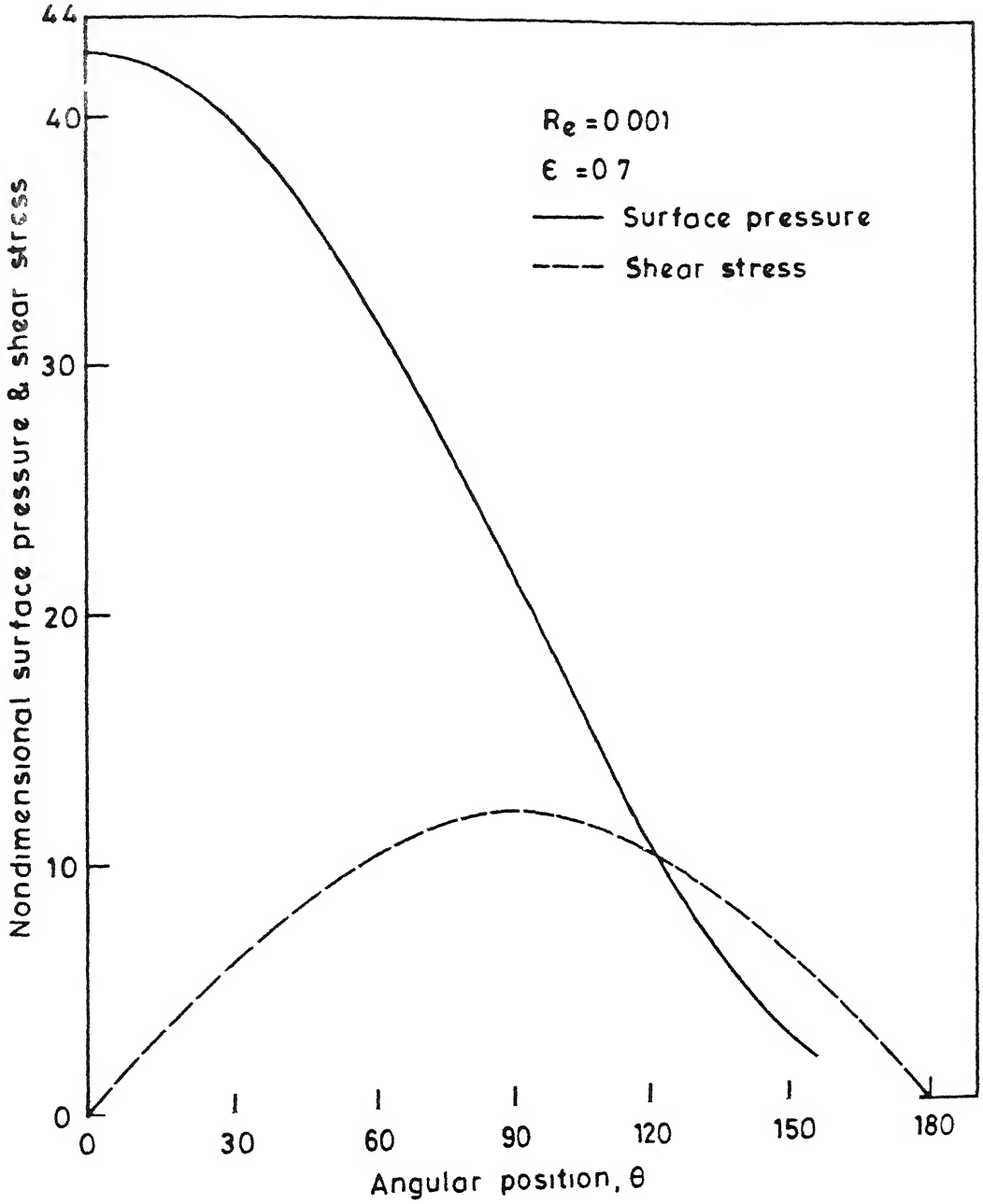

Fig. 5.12 Relative magnitudes of nondimensional surface pressure $p_s/(\eta\ U_\infty/R_p)$ and shear stress $\tau_s/(\eta\ U_\infty/R_p)$, for $\epsilon = 0.7$ and Re = 0.001.

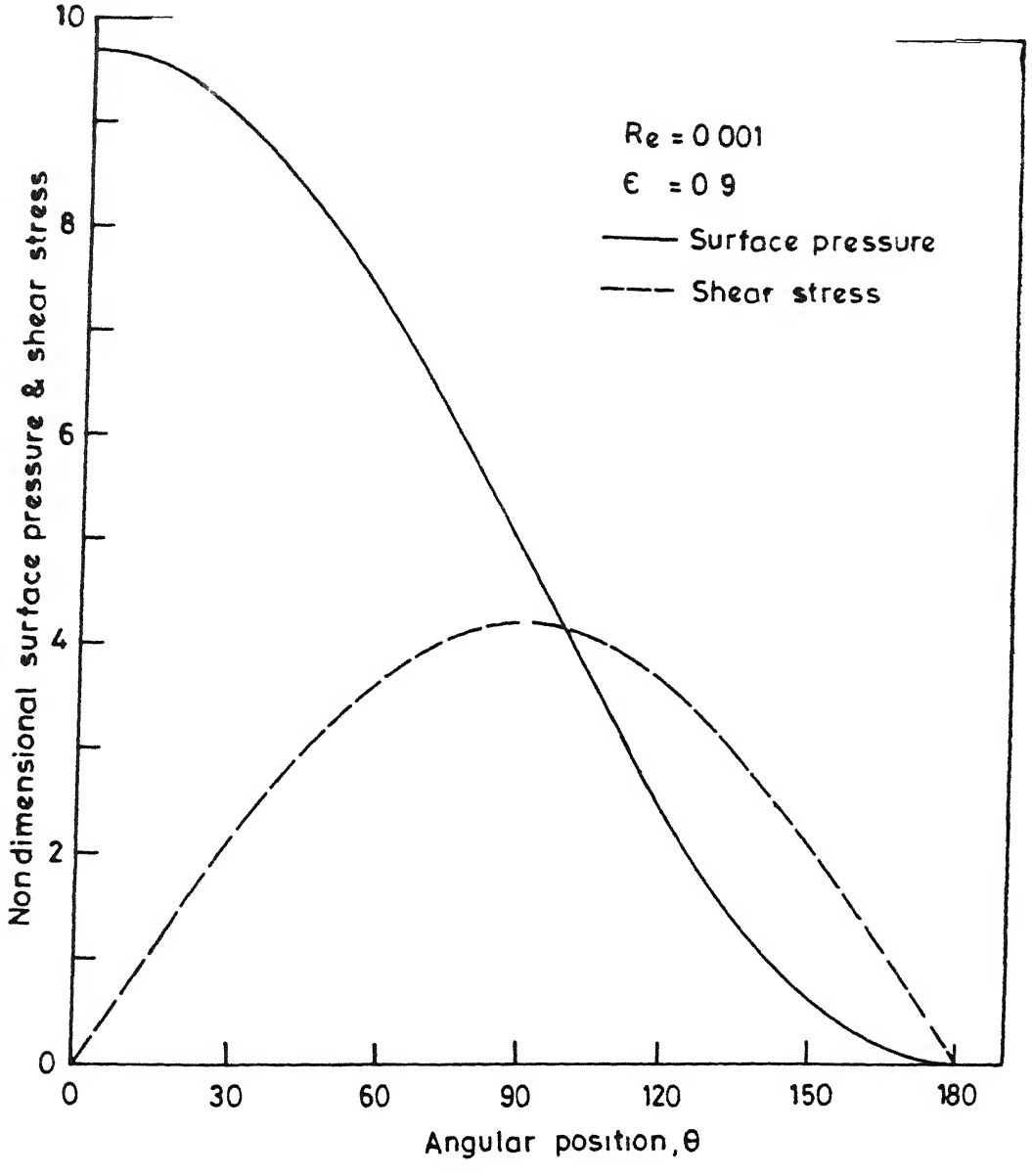

Fig. 5.13 Relative magnitudes of nondimensional surface pressure $p_s/(\eta\ U_\infty/R_p)$ and shear stress $\tau_s/(\eta\ U_\infty/R_p)$, for ϵ = 0 9 and Re = 0 001.

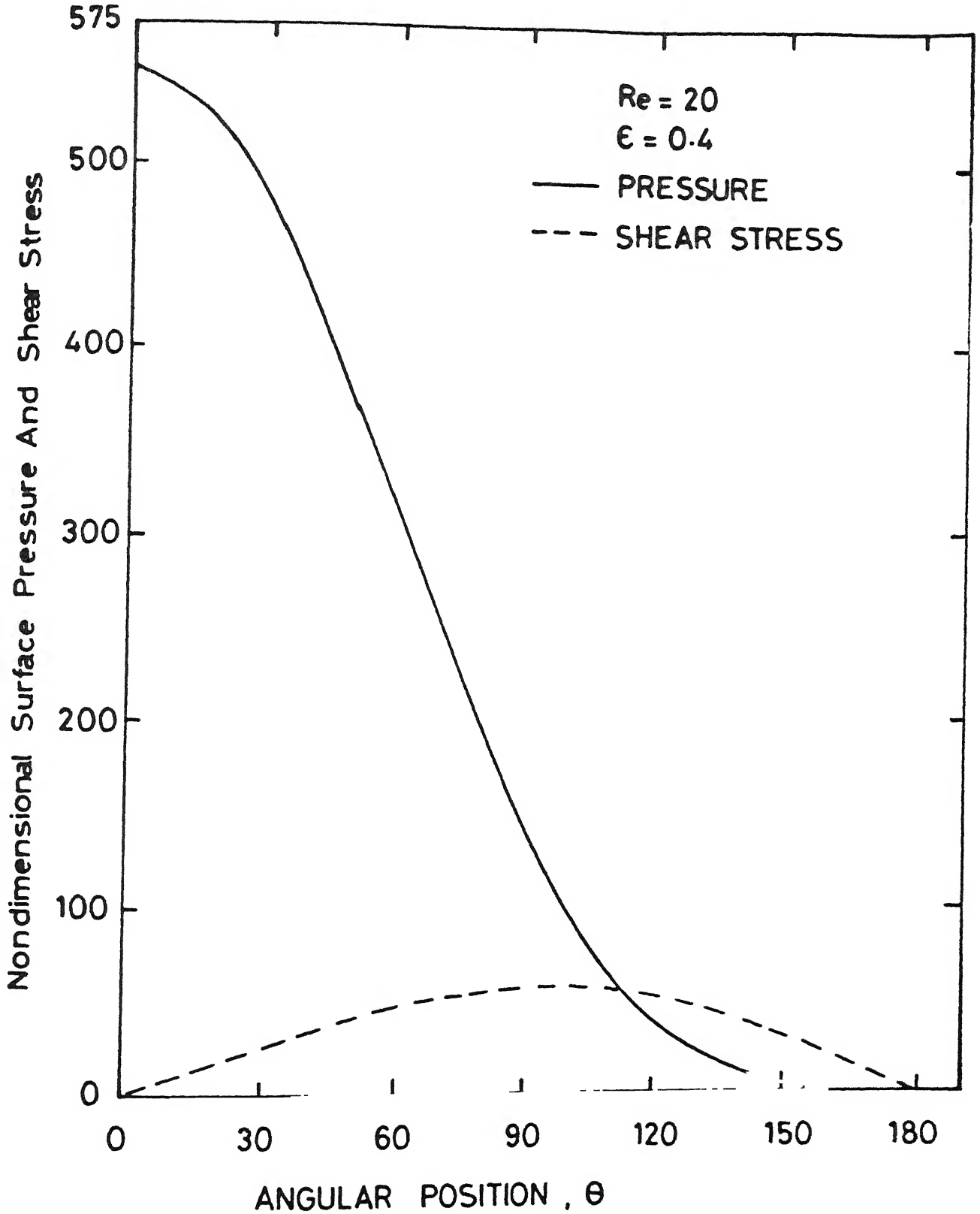

Fig. 5.14 Relative magnitudes of nondimensional surface pressure $p_s/(\eta\ U_\infty/R_p)$ and shear stress $\tau_s/(\eta\ U_\infty/R_p)$, for $\epsilon = 0.4$ and Re = 20.

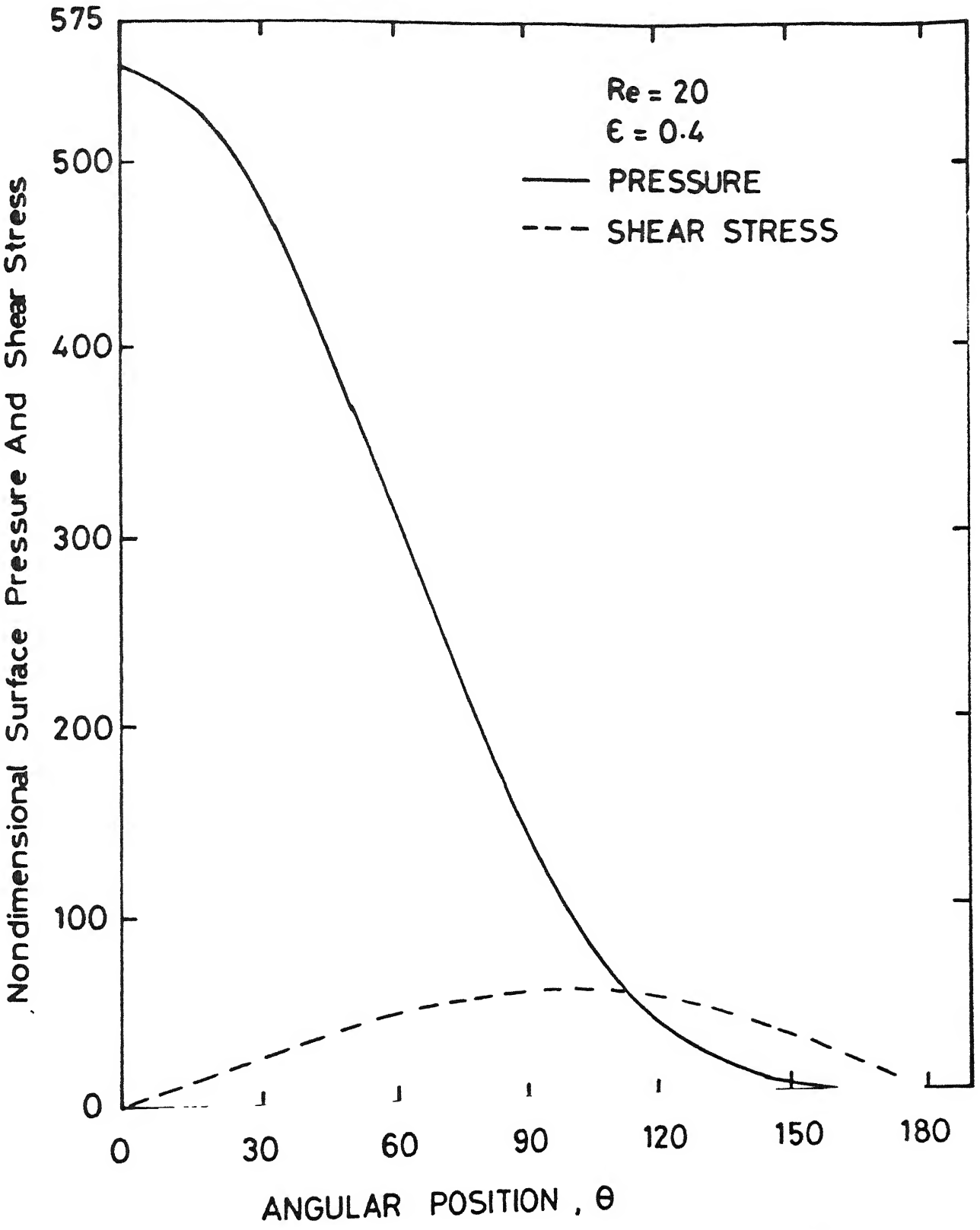

Fig. 5 14 Relative magnitudes of nondimensional surface pressure $p_s/(\eta\ U_\infty/R_p)$ and shear stress $\tau_s/(\eta\ U_\infty/R_p)$, for $\epsilon = 0.4$ and Re = 20.

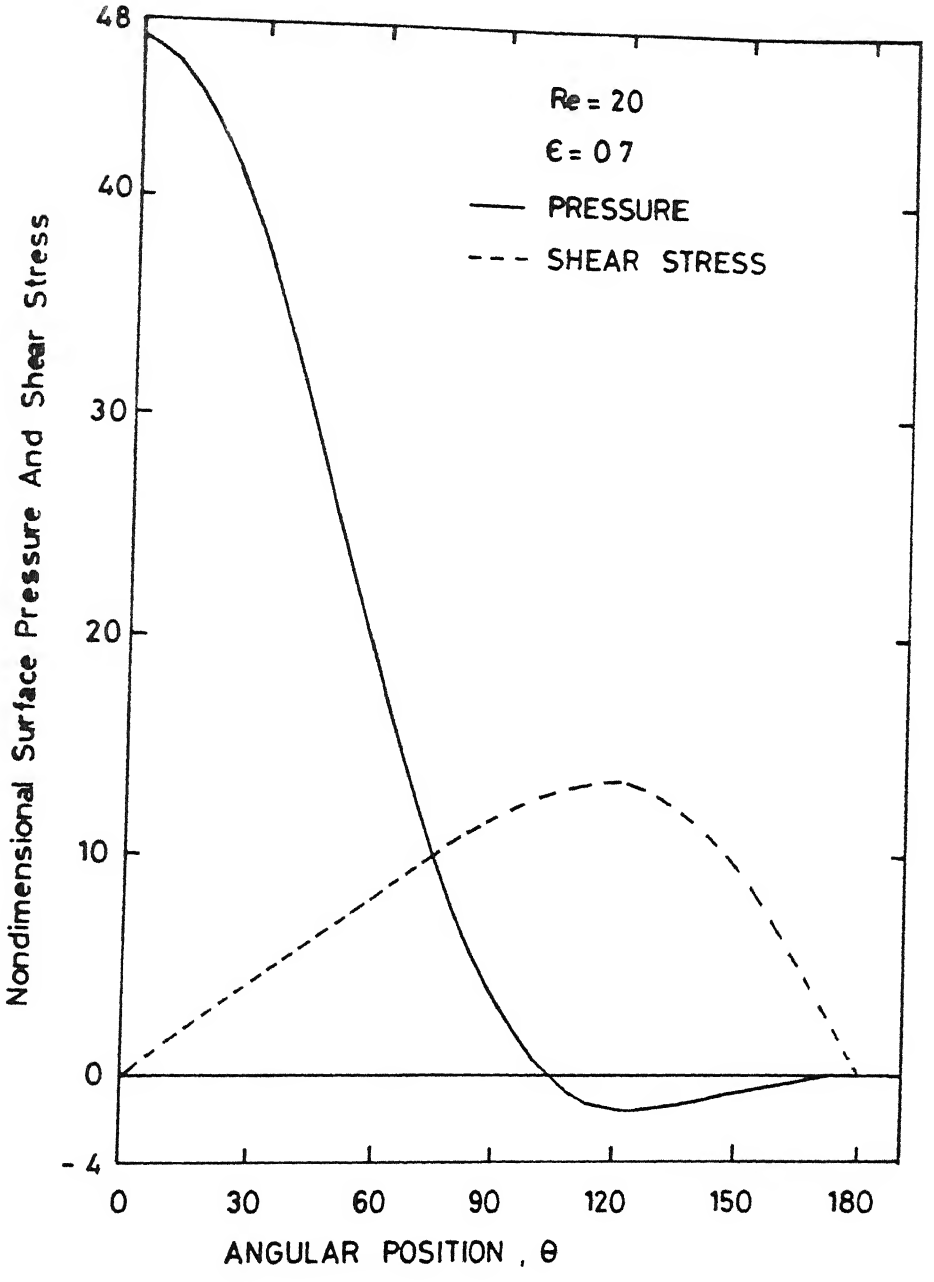

Fig. 5.15 Relative magnitudes of nondimensional surface pressure $p_s/(\eta\ U_\infty/R_p)$ and shear stress $\tau_s/(\eta\ U_\infty/R_p)$, for ϵ = 0.7 and Re = 20.

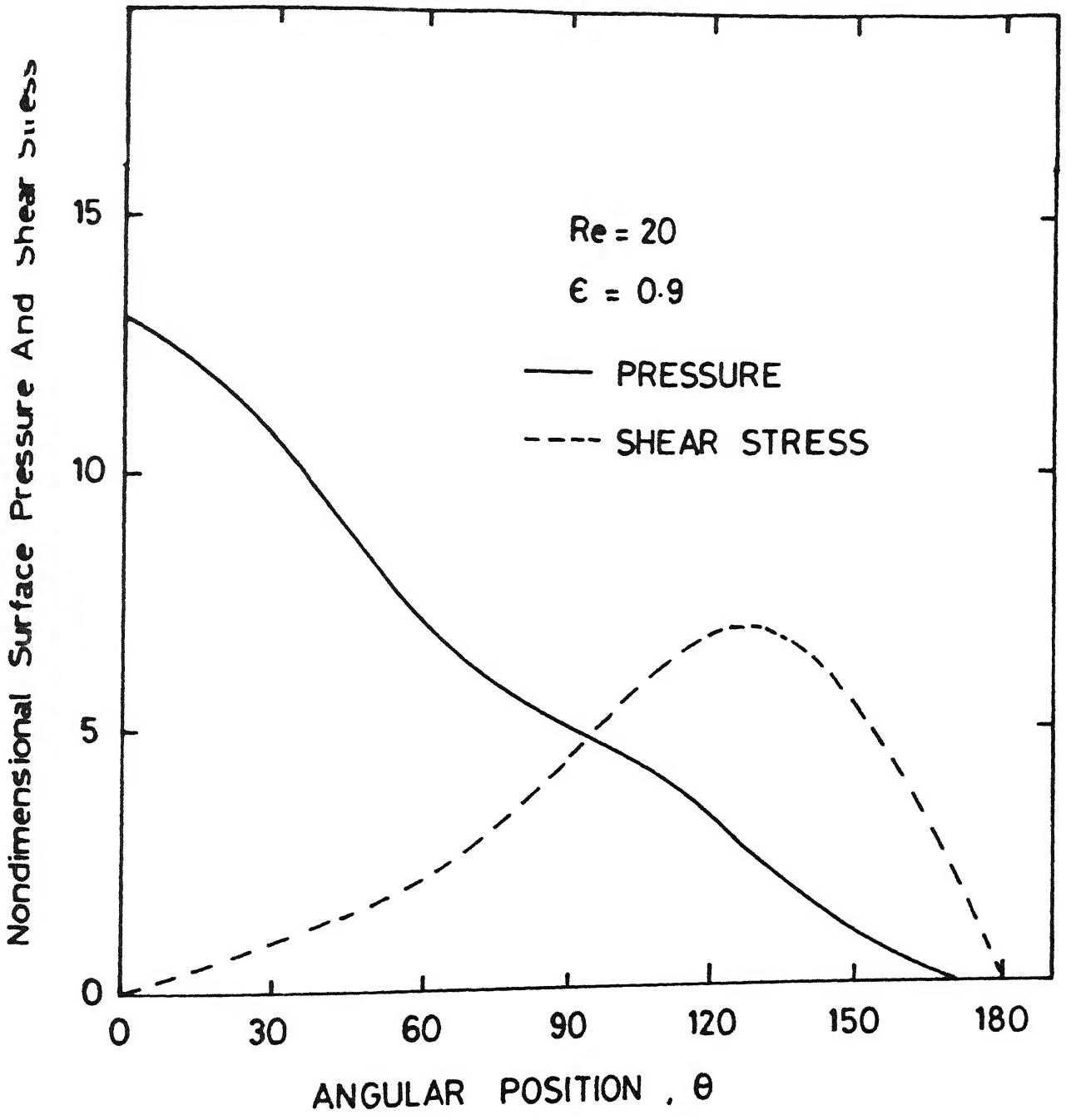

Fig. 5.16 Relative magnitudes of nondimensional surface pressure $p_s/(\eta\ U_\infty/R_p)$ and shear stress $\tau_s/(\eta\ U_\infty/R_p)$, for $\epsilon = 0.9$ and Re = 20

and the rear portion by surface shear stress. This becomes increasingly evident as the bed voidage increases. Finally, with the increasing dilution of the assemblage, the ratio (P_{max}/τ_{max}) decreases from about 9 to 2 for the creeping flow range (Re = 0 001) At ϵ = 0.9, the variations in the surface pressure and shear stress becomes comparable so that the relative drag contributions are also of the same order

The effect of change in Reynolds number on the relative magnitudes of the local values of surface pressure and shear stress is shown in Figures 5.14 - 5 16 wherein the results are plotted for Re = 20 The trends are qualitatively similar to the creeping flow range In the packed bed range (ϵ = 0 4), the surface pressure dominates over the corresponding surface shear stress over a major part of the sphere surface ($0^{\circ} \leq \theta \leq 110^{\circ}$). However, for distended beds (ϵ = 0.9), the pressure dominated region is reduced ($0^{\circ} \leq \theta \leq 60^{\circ}$) while the ($\theta > 100^{\circ}$) region is clearly dominated by surface shear, with a transition zone in between these two parts For Re = 20, the value of P_{max}/τ_{max} falls from 11 to 2, a drop comparable to that in the creeping flow region

5.3 ANGULAR AND RADIAL VELOCITY PROFILES

It is generally realized that the local values of surface shear and pressure are directly determined by the local velocity gradients prevailing in the flow field, in particular, gradients of the angular velocity component

Figures 5 17 and 5 18 show the typical variation of normalized V_θ for ϵ = 0 4 and 0 9 in the creeping f ow regime (Re = 0 001 and 1) An examination of the results plotted in these two figures suggests that complete fore and aft symmetry prevails as the values of V_θ corresponding to θ = 30° and 150°, and θ = 60° and 120° coincide with each other. The results for the remaining values of voidage (not shown here) also conform to this behaviour. At such low values of Reynolds number, the angular velocity seems to change its direction close to the sphere surface, at r ~ 1.02 for ϵ = 0.4 and at r ~ 1.033 for ϵ = 0.9. Furthermore, regardless of the value of Reynolds number, it would be reasonable to expect steeper velocity gradients in low voidage multi-particle systems than those for dilute systems (See Appendix-I) and this assertion is indeed corroborated by the results shown in Figures 5.17 to 5 20.

The effect of Reynolds number on the angular velocity profiles is brought out in figures 5.19 and 5.20. Clearly, the flow is no longer symmetrical (also revealed by surface shear stress profile), and more significantly, the change of direction of the angular velocity now takes place at varying radial distances depending upon the angular coordinate (θ). The angular velocity gradient being maximum in the vicinity (some where on the right) of θ = 90° plane, the shear stress is expected to go through a maximum value at the same location on the sphere surface. This is approximately borne out by shear stress profiles also.

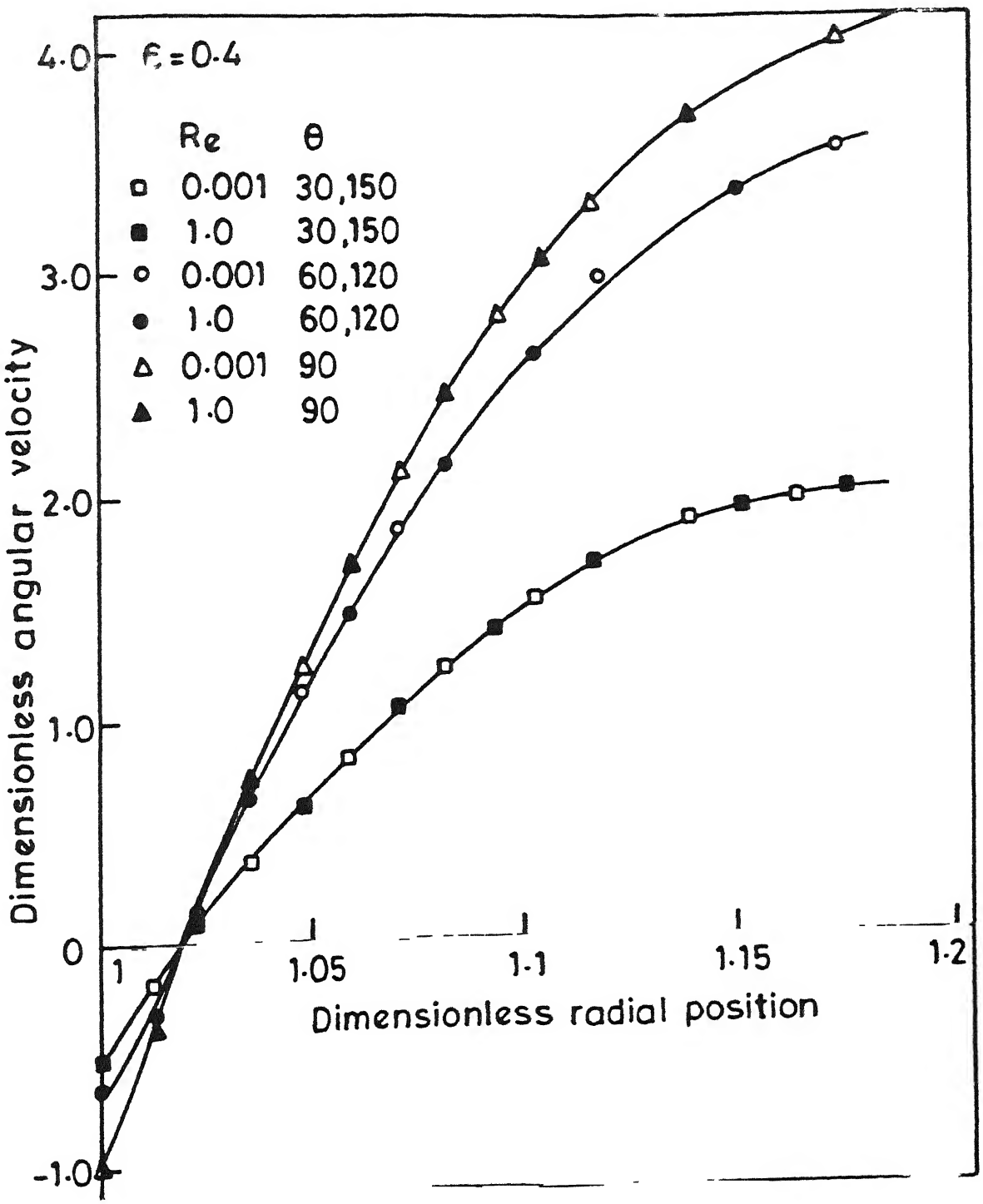

Fig. 5.17 Variation of nondimensional angular velocity in radial direction for ϵ = 0.4; Re = 0.001 and 1.0

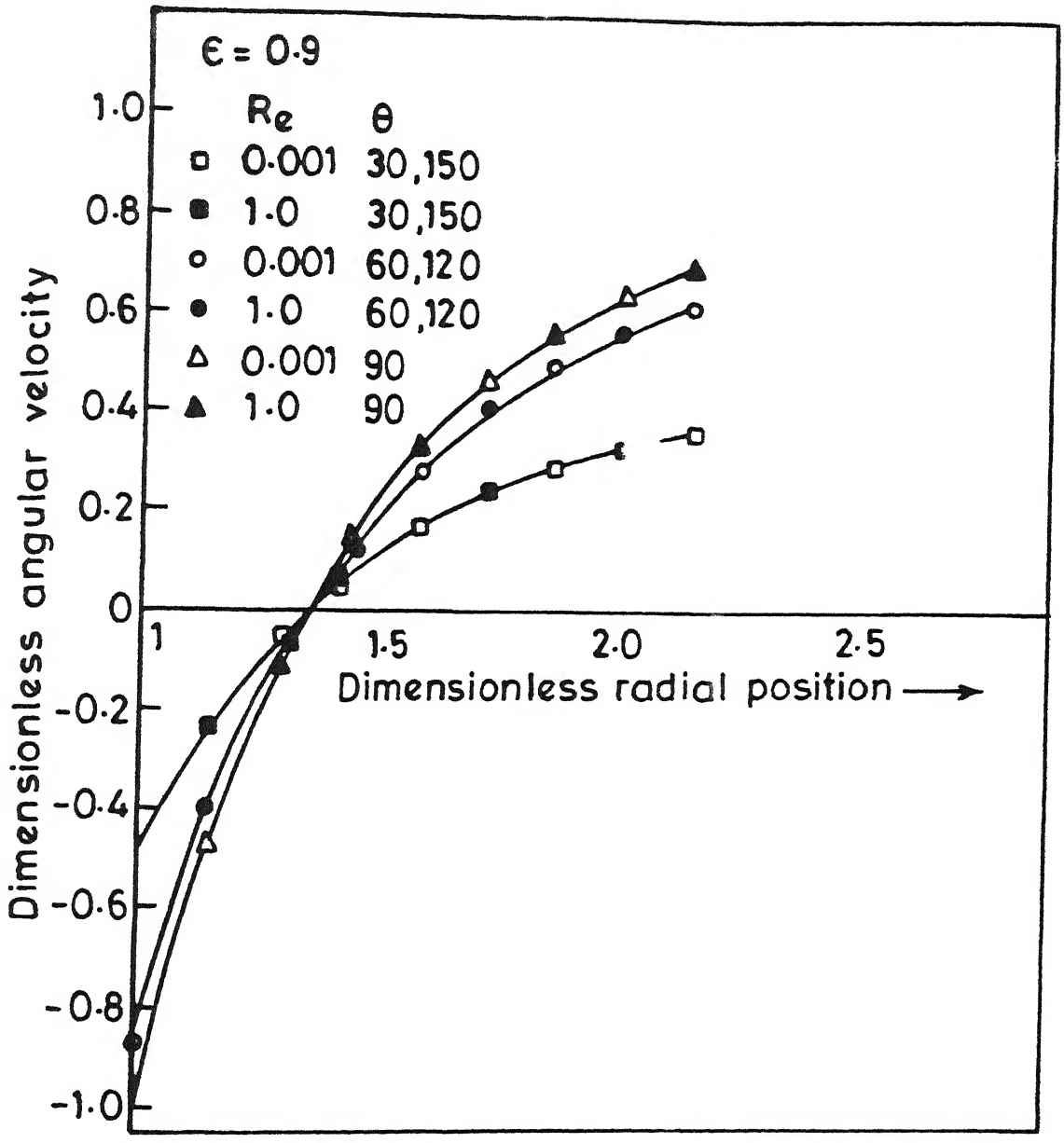

Fig. 5.18 Variation of nondimensional angular velocity in radial direction for ϵ = 0.9; Re = 0.001 and 1.0

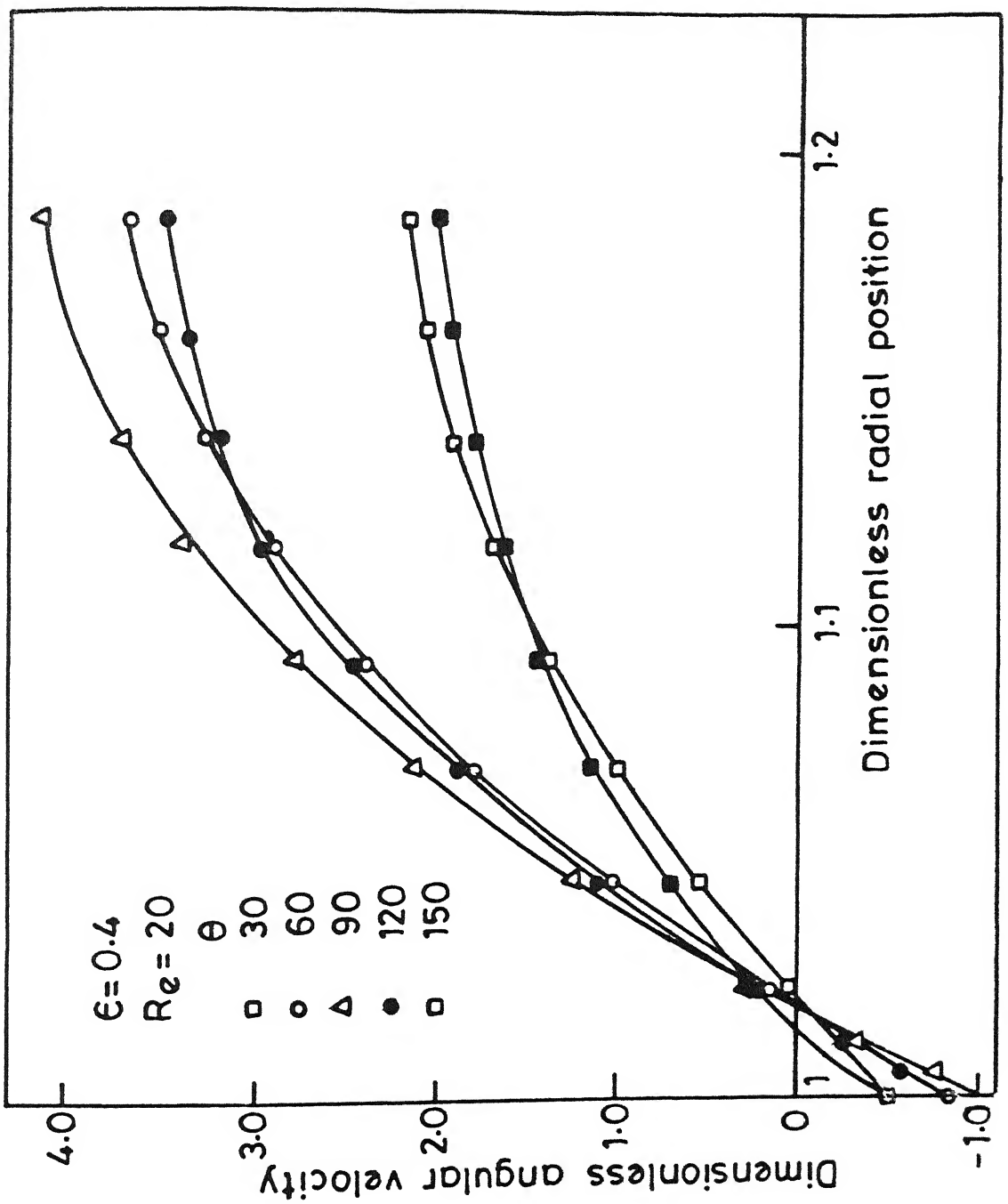

Fig. 5.19 Variation of nondimensional angular velocity in radial direction for $\epsilon = 0.4$ and $Re = 20$

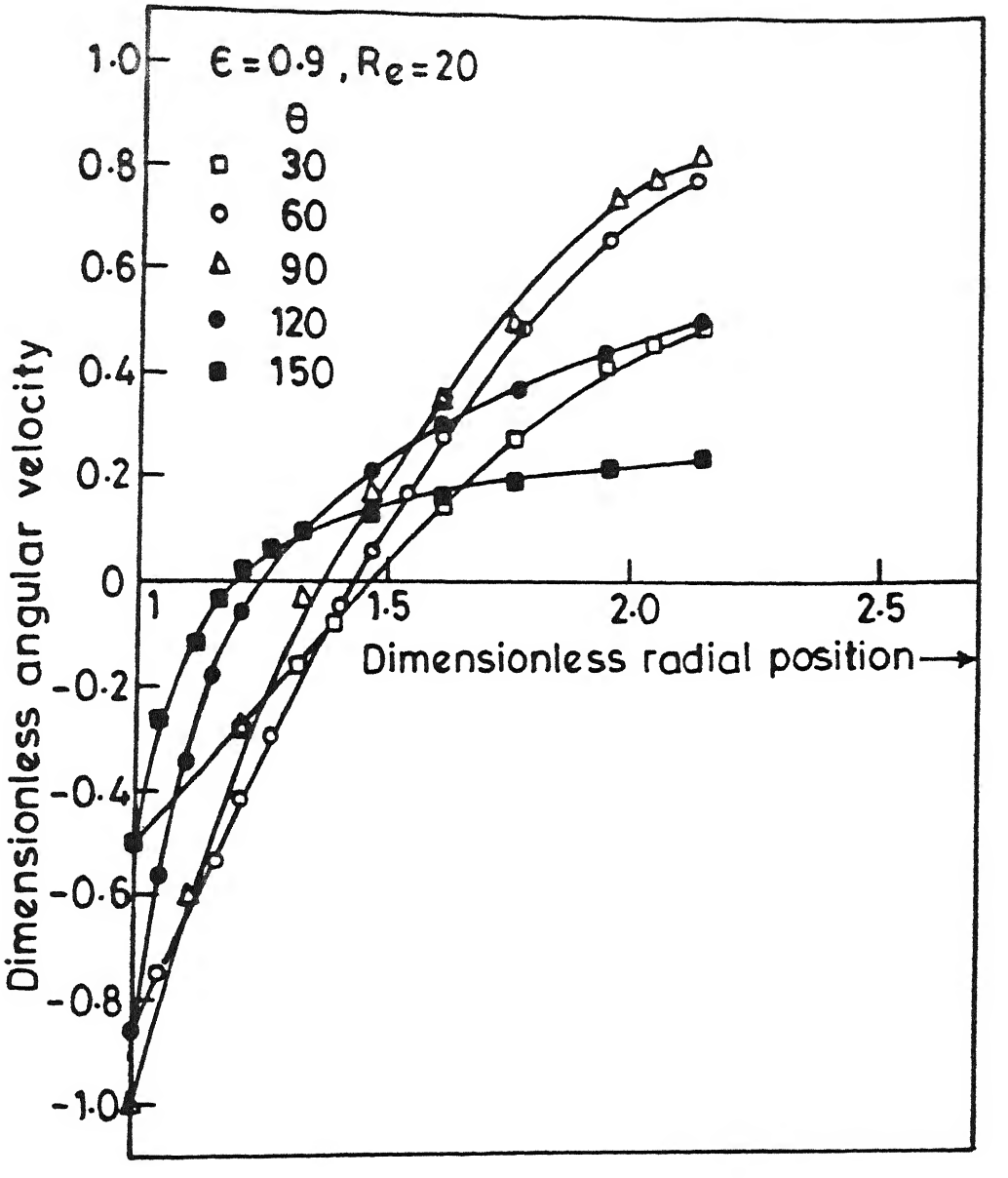

Fig. 5.20 Variation of nondimensional angular velocity in radial direction for ϵ = 0.9 and Re = 20.

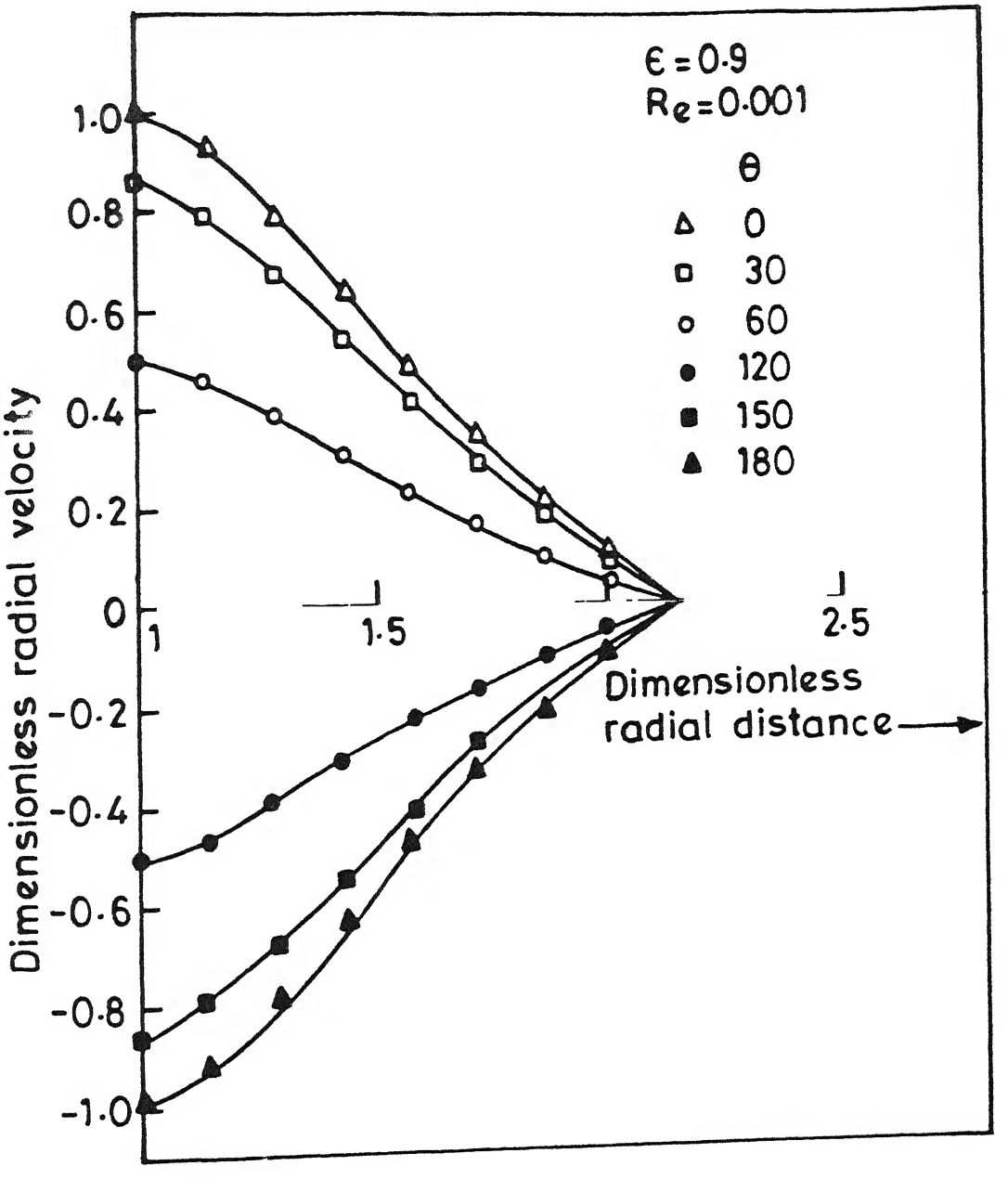

Fig. 5.21 Variation of nondimensional radial velocity in radial direction for ϵ=0.9 and Re = 0.001.

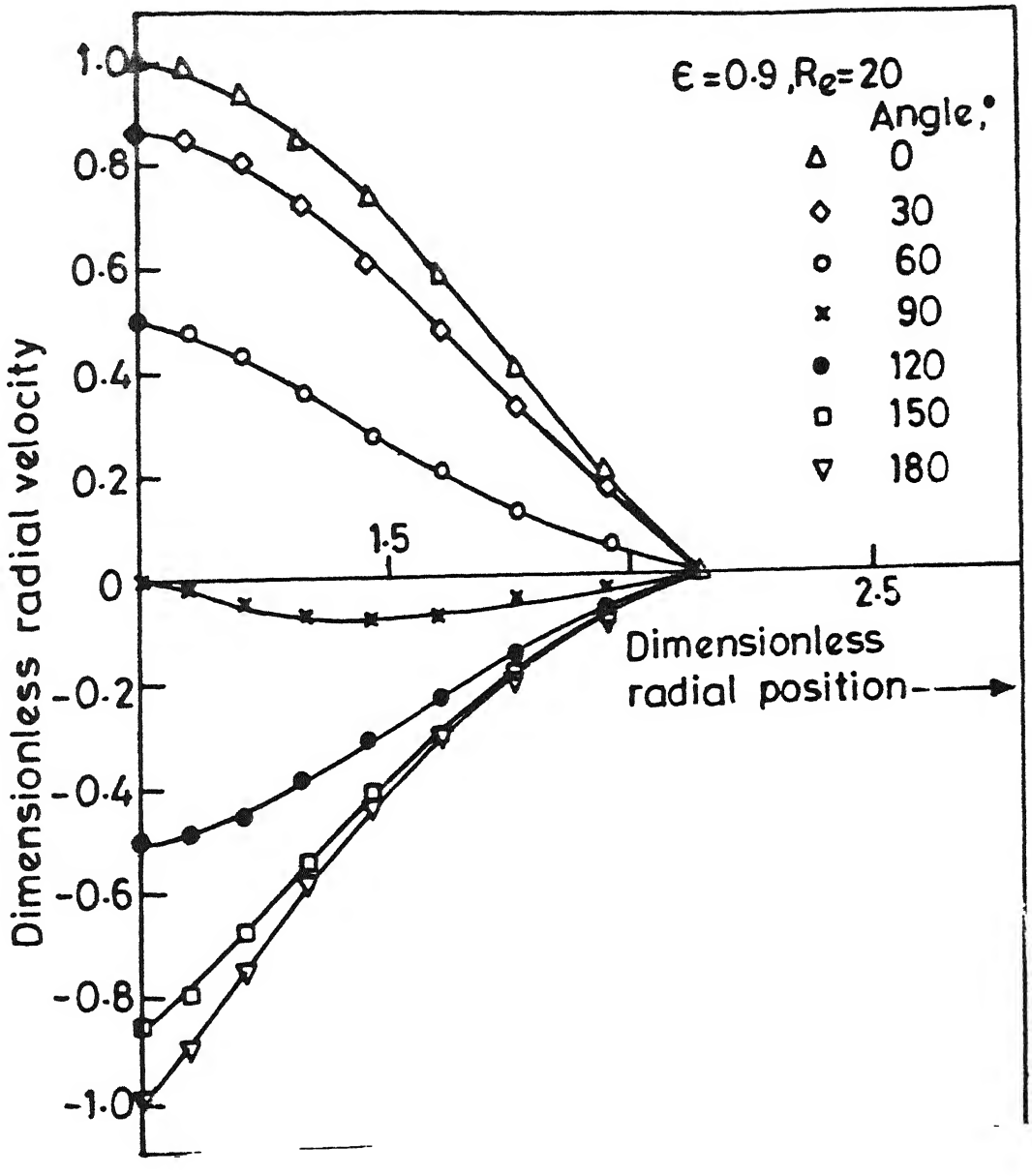

Fig 5 22 Variation of nondimensional radial velocity in radial direction for ϵ = 0.9 and Re = 20.

Though it is generally recognized that in the type of flow being considered here, the angular velocity plays a more important role than the radial velocity, it is together informative to provide some representative results on the radial velocity profiles. Owing to the imposed boundary conditions of no slip and the free stream velocity at the two boundaries, the normalized radial velocity varies between 0° and $\pm \cos \theta$ in the radial direction Typical variation of V_r with r for a range of values of θ and for $\epsilon = 0.9$, is shown in figures 5 21 and 5.22 for two different values of Reynolds number. The results for other values of voidage also show qualitatively similar trends.

5.4 STREAMLINE PATTERNS

Streamline plots provide a qualitative picture of the flow patterns occurring in the flow field, and also facilitate the identification of points of separation, flow reversal, etc. Figure 5.23 and 5.24 (drawn to the scale) depict the streamlines for two values of Reynolds number (0.001 and 20) for $\epsilon = 0.9$. Evidently, complete symmetry exists at Re = 0.001 (Figure 5.23) while the analogous plot for Re = 20 (Figure 5.24) shows that asymmetry has set in. Streamline patterns for other values of voidage also show similar trends except that lower the value of ϵ, higher is the value of Reynolds number upto which the symmetry persists. However, no separation in flow was observed under any combination of conditions of Re and ϵ studied herein.

After discussing the detailed flow results obtained here, it is desirable and instructive to examine their utility through comparisons with the available experimental results for dense and

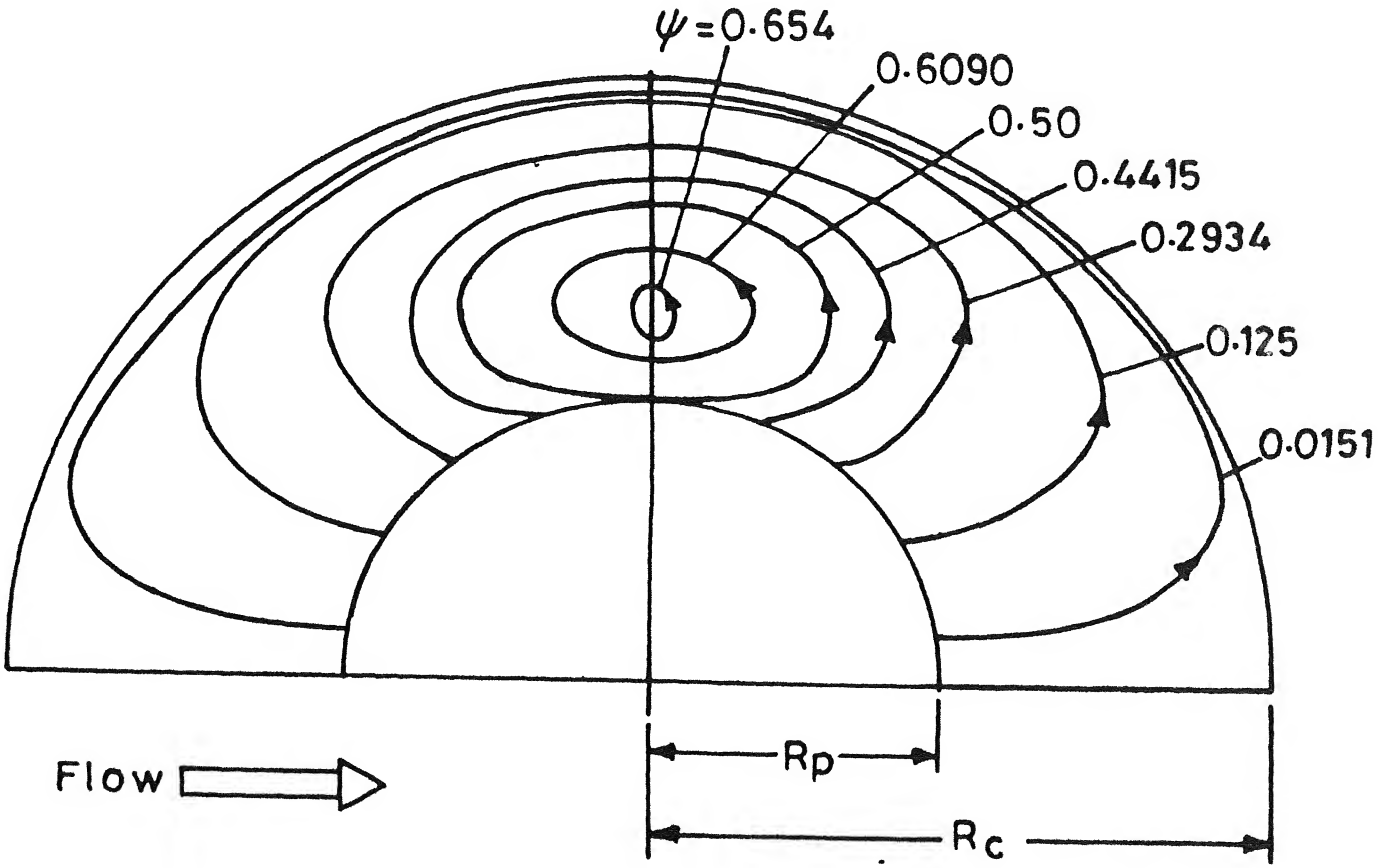

Fig. 5.23 Streamline pattern for ϵ = 0.9 and Re = 0.001.

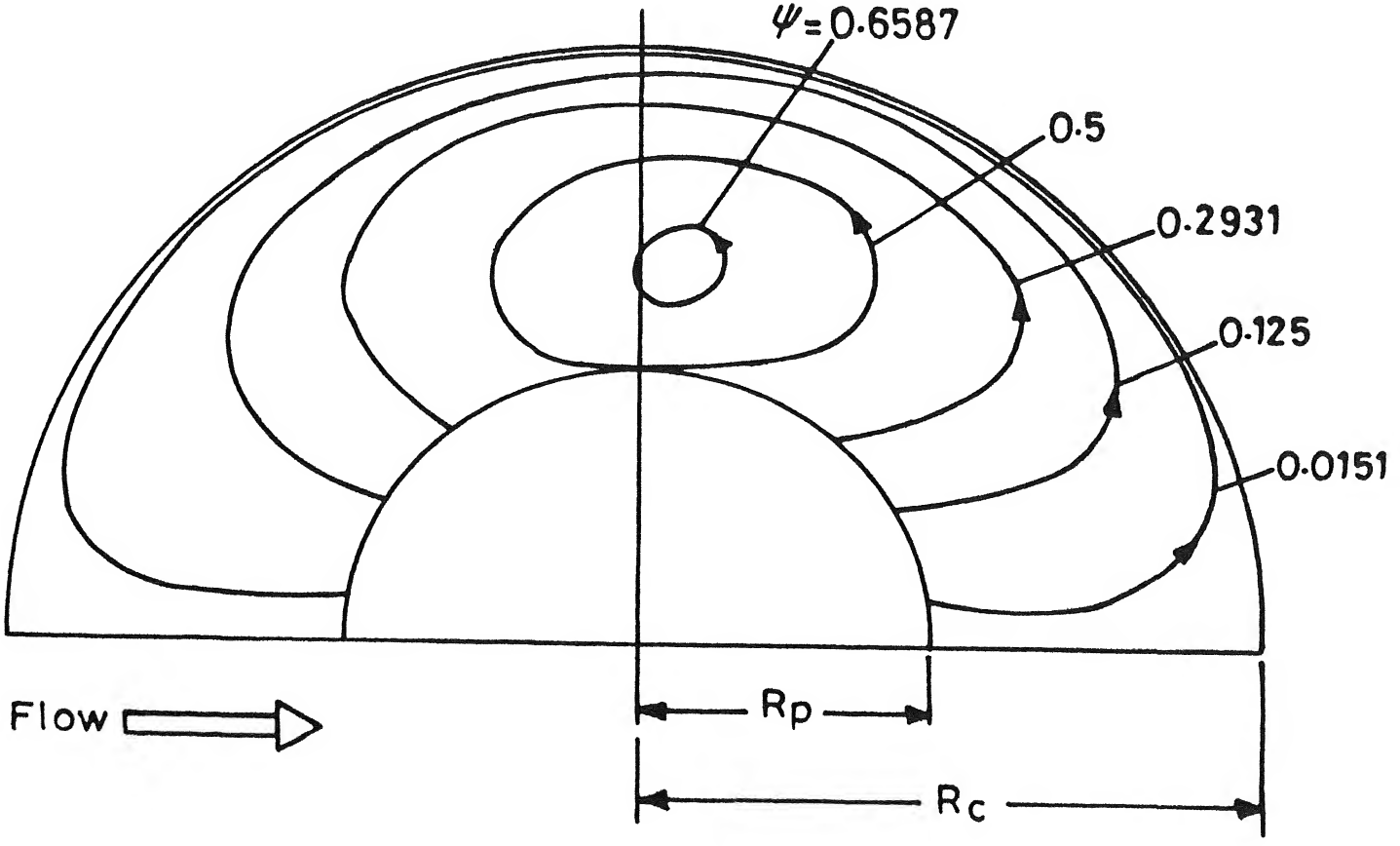

Fig 5 24 Streamline pattern for ∈ = 0 9 and Re = 20

dilute assemblages Such comparisons facilitate to identify the range of applicability of the free surface cell model.

5.5 COMPARISON OF PREDICTED RESULTS WITH EXPERIMENTAL DATA FOR PACKED BEDS

The results presented in the previous chapter indicated that excellent correspondence exist between the present results and analytical results of Happel (1958) for a creeping flow situation. Happel (1958) in his paper made the comparisons of the free-surface cell theory results in the Stokes flow range with the results of other theoretical analyses and the experimental data then available in the literature. The close agreement of theory with the well known Carman-Kozeny or Fair-Hatch equations which are widely used to correlate experimental data on packed beds, was emphasised. The average deviation of Happel's results from the prediction of Carman-Kozeny relation (with Kozeny constant, k = 5.0) over the range of voidage ϵ = 0.2 to 0.7, was reported to be 8%. The maximum deviation which occurred for the voidage, ϵ = 0.7, was found to be 13%. Therefore, the validity of the free surface cell model for the creeping flow of a Newtonian fluid through a packed bed is fairly well-established The objective of the present investigation is to identify the applicability of the free surface cell model in the intermediate Reynolds number regime.

In the intermediate Reynolds number regime, the Ergun equation (1952) purports to represent most of the available experimental pressure drop data on flow through packed beds with reasonable accuracy. The Ergun equation is written as,

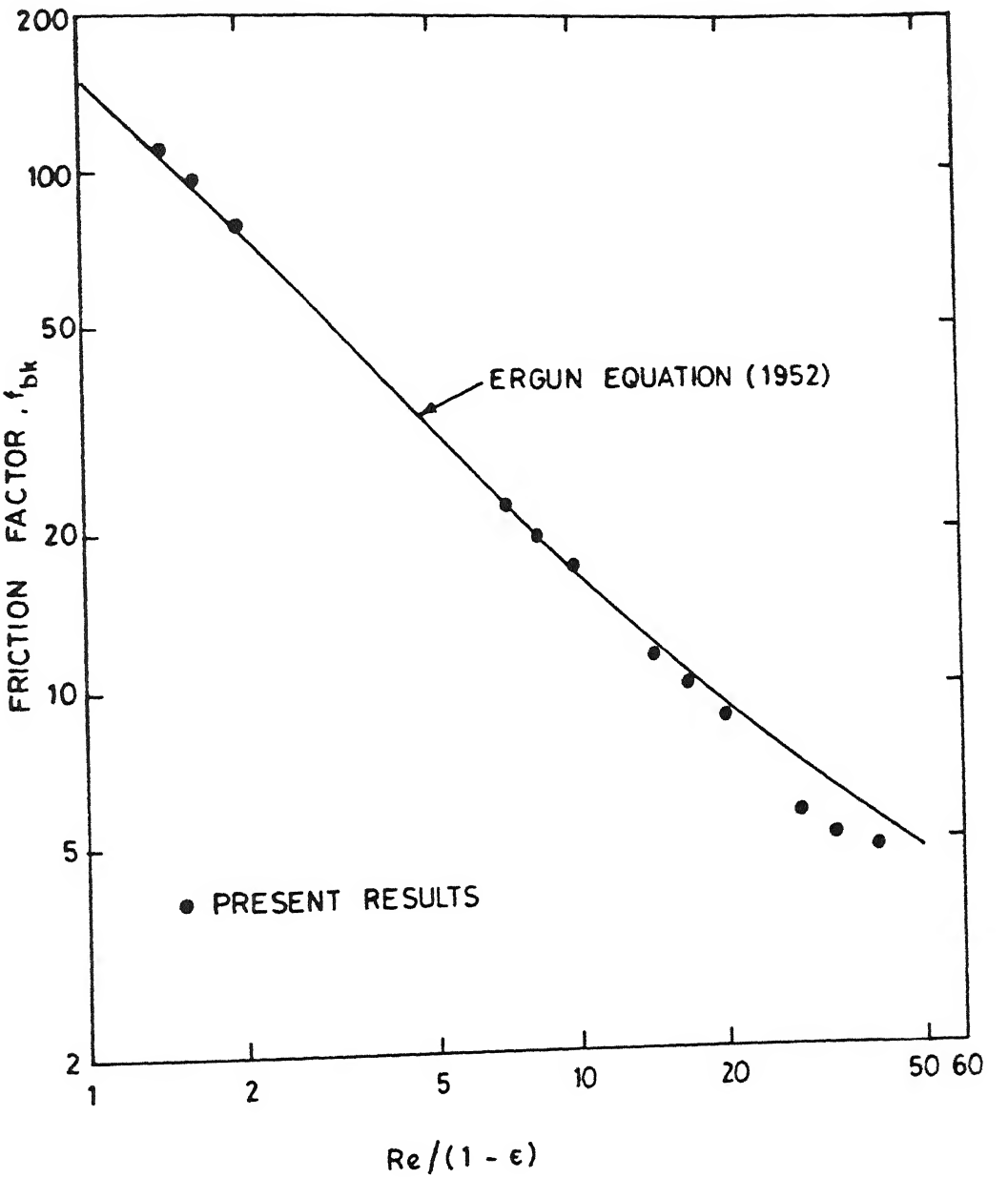

Fig 5.25 Comparison of present numerical results with the predictions of Ergun equation for flow through packed bed range ($0.3 \leq \epsilon \leq 0.5$).

$$f_{bk} = 150 \frac{(1-\epsilon)}{Re} + 1.75 \qquad (5.1)$$

As mentioned earlier in Chapter IV, El-Kaissy and Homsy (1973) extended the analysis of Happel (1958) to the intermediate Reynolds number range by carrying out a regular perturbation analysis. A comparison between their and present results in terms of friction factor was shown in Table 4.6. In the same table the values of f_{bk} calculated using the Ergun's equation are also included. The comparison of the present results with those of Ergun is shown in Figures 5.25. Evidently, the present results as well as those of El-Kaissy and Homsy (1973), are in reasonable agreement with the predictions of Ergun's equation upto about Re ~ 20 in the range $0.3 \leq \epsilon \leq 0.5$. Beyond this value of voidage, the correspondence between the two deteriorates rapidly and the divergence becomes almost 100% at Re = 100. If it is assumed here that the Ergun equation faithfully represents the experimental data, it is then obvious that the free surface cell model, originally developed for creeping flow conditions, breaks down at about Re ~ 20. This is possibly due to appreciable convective effects and it is no longer possible to retain the spherical symmetry of the cell. In view of this, the utility of the results presented by Fukuchi and Ishii (1983) and Nishimura and Ishii (1980a) for the range $10 \leq Re \leq 10^5$ is questionable.

5.6 COMPARISON OF PREDICTED RESULTS WITH EXPERIMENTAL DATA FOR FLUIDIZED BEDS:

In the theoretical modelling of flow through fluidized beds, considerable efforts have been spent on the prediction of minimum

fluidization velocity and establishing the bed-expansion characteristics. Based on experimental evidence, some researchers developed equations relating the relative velocity ratio of the assemblage to the bed void fraction. Here the relative velocity ratio refers to the ratio of the actual velocity of the assemblage U_∞, to the terminal free fall velocity of the single sphere U_o. The pioneering work in this direction concerning a homogeneous fluidized bed was by Richardson and Zaki (1954). Several other investigators such as Lewis and Bowerman (1952), Letan (1974), Garside and Al-Dibouni (1977) followed the same approach and proposed somewhat different forms of equations. These correlations have been summarised by Couderc (1985), Khan and Richardson (1985), etc.

The drag results of the present study were used to provide a general fluidization correlation which is more useful for design and analysis (Zenz & Othmer, 1960) by replotting the drag coefficient variation with Reynolds number and porosity data in terms of $(C_D\ Re^2)^{1/3}$ against $(Re/C_D)^{1/3}$ with porosity as a parameter. Such a plot is presented in Figure 5.26 The plot is useful as it essentially relates the particle velocity particle diameter with physical properties as fixed parameters, i.e.

$$(C_D\ Re^2)^{1/3} = d_p \left(\frac{4}{3} \frac{\rho(\rho_p-\rho)\ g}{\eta^2} \right)^{1/3} \qquad (5.2)$$

$$(Re/C_D)^{1/3} = U_\infty \left(\frac{3\rho^2}{4\eta\ (\rho_p-\rho)\ g} \right)^{1/3} \qquad (5.3)$$

The relationship between the relative velocity ratio, (U_∞/U_o) and the porosity ($\in$) can be obtained simply by drawing a line parallel

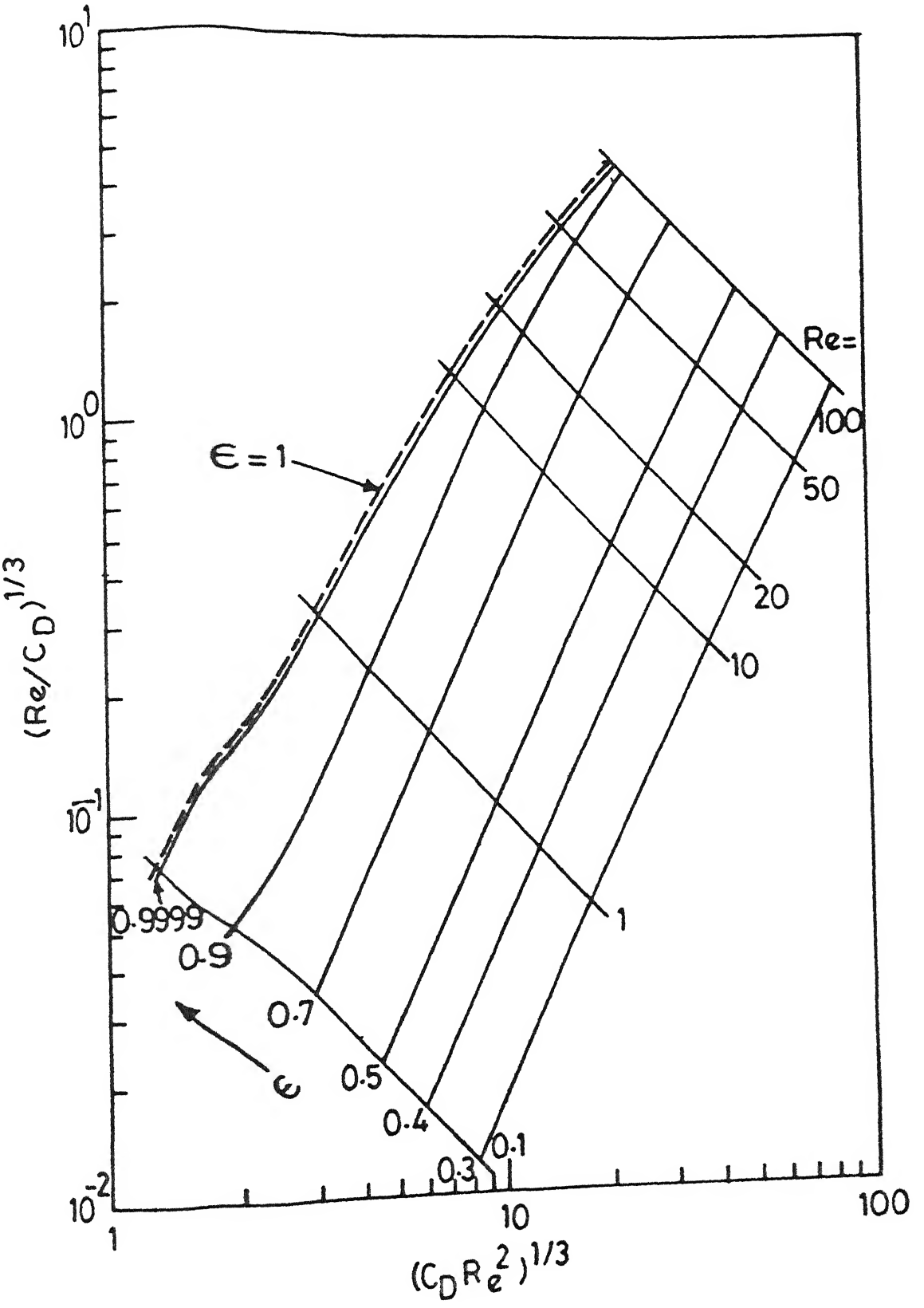

Fig 5.26 Zenz correlation for fluidization.

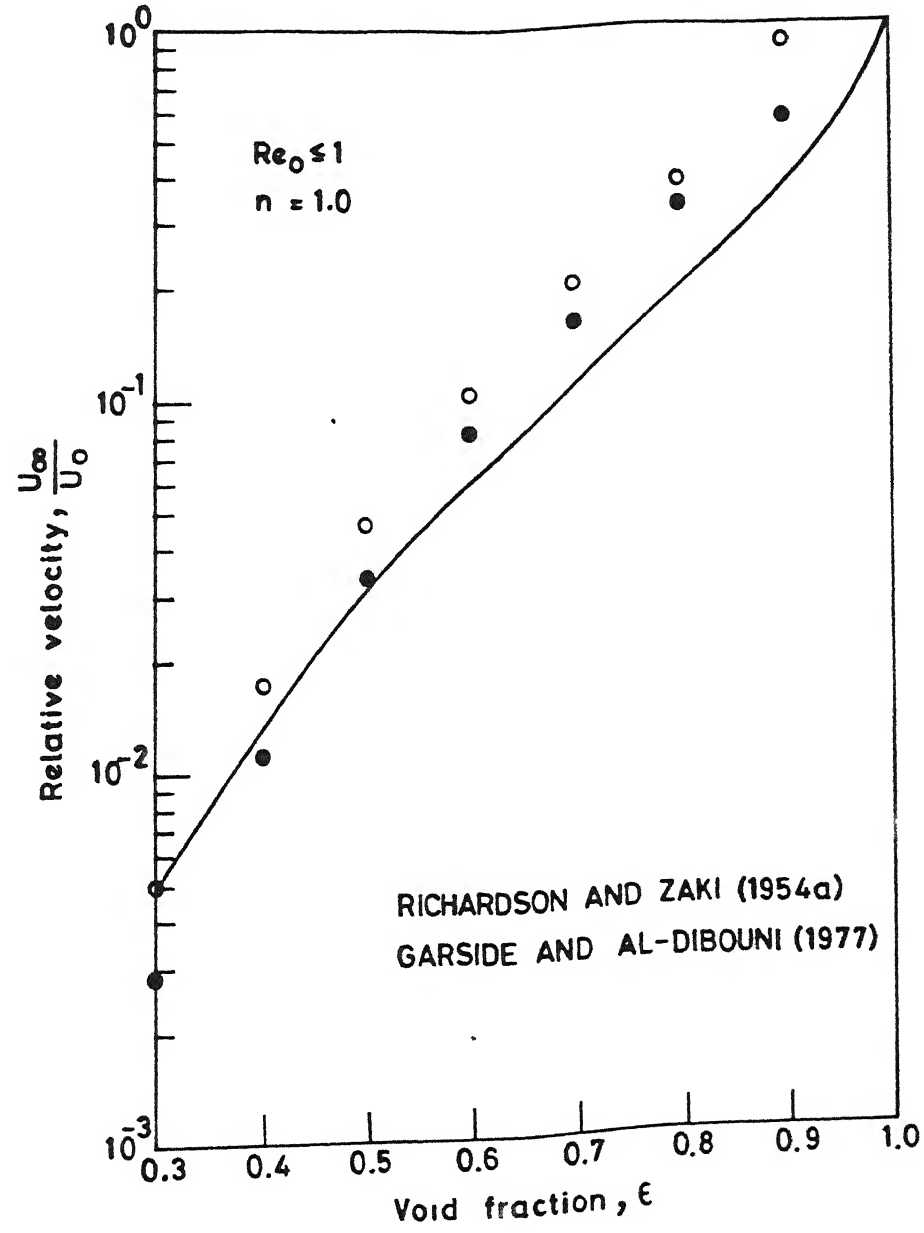

Fig. 5.27 Variation of relative velocity ratio (U_∞/U_o) with voidage for $Re_o \leq 0.1$. Comparison with the predictions of Richardson and Zaki (1954a) and Garside and Al-Dibouni (1976).

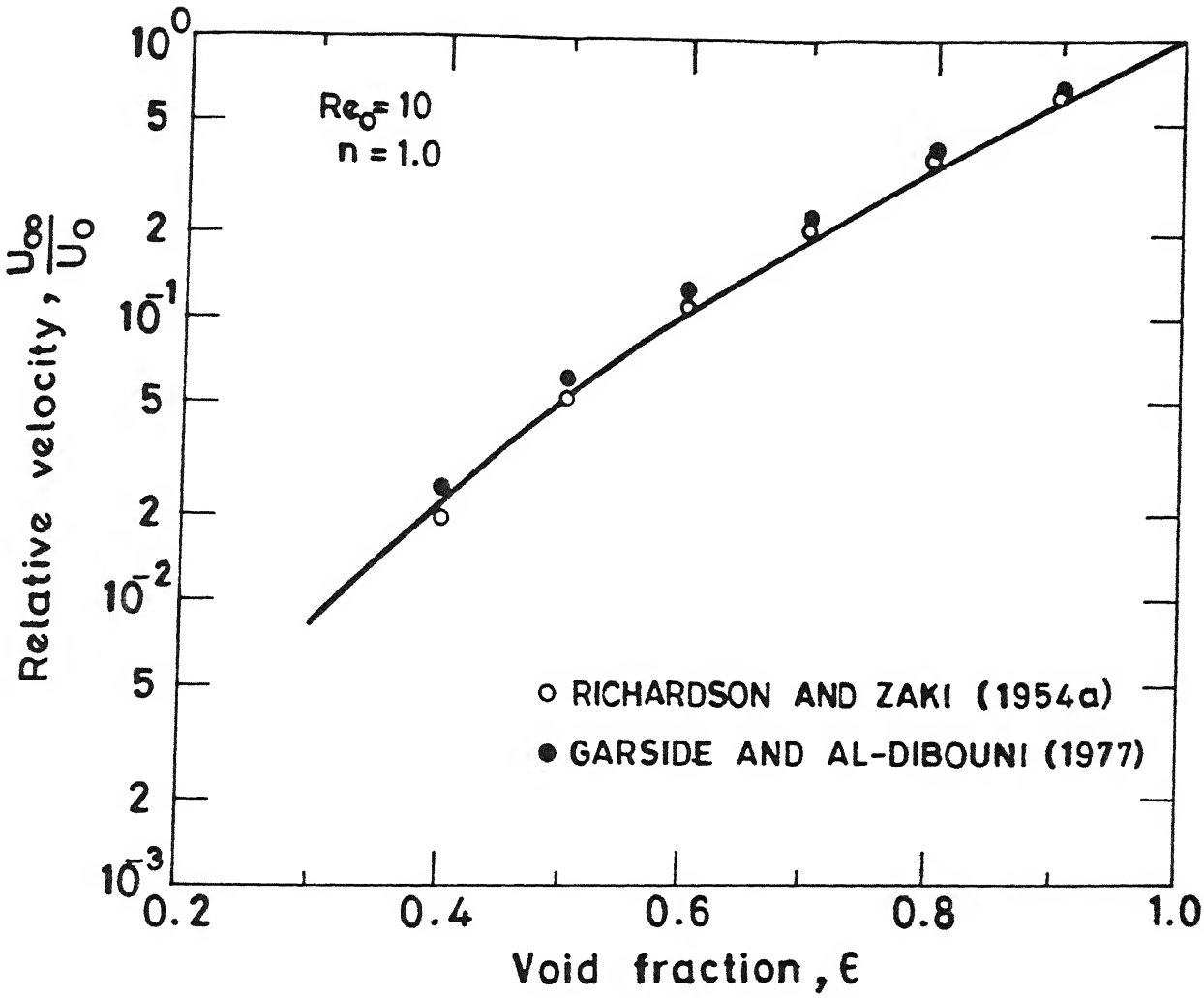

Fig. 5.28 Variation of relative velocity ratio (U_∞/U_o) with voidage for Re_o = 10. Comparison with the available results.

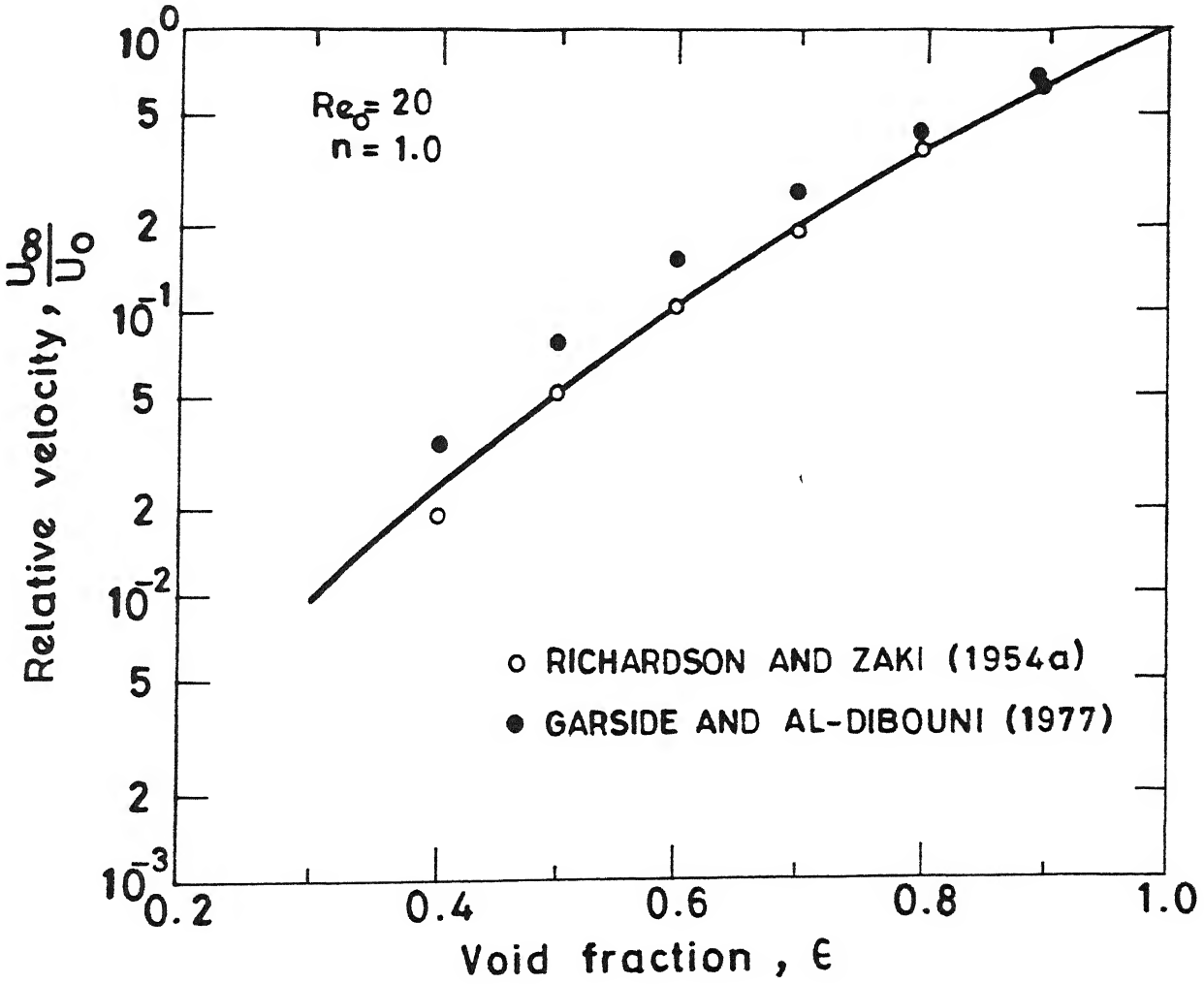

Fig. 5.29 Variation of relative velocity ratio (U_∞/U_o) with voidage for Re_o = 20. Comparison with the available results.

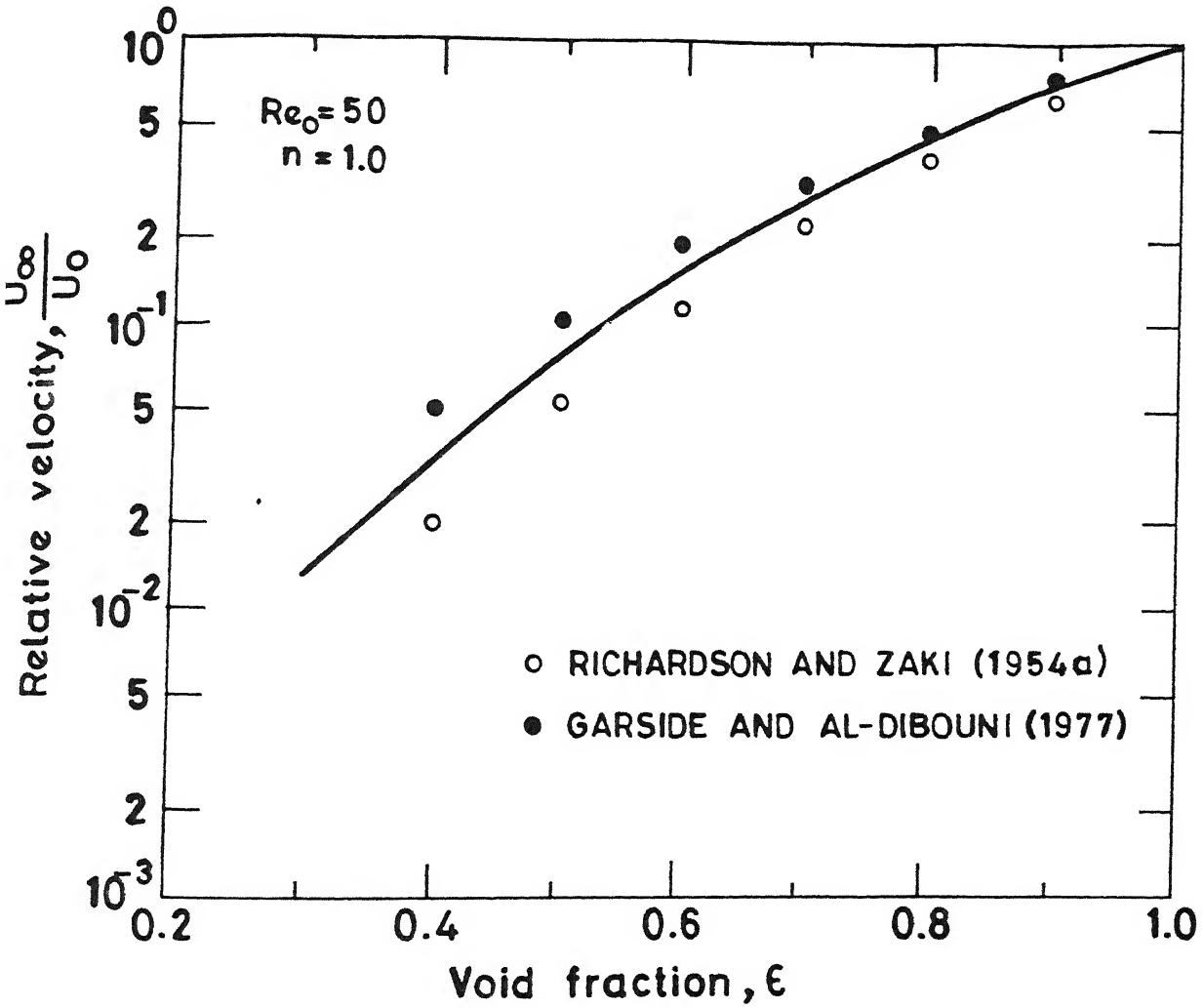

Fig 5.30 Variation of relative velocity ratio (U_∞/U_o) with voidage for Re_o = 50 Comparison with the available results.

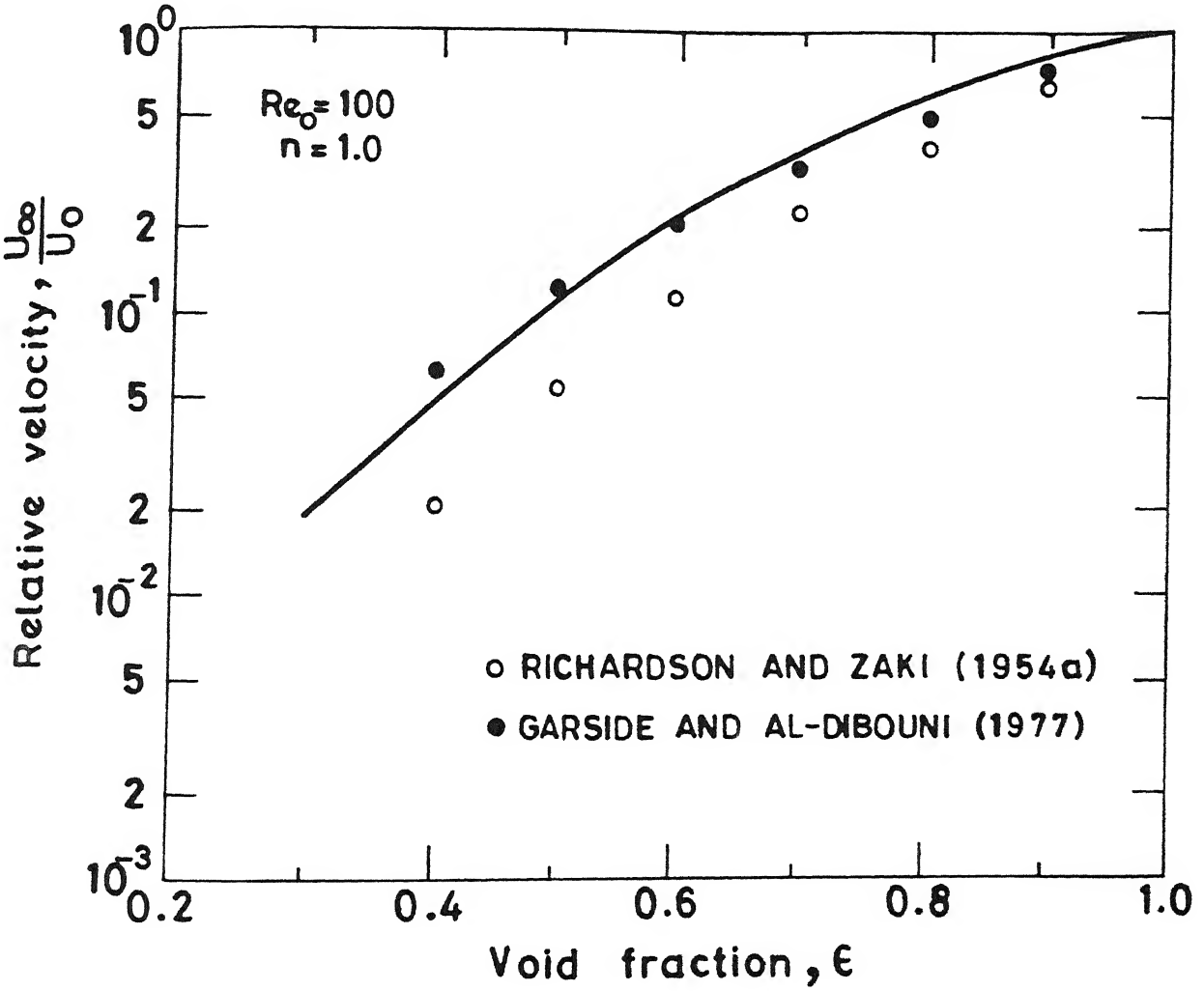

Fig. 5.31 Variation of relative velocity ratio (U_∞/U_o) with voidage for Re_o = 100 Comparison with the available results.

to $(Re/C_D)^{1/3}$ axis through the particular particle diameter or free settling Reynolds number desired The variation of relative velocity ratio over a range of voidage (0 4 to 1.0) at several different Reynolds numbers (Re_o = 0 1, 10, 20, 50, 100) are shown in Figures 5.27 to 5.31. On these figures, the predictions of correlation by Richardson and Zaki (1954a) which is believed to represent reasonably most of the experimental data are also shown for comparison purpose. In order to provide more comparison with experimental data, the predictions of the popular correlation by Garside and Al-Dibouni (1977) are also shown in these figures

For low Reynolds number ($Re_o \leq 0.1$), the present numerical results lack good agreement with the predictions of Richardson and Zaki as well as Garside and Al-Dibouni. At the lowest end of fluidized bed voidage, ϵ = 0 4, the present results are found to deviate from those of Richardson and Zaki by 17% which increases to about 30% at ϵ = 0 5. At still higher voidage ($\epsilon > 0.5$) the deviation increases to 50% or more. Earlier Happel (1958) made exhaustive comparison of free surface cell model results for creeping flow with large number of experimental results of several investigators for fluidized beds. He also observed the lack of agreement between theoretical predictions and experimental results. One of the reasons for such disagreement could be the agglomeration and circulation effects which will result in increased value for relative velocity. It is to be mentioned here that the voidages measured in experiments are average quantities and the actual distribution of particles may not be uniform,

whereas, the free surface cell model assumes a uniform particle distribution.

At intermediate Reynolds number ($1 \leq Re_o \leq 100$) the agreement between the present numerical results and predictions of Richardson and Zaki (1954) considerably improves. At $Re_o = 20$, the two results show excellent agreement and except at $\epsilon = 0.4$ where the deviation between the two results is 25%, at all other voidages the two results differ by less than 6% At $Re_o = 50$, the deviation between present results and those of Richardson and Zaki again increases At low voidages ($\epsilon = 0.4$ and 0.5), it is observed to be about 50% which is found to be limited to 20% at higher voidages ($0.9 \leq \epsilon \leq 0.6$) At $Re_o = 100$, the deviation between the two results are found to be more than 60% at lower voidage and around 40% for higher voidage. There are several possibilities for the observed trend of results; (a) The free surface cell model breaks down beyond $Re_o > 20$, (b) Secondary effects take place in actual experiments

5.7 COMPARISON OF PREDICTED RESULTS WITH EXPERIMENTAL RESULTS FOR SINGLE SPHERES:

The behaviour of free surface cell model in dealing with the extremely dilute assemblages has been identified by comparing the present results with the prediction of the empirical correlations to estimate the resistance experienced by a single sphere in its motion through a fluid. It is well known that an analytical solution has been so far possible only for the creeping flow past a sphere ($Re \leq 0.1$). For intermediate Reynolds number, numerical solutions (Hamielec et.al., 1967; Rimon and Cheng, 1969) are

available but they are limited to Re ≤ 400 Numerous empirical correlations based on experimental data have been proposed by investigators to cover a wider range of Reynolds number. The effect of boundary has also been extensively studied These empirical correlations have been summarised by Clift et.al. (1978) in their excellent treatise. More recently Khan and Richardson (1987) reviewed various empirical correlations available in literature. One of the correlations given by Lapple and Shephard has also been reproduced in Chemical Engineers Handbook (Perry and Chilton, 1973).

In a theoretical modelling, one would intuitively expect that when the cell radius becomes infinitely large the cell model should approach the limiting case of a single sphere moving in an infinite expanse of fluid. However, it is virtually impossible to simulate these conditions in numerical work owing to the computing requirement becoming prohibitively exorbitant. Thus, one has to arbitrarily fix the cell boundary at a sufficiently large distance to simulate the conditions corresponding to that of a single sphere. In the present study, a very high value of voidage (ϵ = 0.9999) has been used to investigate the limiting behaviour of the free surface cell model. The above value of ϵ refer to the cell to particle radius ratio of 21 47.

From the available evidence on wall effects (Clift et.al. 1978) for spheres-in-tube configuration, it is known that the wall effect decreases with the increasing Reynolds number One expects at least qualitatively a similar effect of cell radius in case of sphere-in-sphere configuration of the spherical cell model.

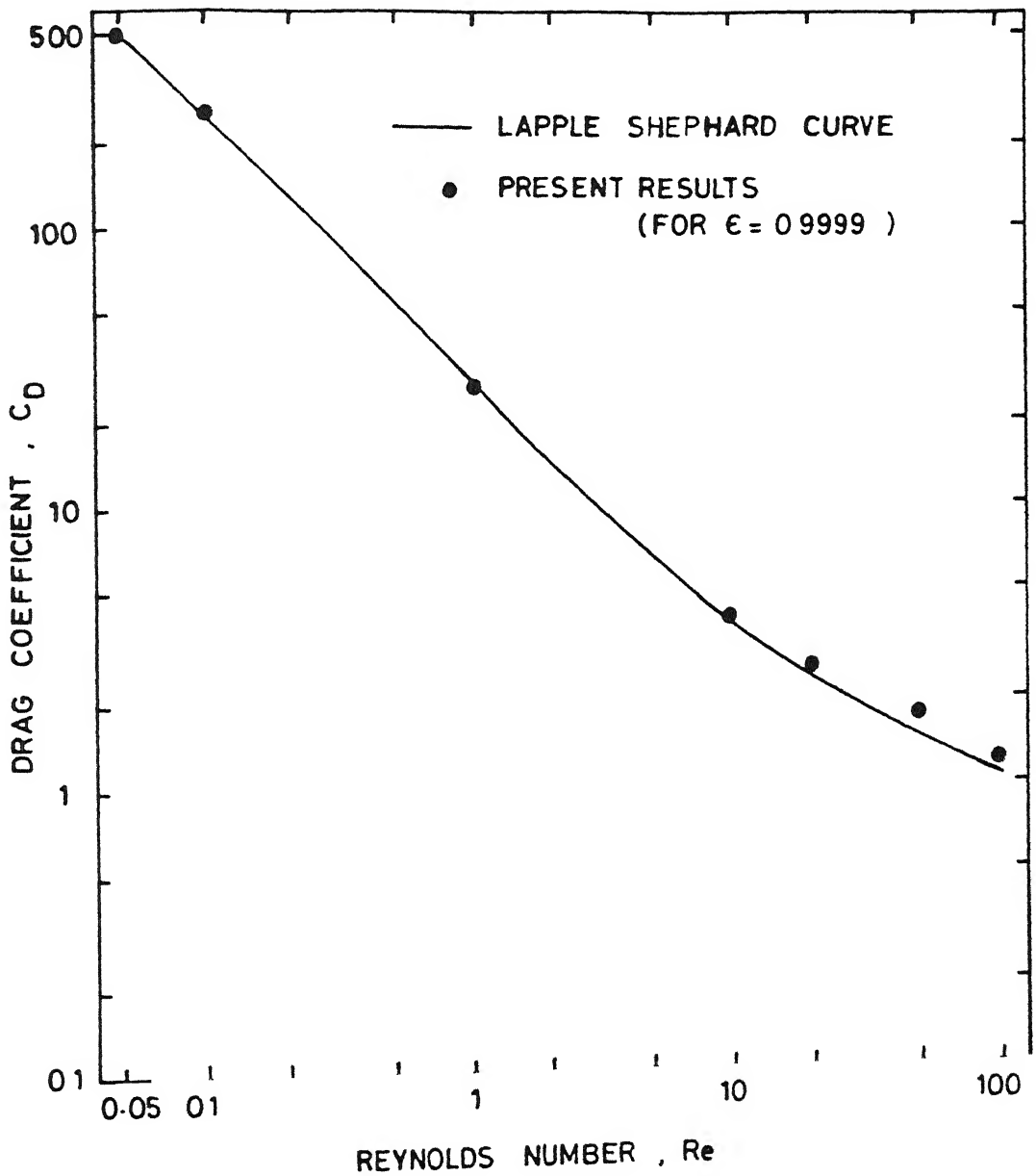

Fig. 5.32 Comparison of present numerical results (ϵ = 0.9999) with Lapple Shephard curve for single spheres.

The present numerical results (for ϵ = 0 9999) are compared in Figure 5.31 with the widely used Lapple-Shephard curve in the range $0.001 \leq Re \leq 100$. The results are in good agreement (within 5% or so) upto about $Re \simeq 30$ but begin to diverge appreciably at higher Reynolds number values It is, however not at all clear whether such a poor correspondence (for $Re > 30$) is due to inaccuracy of numerical results or due to degree of uncertainty inherent in Lapple-Shephard equation or due to the combination of both. With regards to the creeping flow regime, it was mentioned in Chapter IV that present drag results for $\epsilon = 0.9999$ are in close agreement (within 1.3%) with the analytical results of Happel (1958). It is also to be mentioned here that Gu and Tanner (1985) studied the creeping motion of a sphere in the power law type non-Newtonian fluids Though they have not stated it explicitly, their flow configuration and boundary conditions are equivalent to the one used in the present study. They have given a formulae which allows the estimation of the extent of wall effects (for sphere-in-sphere configuration) on drag coefficients for the creeping motion of a sphere in Newtonian fluid. This is expressed as

$$C_D = C_{Dst} \left[1 - 1.5 \frac{R_c}{R_p} + 0 \left(\frac{R_c}{R_p} \right)^5 \right]^{-1} \qquad (5.4)$$

where C_{Dst} is the Stokes drag ($C_{Dst} = 24/Re$) R_c and R_p are the cell radius and particle radius respectively. For $\epsilon = 0.9999$ and $Re = 0.001$, the present result agrees with that of Gu and Tanner within 1.3%. In fact, the drag coefficient evaluated from above expression is exactly equal to the drag coefficient obtained from

the analytical expression by Happel (1958). In the light of foregoing discussion, it is evident that free surface cell model satisfactorily predicts the momentum transfer in a dilute assemblage of particles upto Re $\simeq$ 20 and this may safely be taken as the upper limit for applicability of free surface cell model.

Before concluding this chapter, it is felt desirable to compare the performance of present model with other spherical model, namely, the zero-vorticity cell model in the following section.

5.8 COMPARISON WITH ZERO VORTICITY CELL MODEL

It is of interest to assess the relative performance of the free surface and zero vorticity cell models over a range of Reynolds numbers. Numerical results for the latter model have been presented by Leclair and Hamielec (1968). The predictions of the two models for packed beds ($0.3 \leq \epsilon \leq 0.6$) have been compared in Table 5.2. The predictions of Ergun equation are also included in this table. In the packed bed range there are only two values of voidage which are common to both studies. An examination of Table 5.2 shows that the free surface cell model performs consistently better than the zero vorticity model in the creeping flow region (Re $\leq$ 10) whereas, the latter is a better predictor in the range Re $>$ 10 or so. Furthermore, it is clearly seen that the zero vorticity cell model always yields the values of friction factor which are higher than those based on free surface cell model. This is mainly due to the exchange of energy with other cells in the case of zero vorticity model. This conclusion is in

Table 5.2: Relative performance of free surface and zero vorticity cell models against the predictions of Ergun's equation.

Re	Ergun's Eqn.	Zero Vorticity Model (Le Clair & Hamielec)		Free Surface Cell Model (Present)	
	f_{bk}	f_{bk}	% Deviation from Ergun	f_{bk}	% Deviation from Ergun
VOIDAGE (ϵ) = 0 4					
0.1	901.75	1084.8	+ 20.29	983.0	+ 9.01
1.0	90.75	108.48	+ 18.23	98.30	+ 7.13
5.0	19.75	-	-	19.66	- 0.45
10.0	10.75	10.89	+ 1.30	9.88	- 8.09
20.0	6.25	5.472	- 12.44	4.927	- 21 68
50.0	3.55	2.304	- 35.09	1.99	- 43.94
VOIDAGE (ϵ) = 0.5280*					
0.1	709.75	1019.099	+ 43.58	821.25	+ 15.71
1.0	72.55	101.908	+ 40.55	82.125	+ 13.11
10.0	8.83	10.251	+ 16.09	8.2246	- 6 856
20.0	5.29	5.218	- 1.36	4.1311	- 21.90
50.0	3.166	2.313	- 26.94	1.6975	- 46.384

* Calculated only for the purpose of comparison with the results of Le Clair & Hamielec (1968).

line with the findings of others (e g. Happel and Brenner, 1965; El-Kaissy and Homsy, 1973)

The performance of the two models in predicting the relative velocity ratio (Superficial velocity/Free fall velocity of a single sphere) for flow through fluidized beds at low Reynolds number has been compared in Fig. 5.28 The results of free surface cell model are found to be in close agreement with the predictions of Richardson and Zaki correlation.

5.9 CONCLUSIONS

Detailed comparison with the analytical solution of Happel suggests that the present numerical results are accurate to within 1.5% in the creeping flow regime It also suggests that the free surface cell model, owing to strong convective effects, does not provide a good description of flow through multi-particle systems for Re $\geq$ 30. The analysis of detailed results has also clearly demonstrated that as far as the drag values are concerned, the approximation of creeping flow ($C_D Re$ = constant) holds good upto about Re $\approx$ 10-20 depending upon the value of bed voidage. This conclusion is also corroborated by the surface pressure and shear stress variations in the same range of Reynolds number values. Streamline plots lend further support to this conclusion. The pressure field deviates most from the creeping flow results among all the flow variables as Reynolds number is increased, although this does not affect the drag behaviour significantly. The total drag coefficient draws varying proportions of contributions from pressure and surface shear stress respectively depending upon the value of voidage. In low voidage systems, the drag is dominated

by pressure but the latter contribution decreases as the voidage increases This phenomenon has been explained qualitatively via the angular velocity profiles In the limiting case of a single sphere, notwithstanding the complexity of wall effects, the present results in the creeping flow region show an excellent agreement with the existing analytical solution, however, the correspondence is only moderate for Re > 20

The relative velocity ratio data for fluidized beds show lack of agreement with the predictions of Richardson and Zaki correlation in the creeping flow regime However, the agreement between the two improves with increasing Reynolds number, at Re = 20, the deviation between the two results for all voidages corresponding to fluidized bed system ($0.8 \geq \epsilon \geq 0.4$), is found to be less than 8%. With further increase in Reynolds number, the two results begin to diverge again

Based on the comparison with the widely used Ergun equation for flow through packed beds, it appears that the free surface cell model is a better predictor upto about Re < 10 and beyond this value, the zero vorticity cell model is superior, thereby making them complimentary to each other.

CHAPTER VI

RESULTS AND DISCUSSION - NON-NEWTONIAN FLOW PAST MULTI-PARTICLE ASSEMBLAGES

Steady flow of an incompressible power law type non-Newtonian fluid through an assemblage of rigid spherical particles has been investigated. Comprehensive results on the detailed structure of flow field as well as the macroscopic parameters such as drag coefficients have been obtained over a wide range of fluid behaviour ($1 \leq n \leq 0.2$), bed voidage ($0.3 \leq \epsilon \leq 0.9999$) and flow conditions ($20 \leq Re \leq 0.001$). The variation of the total and the individual drag coefficients (C_D, C_{DP} and C_{DF}) under the combined influence of the non-Newtonian characteristics of the fluid and the concentration of assemblage are highlighted with the help of the corresponding stress and velocity profiles existing around a typical particle. Although, drag coefficients and flow field results have been computed numerically at several values of Reynolds number in the range $1 \leq Re \leq 20$, only the drag behavior at $Re = 20$ has been discussed with the aid of the surface stresses in section 6.2, for the sake of brevity. Finally, the numerical results reported herein are compared with the appropriate theoretical and experimental results available in literature for packed beds, fluidized beds and flow around single spheres.

The objective of the present investigation has been to elucidate the effects of n and ϵ on the flow field and drag

coefficients for both creeping and intermediate Reynolds number flows. The flow field at intermediate Reynolds number is inherently different from the creeping flow field due to the presence of inertial forces. Therefore, in order to distinguish the effects of inertial forces, the results for low and intermediate Reynolds number flows have been discussed here in two separate sections.

6.1 LOW REYNOLDS NUMBER FLOW

In this section, the results are presented for only one value of Reynolds number, i e. Re = 0.001; this value of Re is considered to be sufficiently small so as to render the inertial effects negligible. As stated earlier, the objective has been to identify the combined influence of flow behaviour index and bed voidage on flow field and drag coefficients.

6.1.1 Drag Phenomena

Friction, pressure and total drag coefficients for the range of voidages ($\in$ = 0.3 to 0.9999) and power law indices (n = 0.2 to 0.8) are plotted in figures 6.1, 6.2 and 6.3. For reference purpose the drag coefficients are also summarized in Table 6.1.

With reduction in n, the viscous resistance weakens owing to the shearthinning behaviour of the fluid and this is manifested by a decrease in friction drag coefficient. The variation of log C_{DF} with n is almost linear from n = 1 to 0.5 and appears to obey a relationship of the form $C_{DF} \propto x^n$, upto about $n \simeq 0.5$. However, as the value of n drops below 0.5, the numerical results veer away from the postulated power law behaviour. By analogy with the power law fluid model, one would intuitively expect the quantity x

Table 6.1 Drag Coefficients for Creeping (Re = 0.001) motion of an assemblage of spheres in power law fluid

n	C_{DP}	C_{DF}	C_D	$\frac{C_{DP}}{C_{DF}}$	$Y = \frac{C_D Re}{24}$
ϵ = 0.3					
1.0	0.4333×10^7	$0\ 1210 \times 10^7$	$0\ 5543 \times 10^7$	3 580	230 95
0.9	0.2590×10^7	$0\ 7338 \times 10^6$	$0\ 3323 \times 10^7$	3 529	138 45
0.8	0.1538×10^7	0.4473×10^6	$0\ 1985 \times 10^7$	3 438	82.70
0.6	0.5298×10^6	0.1554×10^6	$0\ 6873 \times 10^6$	3.3638	28 63
0.4	0.1709×10^6	0.5731×10^5	$0\ 2282 \times 10^6$	2.982	9 50
0.2	0.3796×10^5	0.2020×10^5	0.5816×10^5	1 879	2 423
ϵ = 0.4					
1.0	0.1438×10^7	0.6086×10^6	$0\ 2047 \times 10^7$	2 362	85.291
0 9	0.9199×10^6	0.3960×10^6	0.1315×10^7	2 322	54 79
0.8	0.5846×10^6	0.2586×10^6	$0\ 8432 \times 10^6$	2.260	35 133
0 6	0.2297×10^6	$0\ 1043 \times 10^6$	$0\ 3340 \times 10^6$	2 20	13.916
0.4	0.8303×10^5	$0\ 4371 \times 10^5$	0.1267×10^6	1.89	5.279
0.2	0.2341×10^5	0.1794×10^5	$0\ 4135 \times 10^5$	1.30	1.722
ϵ = 0.5					
1.0	0.5645×10^6	0.3433×10^6	$0\ 9077 \times 10^6$	1 644	37.82
0.9	0.3846×10^6	0.2373×10^6	0.6219×10^6	1.62	25.91
0.8	0.2589×10^6	$0\ 1644 \times 10^6$	$0\ 4233 \times 10^6$	1 574	17.63
0.6	0.1133×10^6	$0\ 7524 \times 10^5$	$0\ 1885 \times 10^6$	1.505	7.854
0.4	0.4483×10^5	0.3523×10^5	0.8006×10^5	1.27	3.335
0.2	0.1259×10^5	0.1605×10^5	0.2864×10^5	0.78	1.193
ϵ = 0.7					
1.0	0.1144×10^6	0.1289×10^6	$0\ 2433 \times 10^6$	0.887	10.13
0.9	0.8651×10^5	0.9898×10^5	0.1854×10^6	0.874	7.725
0.8	0.6486×10^5	0.7598×10^5	0.1408×10^6	0.853	5.86
0 6	0.3384×10^5	0.4332×10^5	0.7716×10^5	0 781	3 215
0 4	0.1566×10^5	0.2475×10^5	0.4041×10^5	0.632	1 683
0.2	0.5986×10^4	0.1376×10^5	0.1975×10^5	0 434	0.822

$\epsilon = 0.9$

0 1	0.2643×10^5	0.4803×10^5	0.7446×10^5	0 550	3.102
0 8	0.2007×10^5	0.3660×10^5	0.5607×10^5	0 557	2 361
0 6	0.1421×10^5	0.2621×10^5	0.4042×10^5	0 542	1 684
0.4	0.9564×10^4	0.1817×10^5	0.2770×10^5	0.526	1 154
0 2	0.6078×10^4	0.1166×10^5	0.1774×10^5	0 520	0 739

$\epsilon = 0.99$

1 0	0.1170×10^5	0.2387×10^5	0.3557×10^5	0.490	1 482
0 8	0.1195×10^5	0.2266×10^5	0.3461×10^5	0 527	1.442
0 6	0.1222×10^5	0.2054×10^5	0.3267×10^5	0 597	1.361
0.4	0.1197×10^5	0.1648×10^5	0.2845×10^5	0 725	1.185
0.2	0.1162×10^5	0.1132×10^5	0.2294×10^5	1 025	0.9562

$\epsilon = 0.999$

1.0	0.1012×10^5	0.2114×10^5	0.3129×10^5	0.480	1.303
0 8	0.1151×10^5	0.2182×10^5	0.3333×10^5	0.527	1.380
0.6	0.1273×10^5	0.2060×10^5	0.33338×10^5	0 617	1.389
0.4	0.1372×10^5	0.1664×10^5	0.3036×10^5	0 824	1.265
0.2	0.1410×10^5	0.1144×10^5	0.2554×10^5	1.232	1.064

$\epsilon = 0.9999$

1 0	0.8226×10^4	0.1784×10^5	0.2607×10^5	0.461	1.086
0.8	0.1036×10^5	0.2042×10^5	0.3078×10^5	0.5073	1.2825
0.6	0.1192×10^5	0.1977×10^5	0.3169×10^5	0.602	1.320
0.4	0.1305×10^5	0.1598×10^5	0.2903×10^5	0.816	1 209
0.2	0.1362×10^5	0.1134×10^5	0.2496×10^5	1.20	1.04

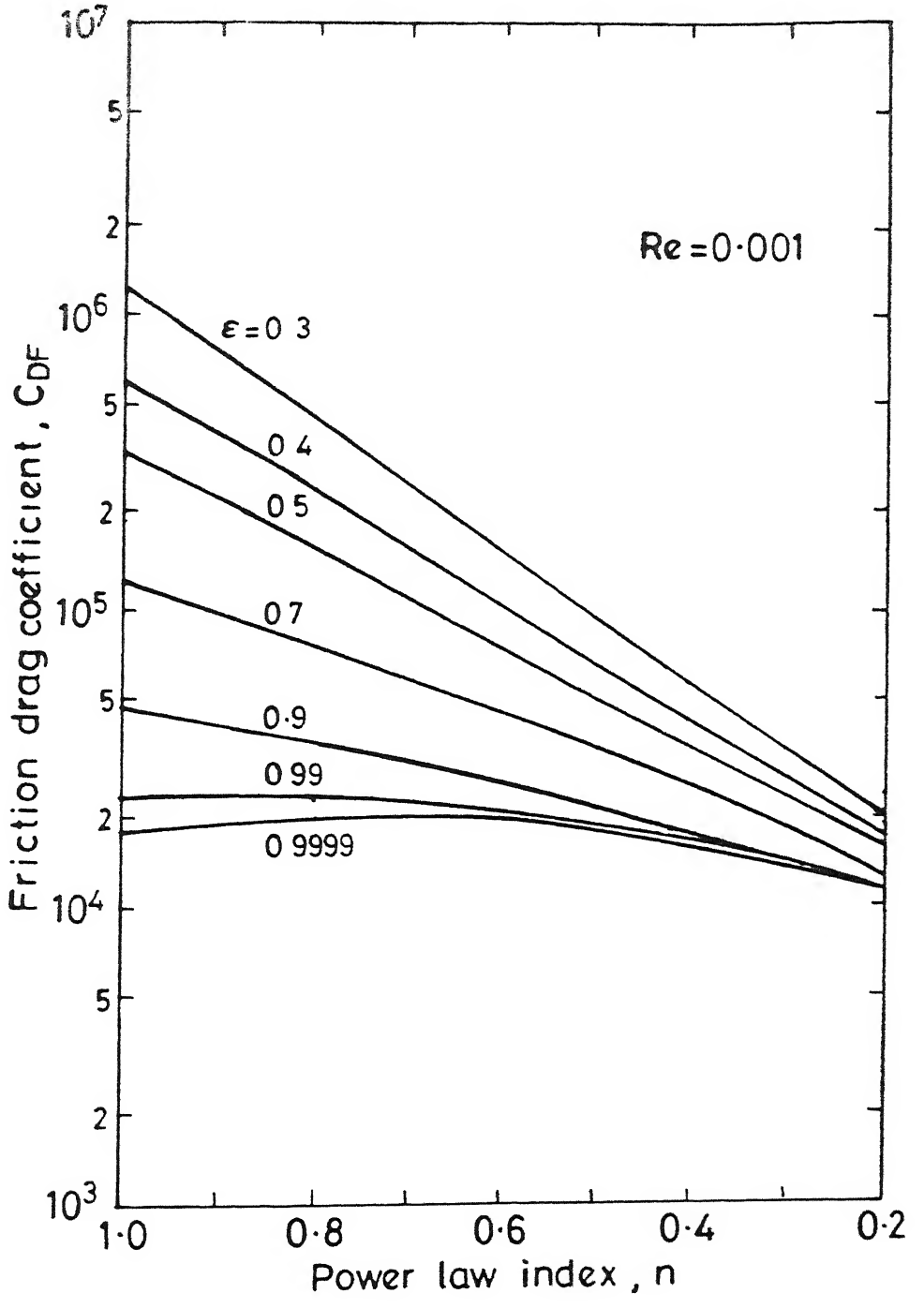

Fig. 6 1 Variation of friction drag coefficient with power law index and voidage, for Re = 0.001

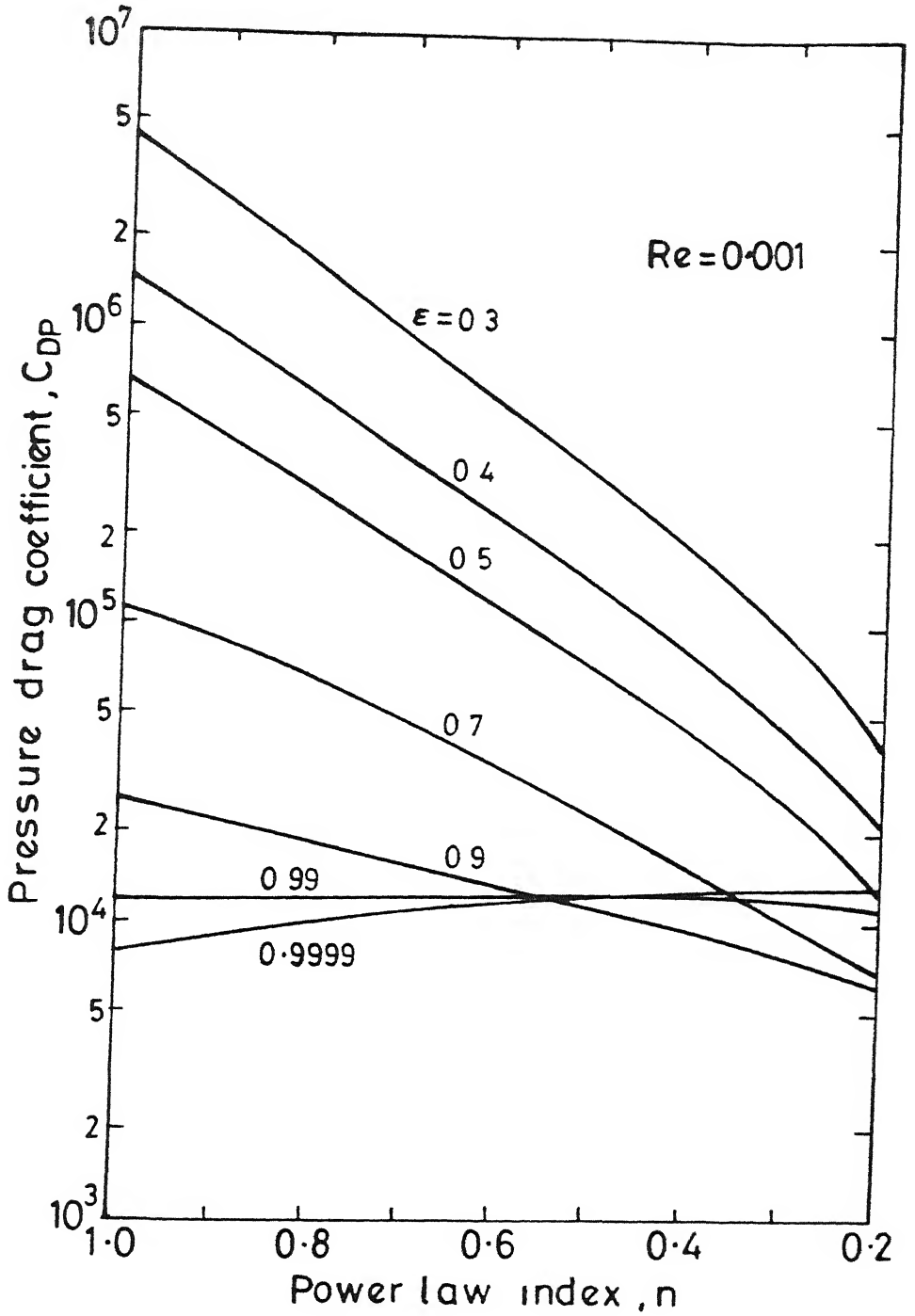

Fig. 6.2 Variation of pressure drag coefficient with power law index and voidage, for Re = 0.001.

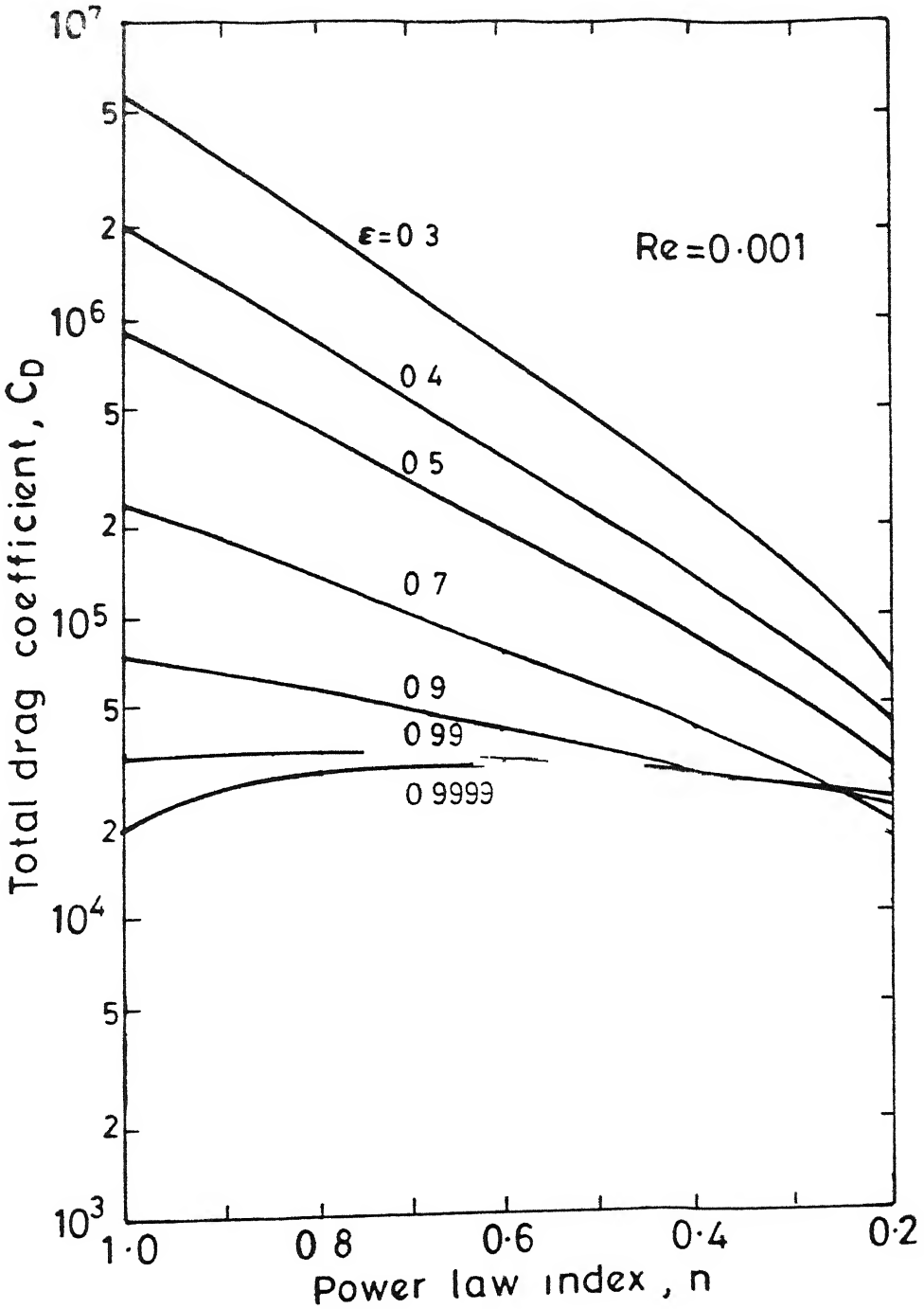

Fig. 6.3 Variation of total drag coefficient with power law index and voidage, for Re = 0.001.

to be some sort of average shear rate on the particle surface. An order of magnitude analysis (outlined in Appendix - II) indeed suggests that the value of x is approximately proportional to the average surface shear rate of a corresponding Newtonian fluid flow situation with the same values of Re and ϵ

A further examination of figure 6 1 reveals a decrease in the value of C_{DF} with increasing voidage (i e inter-particle separation) for a given value of n. It can be readily shown that in the case of dense assemblages, the average shear rate on the particle surface varies as $O(1/\delta^2)$, for a fixed value of n. Here δ refers to the radial gap between the particle and cell surface. It is also observed that the slope of log C_{DF} vs. n curve decreases with voidage. This lends further credence to the power law type of relation suggested above.

In the case of an extremely dilute assemblage ($\epsilon \simeq 0.9999$; $R_c/R_p \sim 20$), the dependence of C_{DF} is characterised by an initial increase ($0.6 \leq n \leq 1$) followed by a downward trend with increasing degree of shearthinning behaviour ($n \leq 0.6$). It is presumably so due to the fact that C_{DF} is predominantly determined by the shear stress prevailing in the vicinity of $\theta = \pi/2$ plane. The observed trend of C_{DF} with respect to n as $\epsilon \rightarrow 1.0$ is a direct consequence of shear stress behaviour around $\theta = \pi/2$ and this aspect is discussed in detail subsequently.

Now turning our attention to the behaviour of the pressure drag coefficient (C_{DP}) shown in Figure 6.2, it is seen that C_{DP} varies with n and ϵ in a qualitatively similar manner to that of C_{DF}. This is hardly surprising, since in creeping flow regime, the pressure and viscous forces locally balance each other

everywhere in the flow field In the case of dense assemblages (low values of ϵ), the pressure drag coefficient contributes more towards the total drag coefficient, this trend continues all the way upto ϵ = 0 99. However, as the limit of single sphere is approached, this trend reverses, i e , the total drag coefficient draws a larger contribution from the frictional drag than from the pressure drag This phenomenon can be clearly seen in Figure 6 4 where the ratio (C_{DP}/C_{DF}) is plotted as a function of n and ϵ. The switch over in the behaviour of C_{DF} and C_{DP} with variation in n in the limit of flow over a single sphere is possibly the reason for the drag coefficient attaining a maximum value around n ~ 0.6 or so, as has been reported by Crochet et.al., (1984) and Gu and Tanner (1985).

The fact that the total drag coefficient draws a larger contribution from the pressure drag in the case of dense assemblages, can be explained by the following simplified analysis. The momentum equation on the particle surface in θ direction can be written as

$$\frac{1}{r}\frac{\partial}{\partial r}(r\,\tau_{r\theta}) = \frac{1}{r}\frac{\partial p}{\partial \theta} \qquad (6.1)$$

Using the boundary conditions (3.20a, b) of the present formulation, the surface shear stress can be simlified as:

$$\tau|_{r=1} = (\eta\,\frac{\partial v}{\partial r})|_{r=1} \qquad (6.2)$$

Now, the orders of magnitudes of $\tau_{r\theta}$ and p appearing in equation (6.1) can be shown (See Appendix-II) to depend upon δ as:

$$\tau_{r\theta}|_{r=1} \propto 1/\delta^{2n} \qquad (6.3)$$

$$p|_{r=1} \propto 1/\delta^{2n+1} \qquad (6.4)$$

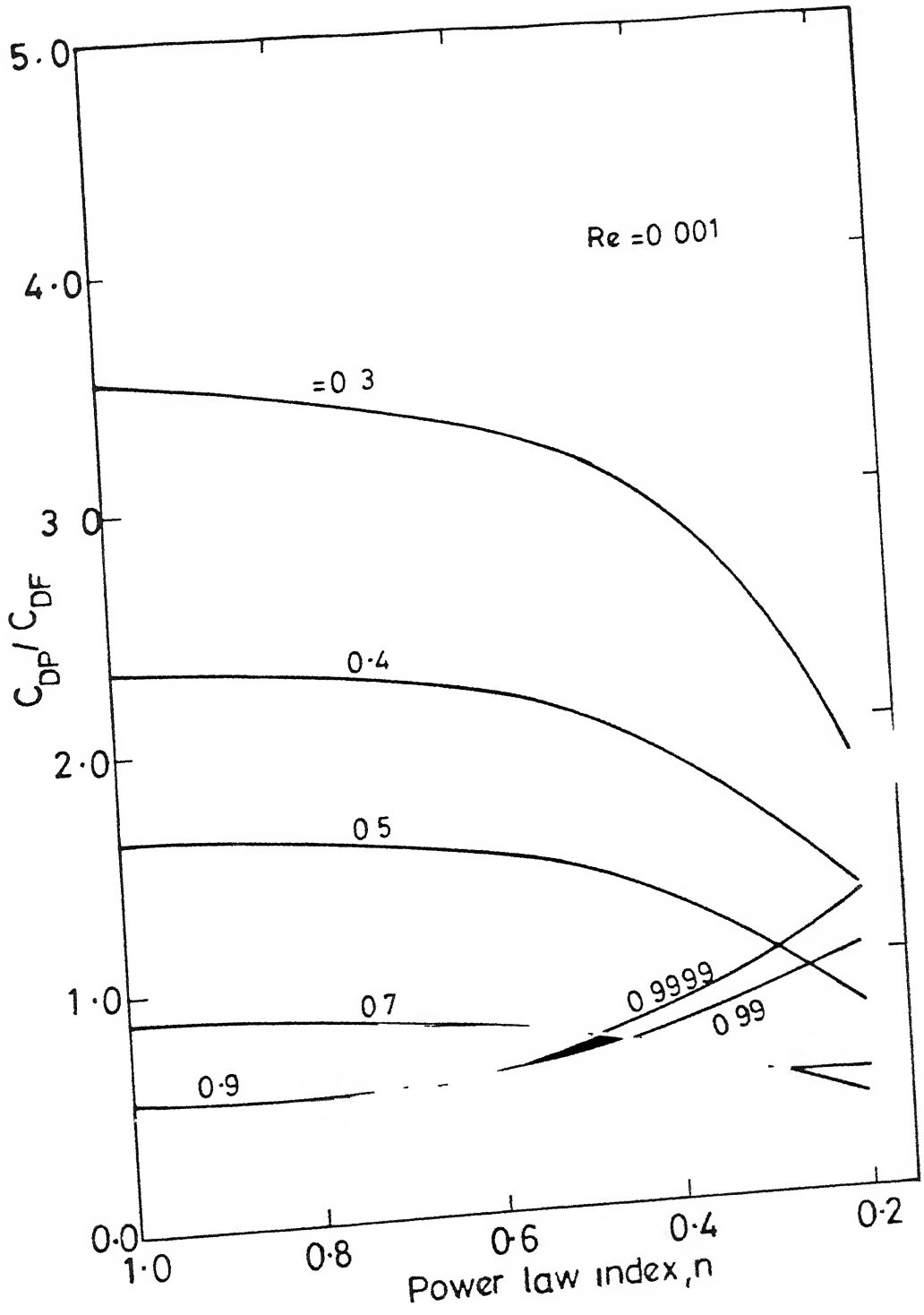

Fig. 6.4 Effect of the power law index and voidage on the ratio (C_{DP}/C_{DF}).

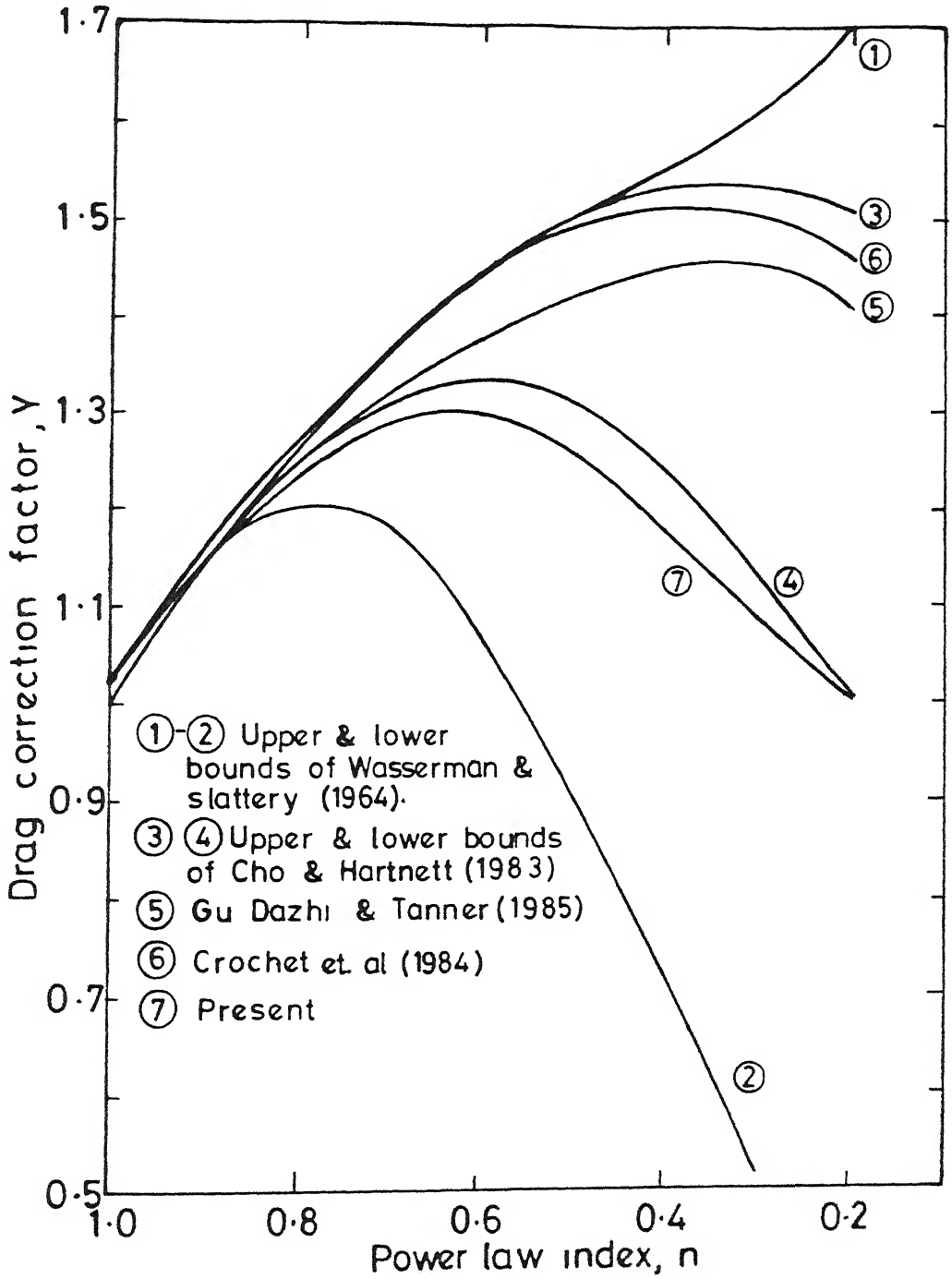

Fig. 6.5 Comparison of present numerical results (ϵ = 0.9999) with the results of other investigators for single sphere.

to be applicable in the range $0.5 \leq n \leq 1.0$ for the total drag coefficient also. This feature could be helpful in testing the rheological properties of a fluid vis-a-vis the power law model

The total drag behaviour in the extremely dilute range ($\epsilon \geq 0.9999$) which is close to the case of a single sphere, is shown in Figure 6.5. It is to be noted that at this voidage, the pressure and friction drag behaviour with respect to n are not similar. For instance, the pressure drag monotonically increases with decreae in n while the friction drag shows an initial mild increase and then a drop in the value beyond $n \simeq 0.5$. The combined effect of such variations of C_{DP} and C_{DF} leads to an initial rise in the value of C_D with its maximum occurring around $n \simeq 0.6$ followed by a sharp reduction for $n < 0.6$. It is to be mentioned here that for a single sphere situation the initial rise of total drag C_D is predominantly contributed by the pressure drag component while the subsequent drop in its value is solely due to friction drag component. In Fig. 6.5, the results of several other investigators available in literature are also plotted with the present results for the sake of comparison. A moot point to be noted is the wide deviation existing between the predictions of different investigators. This has already been illustrated earlier by Chhabra et.al. (1980). The present numerical results are closest to the lower bound predictions of Cho and Hartnett (1983).

6.1.2 Surface Stresses

It is generally acknowledged that the values of the integrated quantities such as drag coefficients, are determined by the stress fields prevailing around the particles, although exact

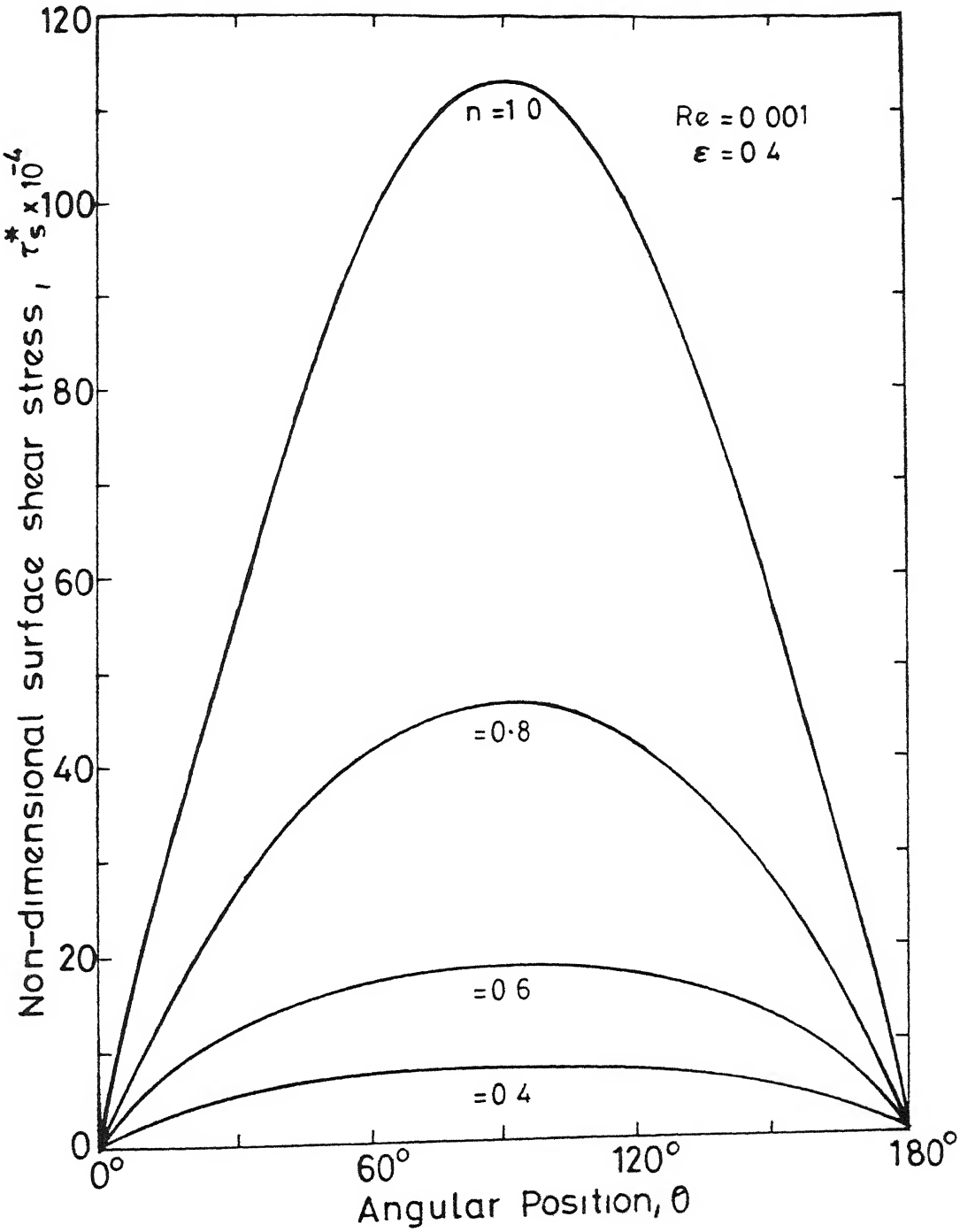

Fig 6.6a Variation of non-dimensional surface shear stress ($\tau_s/\rho U_\infty^2$) with angular position for various values of power law index and ϵ = 0.4.

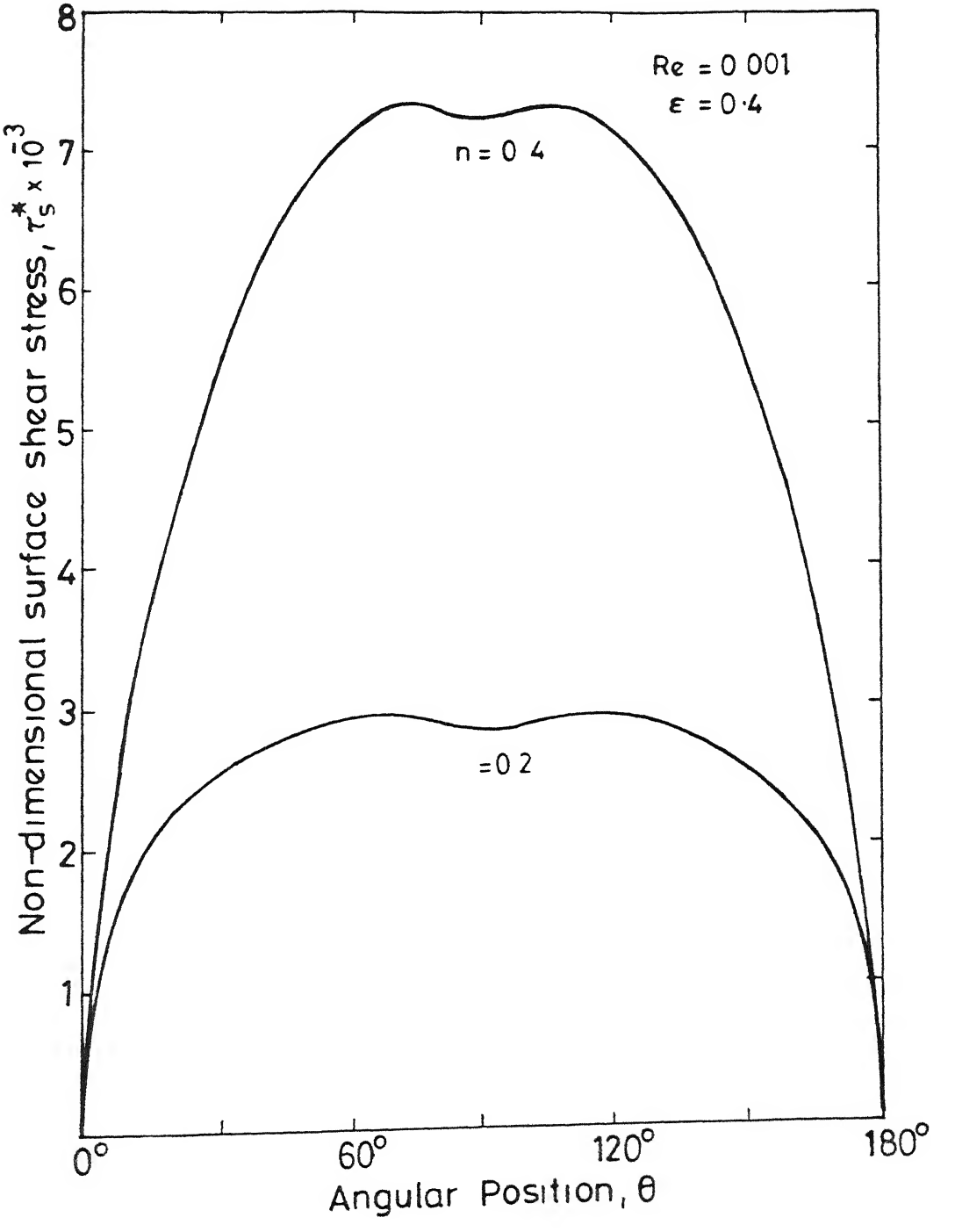

Fig. 6.6b Variation of surface shear stress ($\tau_s/\rho U_\infty^2$) with angular position for highly shearthinning fluids (n = 0.4 and 0.2) and ϵ = 0.4.

correspondence may not be exhibited between the surface stresses and drag. One can thus possibly attempt to explain the dependence of C_{DF}, C_{DP} and C_D on n and ϵ by examining the pressure and shear stress distribution over the particle surface. Though extensive results embracing wide ranges of values of n and ϵ have been obtained in this study, only representative stress profiles are discussed in greater detail here for the sake of brevity.

Figures 6.6a and 6.6b display the variation of surface shear stress with the power law index (n) for a constant value of ϵ = 0 4. As expected, the shear stress exhibits complete fore and aft symmetry for all values of n studied here, and also it varies in a sinusoidal manner for the Newtonian case. However, as the degree of shearthinning gradually increases, the surface shear stress shows an increasing tendency to flatten out, though still being symmetrical about $\theta = 90^{\circ}$ plane. This is solely attributable to the combined effects of the variation of local viscosity and shear rate. The local viscosity decreases from the axis upto the mid-plane ($\theta = 90^{\circ}$), whereas, the surface shear rate increases over the same domain. These two competing mechanisms appear to nullify each other around $\theta = 90^{\circ}$ plane, thereby leading to a plateau in shear stress profile. The flattening of the shear stress profile becomes increasingly evident as the value of n drops below 0.6. Furthermore, it is clearly seen in Figures 6.6a and 6.6b that for the range $0.6 \leq n \leq 1$, the maximum shear stress occurs at $\theta = 90^{\circ}$ plane, whereas, for highly shearthinning behaviour ($n \simeq 0.4$), the shear stress exhibits two maxima between $70^{\circ} \leq \theta \leq 110^{\circ}$, thereby giving rise to a cusp. This feature is clearly shown in Figure 6.6b on an expanded scale. Qualitatively

one can ascribe the formation of cusp to the aforementioned two competing mechanisms, i.e., the different rates of variation of viscosity and shear rate over the particle surface. A quantitative explanation for this phenomenon was sought by using the closed form stream function solution due to Kawase and Ulbrecht (1981a). However, a detailed analysis revealed only one extremum in shear stress at $\theta = 90^{o}$ plane It is not at all surprising as the analysis of Kawase and Ulbrecht is applicable only for n close to 1 whereas, the cusp is observed for highly shear thinning behaviour, i.e., $n \approx 0.4$ No more explanation can be given for this behaviour at this stage. It is also of interest to note that as the vlaue of n drops further from unity, the maximum surface shear stress decreases.

The surface shear stress distribution for a sparse assemblage ($\epsilon = 0.9$) is shown in figure 6.7 for various values of n. The variation is seen to be qualitatively similar to that for $\epsilon = 0.4$. The maximum shear stress decreases more or less uniformly with decreasing value of n, which can be explained by the gradual reduction in average shear rate on account of the large inter-particle distance.

Finally, the surface shear stress profile for an extremely dilute assemblage (in the limit of a single sphere) for $\epsilon = 0.9999$ ($R_c/R_p \approx 20$) is plotted in Figure 6.8. The maximum shear stress shows interesting trends with respect to the power law index (n). The value of τ_{max} seems to increase with power law index upto about $n \simeq 0.8$ Any further reduction in the value of n brings about a slow decrease in maximum shear stress initially, followed by a steep drop in τ_{max} for low values of n. Unlike in

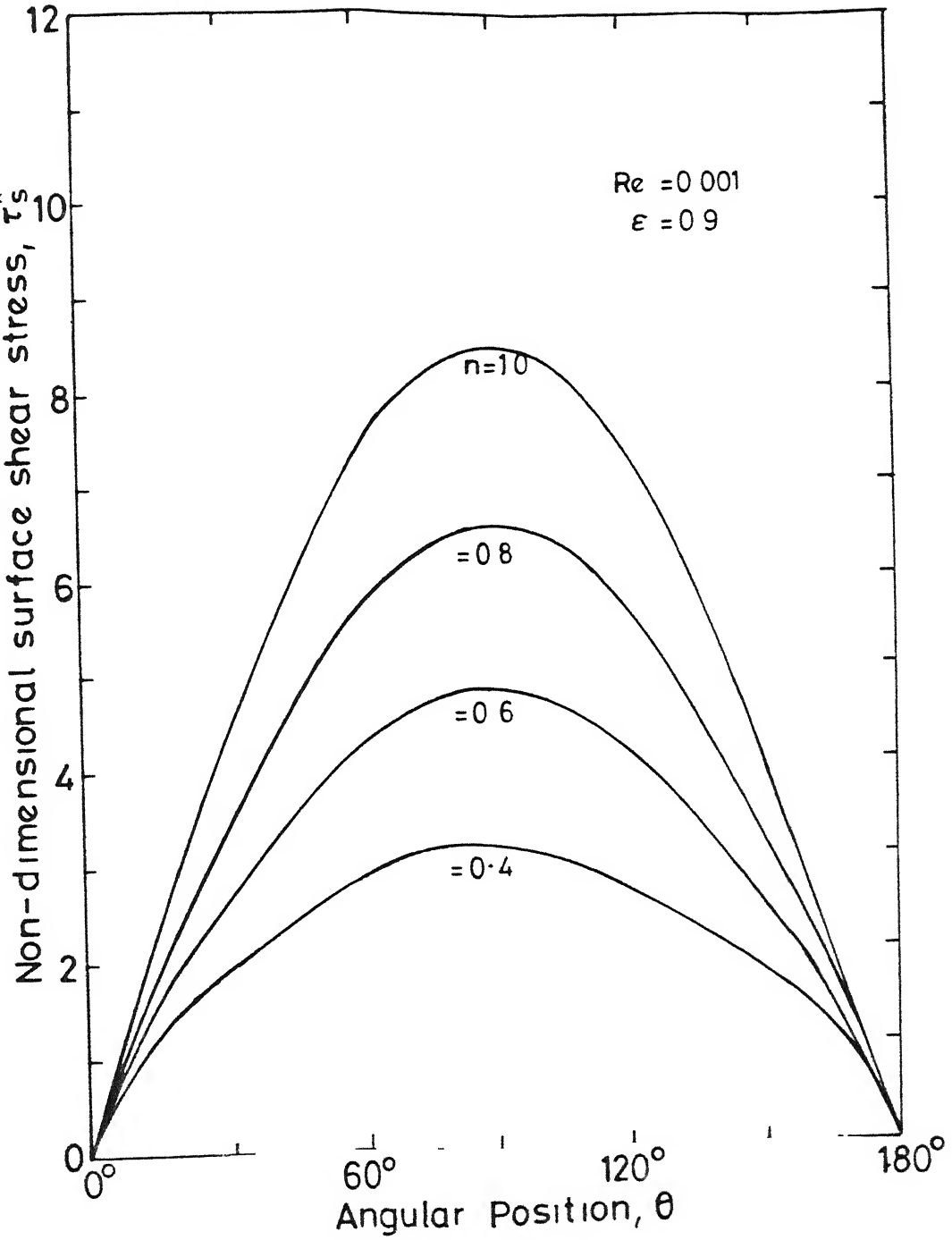

Fig. 6.7 Variation of non-dimensional surface shear stress ($\tau_s/\rho U_\infty^2$) with angular positions for various values of power law index and ϵ = 0.9.

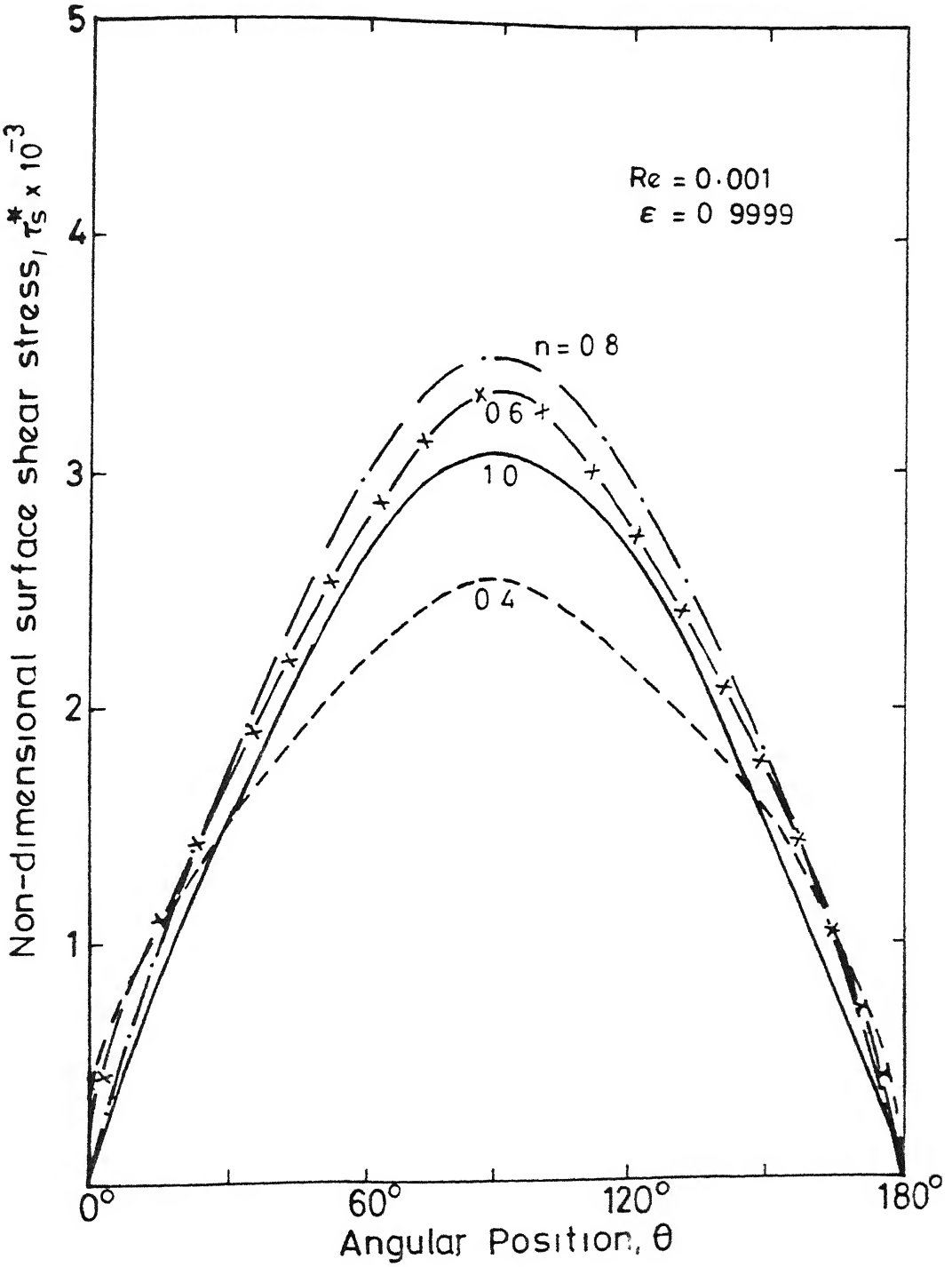

Fig 6.8 Variation of non-dimensional surfac shear stress ($\tau_s/\rho U_\infty^2$) with angular positions for various values of power law index and ϵ = 0 9999.

the case of dense assemblages, it appears that in the case of single sphere, the rate of increase of shear rate outweighs the corresponding decrease in viscosity, thereby resulting in net increase in the value of surface shear stress in the range ($1 \leq n \leq 0.8$). As the value of n drops from 0.8 to 0.6, the two effects compensate each other, exhibiting near constancy for the surface shear stress. The only noticeable change seems to be a slight drop (less than 4%) in the value of τ_{max} with a concomitant increase in the value of shear stress near the axis. This is in line with the discussion earlier made regarding flattening of shear stress profile with decrease in power law index. For lower value of n (< 0.6), the reduction in viscosity is much larger than the increase in shear rate. Therefore, τ_{max} decreases rapidly with decrease in n.

A further insight into the variation of surface shear stress under a range of conditions can be obtained by examining the variation of dimensionless surface viscosity and shear rate. Figures 6.9 to 6.11 show these results for a range of conditions. Evidently, as one would expect, the surface viscosity attains a maximum value on the axis ($\theta = 0^{\circ}$ and 180°) due to the occurrence of lowest velocity gradients at these locations. Similarly, it assumes a minimum value at $\theta = 90^{\circ}$. Recalling that in the case of Newtonian fluid, the dimensionless viscosity at the sphere surface is constant, it appears that in multi-particle systems a major part of the particle surface is exposed to a constant value of viscosity (but much lower in magnitude than the Newtonian case). This prompts one to conclude that the variable viscosity effects are confined mainly to a small region in the vicinity of the axis

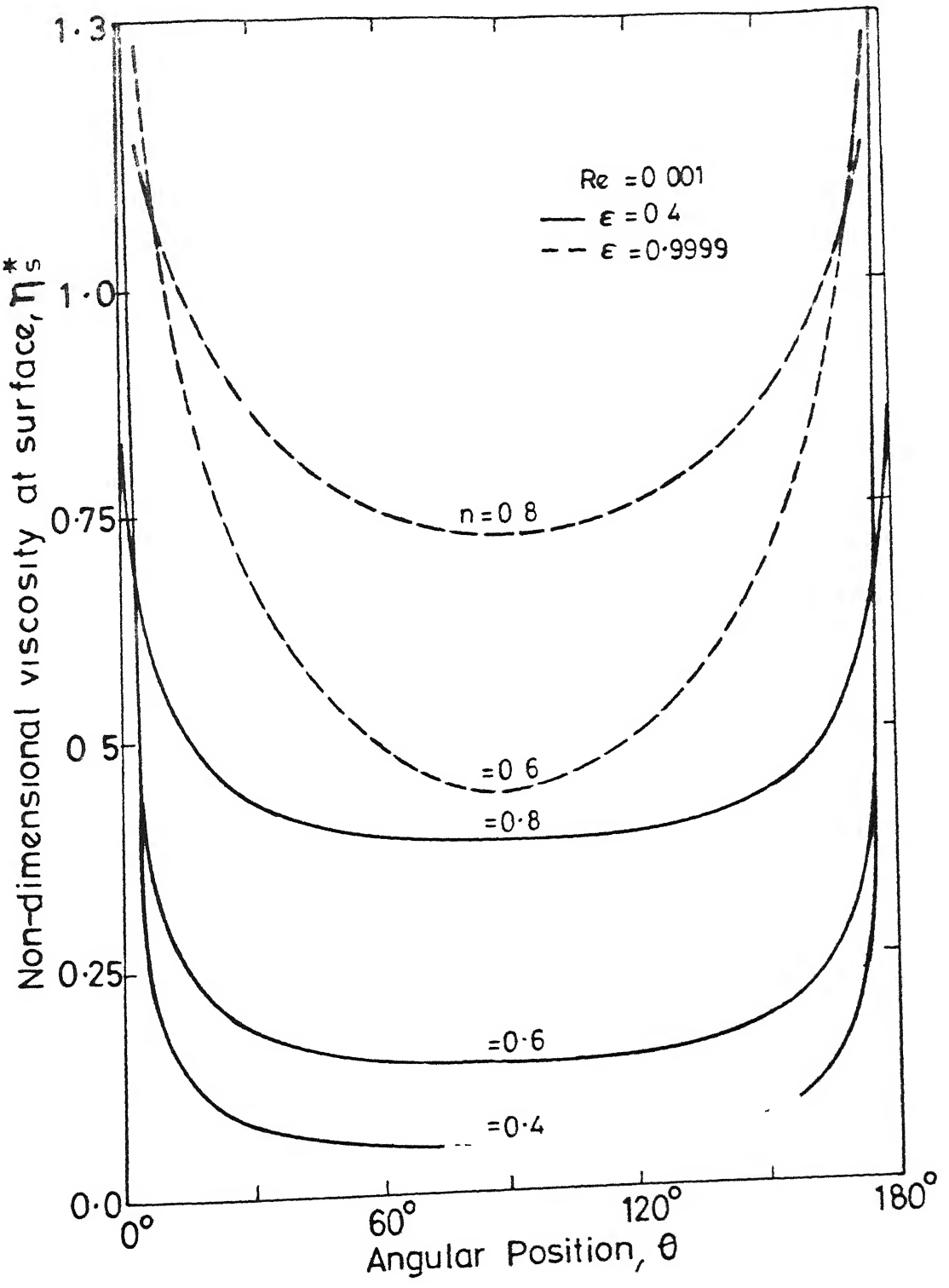

Fig. 6.9 Variation of non-dimensional viscosity on the particle surface with angular position for different values of power law index and two values voidage (ε = 0.4, and 0.9999).

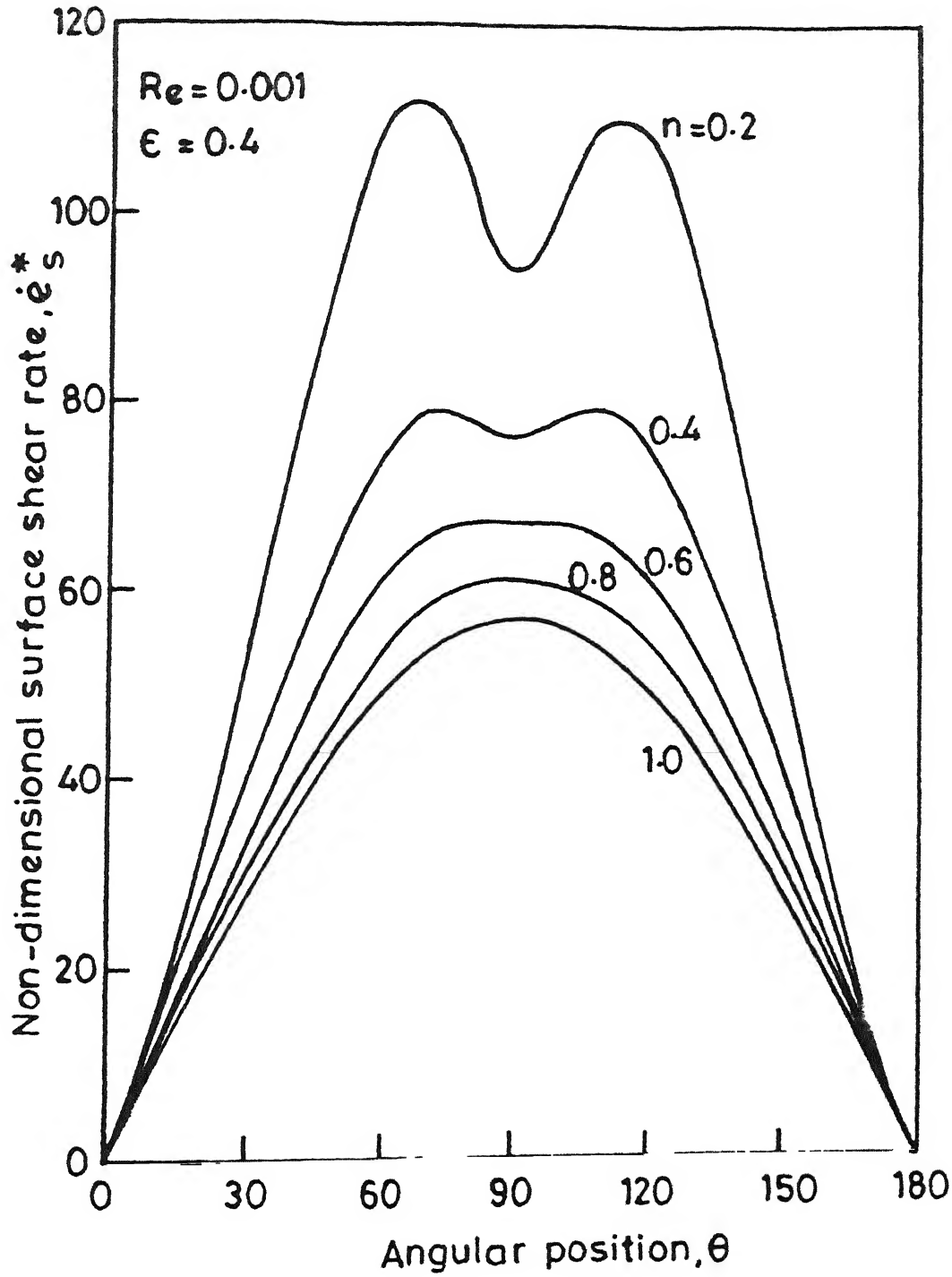

Fig. 6.10 Variation of non-dimensional surface shear rate with angular position for different values of power law index at low voidage (ϵ = 0.4).

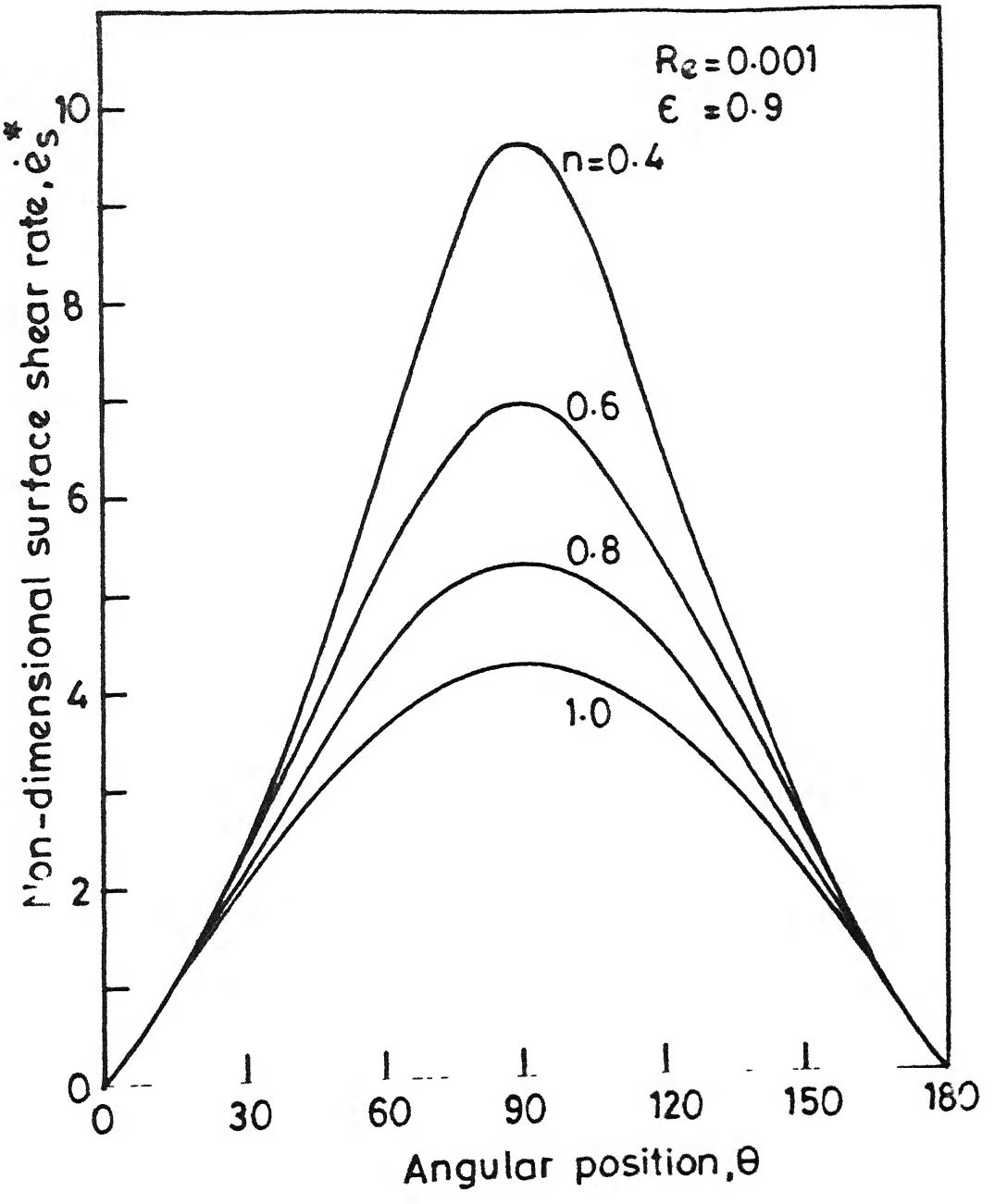

Fig. 6.11 Variation of non-dimensional surface shear rate with angular position for different values of power law index at high voidage (ϵ = 0.9).

(θ = 0^{o} and 180^{o}).

For Newtonian and moderately shearthinning fluids, the surface shear rate conforms to sinusoidal variation;departures are, however, observed for dense assemblages and highly shearthinning conditions (Figures 6.10 and 6 11). The surface shear rate also shows a cusp similar to that seen in shear stress profile. It appears that the interactions between the dependences of shear rate and local viscosity on n exert an appreciable influence in determining the value of τ_{max} around θ = 90^{o} plane. For instance, when n = 0.8 and ϵ = 0.4, the drop in the value of viscosity from θ = 0^{o} to θ = 90^{o} is of the order of 60%, whereas, the corresponding change for ϵ = 0.9999 is only 30%. This is precisely why the surface shear stress shows different types of dependence on n for dense and dilute assemblage.

The trends of shear stress along with the surface shear rate and viscosity variations are helpful in shedding light upon the behaviour of friction drag coefficient (C_{DF}) for various voidages and power law indices. For instance, at low voidage the friction drag decreases monotonically with sharp drop near n = 1.0 and slower drop at lower values of n. At a higher voidage (ϵ = 0.9), the friction drag still decreases monotically, but at a slower rate. However, while approaching the single sphere limit (ϵ = 0.9999), C_{DF} manifests a mild increase in the beginning followed by a sharp decrease as n is progressively reduced. These trends are in exact correspondence with the overall behaviour of shear stress profiles discussed earlier.

The pressure drag coefficient is likewise determined by the pressure distribution on the surface of the particle. Typical

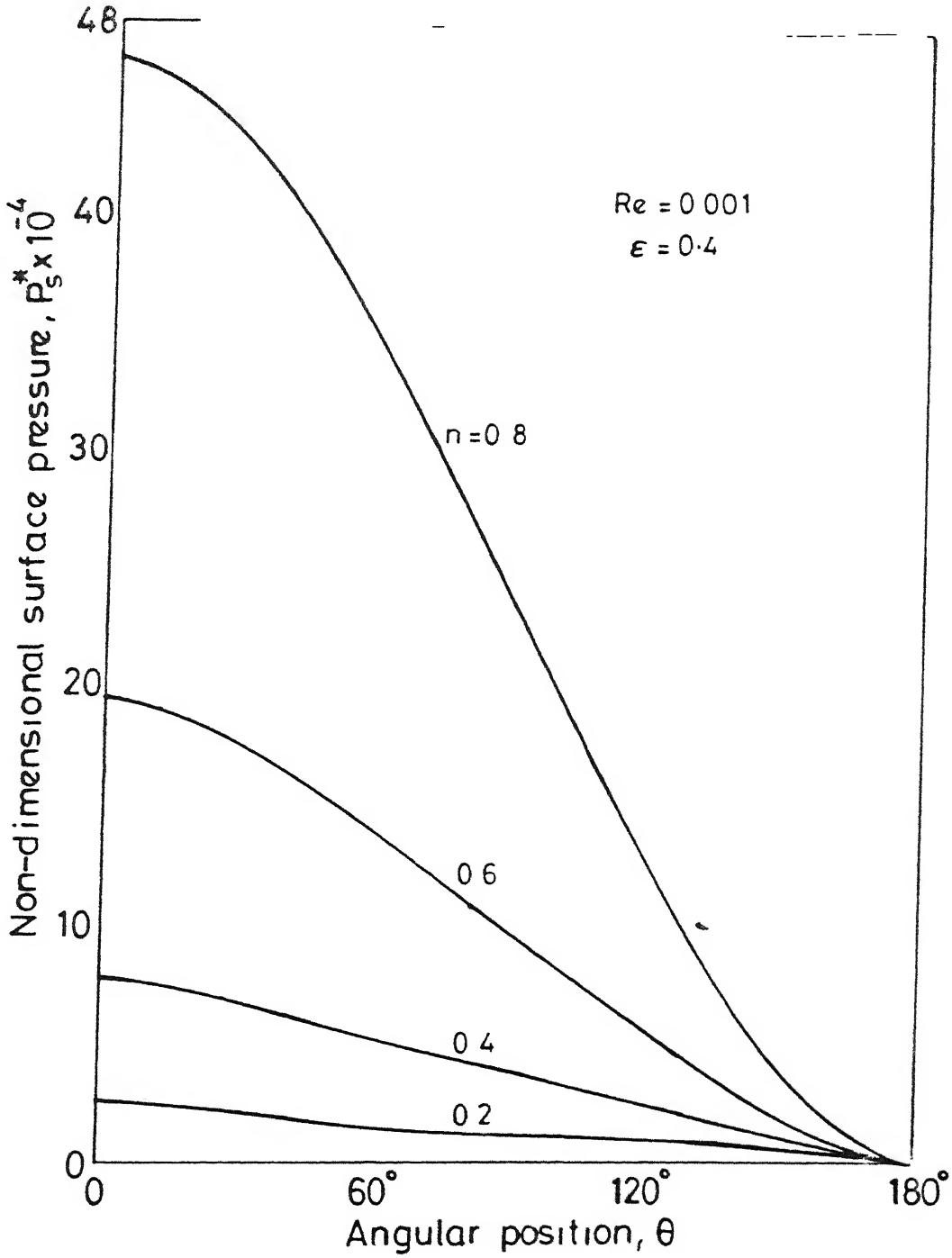

Fig. 6.12 Variation of non-dimensional surface pressure ($P_s/\rho U_\infty^2$) with angular position for different values of power law index and ϵ = 0.4.

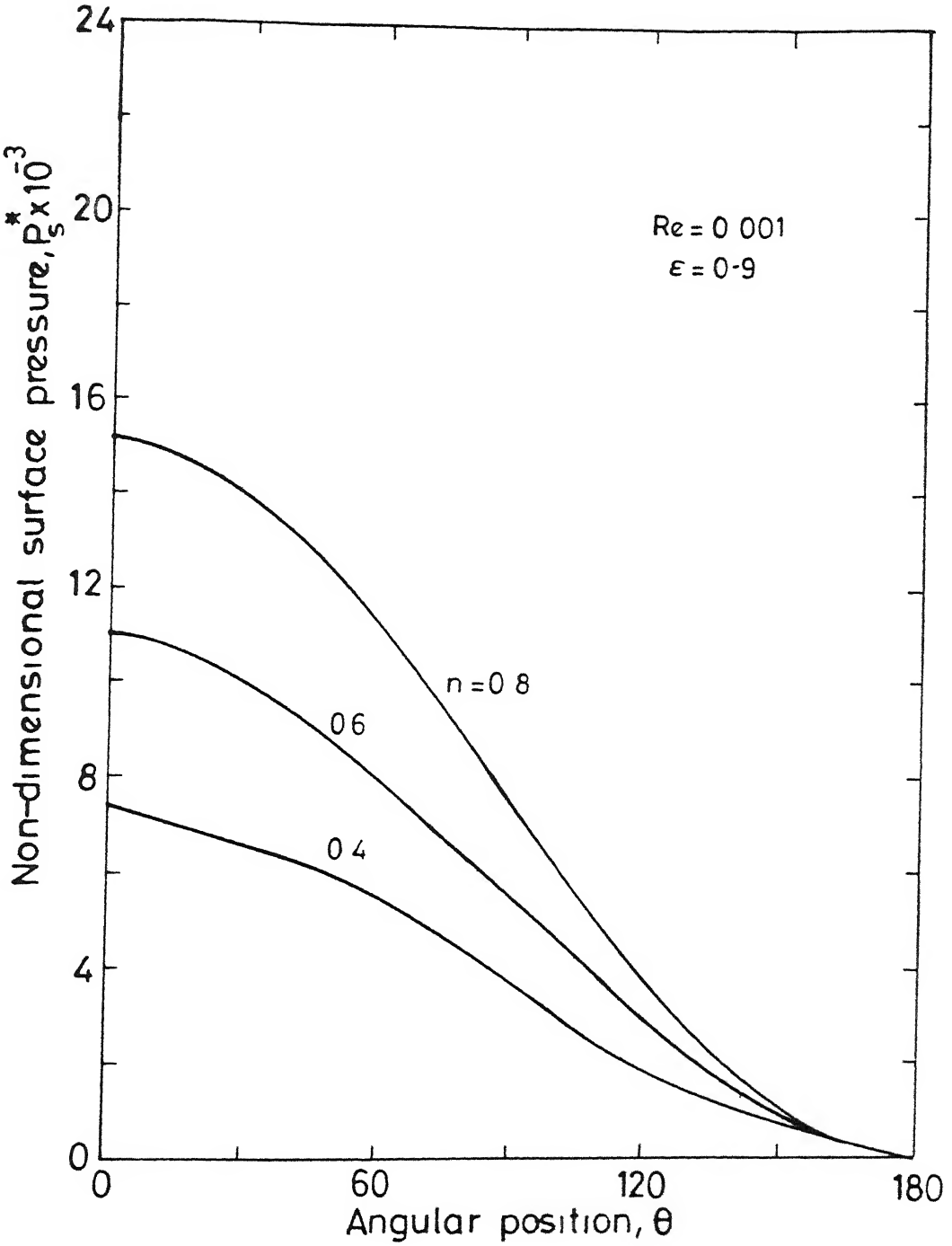

Fig. 6.13 Variation of non-dimensional surface pressure ($P_s/\rho U_\infty^2$) with angular position for different values of power law index and ϵ = 0.9.

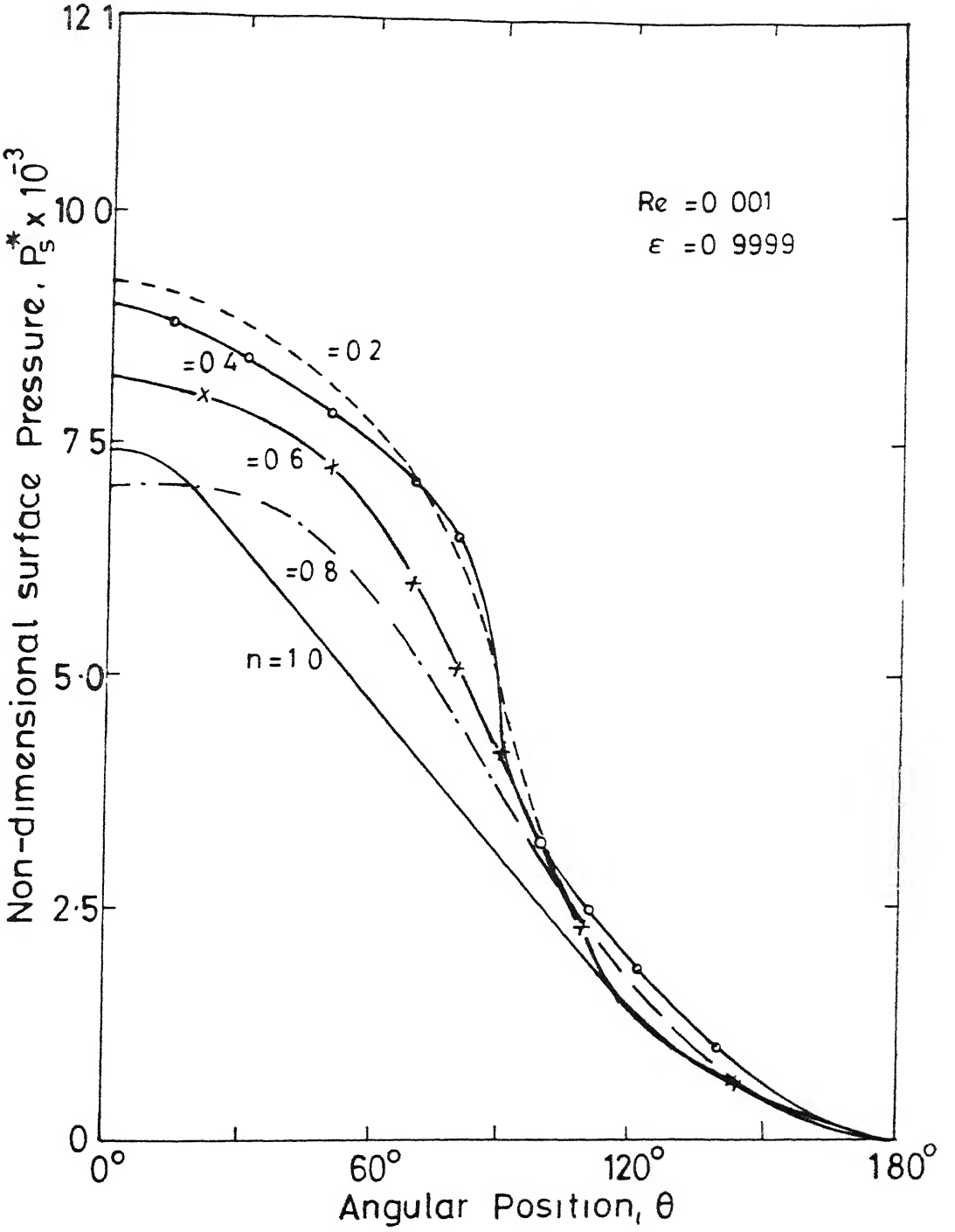

Fig. 6.14 Variation of non-dimensional surface pressure($P_s/\rho U_\infty^2$) with angular position for different values of power law index and ϵ = 0.9999.

surface profiles are shown in Figures 6.12 to 6.14. Note that in these figures, the value of pressure at $\theta = 180^{\circ}$ has been used as the reference point. For dense assemblages (in the packed bed range), the maximum surface pressure ($\theta = 0^{\circ}$), is seen to decrease rapidly with the decreasing value of n, akin to the surface shear stress. Interestingly, for any two values of n, the ratios of maximum surface shear stress and surface pressure are nearly the same. It comes as no surprise since pressure and viscous forces balance each other in the absence of inertia. For the creeping flow of Newtonian fluids, the surface pressure is known to vary as cos θ; however, a departure from this behaviour is observed for highly shearthinning conditions, showing a milder pressure gradient in angular direction than suggested by cosine dependence in the neighbourhood of $\theta = 90^{\circ}$ plane. As the concentration of assemblage is reduced ($\epsilon = 0.9$), the variation of pressure with θ for different values of n is more or less uniform (See Figure 6.13). Here also, the behaviour is at variance from cosine dependence for low values of n.

6.1.3 Flow Field in the Cell

Typical dimensionless pressure and velocity profiles within the cell are shown in Figures 6.15 to 6.20 for various values of n and ϵ An inspection of figure 6.15 suggests that in the packed bed region ($\epsilon = 0.4$), the pressure decreases primarily due to the variation in θ direction for all values of n considered. In the radial direction, the pressure variation is significant only in the region adjacent to the axis, where the flow is predominantly radial At $\theta = 90^{\circ}$, there is no radial variation of pressure at ny voidage or power law index, since the flow is purely in θ

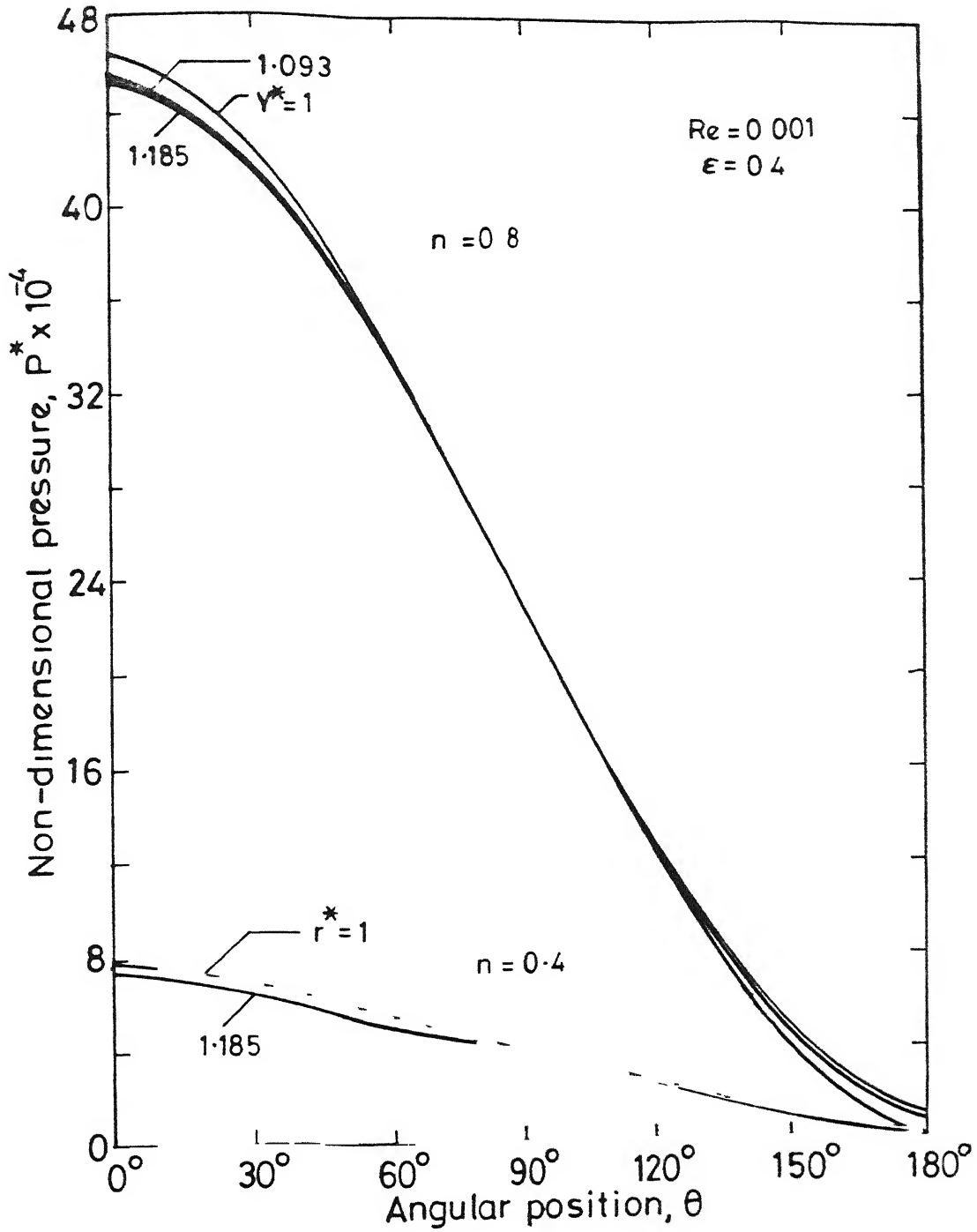

Fig. 6.15 Non-dimensional pressure distribution in the cell at ϵ = 0.4. Effect of shearthinning (n = 0.8 and 0.4).

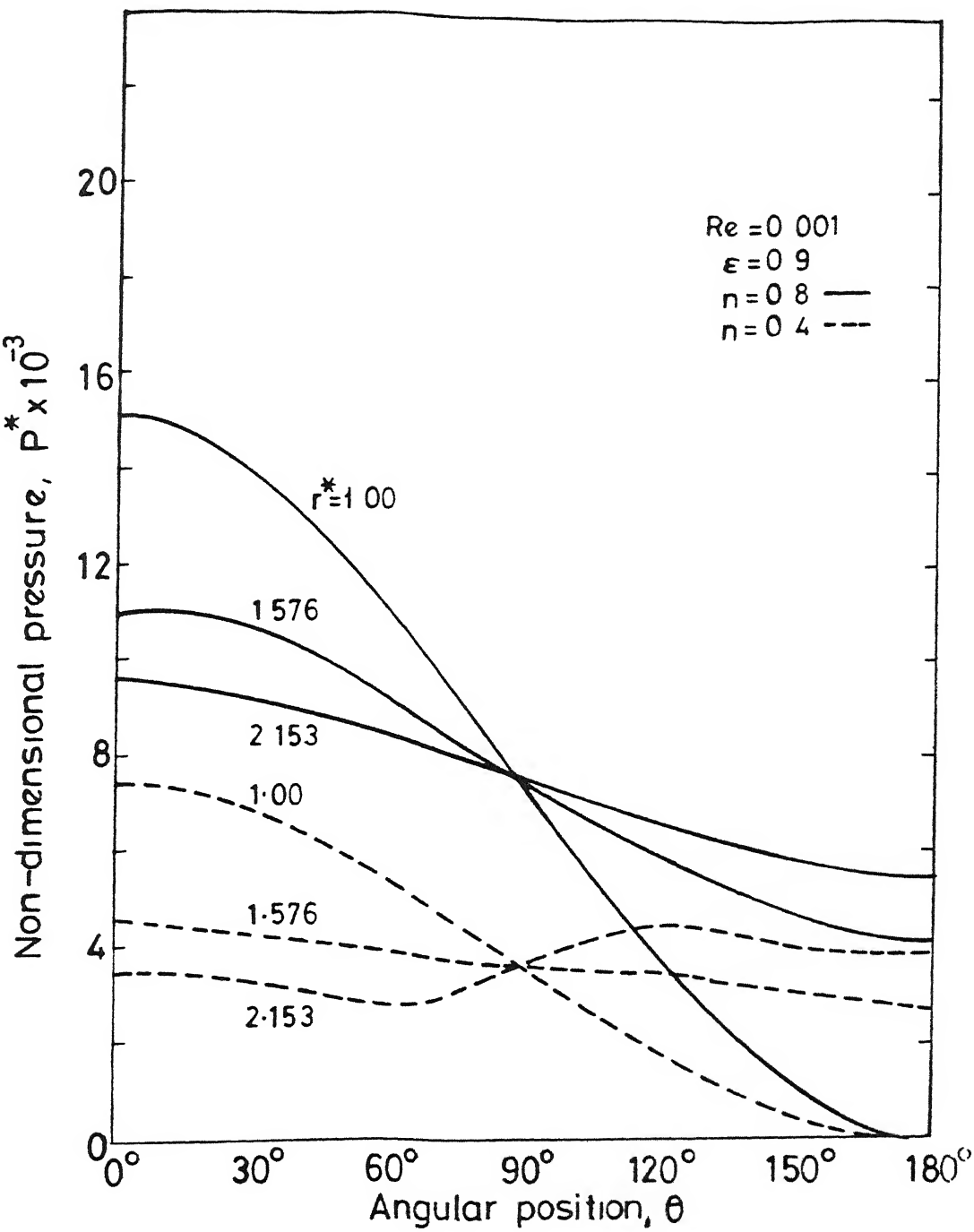

Fig. 6.16 Non-dimensional pressure distribution in the cell at ϵ = 0.9. Effect of shearthinning (n = 0.8 and 0.4).

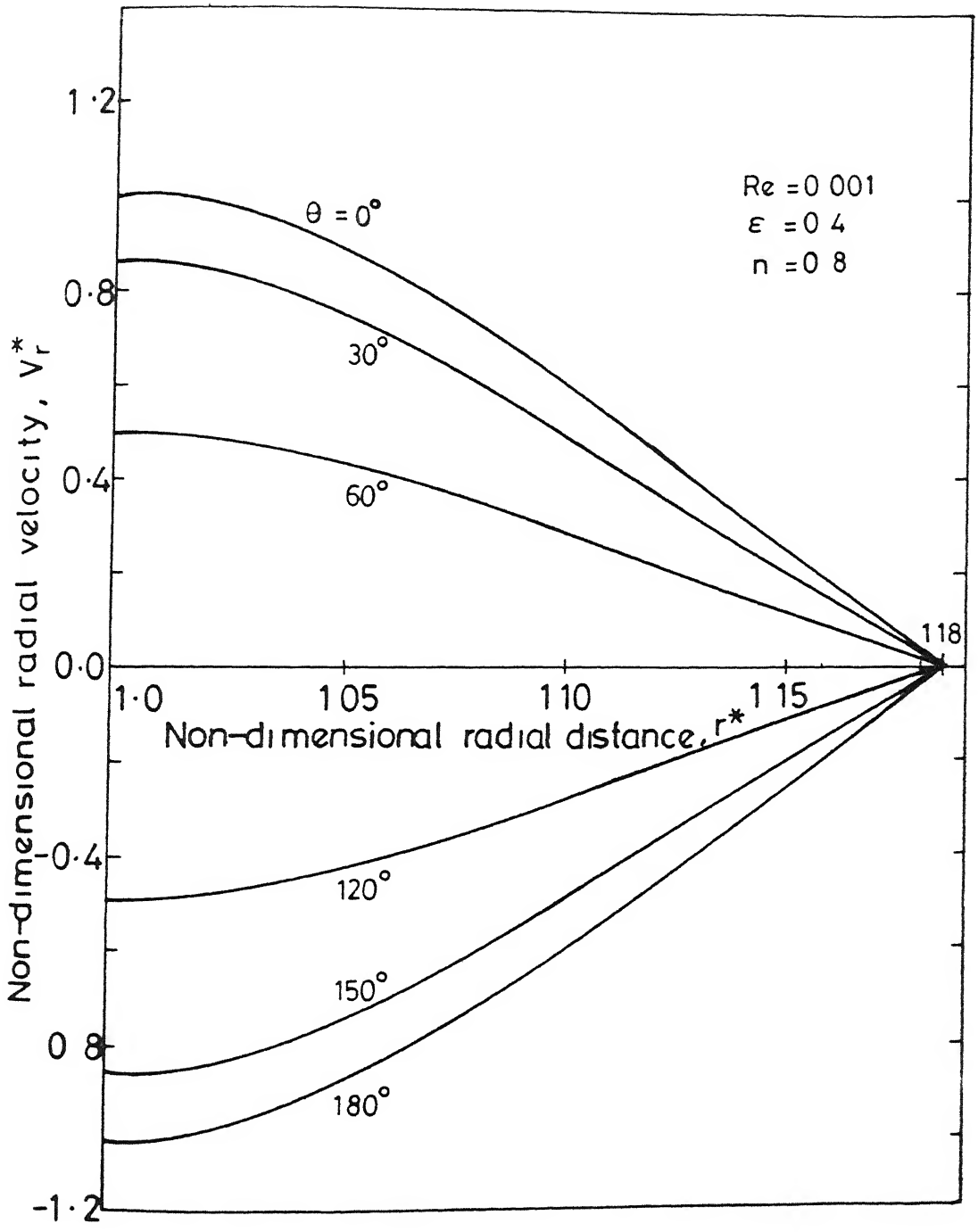

Fig. 6.17 Variation of non-dimensional radial velocity (V_r/U_∞) in radial and angular directions at ϵ = 0.4 and n = 0.8.

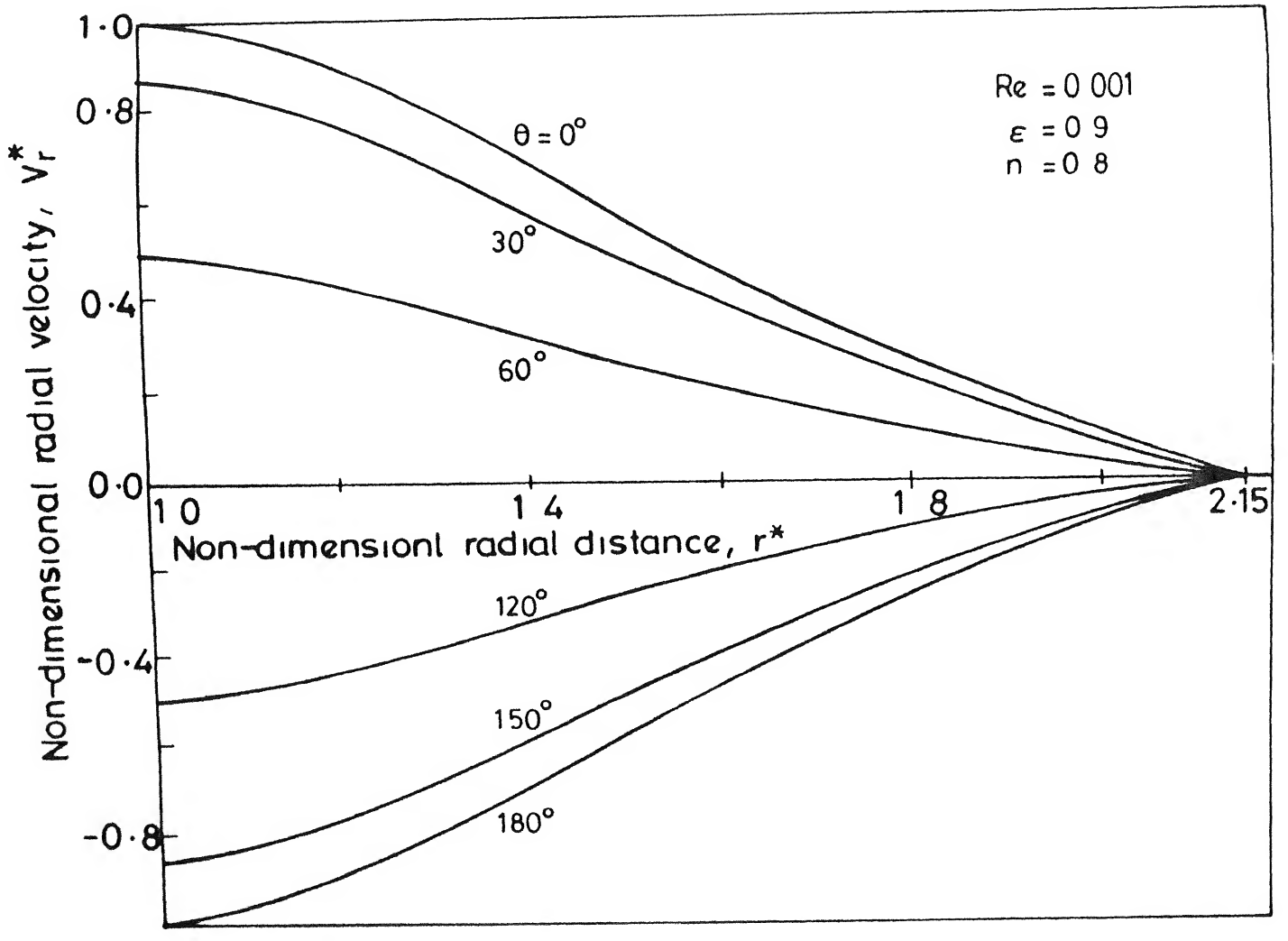

Fig. 6.18 Variation of non-dimensional radial velocity(V_r/U_∞) in radial and angular direction at ϵ = 0.9 and n = 0.8.

direction at the mid-plane The small radial variation of pressure at low voidage is a consequence of small available radial gap and this feature has similarities to the usual approximations invoked in boundary layer theory. It is seen that the rate of change of pressure in radial direction is larger near the particle surface than at free boundary of the cell for all angles. This is simply due to the fact that as one traverses from the particle surface to the cell boundary, there is gradual reduction in radial flow which eventually vanishes at the cell boundary and hence $(\partial p/\partial r)$ goes to zero at the cell surface.

On the other hand, in case of dilute assemblages (ϵ = 0.9), the variation of pressure in radial and angular directions is of comparable magnitude (See Figure 6.16) This is due to the fact that distance travelled by a fluid element in these two directions is of the same order. At ϵ = 0.9 also, the drop in pressure in radial direction is higher near the particle surface than the drop near the cell surface. For Newtonian and mildly shearthinning fluid behaviour, the pressure varies monotonically over the entire flow domain, whereas , there seems to be an adverse pressure gradient on the cell surface for highly shearthinning fluids. Such an adverse pressure gradient would retard the fluid flow.

Both pressure and shear stress distributions are directly linked with the velocity profiles existing in the flow field. The variations of radial velocity with angular and radial positions are shown in Figures 6.17 and 6 18, for two values of voidage (0 4 and 0.9) for a moderately shearthinning fluid (n = 0.8). In both cases, the radial velocity decreases from its maximum value at the particle surface to zero at the cell surface, and it is

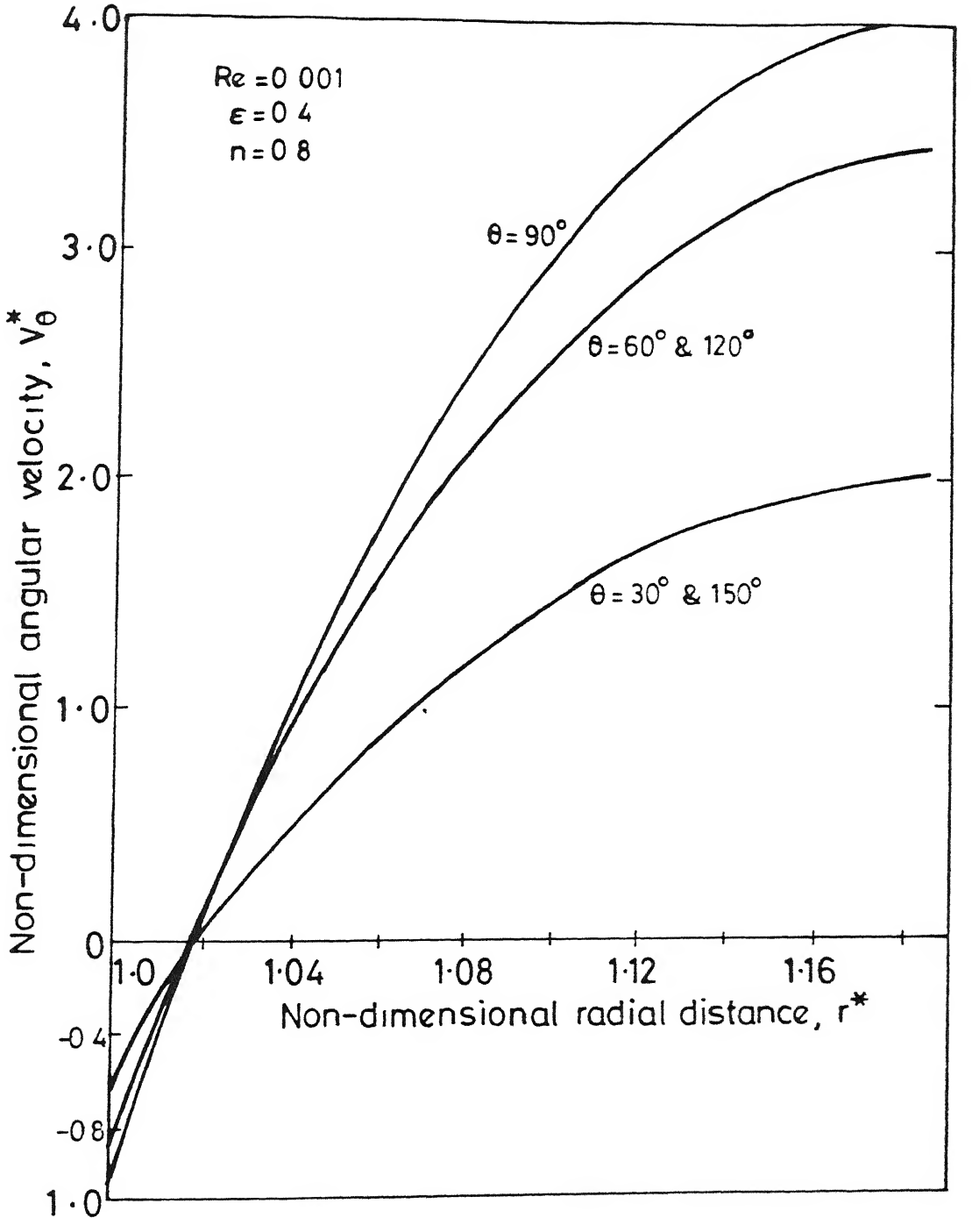

Fig 6.19 Non-dimensional angular velocity (V_θ/U_∞) variation in radial and angular directions at ϵ = 0.4 and n = 0.8.

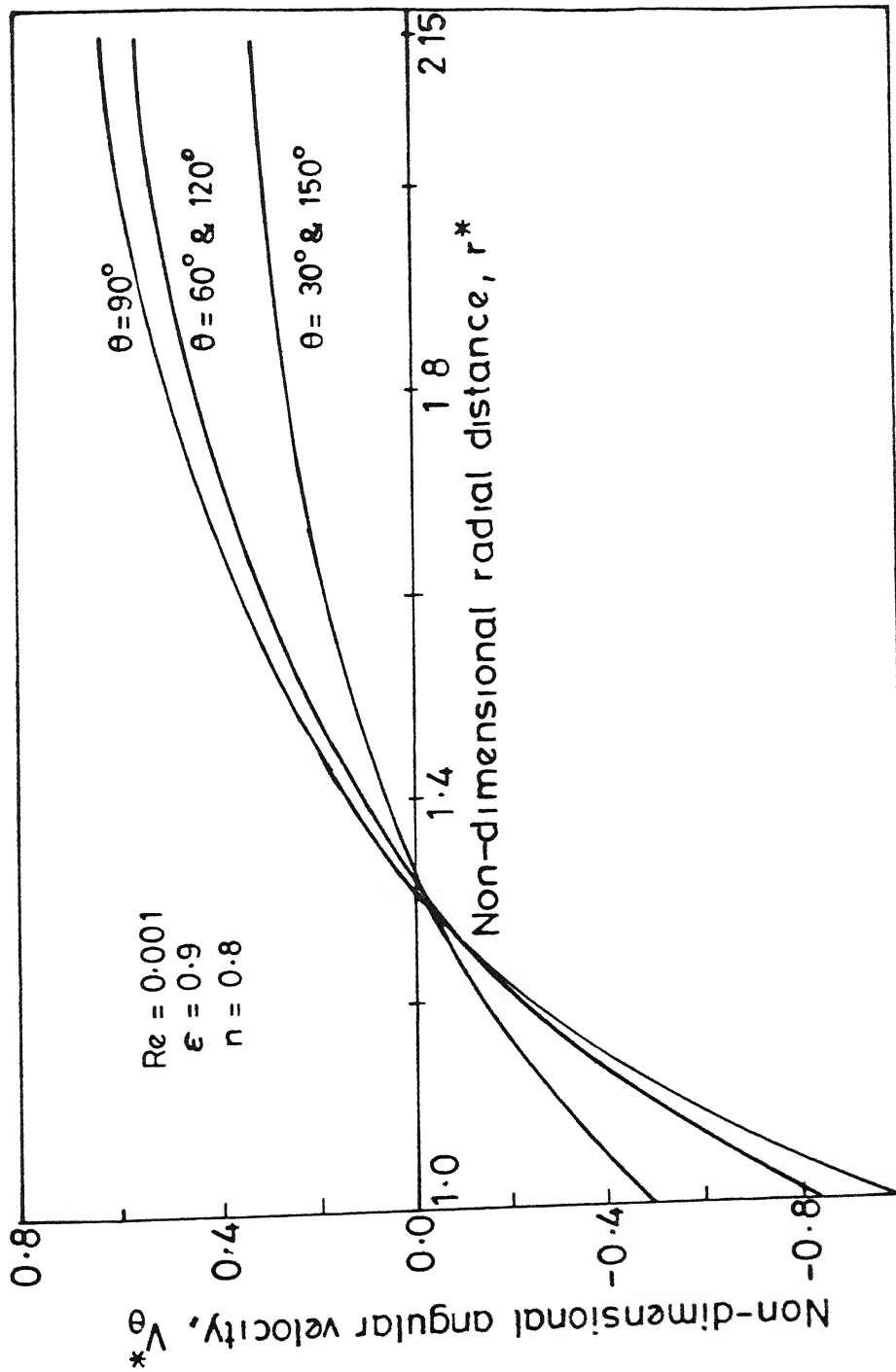

Fig. 6.20 Non-dimensional angular velocity (V_θ/U_∞) variation in radial and angular directions at ε = 0.9 and n = 0.8.

symmetrical about $\theta = 90^{\circ}$ plane which is typical of creeping flow The slope of radial velocity curve is zero on the particle surface. Using continuity equation in conjunction with the boundary conditions ($V_r = \cos\theta$ and $V_\theta = -\sin\theta$), it can readily be shown that $\partial V_r/\partial r$ is indeed zero at the particle surface. Consequently, the normal stress consists of only pressure and the friction drag arises only due to the shear stress. It is also of interest to note that the radial velocity conforms to a cosine dependence on angle at any radial position within the cell. Qualitatively similar trends are observed for other values of power law index ($1 \geq n \geq 0.2$).

Typical angular velocity profiles are displayed in Figures 6.19 and 6.20. From the particle surface towards the cell boundary, V_θ undergoes a change of sign from -ve to +ve somewhere close to the particle surface at all angular positions. Also, complete fore and aft symmetry is displayed. This feature would correspond to the streamlines originating from the particle surface, turning back somewhere near the particle and finally attaching themselves back to the particle in the rear. The radial location where V_θ becomes zero would obviously coincide with the turning point of streamlines. At low values of voidage, the locus of such turning points of streamlines appears to be a spherical surface however, this is so only upto about $n \sim 0.8$ and with further drop in the value of n, it gets distorted into an ellipsoid. Indeed, some of these features can be clearly seen in streamline patterns depicted in Figures 6.21 and 6.22. In general, the magnitude of V_θ at the cell surface is seen to be much higher than the particle velocity except near the axis. Once

again using the overall continuity, it can be demonstrated that V_θ at the cell surface increases as $(1/\delta)$ Further detailed examination of the results suggests that the velocity profiles are relatively insensitive to the power law index in dense assemblages. For dilute assemblages (ϵ = 0.9), the angular velocity conforms to the expected sinusoidal variation only for Newtonian and mildly shearthinning fluids. For highly shearthinning conditions ($n \leq 0.4$) and large values of voidage, the dividing surface takes an ellipsoidal shape. Another interesting feature exhibited by V_θ profiles is that at cell surface the velocity value remains more or less constant over a range of angular positions from $\theta \simeq 60^\circ$ to 120°. A reference was made in this regard while discussing the pressure profiles to the existence of adverse pressure gradient at the cell surface for the range of angles mentioned above. These pressure gradients seem to be partly responsible for V_θ remaining constant around the mid plane. For all conditions of ϵ and n, the radial gradient of angular velocity is the steepest at the particle surface and it decreases gradually as the cell boundary is approached. This is simply due to the condition of zero shear stress at the cell surface.

6.1.4 Streamline Patterns

Owing to the difficulty of plotting, the streamline patterns are shown only for a dilute assemblage (ϵ = 0.9) for two values of power law index in Figures 6 21 and 6.22. As noted earlier, the streamlines are made up of closed loops originating in the front and terminating in the rear of the particle. In addition, one can also discern closed streamlines forming a vortex adjacent to the

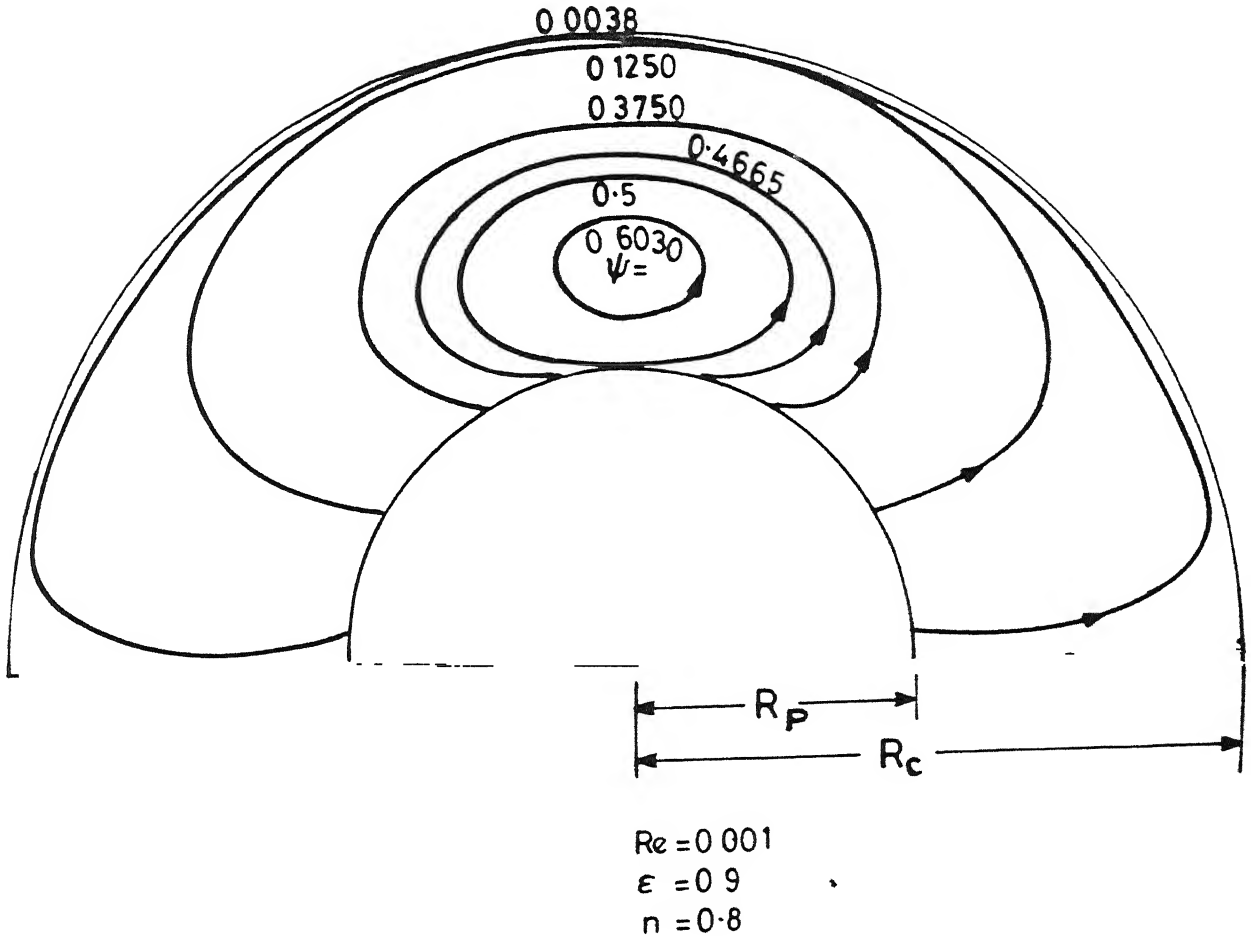

Fig. 6.21 Streamline pattern for mildly sheartninning fluid (n = 0.8) for ϵ = 0.9, under creeping flow (Re = 0.001) condition.

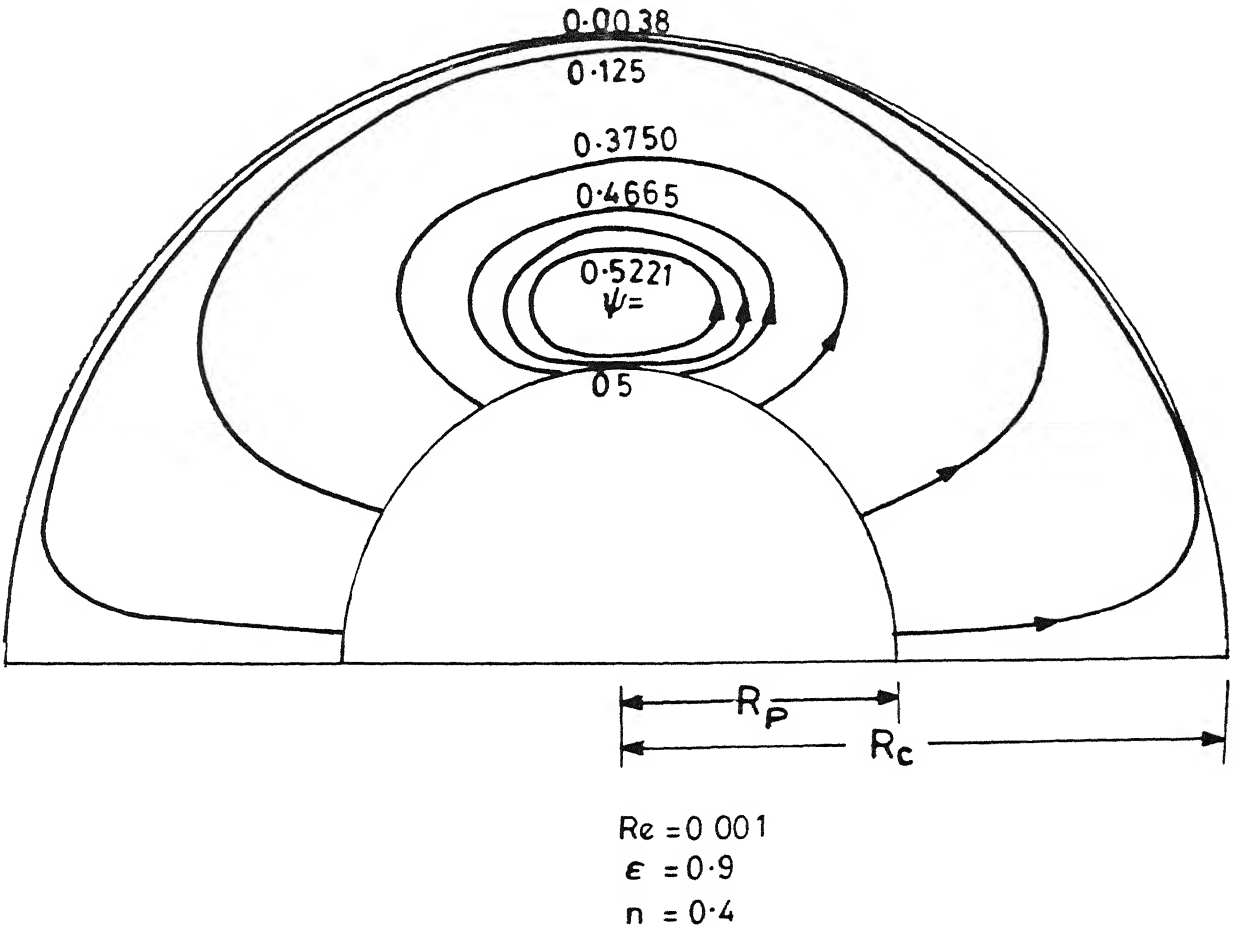

Fig. 6.22 Streamline pattern for strongly shearthinning fluid (n = 0.4) for ϵ = 0.9 under creeping flow (Re = 0.001) condition.

particle However, all streamlines display complete fore and aft symmetry for both the values of power law indices, as expected in creeping flow regime Furthermore, the vortex diminishes in size with increasing degree of shearthinning It is to be recognised that the vortex is sustained by the shear stress caused due to flow of fluid displaced by the moving particle. At lower values of n, the shear stress exerted by the displaced fluid is smaller due to the decrease in effective fluid viscosity. This, in turn, results in reduction of the strength and the size of vortex. It is also seen that as the value of n drops from 0.8 to 0.4, the centre of vortex shifts closer to the particle surface, thereby providing more area for fluid flow to occur. Concurrently, the tangential velocity decreases as has been noted in the angular velocity profiles (Figures 6.19 and 6.20).

6.1.5 Comparison with Available Results

It is of interest to compare the present predictions of the total drag coefficient with the other contemporary studies in this field. It is customary to express drag coefficients of creeping flow through multiparticle assemblages in the form of deviation from the Stokes drag. This is accomplished by introducing a drag correction factor (Y) defined as

$$Y = \frac{C_D \, Re}{24} \qquad (6.5)$$

The quantity Y is expected to be a function of n and ϵ for multi-particle assemblages. The variation of Y with n and ϵ is shown in Figure 6.23.

Mohan and Raghuraman (1976a) obtained upper and lower bounds on the drag coefficient of assemblages for $1 \geq n \geq 0.5$ and

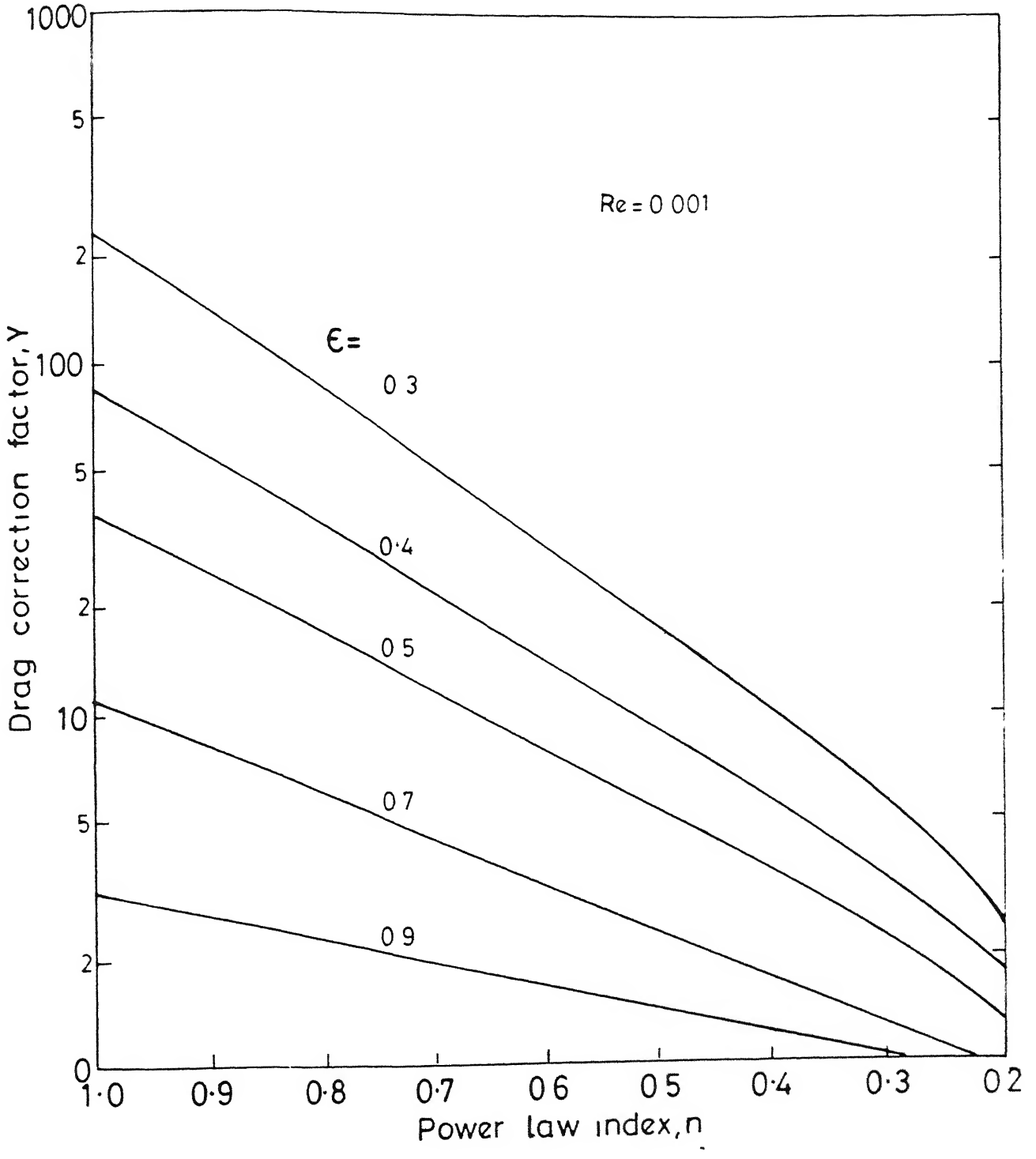

Fig. 6.23 Variation of drag correction factor with voidage and power law index for creeping flow (Re = 0.001) condition.

Table 6 2 Comparison of the present numerical results with the available results on drag correction factor for creeping power law fluid flow.

ϵ	n	Y (present)	Y_U (a)	Y_L (a)	$Y_{av.}$ (a)	Y (b)
0.4	1.0	85.291	85.12	85.12	85.12	85.14
	0.9	54.790	56.18	56.04	56.11	54.95
	0.8	35.133	37.06	37.00	37.03	35.81
	0.6	13.916	16.08	15.92	16.00	15.87
	0.4	5.279	–	–	–	7.84
	0.2	1.722	–	–	–	5.12
0.5	1.0	37.820	37.91	37.91	37.91	37.92
	0.9	25.910	26.61	26.48	26.54	26.75
	0.8	17.630	18.67	18.50	18.58	19.02
	0.6	7.854	9.17	9.11	9.14	9.99
	0.4	3.335	–	–	–	5.83
	0.2	1.193	–	–	–	4.47
0.7	1.0	10.13	10.13	10.13	10.13	10.14
	0.9	7.73	7.94	7.91	7.93	8.29
	0.8	5.86	6.22	6.21	6.21	6.80
	0.6	3.22	3.81	3.78	3.79	4.72
	0.4	1.68	–	–	–	3.58
	0.2	0.82	–	–	–	3.52
0.9	1.0	3.102	3.11	3.11	3.11	3.11
	0.8	2.361	2.44	2.43	2.43	2.74
	0.6	1.684	1.90	1.88	1.89	2.44
	0.4	1.154	–	–	–	2.31
	0.2	0.739	–	–	–	2.74
0.99	1.0	1.482	1.48	1.48	1.48	1.48
	0.8	1.442	1.47	1.46	1.465	1.62
	0.6	1.361	1.45	1.39	1.42	1.74
	0.4	1.185	–	–	–	1.91
	0.2	0.956	–	–	–	2.46

(a) Mohan and Raghuraman (1976a)

(b) Kawase and Ulbrecht (1981a)

0.99 ≥ ε ≥ 0.4. A comparison between their results and those of the present study, is shown in Table 6.2. An examination of this table shows that two values are in excellent agreement upto abhout n = 0.8 and as the value of n drops further, the two values differ increasingly. Kawase and Ulbrecht (1981a) also presented a closed form expression for Y and their values are also included in Table 6.2. Their analysis seems to be in reasonable agreement with the present study only upto n ≃ 0.8. It is believed that the results of the present study should be more accurate since they are derived from a full scale numerical solution of the equations of motion and continuity. On the other hand, the analyses of the previous authors were based on approximate solution techniques.

Admittedly, numerous experimental studies concerning the flow of power law fluids through packed beds have been reported in literature but not all authors have provided the complete information for their results to be recalculated in the form required here. Representative experimental results of some investigators were analysed and recast in a form which facilitates comparison with the present results as shown in Figure 6.24. All these results are pertaining to the packed beds with the value of voidage close to 0.4. The power law index of the fluid in these experimental results ranges from nearly 0.8 to 0.4. Each of these experimental results represents the average value of several runs. Keeping in view the idealizations involved in the present model such as the absence of wall effects, uniformity of particle distribution, etc and usual experimental errors in measurement of non-Newtonian flow through packed beds, the agreement between the experimental and present numerical results is seen to be

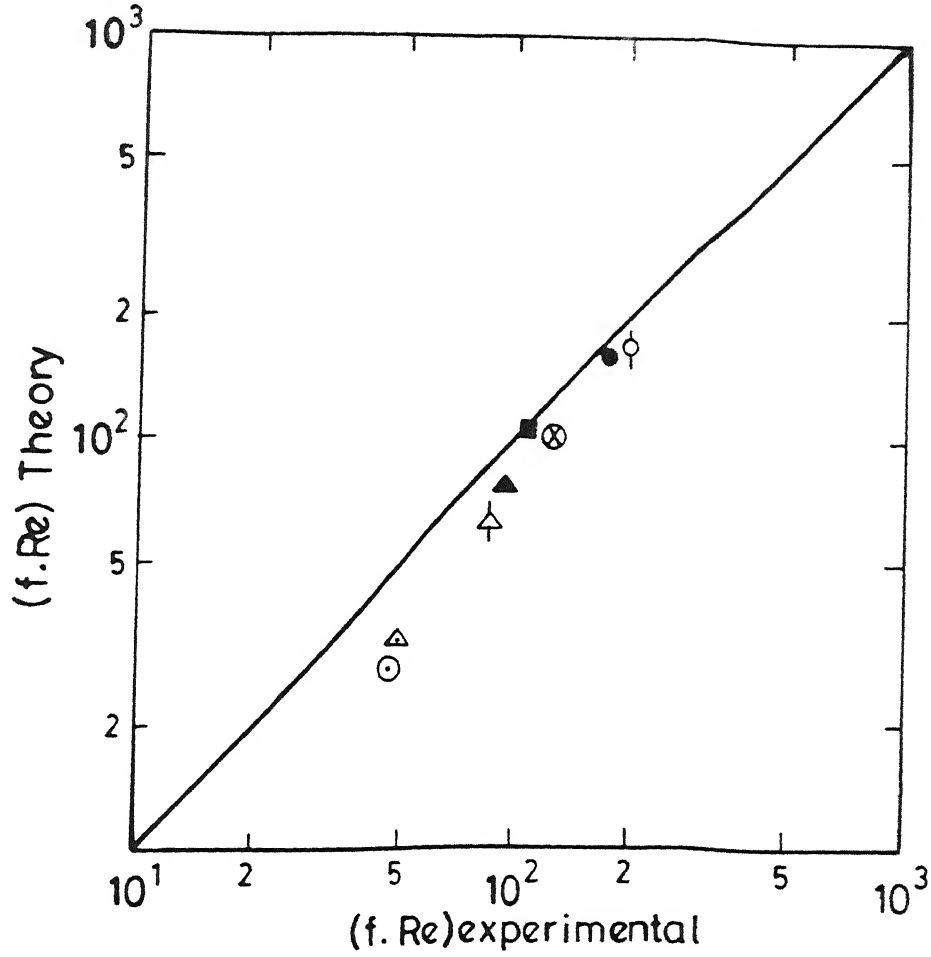

ϵ	n	SYMBOL	REFERENCE
0·4237	0·4104	⊙	Park (1972)
0·4237	0·4566	△	Park (1972)
0·3818	0·744	●	Sadowski (1963)
0·3818	0·570	▲	Sadowski (1963)
0·3870	0·750	⊖	Kemblowski & Mertl (1974)
0·3830	0·620	⊗	Kemblowski & Mertl (1974)
0·3830	0·510	⏄	Kemblowski & Mertl (1974)
0·471	0 81	■	Yu et. al (1968)

Fig. 6.24 Comparison of experimental results of other investigators with the present numerical results for flow through the packed beds.

satisfactory

Development of a general fluidization correlation and comparison with the available results on bed expansion characteristics of fluidized beds has been discussed in Sec.6.3.

6.2 FLOW AT INTERMEDIATE REYNOLDS NUMBER

The objective of the study reported in this section has been to identify the effects of inertia on transport phenomena associated with non-Newtonian fluid flow through multi-particle systems. This effectively boils down to the analysis of drag behaviour and detailed flow field structure at several Reynolds numbers beyond creeping flow regime, with voidage and power law index as parameters. Although, numerical results have been obtained in this study covering a range of parameters ($1 \leq Re \leq 20$, $0.3 \leq \epsilon \leq 0.9$, $0.4 \leq n \leq 1.0$), only drag results have been presented in all the cases investigated, for the sake of brevity. Furthermore, surface pressure and surface shear stress distributions have been analysed in detail for Re = 20 only. This value of Reynolds number was chosen based on the consideration that the inertial effects may begin to manifest in a prominent manner around Re = 20; also, for higher values of Reynolds number the free surface cell model is likely to become inapplicable as discussed in Chapter V. An insight into the nature of flow field prevailing around a particle in an assemblage is provided by the streamline patterns shown for two values of power law index (n=0.8 and 0.4). Finally, detailed comparisons with appropriate experimental results on flow past packed beds and single spheres are presented.

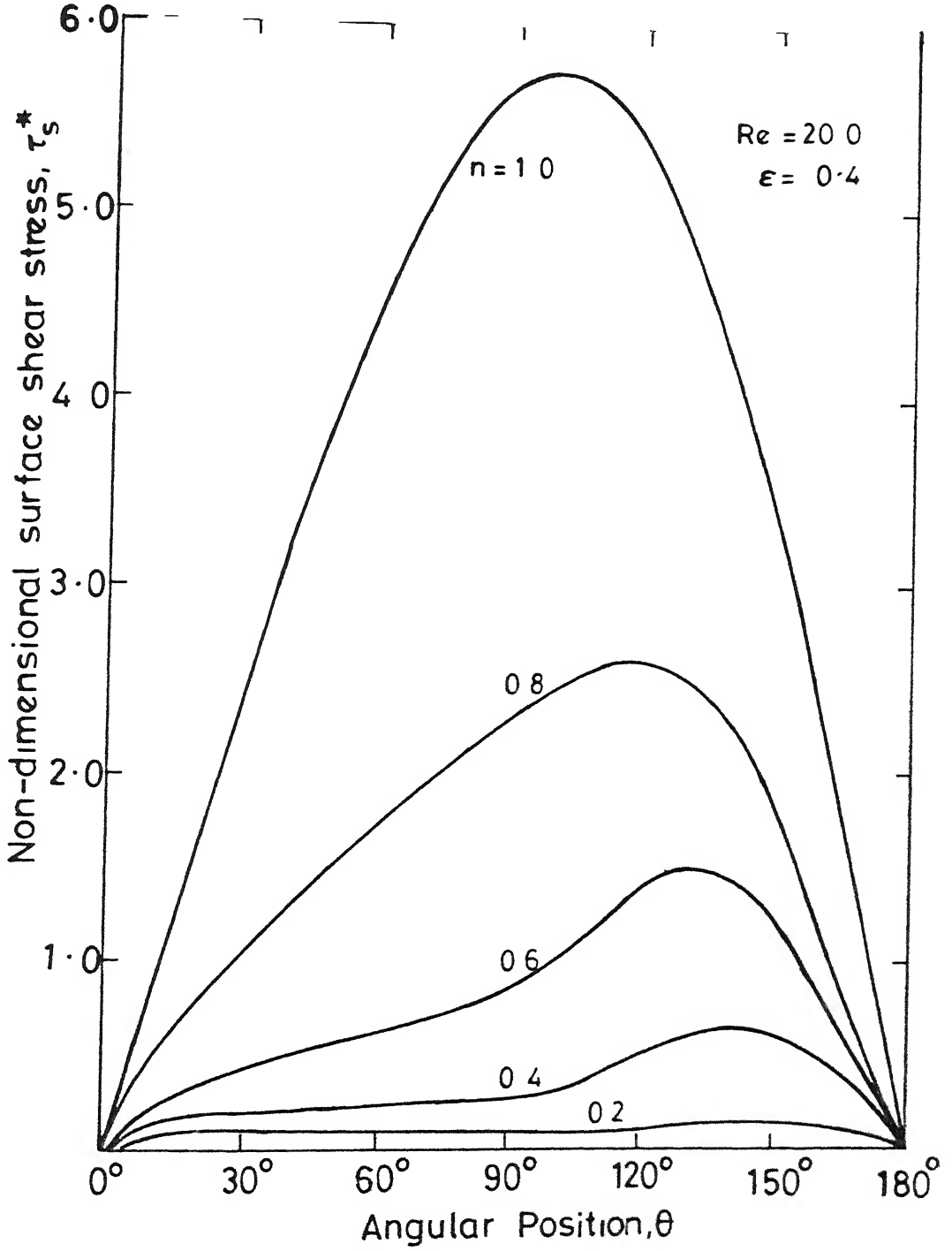

Fig. 6.25 Non-dimensional surface shear stress ($\tau_s/\rho U_\infty^2$) distribution at several values of power law index for ϵ = 0 4 and Re = 20.

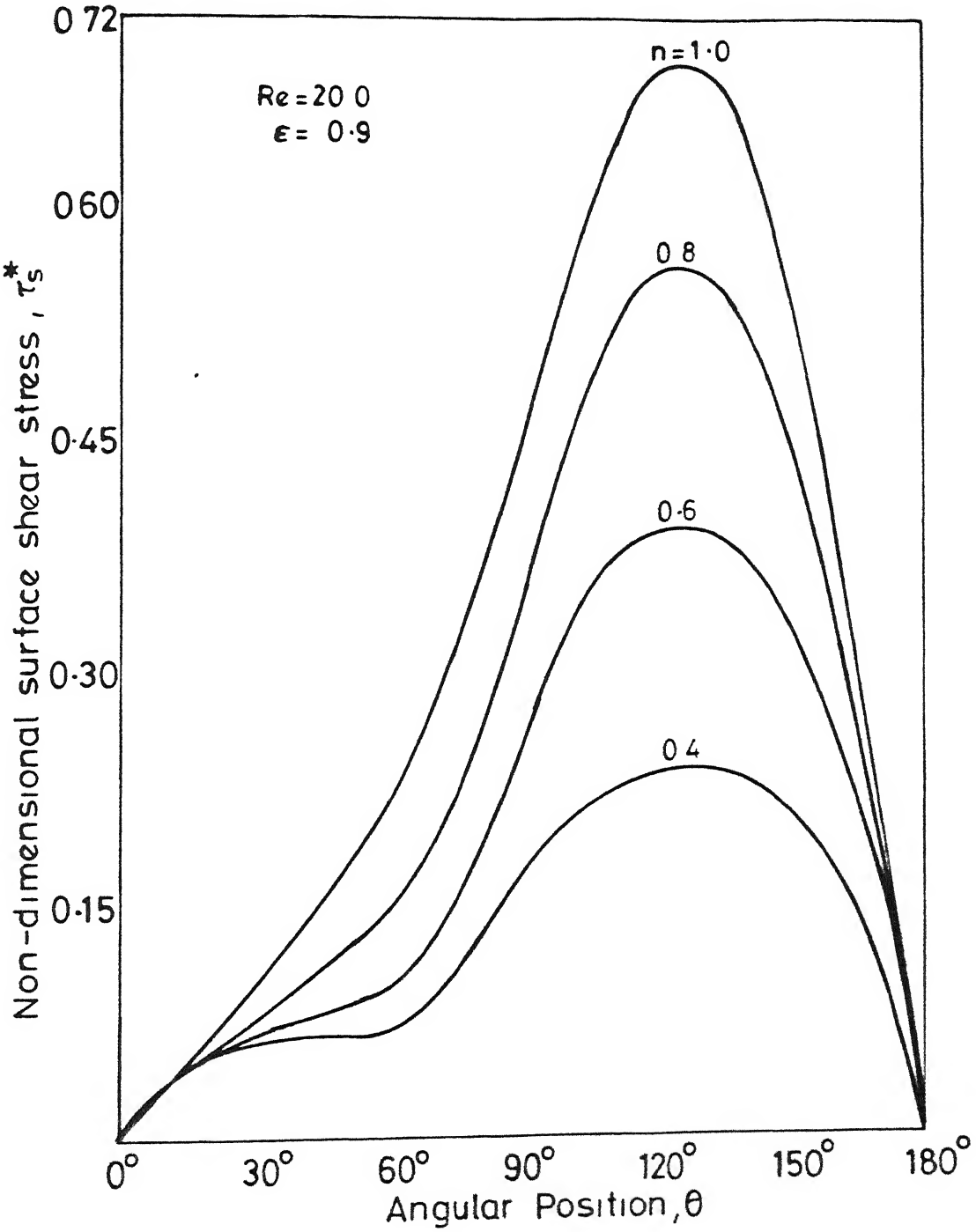

Fig 6.26 Non-dimensional surface shear stress ($\tau_s/\rho U_\infty^2$) distribution at several values of power law index for ϵ = 0 9 and Re = 20

6.2.1 Surface Shear Stress and Pressure Profiles

Figures 6.25 and 6.26 show the typical shear stress profiles on particle surface for two values of voidage (0.4 and 0.9) and for a range of values of power law index ($1 \geq n \geq 0.2$) at Re = 20. Unlike in the case of creeping flow regime, the shear stress is seen to be asymmetric about the mid-plane ($\theta = 90^{o}$) and attains a maximum value in the rear of the particle. It is reasonable to expect that due to inertial effects in the intermediate Reynolds number regime, a mass of fluid will be moving along with the particle in the front region with more or less same velocity as the particle. This phenomenon is more clearly seen in the streamline plots presented in Figures 6.40 and 6.41. Such a feature is akin to the presence of stagnation region in the case of fluid flow over a fixed particle The stagnation region for a fixed particle occurs in the rear portion, causing maximum shear stress to shift to the front region. In the present case, however, the stagnant region occurs in the front of the particle and the maximum shear stress shifts towards the rear region This is because in Happel cell model, particles are assumed to be in motion while the fluid at large is stationary.

With regard to the influence of power law index(n), examination of Figures 6.25 and 6.26 reveals a systematic drop in the value of shear stress at all angular locations with decrease in the value of n. This is a direct consequence of the shearthinning behaviour. The variation in shear stress appears to have an approximate power function type dependence on n, showing sharp drop for mildly shearthinning fluids (n close to 1.0) compared to the strongly shearthinning fluids ($n \leq 0.5$). It is

also interesting to note that even at Re = 20, the shear stress for Newtorian fluid (n = 1.0) varies in a nearly sinusoidal manner in dense assemblages ($\epsilon \approx 0.4$) This is similar to the variation observed in creeping flow regime and is believed to be a consequence of the strong influence of viscous force in the confined geometry of the multi-particle system, even at a fairly high Reynolds number of 20. With a decrease in the value of n, the shear stress profile becomes flatter, indicating a trend similar to that of the creeping flow regime At lower values of n (≤ 0.6), the shear stress profile is found to be flat even beyond the midplane ($\theta = 90^{\circ}$) In the rear portion, it slowly rises to reach maximum value and then suddenly drops to zero near the rear axis. The flatness of the shear stress profile in the front region can be attributed to the mutually offseting trends of the increase in surface shear rate and the decrease in surface viscosity with respect to angular position. Furthermore, due to inertial effects of the fluid in front of the particle, the velocity gradients are small in that region. As described earlier, this leads to an asymmetric shear profile with maximum shifted towards the rear of the particle.

As the inter-particle separation increases (by increasing the bed voidage), the magnitude of the shear stress drops. This is a direct consequence of the reduction in surface shear rate, due to lower velocity gradients in the gap between the particle and the cell surface. The flattening of the shear stress profile with reduction in n is also pronounced at $\epsilon = 0.4$, for the same reason. Comparison of the shear stress profiles corresponding to both voidages ($\epsilon = 0.4$ and 0.9) for a fixed value of non-Newtonian

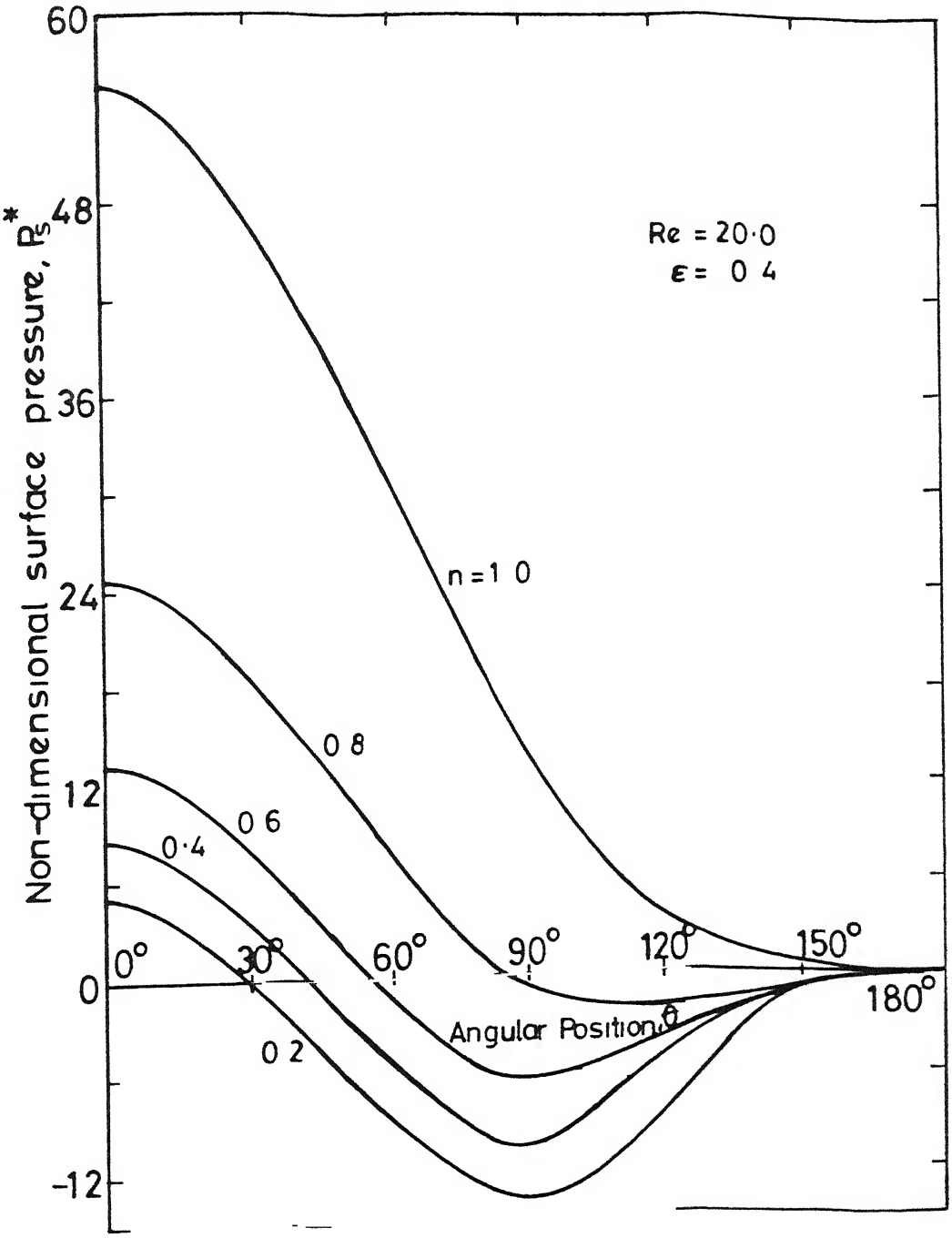

Fig. 6.27 Non-dimensional surface pressure ($p_s/\rho U_\infty^2$) distribution at several values of power law index for ϵ = 0.4 and Re = 20.

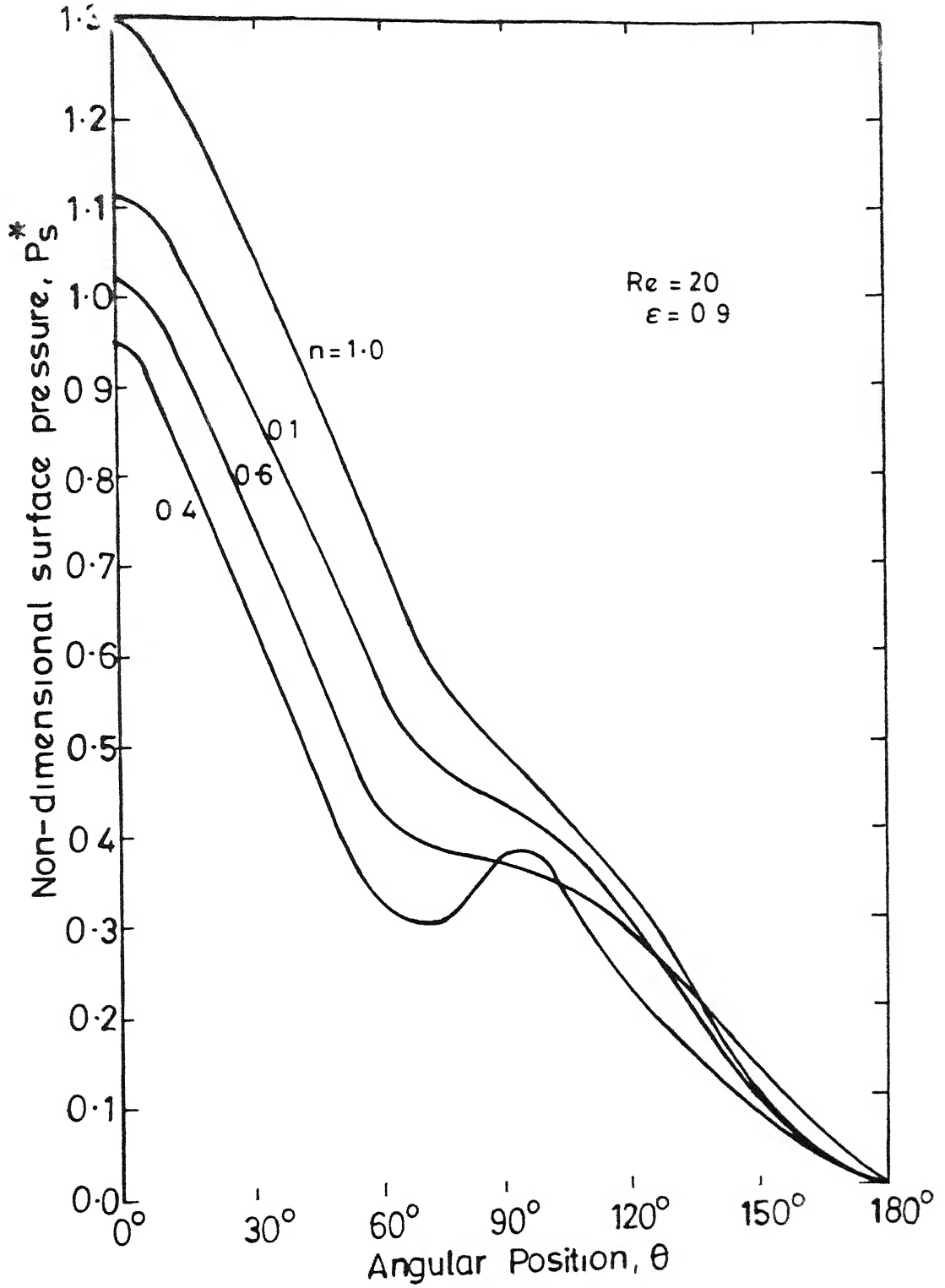

Fig. 6.28 Non-dimensional surface pressure ($p_s/\rho U_\infty^2$) distribution at several values of power law index for ϵ = 0.9 and Re = 20.

fluid behaviour index (n = 0.4), shows that at higher voidage (ϵ = 0.9) the flat region is confined to $0^{\circ} < \theta < 60^{\circ}$, whereas, at lower voidage (ϵ = 0.4), it extends upto $\theta = 100^{\circ}$. Another important difference between the results of two voidages is that in sparse assemblages even the Newtonian shear stress profile does not follow the sinusoidal variation It is also observed that the location of maximum shear stress with respect to the angular position remains almost invariant with the change in the value of power law index. The implication of this feature is that the flow field remains insensitive to the variation in local Reynolds numbers at higher voidage.

The corresponding pressure profiles for the same values of the kinematic (Re $\approx$ 20) and physical parameters (ϵ 0.4 and 0.9) are presented in Figures 6.27 and 6.28 over a range of power law indices ($0.2 \leq n \leq 1.0$). For densely packed systems (ϵ = 0.4), the pressure profile for Newtonian flow approximates a cosine profile, eventhough Re = 20 is well beyond the creeping flow regime. This affirms the contention that viscous forces are important for densely packed assemblages even at Re = 20. Furthermore, it is observed that pressure profile increasingly deviates from cosine dependence on angle as the degree of non-Newtonian behaviour becomes more and more pronounced. Indeed, for low values of n, the surface pressure is seen to attain a minimum value in the vicinity of $\theta = 90^{\circ}$ plane. These features are qualitatively similar to that of a potential flow pressure profile. Thus, the occurrance of minimum pressure around $\theta = 90^{\circ}$, is a consequence of flow acceleration around the mid plane. Indeed by combining the fact that V_{θ} is maximum at mid plane with

the Bernoulli's equation, it can be shown that the pressure goes through a minimum value around the mid plane. Between $\theta = 90^{o}$ and $\theta = 180^{o}$, the pressure increases due to flow decleration However, the pressure recovery is not complete due to viscous dissipation of the momentum Thus for any given value of n, the rear stagnation pressure is lower than the frontal stagnation value. It is also interesting to note that the change registered in the value of surface pressure with the change in power law index, decreases as n is reduced. Effectively, this means that when n is changed from 1 0 to 0 8, the decrease in pressure is more compared to that which occurs for change in n from 0.6 to 0 4. Qualitative explanation for such a behaviour can be taken from the dependence of viscosity on power law index discussed earlier in context with the creeping flow situation (Figure 6.9). As viscosity becomes very small at low values of n, the scope for further reduction in it remains limited Therefore, only minor changes occur in the pressure profile, with reduction in n at lower values of n. In the case of a hypothetical fluid with $n \approx 0$, the pressure profile will correspond to that of an ideal fluid flow occurring within the cell and such pressure profile would exhibit fore and aft symmetry about the mid plane. Indeed the present results are seen to approach this limiting behaviour.

At high voidage ($\epsilon = 0.9$),the surface pressure profile monotonically decreases from the front stagnation value to the rear with few minor exceptions. The monotonic decrease indicates that viscous effects are significant for all power law indices considered ($0.2 \leq n \leq 0\ 8$) even at Re = 20. Infact, the velocity within the cell gap varies as $(1/\delta)$, where δ is the radial gap

between the particle and the cell surface (See Appendix-II). The inertial effects are therefore ~ $O(1/\delta^2)$ while the viscous effects are $O(1/\delta^{2n})$ Thus, at high voidage and Re = 20, the inertial effects are not as important as in the case of low voidage. It is also worthwhile to note that the change in pressure with the power law index is much more gradual in this case than seen in Figure 6.27. This is due to a reduction in the average shear rate arising from the larger radial gap within the cell. At low values of n ($\leq$ 0.4), the pressure profile is seen to fluctuate around θ = 90^{o} plane Though the precise reasons for this behaviour are not immediately obvious, this may be attributed to the onset of inertial domination in the flow for given Reynolds number and voidage.

6.2.2 Drag Phenomena

Pressure, friction and total drag coefficients numerically computed over a range of voidage ($0.3 \leq \epsilon \leq 0.9999$), power law index ($0.2 \leq n \leq 0.8$) and Reynolds number ($1 \leq Re \leq 20$) are summarized in Table 6.3. Figures 6.29 to 6.37 show the variation of the pressure, friction and total drag coefficients with Reynolds number and voidage for three values of the power law index covering moderate to high shearthinning characteristics of the fluid. A preliminary examination of all these figures suggests that the results conform to C_D Re = constant (which is a trend displayed by creeping flow solutions) almost upto Re $\approx$ 10-20 for all values of n and moderate values of ϵ. For the extremely dilute voidages such as $\epsilon \approx 0.9999$ which are closer to the single sphere limit, however, the drag curve veers away from C_D Re = constant around Re $\approx$ 5-10 or so. The proportionalityy of the drag

Table 6 3· Summary of drag (pressure, friction and total) coefficients for power law fluid flow past an assemblage of particles at intermediate Reynolds numbers

n	C_{DP}	C_{DF}	C_D	C_{DP}/C_{DF}
Re = 1				
∈ = 0 3				
1 0	0.4333×10^{4}	$0\ 1210\times10^{4}$	$0\ 5543\times10^{4}$	3 58
0.8	0.1538×10^{4}	$0\ 4472\times10^{3}$	0.1985×10^{4}	3 5391
0 6	0.5306×10^{3}	$0\ 1554\times10^{3}$	0.6860×10^{3}	3 4144
0.4	0.1720×10^{3}	$0\ 5745\times10^{2}$	$0\ 2294\times10^{3}$	2.993
0 2	0.4988×10^{2}	0.2041×10^{2}	$0\ 7029\times10^{2}$	2 44
∈ = 0.4				
1 0	0.1438×10^{4}	0.6086×10^{3}	0.2047×10^{4}	2.362
0.8	0.5847×10^{3}	0.2586×10^{3}	0.8433×10^{3}	2.261
0.6	0.2298×10^{3}	0.1043×10^{3}	0.3341×10^{3}	2 203
0.4	0.8213×10^{2}	0.4369×10^{2}	$0\ 1258\times10^{3}$	1.879
0.2	0.2586×10^{2}	0.1786×10^{2}	$0\ 4372\times10^{2}$	1 44
∈ = 0.5				
1 0	$0\ 5673\times10^{3}$	$0\ 3438\times10^{3}$	$0\ 9111\times10^{3}$	1 650
0.8	0.2590×10^{3}	$0\ 1644\times10^{3}$	0.4234×10^{3}	1 575
0.6	0.1134×10^{3}	$0\ 7527\times10^{2}$	0.1886×10^{3}	1.506
0 4	0.4563×10^{2}	0.3537×10^{2}	$0\ 8100\times10^{2}$	1.290
0 2	0.1346×10^{2}	0.1584×10^{2}	0.2930×10^{2}	0.849
∈ = 0.7				
1.0	0.1143×10^{3}	0.1290×10^{3}	$0\ 2433\times10^{3}$	0.886
0.8	0.6485×10^{2}	$0\ 7594\times10^{2}$	0.1407×10^{3}	0 853
0.6	0.3463×10^{2}	0.4353×10^{2}	0.7816×10^{2}	0.795
0.4	0.1647×10^{2}	$0\ 2488\times10^{2}$	0.4135×10^{2}	0.661
0.2	0.6256×10	0.1372×10^{2}	0.1998×10^{2}	0 455

ϵ = 0 9

1.0	0 2643x10^2	0 4805x10^2	0 7448x10^2	0.550
0 8	0 1995x10^2	0.3645x10^2	0 5640x10^2	0 5473
0.6	0 1421x10^2	0.2611x10^2	0 4032x10^2	0 5440
0.4	0 9640x10	0.1823x10^2	0.2787x10^2	0 5287
0.2	0.6263x10	0.1192x10^2	0 1818x10^2	0 5251

ϵ = 0 99

1.0	0.1171x10^2	0.2394x10^2	0 3565x10^2	0 4891
0.8	0 1204x10^2	0.2278x10^2	0 3482x10^2	0 528
0.6	0.1223x10^2	0.2057x10^2	0 3280x10^2	0 594
0.4	0 1218x10^2	0.1656x10^2	0 2874x10^2	0 735
0.2	0.1163x10^2	0.1130x10^2	0 2293x10^2	1 029

ϵ = 0.9999

1.0	0.8273x10	0.1801x10^2	0.2628x10^2	0 458
0.8	0.1085x10^2	0.2005x10^2	0.3020x10^2	0 506
0.6	0 1182x10^2	0.1962x10^2	0.3144x10^2	0.602
0 4	0.1301x10^2	0.1592x10^2	0.2893x10^2	0.816
0.2	0.1359x10^2	0.1133x10^2	0.2492x10^2	1.199

Re = 10

ϵ = 0 3

1.0	0.4333x10^3	0.1211x10^3	0.5544x10^3	3.578
0.8	0.1540x10^3	0.4486x10^2	0.1988x10^3	3 432
0.6	0 5360x10^2	0.1586x10^2	0.6946x10^2	3.379
0.4	0.1887x10^2	0.5826x10	0.2469x10^2	3.238
0.2	0.5449x10	0 1829x10	0.7278x10	2.978

ϵ = 0 4

1.0	0.1439x10^3	0.6092x10^2	0 2048x10^3	2.362
0.8	0.5860x10^2	0.2600x10^2	0.8460x10^2	2.253
0.6	0.2334x10^2	0.1070x10^2	0.3404x10^2	2.181
0.4	0.9378x10	0.4484x10	0 1386x10^2	2.090
0.2	0.2805x10	0.1607x10	0.4412x10	1.745

$\epsilon = 0.5$

1.0	0.5677×10^{2}	0.3455×10^{2}	0.9122×10^{2}	1.643
0.8	0.2598×10^{2}	0.1657×10^{2}	0.4255×10^{2}	1.567
0.6	0.1161×10^{2}	0.7778×10	0.1938×10^{2}	1.492
0.4	0.5444×10	0.3675×10	0.9119×10	1.48
0.2	0.1949×10	0.1659×10	0.3608×10	1.174

$\epsilon = 0.7$

1.0	0.1146×10^{2}	0.1299×10^{2}	0.2455×10^{2}	0.882
0.8	0.6530×10	0.7760×10	0.1429×10^{2}	0.841
0.6	0.3655×10	0.4594×10	0.8249×10	0.795
0.4	0.2041×10	0.2618×10	0.4659×10	0.779
0.2	0.9504	0.1286×10	0.2237×10	0.739

$\epsilon = 0.9$

1.0	0.5291×10	0.9709×10	0.1500×10^{2}	0.545
0.8	0.4275×10	0.7802×10	0.1207×10^{2}	0.548
0.6	0.2891×10	0.5350×10	0.8241×10	0.540
0.4	0.2031×10	0.3713×10	0.5744×10	0.546
0.2	0.1532×10	0.2341×10	0.3873×10	0.641

$\epsilon = 0.9999$

1.0	0.1887×10	0.4261×10	0.6148×10	0.443
0.8	0.2174×10	0.4337×10	0.6511×10	0.501
0.6	0.2451×10	0.3931×10	0.6382×10	0.623
0.4	0.2642×10	0.3120×10	0.5762×10	0.846
0.2	0.2725×10	0.2286×10	0.5011×10	1.195

Re = 20

$\epsilon = 0.3$

1.0	0.2167×10^{3}	0.6051×10^{2}	0.2769×10^{3}	3.581
0.8	0.7744×10^{2}	0.2289×10^{2}	0.1003×10^{3}	3.382
0.6	0.2783×10^{2}	0.8790×10	0.3662×10^{2}	3.163
0.4	0.9882×10	0.2921×10	0.1280×10^{2}	3.383
0.2	0.2039×10	0.8821	0.2921×10	2.311

$\epsilon = 0.4$

1.0	0.7203×10^{2}	0.3055×10^{2}	0.1026×10^{3}	2 358
0 8	0.2953×10^{2}	0.1333×10^{2}	0.4286×10^{2}	2 215
0 6	0.1215×10^{2}	0.5868x10	0.1801×10^{2}	2 070
0.4	0 4877x10	0 2248x10	0.7125x10	2 169
0.2	0.1188x10	0 7749	0.1962x10	1 533

$\epsilon = 0.5$

1.0	0.2845×10^{2}	0.1732×10^{2}	0.4577×10^{2}	1 643
0.8	0.1313×10^{2}	0 8573x10	0.2170×10^{2}	1 531
0.6	0.6092x10	0 4250x10	0.1034×10^{2}	1 433
0 4	0 2672x10	0 1819x10	0 4491x10	1 468
0.2	0.9237	0 7115	0 1635x10	1 298

$\epsilon = 0.7$

1.0	0.5768x10	0 6656x10	0.1242×10^{2}	0 867
0.8	0.3332x10	0 4104x10	0 7436x10	0 811
0.6	0.1931x10	0 2498x10	0 4429x10	0 773
0.4	0.1029x10	0 1292x10	0 2494x10	0 796
0.2	0.3949	0 6152	0 1010x10	0 642

$\epsilon = 0.9$

1 0	0.1337x10	0 2745x10	0.4082x10	0 487
0.8	0.1044x10	0 2155x10	0.3199x10	0 484
0 6	0.8262	0 1562x10	0.2388x10	0 528
0.4	0.6521	0 9975	0 1649x10	0.653
0 2	0.4536	0 5685	0.1022x10	0.798

$\epsilon = 0.99$

1.0	0.8931	0 2037x10	0.2851x10	0.438
0.8	0.8263	0 1764x10	0.2590x10	0.468
0.6	0 8364	0 1362x10	0 2196x10	0.613
0.4	0.8189	0 9225	0.1741x10	0 887
0.2	0.7259	0 5546	0.1270x10	1.308

$\epsilon = 0.9999$

1.0	0.8491	0.2017x10	0.2866x10	0.421
0.8	0.8342	0.1606x10	0.2440x10	0.519
0.6	0.8170	0.1212x10	0.2029x10	0.674
0.4	0.7915	0.8675	0.1639x10	0.912
0.2	0.7622	0.5790	0.1341x10	1.316

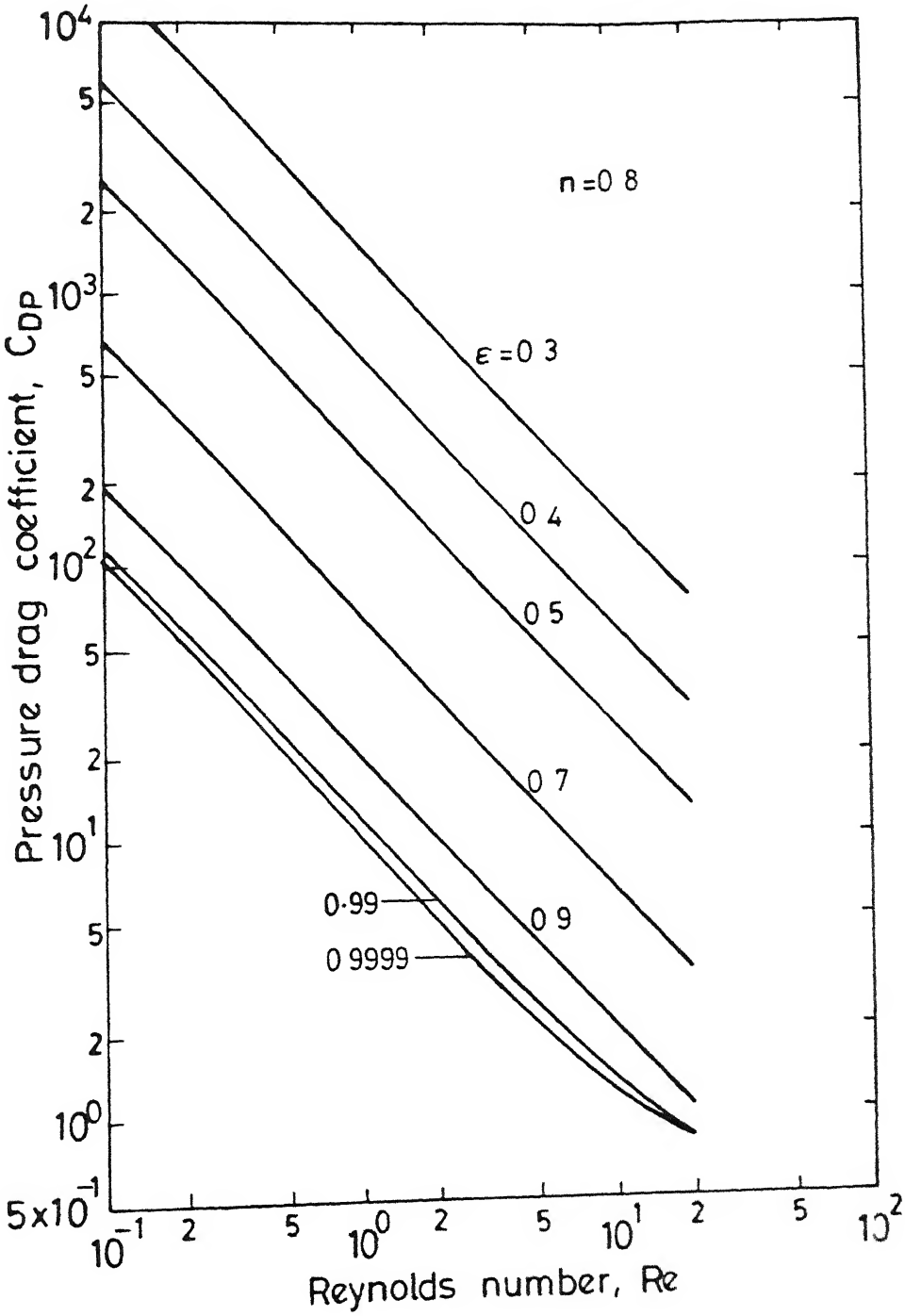

Fig. 6.29 Variation of pressure drag coefficient with Reynolds number and voidage for n = 0.8

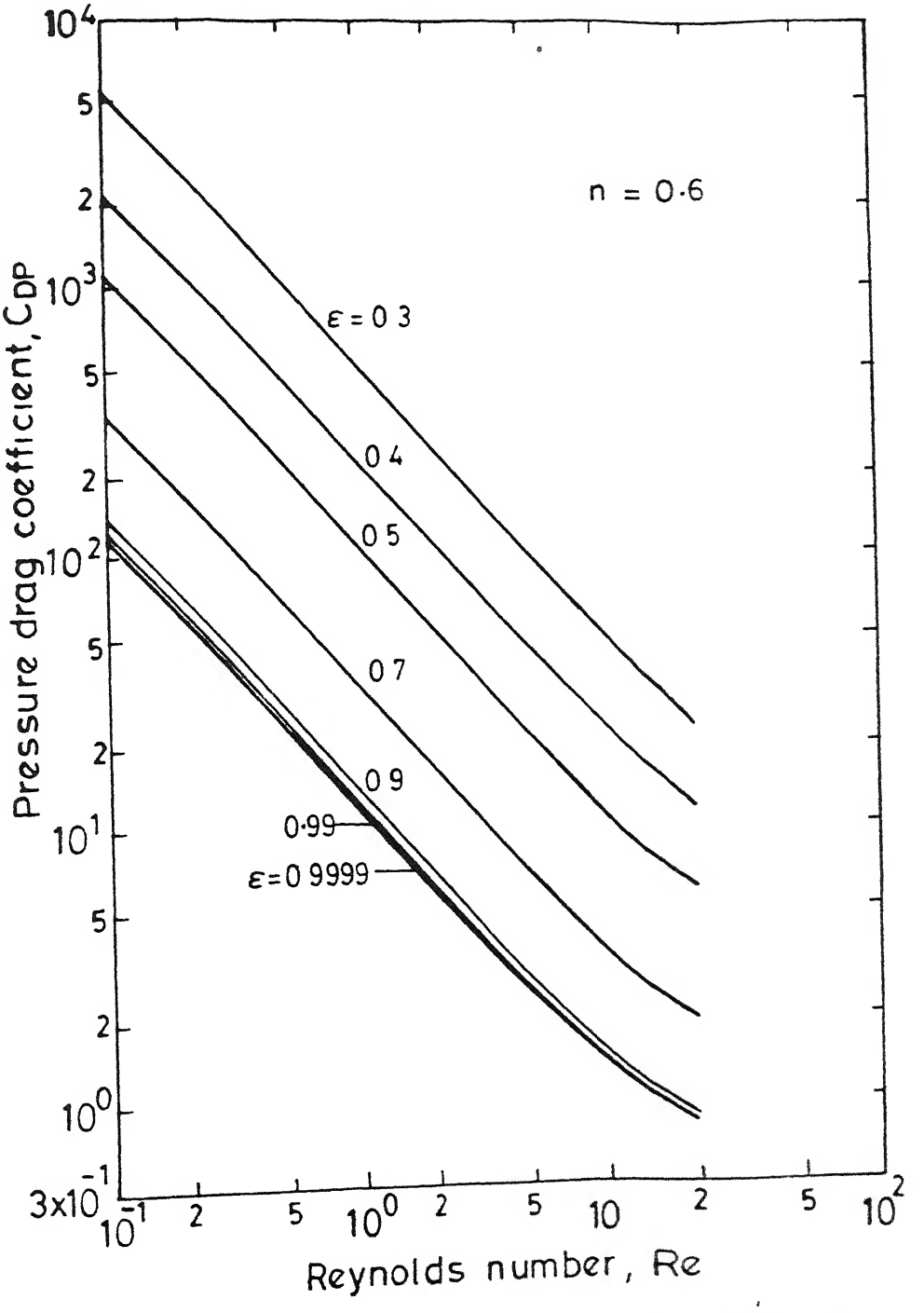

Fig 6.30 Variation of pressure drag coefficient with Reynolds number and voidage for n = 0 6.

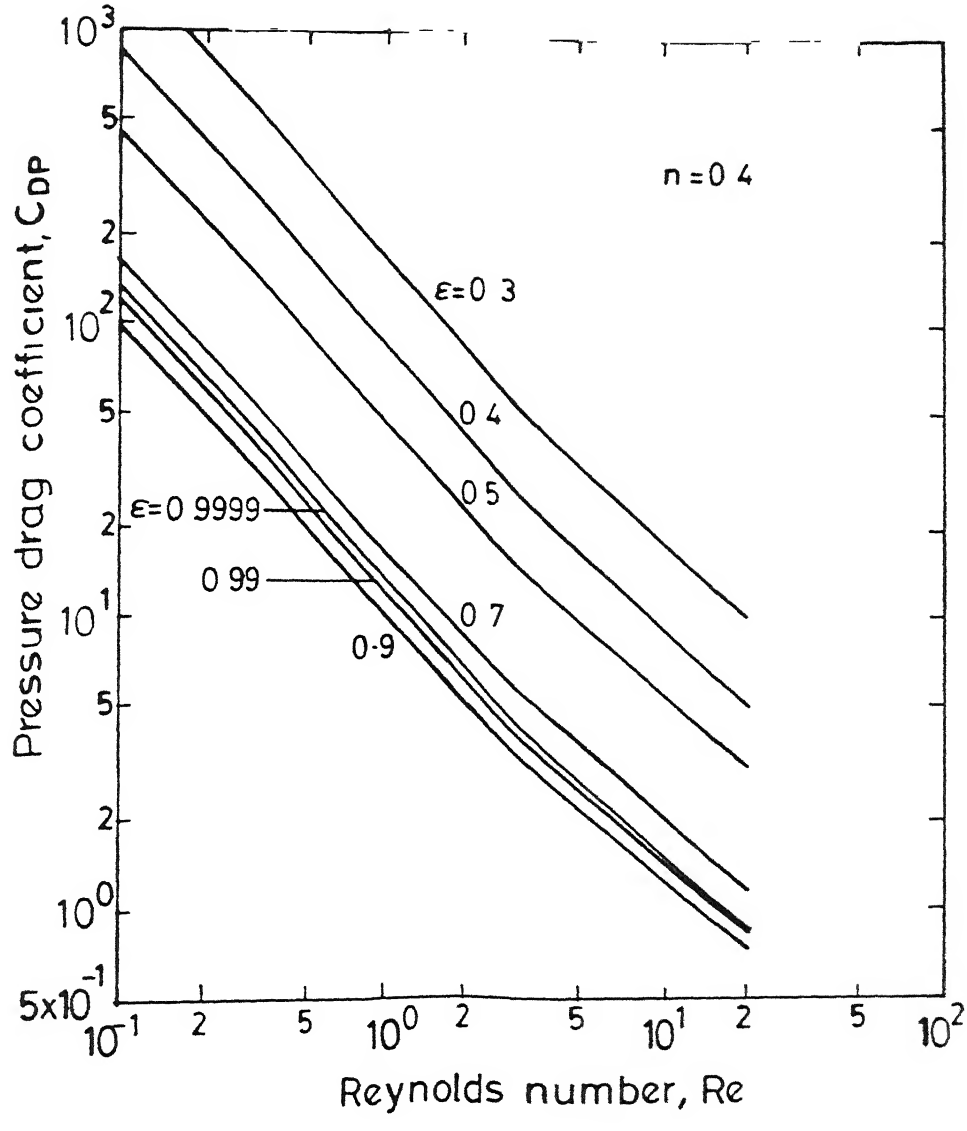

Fig. 6.31 Variation of pressure drag coefficient with Reynolds number and voldage for n = 0.4.

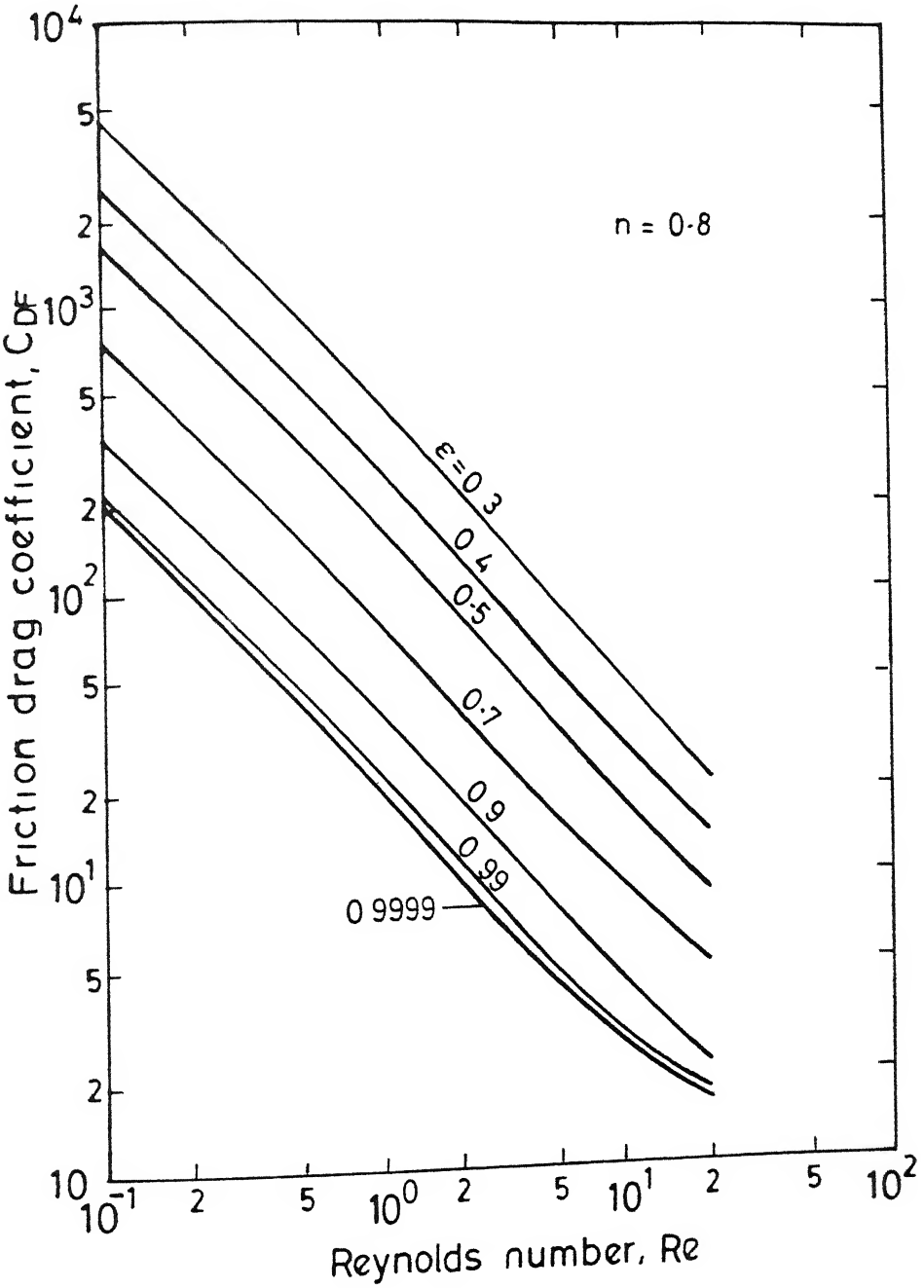

Fig 6.32 Dependence of friction drag coefficient on voidage and Reynolds number for n = 0.8.

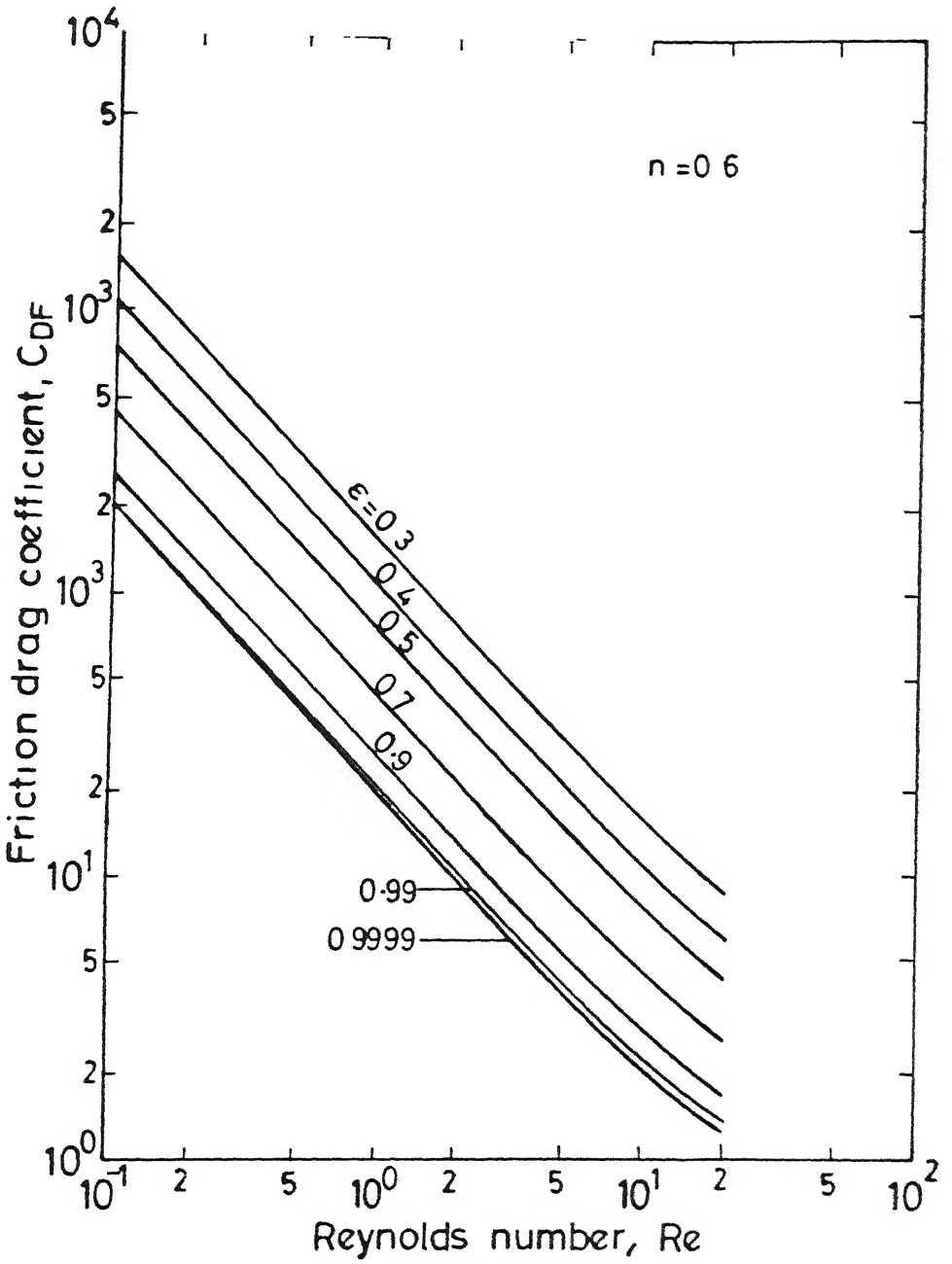

Fig. 6.33 Dependence of friction drag coefficient on voldage and Reynolds number for n = 0.6.

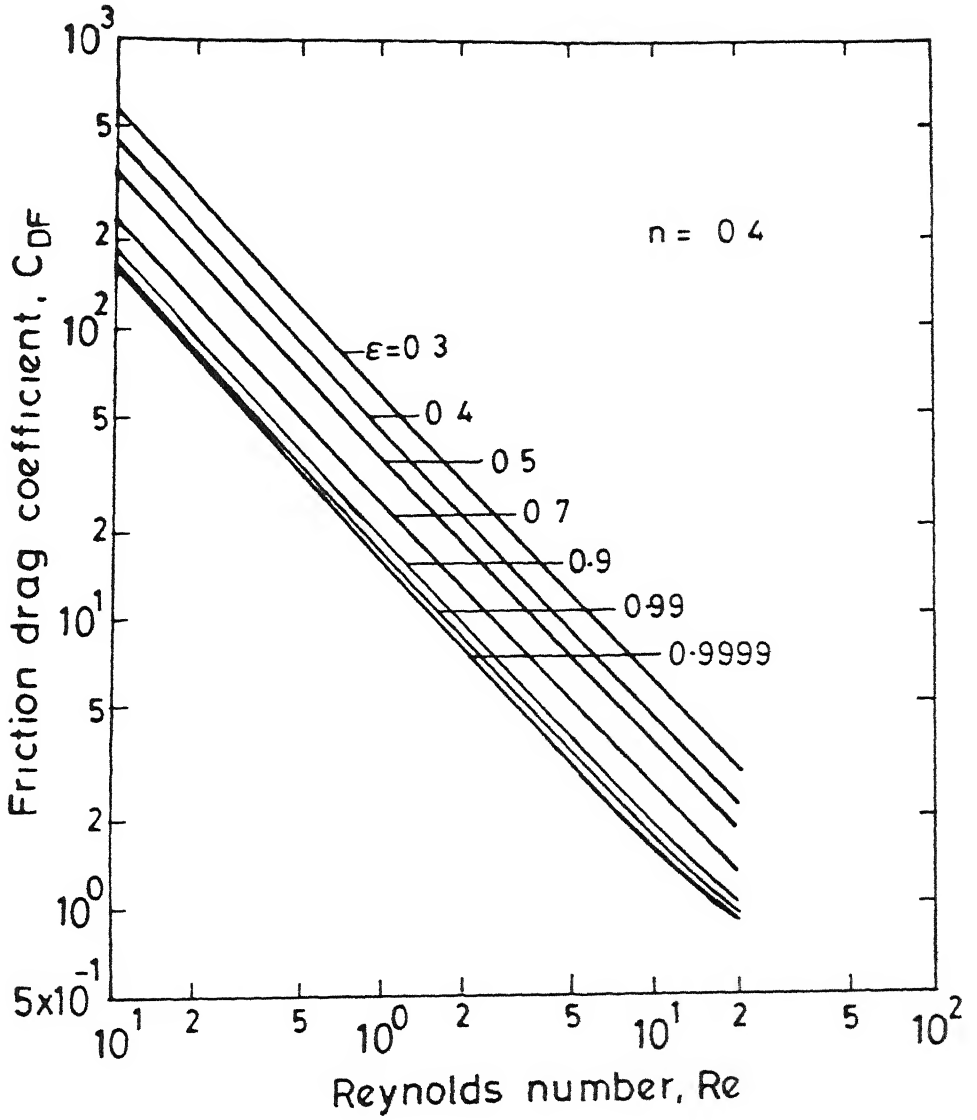

Fig 6.34 Dependence of friction drag coefficient on voidage and Reynolds number for n = 0.4.

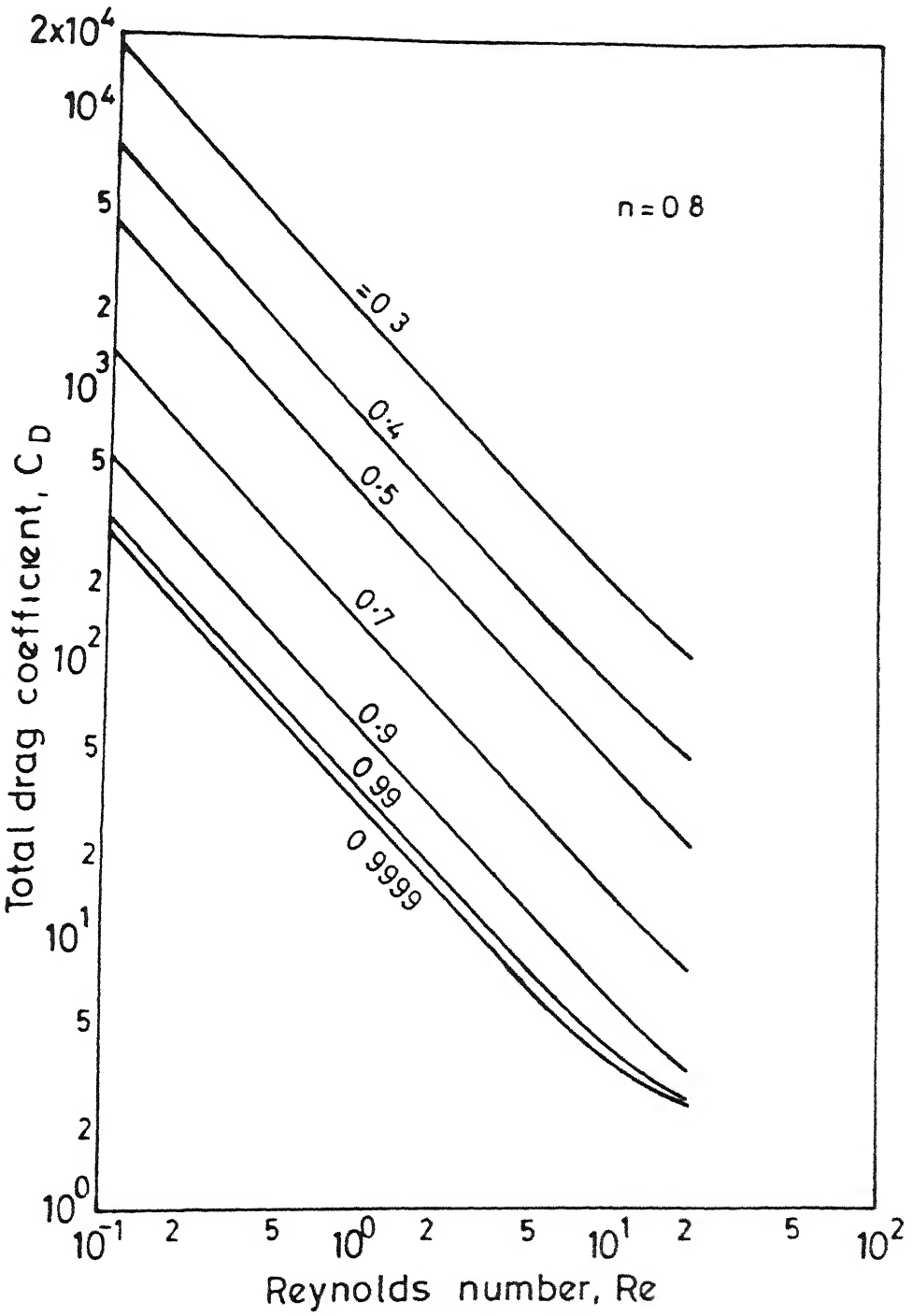

Fig. 6.35 Variation of total drag coefficient with Reynolds number and voidage for n = 0.8.

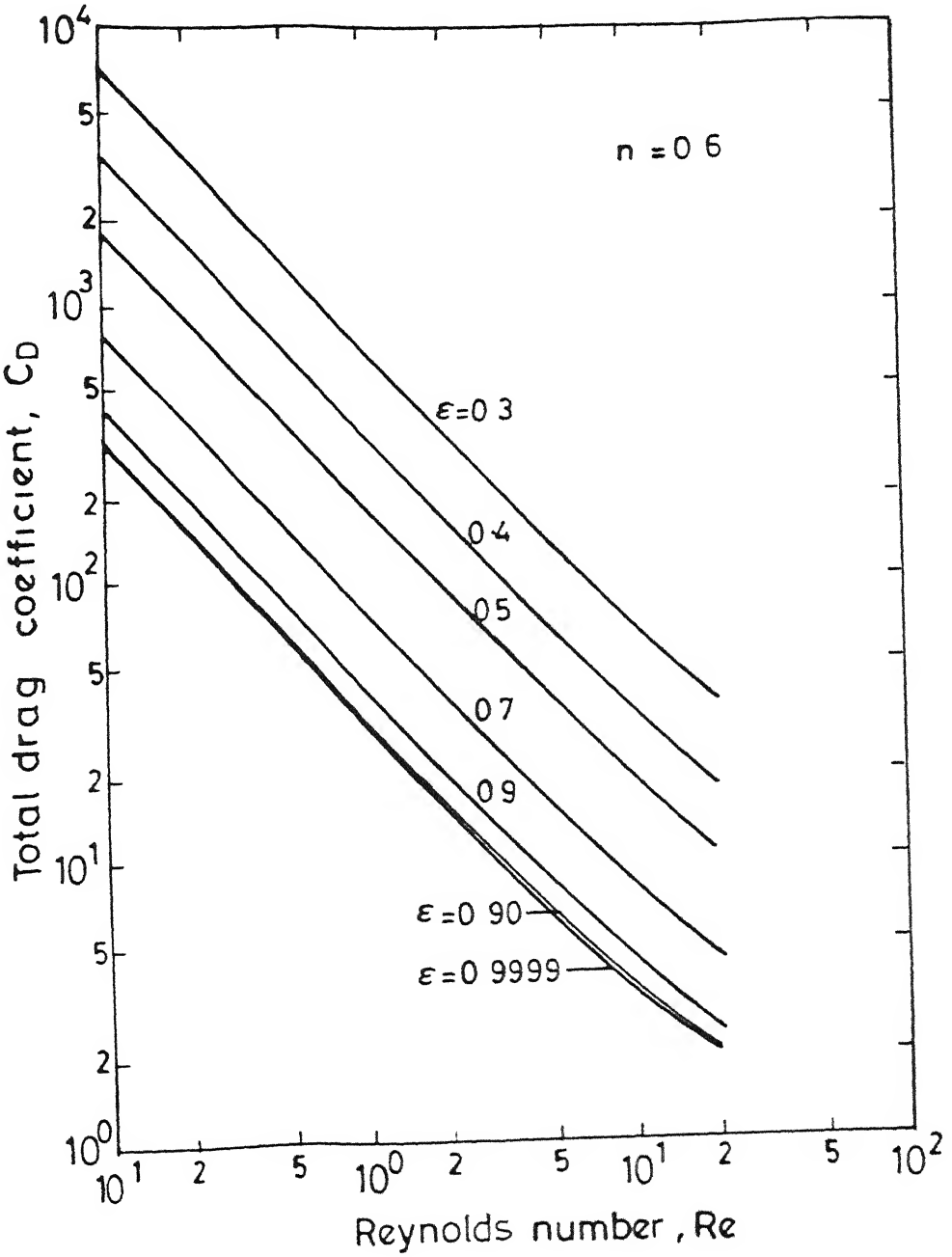

Fig. 6.36 Variation of total drag coefficient with Reynolds number and voidage for n = 0 6.

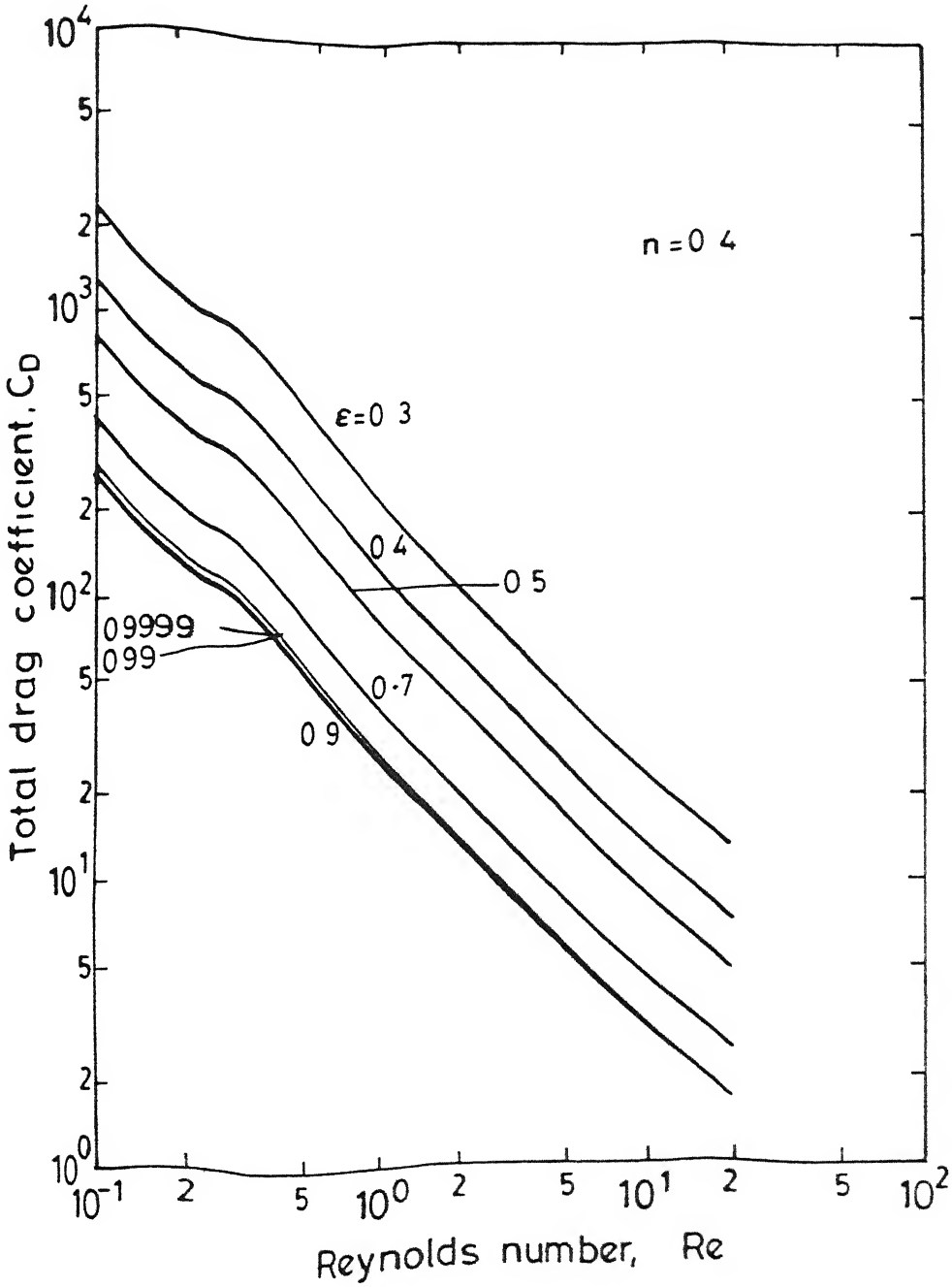

Fig. 6.37 Variation of total drag coefficient with Reynolds number and voldage for n = 0.4.

coefficient to flow Reynolds number reinforces the idea that for multiparticle systems, the viscous force plays a significant role and some of the features of the creeping flow solution are exhibited even upto Reynolds number of 20. Strictly speaking, the critical value of Re at which the behaviour ceases to conform to C_D Re = constant, appears to be dependent on the values of ϵ and n Lower the value of voidage, higher is the critical Reynolds number, whereas, lower the value of the power law index, lower is the critical Reynolds number This observation in respect to the effect of voidage is in qualitative agreement with the findings of El-Kaissy and Homsy (1973). In the light of above discussions, it is safe to conclude that the viscous effects continue to dominate the flow almost upto Re $\approx$ 20 in multiparticle assemblages under commonly encountered shearthinning conditions and voidage.

Further examination of these figures reveals that the total drag coefficient draws a larger contribution from the pressure drag coefficient in the case of dense assemblages, whereas, frictional drag contributes in a greater measure in dilute systems. This reversal appears to occur around $\epsilon \approx 0.7$ or so. It can be shown from an order of magnitude consideration that for a small radial gap (δ) between the particle and cell surfaces,

average angular velocity = $O(1/\delta)$

inertial force = $O(1/\delta^2)$

shear force = $O(1/\delta^{2n})$

and, pressure force = $O(1/\delta^m)$

Here, m = 2 for inertia dominated flows (i.e. low n, and/or high Re) and m = 2n+1 for viscous flow (high n and/or low Re). It then follows that for low voidages, pressure drag contribution will be

larger than friction drag coefficient and vice-versa.

In the limiting case of a single sphere (ϵ = 0.9999), the pressure drag coefficient shows an anomalous dependence on voidage under highly shearthinning conditions (Figure 6.31) i.e. pressure drag increases with increase in voidage. This is believed to be a consequence of the significant changes in the flow field structure as single sphere limit is approached, for an extremely shearthinning fluid. One can possibly explain this by noting that the flow is usually circulatory in a multiparticle assemblage (Figures 6.38 and 6.39) whereas the streamlines are non-circulatory in the case of a single sphere This change in flow structure may cause the increase in pressure drop with voidage for an extremely dilute assemblage. The numerical values of C_{DP}, C_{DF} and C_D indicate that a power function type dependence (as discussed in Sec.6.1.1) is applicable for $n \geq 0.5$ even at Re = 20. However, the drag coefficient (C_D) near the single sphere limit ($\epsilon \approx 0.9999$) is a continuously decreasing curve. With reduction in n, this behaviour is different from that observed for creeping flow at the same voidage. This difference in drag behaviour between the creeping and intermediate Reynolds number flow regimes, is evidently contributed by inertia.

6.2.3 Flow Field

Figures 6.38 and 6.39 depict the typical streamline patterns (Re = 20 and ϵ = 0.9) for two values of power law flow index. The flow is seen to be asymmetric in the gap within the cell about the mid plane. This asymmetry is clearly indicated by a forward shift in location of the vortex in the direction of particle motion. The streamlines are seen to originate from the front portion of

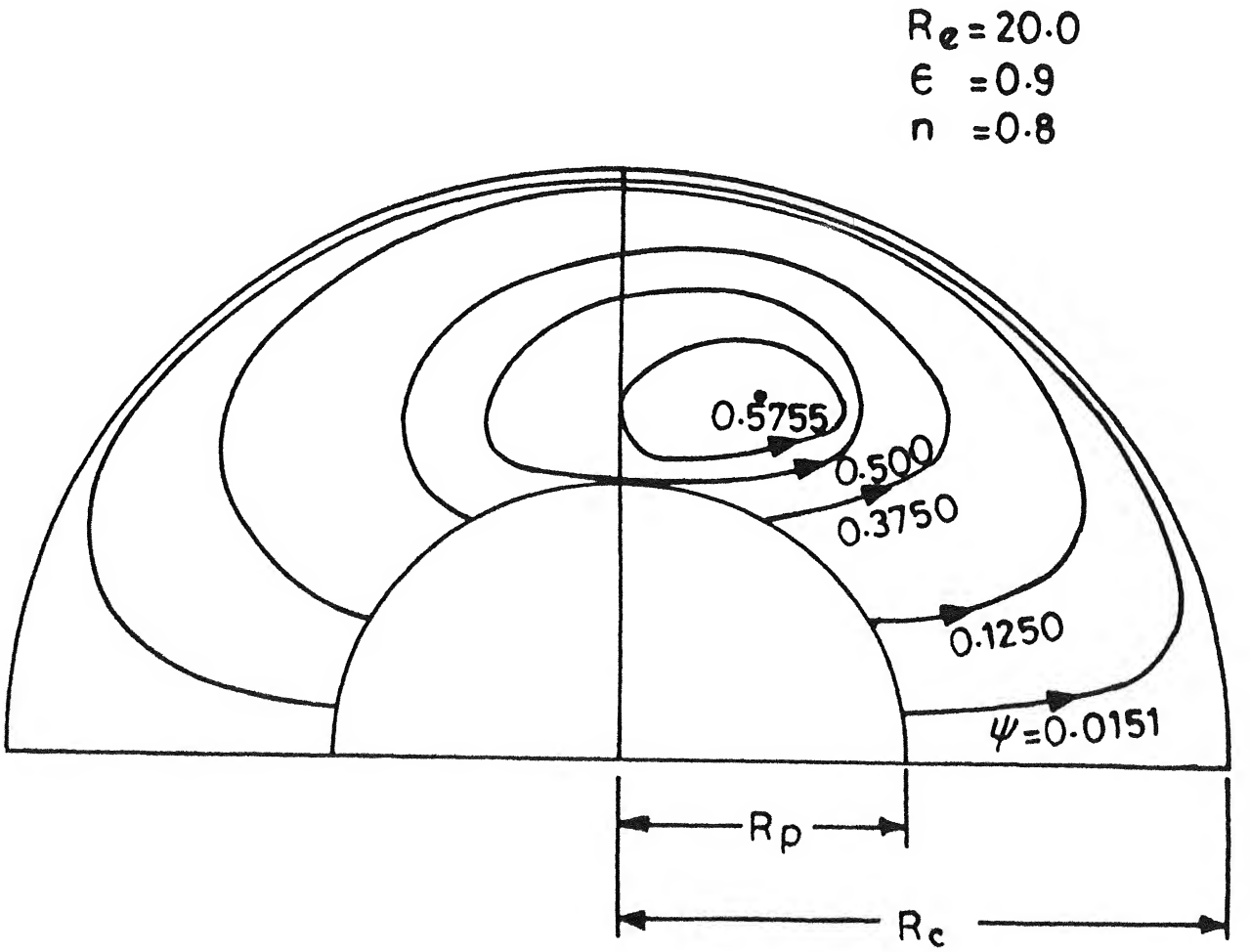

Fig. 6 38 Streamline patterns for Re = 20, ∈ = 0.9 and n = 0 8.

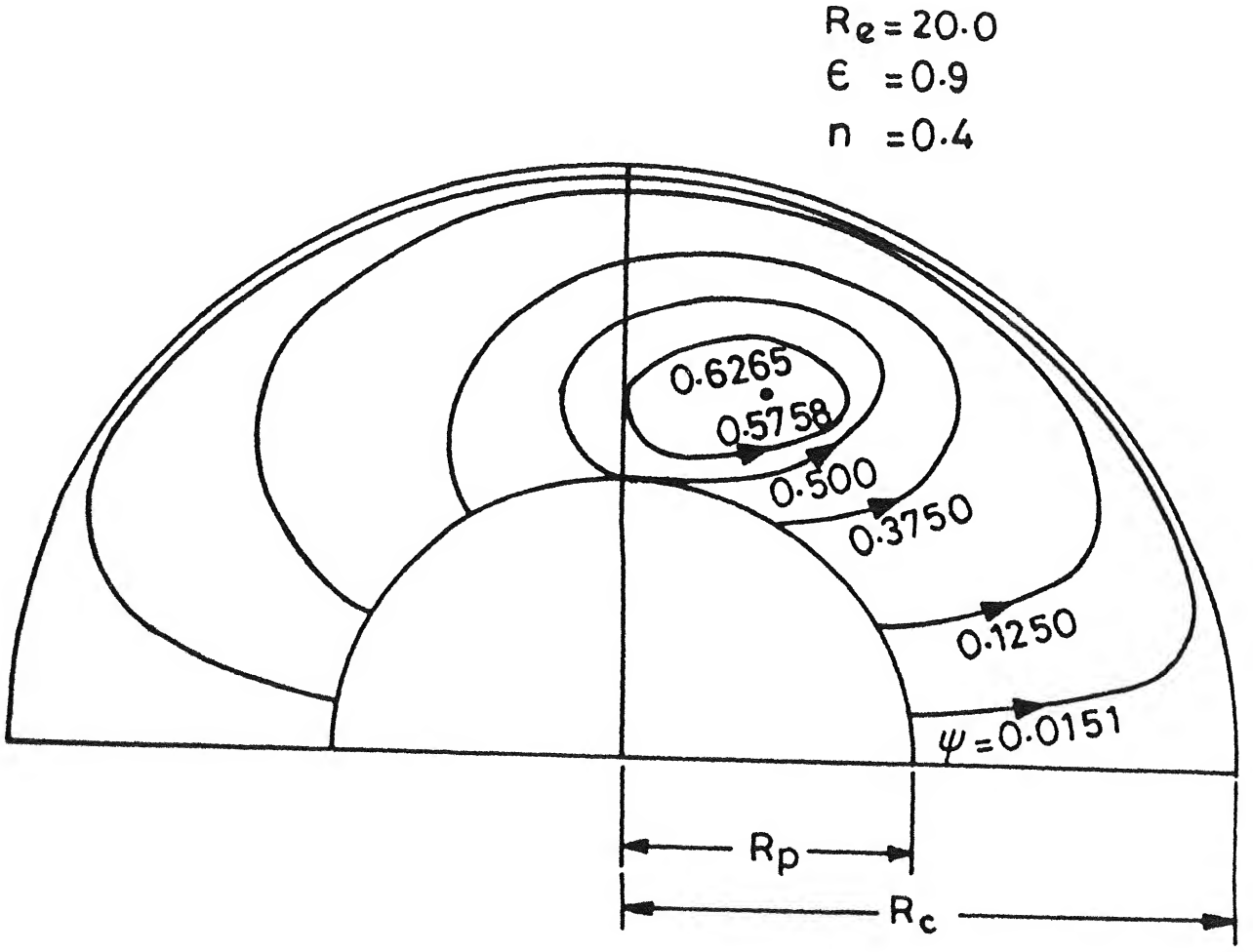

Fig. 6.39 Streamline patterns for Re = 20, ∈ = 0 9 and n = 0 4.

the particle, turn back at a certain distance, and reattach themselves in the rear of the particle It is interesting to note that after leaving the particle surface in the front portion, the streamlines remain parallel to the axis, upto a certain distance away from the particle. In this region the stream function at a point can be roughly calculated as $\psi = \frac{1}{2} y^2$, where y is the distance measured from the axis This is a feature of uniform flow with unit velocity. Therefore, a portion of fluid in front of the particle seems to be moving with the same velocity as the particle due to inertial effects. This uniform flow region adjacent to the particle extends almost upto midplane ($\theta \approx 90^{\circ}$) In addition to the streamlines attached to the particle, one can also discern small vortex like streamlines adjacent to the particle. As power law index is reduced the circulatory vortex adjacent to the particle shrinks in size As the vortex is sustained by shear stress in the fluid, it is hardly surprising that at a lower power law index (hence lower viscosity), the size or the vortex is small. However, it is to be mentioned that compared to creeping flow situation, the reduction in size of vortex with decrease in power law index is less apparent at higher Reynolds number (Re = 20)

6.2.4 Comparison with Available Results

In order to ascertain the reliability of the present theoretical predictions, it is desirable to compare them with available experimental results in literature on flow of power law fluid past multiparticle assemblages at intermediate Reynolds number. However, it is to be admitted that such comparisons are difficult due to the paucity of results at intermediate Reynolds

numbers In a comprehensive study, Kemblowski and Mertl (1974) proposd the following expressions for the flow of power law liquids through the packed beds ($\epsilon \sim 0.39 - 0.4$):

$$f_{bk} = (150/Re'_{bk}) + 1\ 75\ K_1^2 / (\mu_c^2\ (K_1^2 - 1)^2 + K_1^2)^{1/2} \qquad (6\ 6)$$

where,

$$K_1 = \xi_c\ Re'_{bk}$$

$$Re'_{bk} = U_\infty^{2-n}\ (2R_p)\ e/\psi\ (1-\epsilon)$$

$$\psi = K_1\ ((9n + 3)/n^n\ (150\ S\epsilon)^{\frac{1-n}{2}}/12$$

$$S = d_p^2\ \epsilon^3/150\ (1-\epsilon)^2$$

The quantities μ_c and ξ_c were found to be functions of flow behaviour index n only Values of the parameters μ_c and ξ_c for a constant n, were determined employing the method of least squares. Using the fifth order polynomials given by authors to evaluate μ_c and ξ_c, it is found that when

$n = 0.8$

$\xi_c = 0.1924$

$\mu_c = 0.8273$

and when $n = 0\ 6$

$\xi_c = 0\ 1579$

$\mu_c = 0.7128$

Equation (6.6) has been claimed to be applicable for both shearthinning and dilatant materials. However, the experimental data used in obtaining the empirical constants are restricted to $1 \geq n \geq 0.6$. Therefore, the comparison between the present results and those calculated from Eqn. (6.6) is restricted to $1 \leq Re \leq 20$ and $0.6 \leq n \leq 1.0$ only. A summary of the results is shown in

Table 6.4 An examination of this Table suggests that the present theoretical results are in reasonable agreement with the experimental results (assumed here to be represented by Eqn 6 6) only upto Re ~ 10 and n ~ 0 8 The degree of divergence increases rapidly with the increasing non-Newtonian behaviour as well as with increasing value of Reynolds numbers.

Table 6.4 Comparison of Theoretical Predictions with Experimental Results on Packed Beds (ϵ = 0.4).

	n = 0.8		n = 0.6	
Re	f^{+}_{bk}(present)	f_{bk}(expt)	f^{+}_{bk}(present)	f_{bk}(expt)
1.0	40.48	45.87	16.04	22.891
5.0	8.1	10.25	3.25	6.056
10.0	4.06	6.16	1.63	3.903
20.0	2 06	3.95	0.86	2 826

In a recent study, Srinivas and Chhabra (1990) demonstrated that the values of the pressure drop for the flow of power law liquids through packed beds predicted by various empirical expressions available in the literature differ from each other by as much as a factor of 2. Furthermore, Sheffield (1975) re-analysed most of the data on the non-Newtonian fluid flow through fixed beds available in the literature, and concluded that the errors of the order of 60-70% are not uncommon. Bearing in mind these factors, the correspondence between the two results in

---

$$f^{+}_{bk}\ (\text{present}) = \frac{3}{4} C_d \epsilon^3$$

Table 6 2 is believed to be satisfactory upto about Re ~ 10 and n ~ 0 8 For moderately shearthinning fluids (n = 0 6) the agreement with experimental results may be taken as satisfactory only at Re = 1.0.

In order to examine the performance of the free surface cell model at intermediate Reynolds numbers for extremely dilute assemblages (ϵ = 0.9999), the present results are compared with the available experimental results for a single sphere falling under the influence of gravity. At the outset, it is important to recognise that even the condition of ϵ = 0.9999 denotes the (R_c/R_p) ratio of about 21, and based on the experimental results obtained in cylindrical tubes, the wall correction to fall velocity for this situation is of the order of 8%, which in turn, would contribute to drag coefficient in varying amounts depending upon the value of n. Thus, such a comparison must be regarded as only qualitative Figures 6.40 and 6.41 show typical comparisons for n = 0.8 and 0.6 with the experimental results of Chhabra and Uhlherr (1980). The degree of correspondence is seen to be qualitatively satisfactory upto Re ~ 20 for n ~ 0.8 and upto Rc $\leq$ 2.0 for n = 0.6. In concluding this section, it is to be mentioned that flow past packed beds and single spheres represent the two extreme conditions of particle assemblages and the intermediate voidage range is the characteristic of fluidized beds. In the following section, the performance of free surface cell model in dealing with the fluidized beds has been discussed.

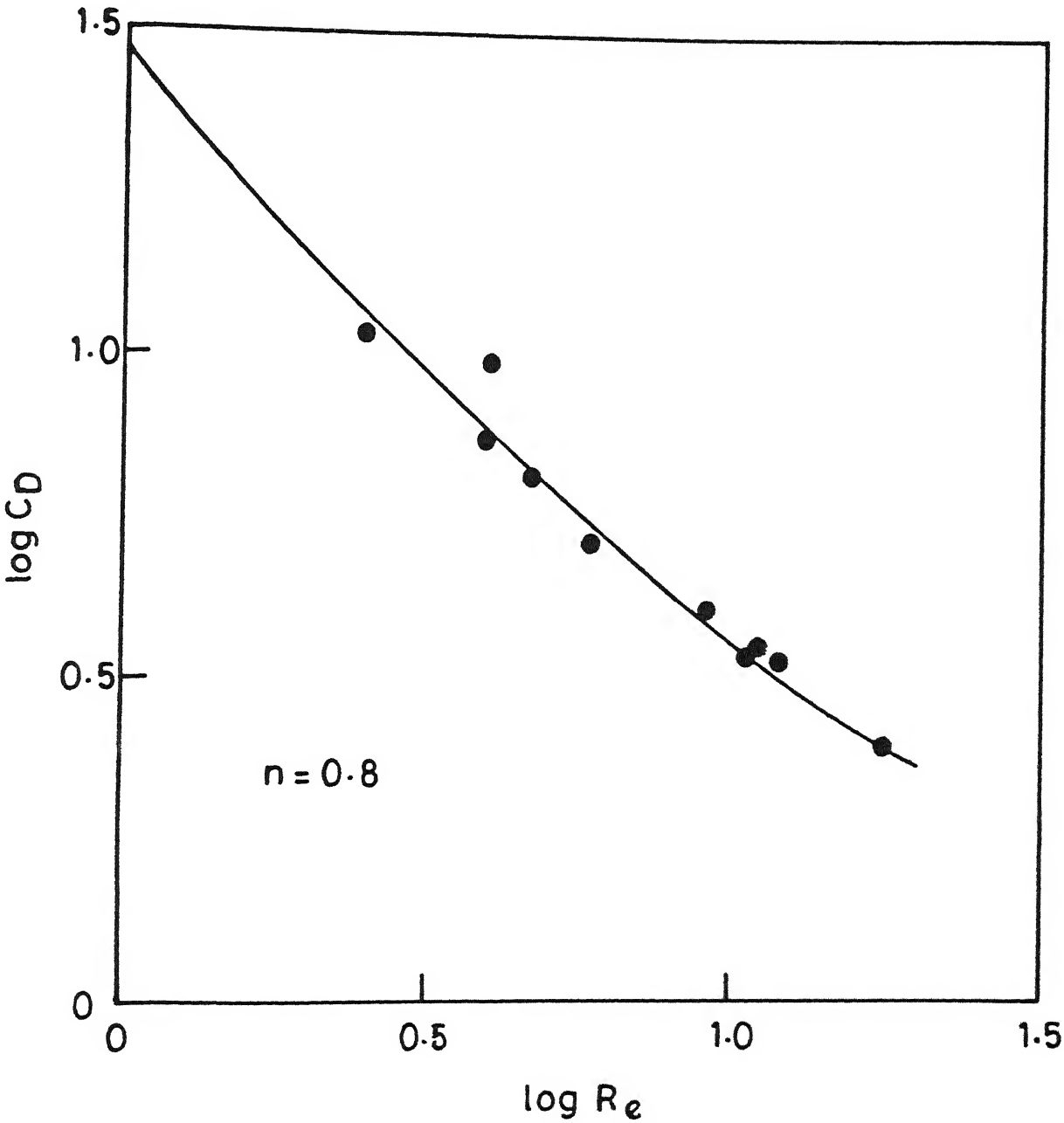

Fig. 6.40 Comparison between theory (ϵ = 0.9999) and experiments for single spheres (n = 0.8) at intermediate Reynolds numbers.

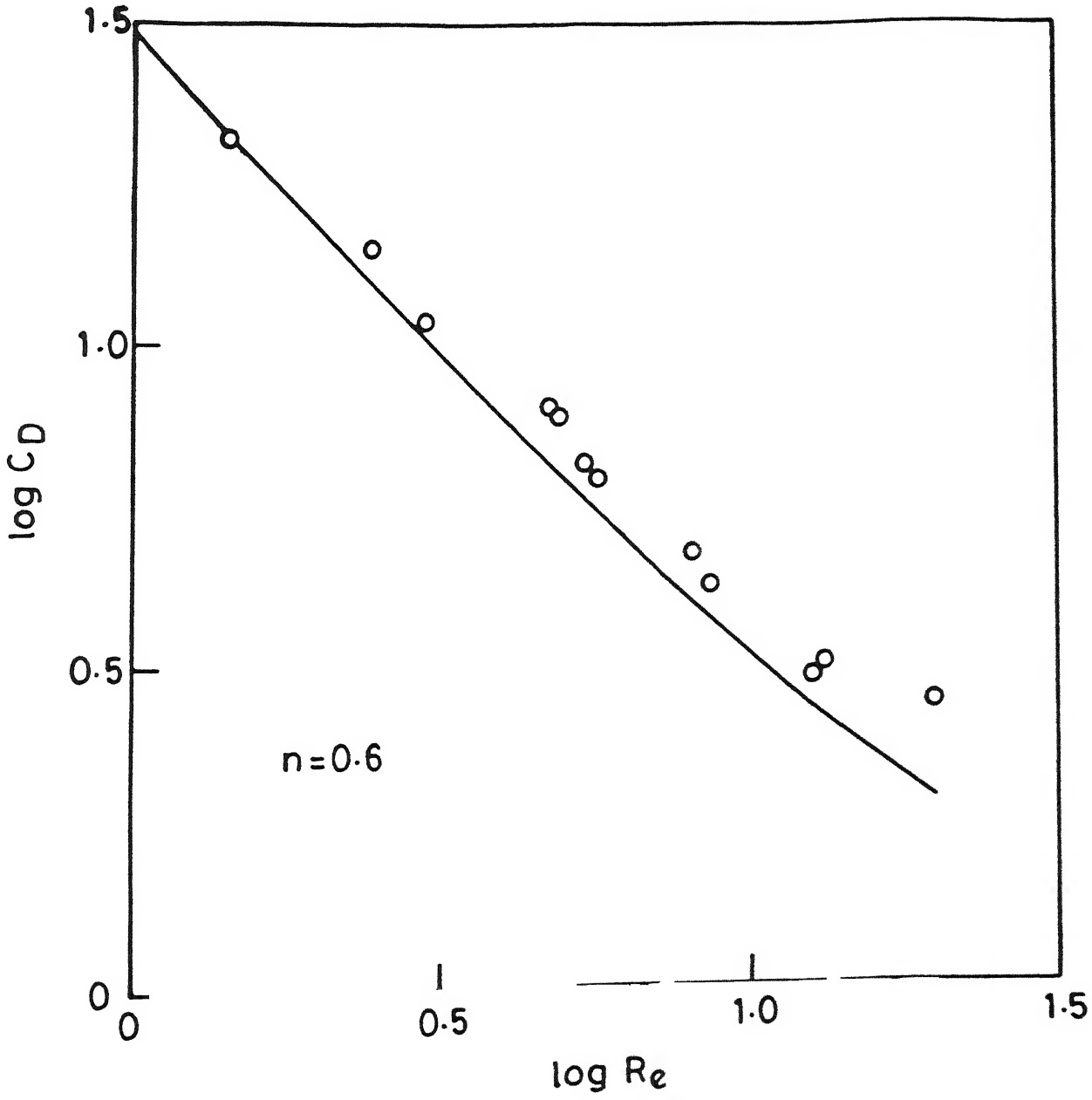

Fig 6.41 Comparison between theory (ϵ = 0.9999) and experiments for single spheres (n = 0.6) at intermediate Reynolds numbers.

6.3 FLUIDIZED BED DATA AND COMPARISON WITH EXPERIMENTAL RESULTS

A general fluidization correlation which may be useful for design and analysis purpose has been prepared essentially by extending the approach described by Zenz and Othmer (1960) for Newtonian fluid, to a power law fluid. This consists replotting the variation of drag coefficient vs. Reynolds number data for a fixed value of n, in terms of $(C_D^{\frac{2-n}{2+n}} \; Re^{\frac{2}{2+n}}$ against $(Re^{1/n}/C_D)^{\frac{n}{n+2}}$ with voidage as parameter Such plots have been prepared for two values of power law index n (0.8 and 0.6),and are presented as Figures 6.42 and 6.43 A plot of this kind is useful as it results essentially in a plot of particle velocity against particle diameter for a given value of n, with physical properties as parameters For a fluidized bed

$$C_D = \frac{4}{3} \frac{g d_p}{U_\infty^2} \frac{(\rho_p - \rho)}{\rho} \tag{6.11}$$

and $$Re = \frac{\rho \, U_\infty^{2-n} \, d_p^{\,n}}{K} \tag{6.12}$$

From these two equations, it can be shown that

$$C_D^{\frac{2-n}{2+n}} \; Re^{\frac{2}{2+n}} = d_p \, \alpha \tag{6.13}$$

and $$\left(Re^{1/n}/C_D \right)^{\frac{n}{2+n}} = U_\infty \, \beta \tag{6.14}$$

where α and β are solely dependent upon physical properties of the particle and the fluid and U_∞ is the superficial flow velocity through the bed. Defining U_o as the free settling velocity of single spherical particle, the relative velocity ratio $\left(\frac{U_\infty}{U_o} \right)$ for any voidage (ϵ) can be obtained simply by drawing a line parallel

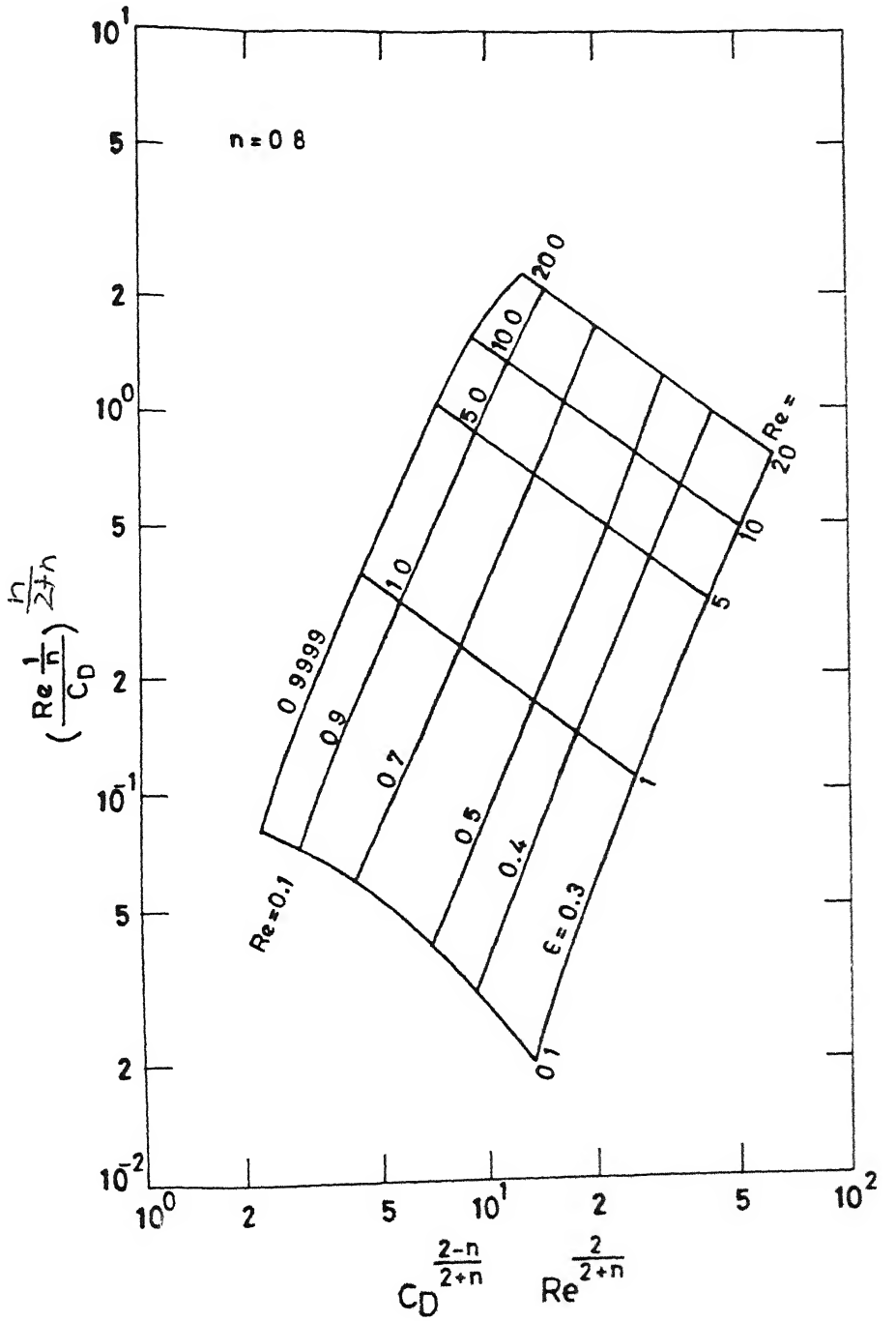

Fig 6 42 Fluidization curve for n = 0 8.

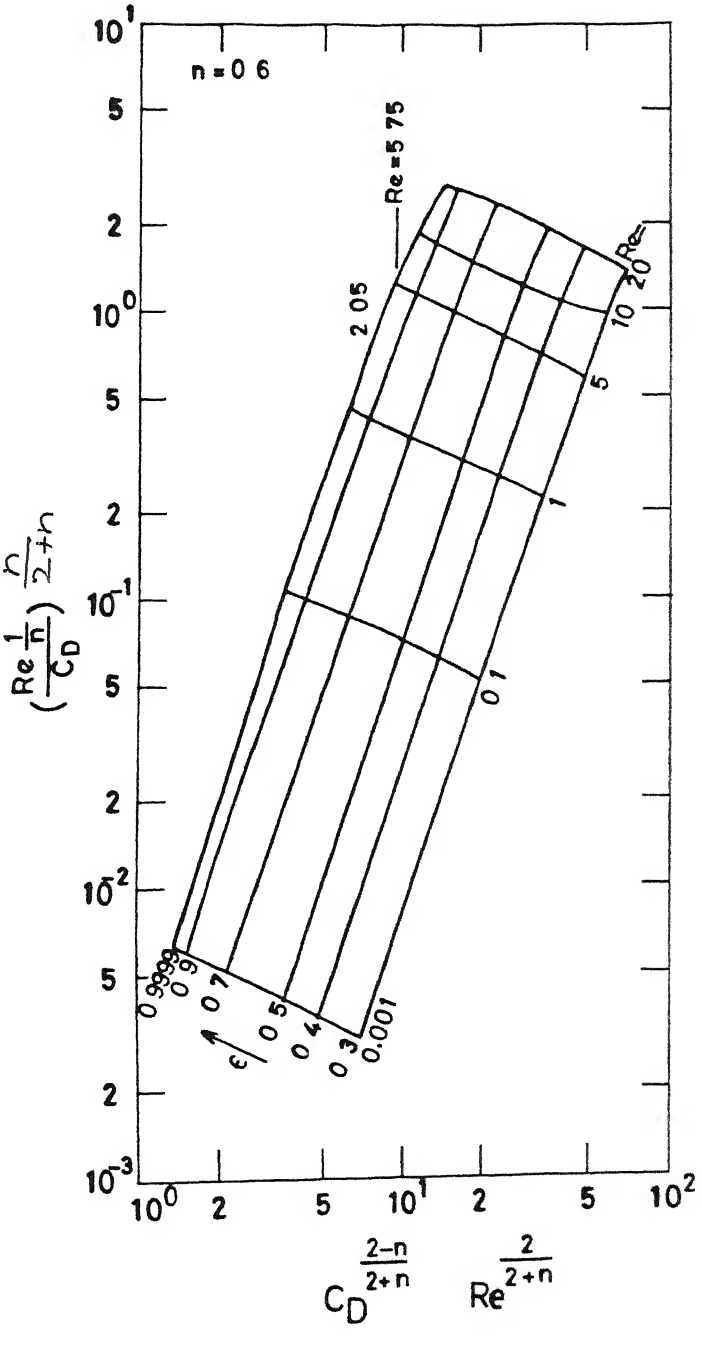

Fig. 6.43 Fluidization curve for n = 0.6.

to the $\left[Re^{1/n}/C_D\right]^{\frac{n}{2+n}}$ axis corresponding to the particular particle diameter. Thus, it is possible to plot the relative velocity ratio over a range of voidages (0 5 to 0.9) for a g . fluid behaviour index (n) and flow conditions (Re) Such a plot is shown in Figure 6.46 for Re = 5.75 and n = 0.6 the selection of the rather unusual value of Reynolds number (Re = 5.75) was made because experimental data collected from several runs were available (Srinivas 1990) for these conditions These experimental points are also shown in Figure 6 44. The agreement between the theoretical predictions and the experimental results are satisfactory only upto a limited range of voidage ($\epsilon \leq 0.6$). At higher voidage, the divergence between the two results increases.

Another correlation to predict the mass and momentum transport to non-Newtonian fluids flowing through the fluidized beds has been due to Kawase and Ulbrecht (1985) The fluidization velocity-voidage relationship has been expressed as

$$\frac{U_o}{U_\infty} = \left[\frac{12.5}{18\ F_1(n)} \left(9 + \frac{3}{r}\right)^n \right]^{1/n} \frac{(1-\epsilon)}{\epsilon^{(1+2n)^n}} \qquad (6.15)$$

where

$$F_1(n) = 3^{\frac{3n-3}{2}} \left[\frac{-22n^2 + 2n + 2}{n(n+2)\ (2n+1)} \right] \qquad (6.16)$$

The predictions of eqn. (6.15) for fluid behaviour index, n = 0.6 have also been shown along with the present results at Re_o = 5.75 in Figure 6.44. It is evident that present results are in good agreement with the predictions of equation (6.15) over a range of voidage varying from 0.4 to 0.65. However, the divergence between the two results begin to increase beyond $\epsilon \geq 0.7$. The exact

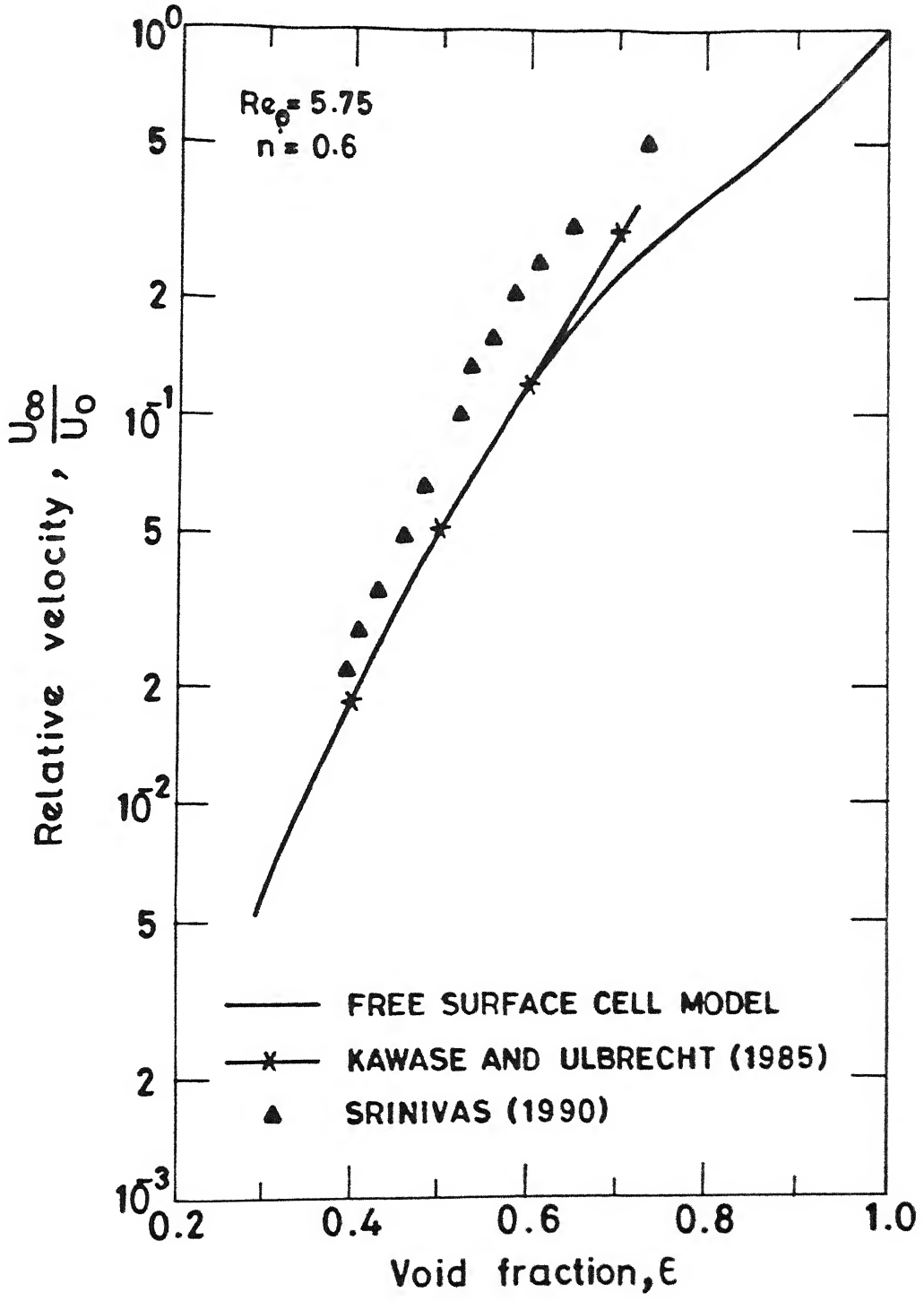

Fig. 6.44 Relative velocity ratio (U_∞/U_o) variation with voidage for Re_o = 5.75 and n = 0.6. Comparison with theoretical predictions and experimental results on power law fluid flow through fluidized beds.

reason for this behaviour is not obvious at this stage. It is to be borne in mind that while calculating the relative velocity ratio in the present study, the free settling velocity of a single sphere in infinite medium has been substituted by superficial velocity in an extremely dilute assemblage (ϵ = 0.9999). Furthermore, it can be readily shown that equation (6.15) is not valid at higher voidage range, and, in the limiting case of $\epsilon \to 1$, it predicts infinite relative velocity ratio which is physically incorrect. Even at ϵ = 0.9 and n = 0.6, it predicts U_∞/U_o = 2.22, whereas this ratio should always be less than unity. It is also appropriate to mention here that equation (6.15) is strictly valid for low Reynolds number flow, though it has not been mentioned exclusively by the authors. However, since creeping flow characteristics persist even upto Re $\approx$ 10, the comparison of present results for Re_o = 5.75 with the predictions of above equation does not entail any significant error. The predictions of relative velocity ratio over a range of voidages ($0.3 \leq \epsilon \leq 0.9$) are shown in Table 6.5 at three different values of Reynolds number (0.1, 5.75, 20.0) for n = 0.6. Also included in the same Table are the predictions of Kawase and Ulbrecht (1985) and those of Brea et al. (1976) which is essentially valid for low Reynolds number flow.

On the basis of these comparisons, the present results are found to be satisfactory over a range of voidage ($0.4 \leq \epsilon \leq 0.6$). Further conclusions regarding the performance of the model can be made only through exhaustive comparisons with established experimental results.

The influence of fluid behaviour index (n) on relative

velocity ratio vs velocity voidage relationship was also studied. The results for two values of fluid behaviour index (n = 0 8 and 0 6) are shown in Table 6 6 at Re_o = 5 75 as well as at Re_o = 20 0 It is evident that the reduction in the value of n from 0.8 to 0 6 does not make any significant impact on velocity-voidage data even upto Re_o = 20. This observation is consistent with the findings of Tonini et al. (1981).

Table 6.5· Relative velocity ratio (U_∞/U_o) for moderate shearthinning (n = 0.6) fluid at different Reynolds numbers-Comparison with available results

∈	Re_o = 0 1	Re_o = 5 75	Re_o = 20	Kawase & Ulbrecht (1985)	Brea et al (1976)
0.4	0.014	0.0166	0 0286	0 018	0 0077
0.5	0.04	0 051	0 0652	0.0514	0.62520
0.7	0.19	0 2296	0.2437	0.2947	0.1504
0.9	0.619	0 5925	0 7391	-	0 5715
0.9999	1.0	1.0	1.0	-	1.0

Table 6.6: Effects of power law index on relative velocity ratio (U_∞/U_o) for non-Newtonian fluid flow through fluidized beds.

∈	Re_o = 5.75		Re_o = 20	
	n=0.8	n=0.6	n=0 8	n=0 6
0 4	0.0173	0.0166	0.029	0.02869
0.5	0.0446	0.051	0.043	0.0632
0.7	0.1986	0.2296	0.2521	0.2437
0.9	0.545	0.5925	0.6173	0.7391
0.9999	1.0	1.0	1.0	1.0

6.4 CONCLUSIONS

Creeping flow is characterised by the dynamic balance between pressure and viscous forces. Thus both pressure drag and friction drag indicate a similar type of dependence on the non-Newtonian

peculiar features are not observed Further, in the limit of approach to a single sphere, the shear stress increases initially and then drops rapidly with reduction in n. For non-Newtonian systems, the pressure profile is also modified from the cosine dependence on angular positions which is displayed in the case of Newtonian fluid flow. Infact, as n is reduced the pressure profile also becomes flat, which is markedly exhibited for the low voidage situation For the single sphere limit (ϵ = 0.9999), surface pressure increases with decrease in n The observed trends of the surface pressure and shear stress with respect to n for a single particle case explain the existance of maximum drag which has been observed by several researchers A plot of surface viscosity variation indicates that a high value of viscosity exists near the axis Indeed, the non-Newtonian viscosity is nearly a constant on the particle surface, except near the axis.

At intermediate Reynolds number flow some of the creeping flow features persist even upto Re $\simeq$ 20 for dense assemblages For instance, each of the individual drag coefficients (pressure and friction drag) is inversely proportional to the Reynolds number at a fixed voidage and power law index. Also pressure drag drops mere steeply with voidage than the viscous drag, as in the case of creeping flow. A roughly power function type of dependence on n is also exhibited. The inertial effects on the drag coefficients are noticeable only for high voidages, high Reynolds number and low values of n The surface pressure and shear stress profiles are significantly altered by inertia in the intermediate Reynolds number regime. The shear stress is very much asymmetric about the mid plane. The pressure profile shows

decrease in value in the front portion and pressure recovery in the rear of the particle This feature is predominantly displayed at low values of n indicating that pressure and inert al forces approximately balance each other in such a situation. The streamline patterns also display asymmetry in the flow direction about the mid-plane of the particle

Comparison of present drag results for creeping flow with upper and lower bound solutions of Mohan and Raghuraman (1976a) and perturbation solution of Kawase and Ulbrecht (1981a) indicates excellent agreement upto $n \approx 0.8$; for $n < 0.8$ the divergence between the present results and those of earlier investigators increases. It is believed that present results should be more accurate as compared to the other approximate analyses. Comparison with available experimental results on creeping flow through packed beds also shows reasonable correspondence.

There is a paucity of both theoretical correlations and experimental data pertaining to the bed expansion characteristics of fluidized beds involving non-Newtonian fluid flow A general fluidization correlation which may be useful for design and analysis purposes has been prepared in the present study by extending the approach described byy Zenz and Othmer (1960) to the flow of power law liquid. The relative velocity ratio (U_∞/U_o) evaluated from this correlation for a range of voidages ($0.3 \leq \epsilon \leq 0.9$) have been compared with the theoretical predictions of Kawase and Ulbrecht (1985) and experimental data of Srinivas (1990). A reasonable agreement is observed between present results and theoretical as well as eperimental results of previous investigators over the range of voidage, $0.4 \leq \epsilon \leq 0.6$.

The present results on variation of drag coefficient with power law index n for the case of ϵ = 0 9999 have been compared, with the theoretical and experimental results available for single sphere falling under the influence of gravity, at low as well as intermediate Reynolds numbers. For creeping flow (Re $\simeq$ 0 001) the present drag predictions are found to be closest to the lower bound values of Cho and Hartnett (1983) The maximum drag is found to occur at n = 0.6 For intermediate Reynolds number, the present predictions have been compared with the experimental results due to Chhabra and Uhlherr (1980) for two values of fluid behaviour index, (n = 0.8 and 0.6) The degree of correspondence is seen to be qualitatively satisfactory.

SCOPE FOR FUTURE WORK

In this work, it has been demonstrated that the use of as highly idealized as the free surface cell model can yield useful information about the transfer processes occuring in multi-particle systems. Further refinements can be made by incorporating particle size distribution as often encountered in real life applications. The gap between theory and experiments can also be narrowed down by assuming more realistic shapes of the surrounding cell, e.g., cylindrical or distorted, etc. Alternately, one can model the flow in multi-particle systems as that in conduits of regular but complex cross-section.

In this study, only shearthinning effects have been considered whereas most real materials display viscoelastic behaviour. The importance of viscoelastic effects in this flow field can be ascertained by replacing the power law model by one of the viscoelastic constitutive equation, e.g., Maxwell fluid

No consideration has been given to wall effects in theoretical developments whereas experimental results always entail a degree, howsoever small, of wall effects. These manifest in two ways: firstly, the container wall does provide additional surface area which comes in contact with fluid; secondly, the bed voidage approaches unity at the wall The latter can be taken into account by using voidage as a function of spatial coordinates.

Available experimental results differ widely even under nominally identical conditions, A part of this descrepancy must be attributed to the incomplete rheological characterisation of test fluids, which have been seldom checked for viscoelastic and/or time dependent effects. Thus, there is a need for further experimental work in this area using well-characterized systems e g purely viscous, purely elastic fluids, etc Furthermore, the importance of wall effects can be ascertained by performing experiments with a range of particle to tube diameter ratios. To date, no experimental measurements on flow patterns prevailing around a typical particle in an assemblage have been reported Such measurements undoubtedly will further our understanding of the physics of flow. Thus, considerable scope exists for experimentalists as well as theoreticians for exploring the rugged terrains of flow in multi-particle systems

REFERENCES

Acharya, A., R A Mashelkar and J.Ulbrecht, "Flow of inelastic and viscoelastic fluids past a sphere", Rheol Acta , 15,454 (1976).

Adler,I.L , Sc. D dissertation, New York University (1958)

Al-Fariss,T F., A new correlation for Non-Newtonian Flow through Porous Media", Comp. Chem Eng ,13 (4/5), 475 (1989).

Allen E. and P.H T. Uhlherr, "Non-homogenous sedimentation in viscoelastic fluids", J. Rheo , 33, 627 (1989)

Al-Naffa, M A. and M. Samiselim, "Sedimentation of polydisperse concentrated suspensions", Can J. Chem Eng , 67, 253 (1989).

Baker, A.J., "Finite element computational fluid Mechanics", Hemisphere Publishing Corporation, New York (1985)

Baker, A J , "Finite Element Solution Algorithm for Viscous Incompressible Fluid dynamics", Int Jour. Num. Meth. Eng. 6, 89(1973)

Balakrishna, M., M S. Murthy and N R Kuloor, "Sedimentation of fine particles in non-Newtonian fluids", Indian Chem.Eng., 13, T12 (1971).

Barnea, E and R L. Mednick, "A generalized approach to the fluid dynamics of particulate systems III - General Correlation for the pressure drop through fixed bed of spherical particles", Chem. Eng. J., 15, 215 (1978).

Barnea, E. and J Mizrahi, "A generalised approach to the fluid dynamics of particulate systems Part 2. Sedimentation and fluidisation of clouds of spherical liquid drops", Can J. Chem. Eng., 53, 461 (1973).

Batchelor, G.K., "Sedimentation in a dilute dispersion of spheres", J. Fluid Mech., 52, 245 (1972)

Batra, V.K., G.D. Fulford and F.A.L. Dullien, "Laminar flow through periodically convergent-divergent tubes and channels", Can. J. Chem. Eng., 48, 622 (1970).

Bear, J., "Dynamics of fluids in porous media", American Elsevier, New York (1972).

Bercovier, M. and M.S. Engleman, "A finite element for numerical solution of viscous incompressible flow", J Comp. Phys., 20, 181 (1979).

Bernstein, B , M K Kadivar and D.S. Malkus, "Steady flow of memory fluids with finite elements, two test problems", Comp Methods Appl Mech. Engng., 27, 279 (1981)

Bird, R B , "Experimental tests of generalised Newtonian models containing a zero shear viscosity and a characteristic time", Can J. Chem Eng., 43, 161 (1965).

Bird, R B , "Useful non-Newtonian models", Ann. Rev. Fluid Mech., 8, 13 (1976).

Bird, R B , "New variational principles for incompressible Non-Newtonian flow", Phys. Fluids, 3, 539 (1960).

Bird, R B , R.C. Armstrong and O Hassager, "Dynamics of Polymeric liquids", Wiley, New York (1977).

Bird, R.B , W E. Stewart and E N. Lightfoot, "Transport phenomena", Wiley,New York (1960), 14th Corrected Printing (1974).

Bhavaraju, S M., R.A. Mashelkar and H W Blanch, "Bubble motion and mass transfer in non-Newtonian fluids", A I.Ch.E J , 24, 1063 (1978).

Blake, F.C., "The resistance of packing in fluid flow", Trans. Am. Inst. Chem. Engrs., 14, 415 (1922).

Brea, F.M., M F. Edwards, and W L Wilkinson, "The flow of non-Newtonian slurries through fixed and fluidized beds", Chem Eng. Sci., 31, 329 (1976).

Brinkman, H.C , "A calculation of viscous force exerted by a flowing fluid on a dense swarm of particles", Appl. Sci. Res , 1, 27 (1947).

Burgers, J.M., "On the influence of concentration of suspensions upon the sedimentation velocity", Proc. Kon. Nederl Akad Wetenschappen (Amsterdam), 44, 1045, 1117 (1941); 45, 9, 126 (1942).

Bush, M.B. and N. Phan-Thien, "Drag force on a sphere in creeping motion through a Carreau model fluid", J. Non-Newt Fluid Mech , 16, 303 (1984).

Burke, S.P. and W B. Plummer, "Gas flow through packed columns", Ind. Eng. Chem., 20, 1196 (1928)

Carman, P.C., "Flow of gases through porous media", Butterworths Scientific, London (1956).

Carman, P.C., "Fluid flow through granular beds", Trans. Inst Chem. Engrs., 15, 150 (1937).

Chhabra, R.P., C Tiu and P H.T Uhlherr, "Shear thinning effects in creeping flow about a sphere, "In Rheology (Eds. G. Astarita, G. Marrucci and L Nicolais), Vol. 2, p 9 Plenum Press, New York (1980)

Chhabra, R.P. and P H.T Uhlherr, "Sphere motion through non-Newtonian fluids at high Reynolds number", Can J. Chem. Eng., 58, 124 (1980).

Chhabra, R P. and J Raghuraman, "Slow non-Newtonian flow past an assemblage of rigid spheres", Chem. Eng Commun , 27, 23 (1984)

Christopher, R.H and S. Middleman, "Power law fluid flow through a packed tube", Ind Eng Chem Fund , 4, 422 (1965)

Clift, R , J.R. Grace and M E Weber, "Bubbles, Drops, and Particles", Academic Press, New York (1978)

Cohen, Y and A.B Metzner, "Wall effects in Laminar flow of fluids through packed beds", A I.Ch E.J., 27(5), 705 (1981).

Collins, R.E., "Flow of fluids through porous materials", Reinhold, New York (1961).

Cooley, M.D.A. and M E. O'Neill, "On the slow motion of two spheres in contact along their line of centres through a viscous fluid", Proc. Camb. Phil. Soc., 66, 407 (1969).

Couderc, J P., "Incipient Fludization and particulate systems", In Fluidization (Eds. Davidson, J F., R Clift and D. Harrison), 2nd edition, Academic Press, London, p. 1 (1985).

Crochet, M.J.,A.R. Davies and K Walters, "Numerical simulation of non-Newtonian flow", Elsevier, New York (1984)

Crochet, M J., "The flow of a Maxwell fluid around a sphere", In finite elements in fluids (Ed Gallagher, R H.), Vol. 4, Wiley, New York, p 573 (1982).

Cunningham, M.A., "On the velocity of steady fall of spherical particles through fluid medium", Proc R Soc. London, A83, 357 (1910)

Darby, R., "Viscoelastic fluids", Marcel Dekker, New York (1976).

Darcy, H., "Les fontaines publiques de la ville de Dijon," Victor Dalmont, Paris (1856).

Davis, R.H and A Acrivos, "Sedimentation of non-colloidal particles at low Reynolds numbers", Ann. Rev Fluid Mech., 17, 91 (1985).

Davis, R.H. and K.H. Birdsell, "Hindered settling of semidilute, monodisperse and polydisperse suspensions", A I.Ch.E.J., 34, 123 (1988).

Dharmadhikari, R V and D.D Kale, "Flow of Non-Newtonian Fluids through porous media", Chem Eng. Sci., 40(3),527 (1985)

Dieber, J.A. and W.R. Schowalter, "Flow through tubes with sinusoidal axial variations in diameter", A.I.Ch.E.J , 25, 635 (1979).

Dullien, F.A.L., "New Network permeability model of porous media", A.I.Ch.E.J., 21, 299 (1975).

Dullien, F A.L , "Porous media-fluid Transport and pore structure", Academic Press, New York (1979).

Dupuit, A J E.J , "Etudes Theoriques et pratiques sur le mouvement des eaux", Paris (1863).

Durst, F., R. Hass and W. Interthal, "The nature of flows through porous media", J. Non-Newt. Fluid Mech , 22, 669 (1987).

El-Kaissy, M.M. and G.M. Homsy, "A theoretical study of pressure drop and transport in packed beds at intermediate Reynolds numbers", Ind. Eng. Chem. Fund., 12 (1) 82(1973)

Engleman, M.S. and R.L. Sani, "Finite element simulation of incompressible fluid flows with a free/moving surface", In Computational Techniques for Fluid Flow, Pineridge Press, Swansea (U.K.), 5, 47 (1986)

Ergun,S., "Fluid flow through packed columns", Chem. Eng Prog., 48 (2) 89 (1952).

Faxen, H., "Die bewegung einter starren kugel längs der Achseeinesmit zäher Flussigheit gefullten rohres", Arkiv. Mat. Astron. Fysik., 17, 1 (1923).

Fedkiw, P. and J. Newman, "Mass Transfer at high Peclet numbers for creeping flow in packed bed reactor", A.I.Ch.E.J., 23, 255 (1977).

Ferry, J.D., "Viscoelastic properties of polymers", Wiley, New York (1970)

Feuillebois, F., "Sedimentation in a dispersion with vertical inhomogeneties", J. Fluid Mech., 139, 145 (1984).

Finalyson, B.A., "The method of weighted residuals and variational principles", Academic Press, New York (1972)

Forchheimer, P., "Wasserbewegung durch Bodem", Z. Ver. Deutsch. Ing., 45, 1782 (1901)

Foscolo, P.U., L G. Gibilaro and S.P. Waldram, "A unified model for particulate expansion of fluidized beds and flow in fixed porous media", Chem Eng. Sci., 38 (8), 1251 (1983)

Fukuchi, T. and T. Ishii, "An analysis of transport phenomena for multi-solid particle systems at higher Reynolds numbers by a 5th order polynomial Karman Pohlhausen method", Lett. App Sci Eng , 20, 121 (1982)

Gaitonde, N.Y. and S Middleman, "Flow of viscoelastic fluids through porous media", Ind Eng Chem. Fund , 6, 145 (1967).

Gal-Or, B. and S. Waslo, "Hydrodynamics of an ensemble of drops and bubbles in the presence or absence of surfactants", Chem. Eng. Sci., 23, 1431 (1968)

Gallagher, R.H., J.T. Oden, C. Taylor and O.C Zienkiewicz, "Finite elements in fluids", Wiley, New York (1978).

Garside, J. and M.R Al-Dibouni, "Velocity-voidage relationship for fluidization and sedimentation in solid-liquid systems", Ind. Eng. Chem. Proc. Des Dev. 16(2), 206 (1977)

Gauvin, W.H. and S. Katta, A.I.Ch E.J., 19, 775 (1973).

Giesekus, H., "Non-linear effects in the flow of viscoelastic fluids through slits and circular apertures", Rheol. Acta , 7, 127 (1968).

Glendinning, A.B and W.B Russel, "A pairwise additive description of sedimentation and diffusion in concentrated suspensions of hard spheres", J. Colloid Interfac. Sci , 89, 124 (1982).

Greenkorn, R.A., "Flow phenomena in porous media", Marcel-Dekker, New York (1983).

Gregory, D.R. and R G. Griskey, "Flow of molten Polymers through porous media", A.I.Ch E.J., 13, 122 (1967).

Gummalam, S. and R.P. Chhabra, "Rising velocity of a swarm of spherical bubbles in a power law non-Newtonian liquid", Can. J. Chem. Eng., 65, 1004 (1987).

Gummalam, S., K.A. Narayan and R.P. Chhabra, "Rise velocity of a swarm of spherical bubbles through a non-Newtonian fluid: Effect of zero shear viscosity", Int. J. Multiphase flow, 14, 361 (1988).

Gu, Dazhi and R.I. Tanner, "The Drag on a sphere in a power lawfluid", J. Non-Newt. Fluid Mech., 17, 1 (1985).

Gunn, D.J. and A.A. Malik, "Flow through expanded beds of solids", Trans. Inst. Chem. Engrs., 44, T371 (1966).

Hamielec, A.E., T.W. Hoffman and L.L. Ross, "Numerical solution of the Navier-Stokes equation for flow past spheres Part I, Viscous flow around spheres with and without mass efflux, A I.Ch.E.J., 13, 212 (1967)

Hanna, M R , W Kozicki and C. Tiu, "Flow of drag reducing fluids through packed beds", Chem Eng J , 13, 93 (1977).

Hanratty, T.J and A Bandukwala, "Fluidization and sedimentation of spherical particles", A.I.Ch.E.J , 3, 293 (1957).

Happel, J , "Viscous flow in multiparticle systems Slow motion of fluids relative to beds of spherical particles", A.I Ch.E.J., 4, 197 (1958)

Happel, J. and H Brenner, "Low Reynolds number Hydrodynamics", Prentice-Hall, Englewood Cliffs, New Jersey (1965).

Happel, J and N. Epstein, "Cubical assemblages of uniform spheres", Ind Eng. Chem. Fund , 46, 1187 (1954)

Happel, J. and P.A. Ast, "The motion of rigid spheres in a frictionless cylinder", Chem. Eng. Sci , 11, 288 (1960)

Hasimoto, H., "On the periodic fundamental solutions of the Stokes equations and their application to viscous flow past a cubic array of spheres", J Fluid Mech , 5, 317 (1959).

Hassell, H L and A. Bondi, "Mixing of viscous non-Newtonian fluids in packed beds", A.I.Ch E.J , 11(2), 217 (1965).

Higashitani, K and A S. Lodge, "Hole pressure error measurements in pressure-generated shear flow", Trans Soc Rheo., 19, 307 (1975).

Higashitani, K and W.G. Pritchard, "A kinematic calculation of intrinsic errors in pressure measurement made with holes", Trans. Soc. Rheo , 16, 687 (1972).

Hinch, E.J., "An averaged-equation approach to particle interactions in a fluid suspensions", J. Fluid Mech., 83, 695 (1977).

Hirose, T and M. Moo-Young, "Bubble drag and mass transfer in non-Newtonian fluids", Can. J. Chem. Eng., 47, 265 (1969).

Hopke, S.W. and J.C Slattery, "Upper and lower bounds on the drag coeficient of a sphere in an Ellis model fluid", A.I.Ch.E.J., 16, 224 (1970).

Hood, P., "Frontal solution program for unsymmetrical matrices", Int. J. Num. Method. Eng., 10(1976).

Hood, P. and C Taylor, "Navier-Stokes equations using mixed interpolation". In Finite elements in flow problems, UAH Press, Huntsville, 55 (1974).

Hua, T.N. and T. Ishii, "Momentum transfer for Multi-solid particle power law fluid systems at high Reynolds numbers", J Non-Newt. Fluid Mech , 9, 301 (1981).

Irons, B.M., "A frontal solution programme for finite element analysis", Int J. Numer. Meth. Eng., 2, 5 (1970).

Jackson, C.P. and K A. Cliffe, "Mixed interpolation in primitive variable finite element formulations for incompressible flow", Int. J. Num Meth. Eng., 17, 1659 (1980)

Jarzebski, A B and J.J. Malinowski, "Drag and mass transfer in multiple drop slow motion in a power law fluid", Chem. Eng Sci., 41, 2569 (1986)

Jean Rong-Her and Liang-Shih Fan, "A fluid mechanic based model for sedimentation and fluidization at low Reynolds numbers", Chem Eng. Sci., 44 (2), 353 (1989).

Johnson, M.W Jr , "Some variational theorems for non-Newtonian fluids", Phys fluids, 3, 871 (1960).

Johnson, M W. Jr , "On variational principles for non-Newtonian fluids", Trans Soc Rheol., 5, 9 (1961).

Joshi, J.B., "Solid-Liquid fluidised beds: some design aspects", Chem. Eng Res. Des , 61, 143 (1983).

Kanellopoulos, N.K., "Capillary models for porous media: Newtonian and non-Newtonian flow", J. Colloid Interfac Sci., 108 (1), 11 (1985).

Kawaguti, M., "A hydrodynamic model for the sedimentation", J. Phy. Soc. Japan., 13, 209 (1958).

Kawase, Y. and J.J. Ulbrecht., Drag and mass transfer in non-Newtonian flows through multi-particle systems at low Reynolds numbers", Chem. Eng Sci., 36, 1193 (1981a).

Kawase, Y and J.J Ulbrecht., "Motion of and mass transfer from an assemblage of solid spheres moving in a non-Newtonian fluid at high Reynolds numbers", Chem. Eng. Commun , 8, 223 (1981b).

Kawase, Y. and J.J Ulbrecht , "Sedimentation of particles in non-Newtonian fluids", Chem. Eng. Commun., 13, 55 (1981c).

Kawase, Y. and J.J Ulbrecht, "Rheological properties of suspension of solid spheres in non-Newtonian fluids", Chem. Eng. Commun., 20, 127 (1983).

Kawase, Y. and J.J Ulbrecht, "Mass and momentum transfer with non-Newtonian fluids in fluidized beds", Chem Eng Commun , 32, 263 (1985).

Kemblowski, Z. and J. Mertl , "Pressure drop during the flow of Stokesian fluids through granular beds", Chem Eng Sci., 29, 213 (1974).

Kemblowski, Z. and M. Michniewicz , "A new look at the laminar flow of power law fluids through granular beds", Rheol. Acta., 18, 730 (1979)

Kemblowski, Z and M. Michniewicz , "Correlation of data concerning resistance to flow of generalised Newtonian fluids through granular beds", Rheol. Acta, 20, 352 (1981).

Khan, A.R and J F Richardson, "The resistance to motion of a solid sphere in Fluid", Chem Eng. Commun , 62, 135 (1987)

Kim, S and W B Russel, "Modelling of porous media by renormalization of the Stokes equations", J Fluid Mech., 154, 269 (1985).

Kozicki, W and C Tiu, "A unified model for non-Newtonian flow in packed beds and porous media", Rheol Acta, 27, 31 (1988).

Kozicki, W , C J. Hsu and C Tiu, "Non-Newtonian flow through packed beds and porous media", Chem Eng. Sci., 22, 487 (1967).

Kozicki, W., A R.K Rao and C. Tiu, "Filtration of polymer solutions", Chem Eng Sci , 22, 615 (1972).

Kumar, S and S N. Upadhyay, "Mass and momentum transfer to Newtonian and non-Newtonian fluids in fixed and fluidized beds", Ind. Eng Chem Fund , 20, 186 (1981)

Kumar, S., J. Kishore, P. Lal and S.N Upadhyay, "Non-Newtonian flow through packed beds and porous media", J Sci. Ind. Res., 40, 238 (1981).

Kunni, D and O. Levenspiel, "Fluidization Engineering", Wiley, New York (1969).

Kuwabara, S., "The forces experienced by randomly distributed parallel circular cylinders or spheres in a viscous flow at small Reynolds numbers", J. Phys. Soc. Japan, 14, 527 (1959).

Leclair, B.P., and A.E. Hamielec, "Viscous flow through particle assemblages at intermediate Reynolds numbers", Ind Eng. Chem. Fund., 7 (4), 542 (1968).

Leva, M., "Fluidization", McGraw-Hill, New York (1967).

Letan, R., "On vertical dispersed two phase flow", Chem Eng Sci., 29, 621 (1974).

Lewis, E.W. and E.W. Bowerman, "Fluidization of solid particles in liquids", Chem. Eng. Prog , 48, 603 (1952).

Leonov, A I., "Extremum principles and exact two side bounds of potential: Functional and dissipaion for slow motions of nonlinear viscoplastic media", J. Non-Newt. Fluid Mech , 28, 1 (1988)

Lodge, A S., "Elastic liquids", Academic Press, London (1967).

Machac, I., M. Blacar and Z Lecjaks, "Creeping flow of non-Newtonian liquids through fluidized beds of spherical particles", Chem Eng Sci. 41(3), 591 (1986).

Machac, I and V Dolejs, "Flow of viscoelastic liquids through fixed beds of particles", Chem. Eng Commun , 18, 29 (1982)

Marshall, R J. and A.B. Metzner, "Flow of viscoelastic fluids through porous media", Ind Eng. Chem. Fund , 6, 393 (1967).

Matsuhisa, S. and R B Bird, "Analytical and numerical solutions for laminar flow of non-Newtonian Ellis fluid", A I Ch E J., 11, 588 (1965).

Metzner, A B., E.A. Uebler and C.F Chan Man Fong, "Converging flows of viscoelastic materials", A.I.Ch E J , 15, 750 (1968).

Mishra, P., D. Singh and I.M. Mishra, "Momentum transfer to Newtonian and non-Newtonian fluids flowing through packed and fluidized beds", Chem. Eng. Sci., 30, 397 (1975)

Mohan, V. and J. Raghuraman, "A theoretical study of pressure drop for non-Newtonian creeping flow past an assemblage of spheres", A.I.Ch.E.J., 22(2), 259 (1976a).

Mohan, V and J. Raghuraman, "Bounds on the drag for creeping flow of an Ellis fluid past an assemblage of spheres", Int. J. Multiphase flow., 2, 581 (1976b)

Molerus, O , "A coherent representation of pressure drop in fixed beds and of bed expansion for particulate fluidized beds", Chem Eng. Sci., 35, 1331 (1980).

Moritomi, H., T.Yamagishi and T Chiba, "Predictions of complete mixing of liquid-fluidized binary solid particles", Chem. Eng. Sci., 41(2), 297 (1986).

Nakazawa, S., J.F.T. Pittman, and O C. Zienkiewicz, "Numerical solution of flow and heat transfer in polymer melts", In finite elements in fluids (ed. R.H. Gallagher), Wiley· New York, Vol. 4, 251 (1982).

Nishimura, Y. and T. Ishii, An analysis of transport phenomena for multi solid particle systems at higher Reynolds numbers by a standard Karman-Pohlhausen method: 1 Momentum transfer", Chem. Eng. Sci. 35, 1195 (1980a).

Nishimura, Y. and T. Ishii, "An analysis of transport phenomena for multi-solid particle systems at higher Reynolds numbers by a standard Karman-Pohlhausen method II, Chem. Eng. Sci., 35, 1205 (1980b).

Olson, M.D and S Y. Tuann , "Primitive variables versus stream function -Finite Element solutions of the Navier Stokes equations", Pro 2nd Int Sym. Finite Element Methods in Flow Problems, (ed S Margherita Liqure) Italy (1976)

O'Brien, R W , "A method for the calculation of the effective transport properties of suspensions of interacting particles", J. Fluid Mech., 8, 256 (1979).

Park, H.C , "The flow of non-Newtonian fluids through porous media", Ph.D. Thesis, Michigan State University, East Lansing, (1972).

Park, H.C , M.C Hawley and R.F Blanks, "The flow of non-Newtonian solutions through packed beds", Polym Eng Sci , 15, 761 (1975).

Payatakes, A C., C Tien and R.M. Turian, "A new model for granular porous media", A.I.Ch.E.J , 19, 58 (1973).

Payatakes, A C. and M.A. Neira, "Model of the constricted unit cell type for Isotropic granular porous media", A I.Ch.E.J , 23, 923 (1977).

Perry, R.H. and C.H. Chilton, "Chemical Engineers Handbook," International student edition, McGraw-Hill, Kagakusha, Tokyo (1973).

Pfeffer, R., "Heat and Mass Transport in Multiparticle systems", Ind. Eng Chem. Fund., 3, 380 (1964)

Pfeffer, R. and J. Happel, "An analytical study of heat and mass transfer in multi-particle systems at low Reynolds numbers", A.I.Ch.E.J., 10, 605 (1964).

Prasad, D , K.A. Narayan and R.P. Chhabra, "Creeping fluid flow relative to an assemblage of composite spheres", Int. J. Eng. Sci., 28, 215-230 (1990).

Popinski, Z and A.J. Baker, "An implicit finite element algorithm for the boundry layer equations", J. Comp. Phys 2(1), 55 (1976).

Powlowski, J., "Uber eine Erweiterung des Helmholtzschen prinzips", Kolloid Z , 138, 6 (1954).

Rae, J., "Finite element solutions for Navier-Stokes equations", Numerical methods for fluid dynamics, Academic Press, New York (1982).

Rallison, J.M and E J. Hinch, "Do we understand the physics in the constitutive equations?", J. Non-Newt. Fluid Mech , 29, 37 (1988).

Ranz, W.E., "Friction and Transfer coefficients for single particles and packed beds", Chem. Eng. Prog., 48 (5), 247 (1952)

Richardson, J.F., In Fluidization (Ed Davidson, J.F. and D. Harrison), Academic Press, Ist ed., 25 (1971).

Richardson, J F. and W N Zaki, "Sedimentation and Fluidization: Part I", Trans Inst Chem Engrs., 32, 35 (1954a).

Richardson, J.F. and W N Zaki, "The sedimentation of a suspension of uniform spheres under conditions of viscous flow", Chem Eng Sci., 3, 65 (1954b)

Sadowski, T.J., "Non-Newtonian flow through porous media", Ph D Thesis, University of Wisconsin, Madison (1963).

Sadowski, T.J. and R B Bird, "Non-Newtonian flow through porous media", Trans. Soc. Rheol , 9(2), 43 (1965).

Sani, R.L., P.M. Gresho and R.L. Lee, "On the spurious pressures generated by certain FEM solutions of the incompressible Navier-Stokes equations", 3rd Int. Conf Finite Elements (in flow problems; Banff, Canada (1980).

Sangani, A.S. and A. Acrivos, "Slow flow through a periodic array of spheres", Int. J. Multiphase flow, 8, 343 (1982).

Savins, J.G., "Non-Newtonian flow through porous media", Ind. Eng. Chem., 61(10), 18 (1969)

Scheidegger, A.E., "The Physics of flow through porous media", University of Toronto Press, Toronto (1974).

Schowalter, W.R., "Mechanics of non-Newtonian fluids", Pergamon Press, Oxford (1978).

Shah, D.O. and R.S. Schechter, (Eds), "Improved oil recovery by surfactant and polymer flooding", Academic Press, New York (1977).

Sheffield, R.E. and A.B. Metzner, "Flow of non-linear fluids through porous media", A I.Ch.E.J., 22, 736 (1976)

Skelland, A H.P., "Non-Newtonian flow and heat transfer", Wiley, New York (1967).

Slattery, J C., "Momentum energy and mass transfer in continua", McGraw Hill, New York, (1972).

Slattery, J C., "Flow of viscoelastic fluids through porous media", A.I.Ch.E.J., , 13, 1066 (1967).

Slattery, J C. and R.B. Bird, "Non-Newtonian flow past a sphere", Chem. Eng. Sci., 16, 231 (1961).

Smoluchowsky, M.S., "On the practical applicability of Stokes' law of resistance and the modification of it required in certain cases", Proc 5th Int. Cong. Math , 2 192 (1912)

Srinivas, B K and R.P. Chhabra, "Effect of particle to bed diameter ratio on pressure drop for power law fluid flow in packed beds", Int J Eng Fluid Mech , in press (1990)

Srinivas, B K , "Non-Newtonian flow through packed and fluidized beds", M tech Thesis, IIT, Kanpur (1990).

Stimson, M and G.B. Jeffery, "The motion of two spheres in a viscous fluid", Proc R. Soc. London Ser. A , 110 (1926).

Steinour, H H , "Rate of sedimentation: Non-flocculated suspension of uniform spheres", Ind Eng. Chem., 36, 618 (1944).

Sundararajan,T. and P.S Ayyaswamy, "Hydrodynamics and heat transfer associated with condensation on a moving drop Solution for intermediate Reynolds numbers", J. Fluid Mech , 149, 33 (1984).

Tal (Thau), R. and W A Sirignano, "Cylindrical cell model for the hydrodynamics of particle assemblages at intermediate Reynolds numbers", A.I Ch.E J , 28(2), 288 (1982)

Tanner, R.I., "Non-Newtonian fluid parameter estimation using conical flows", Ind Eng Chem Fund., 5, 55 (1966)

Taylor, C. and T.G. Hughes, "Finite element programming of Navier-Stokes equation", Pineridge Press, Swansea (1984).

Tiefenbruck, G. and L.G. Leal, "A numerical study of the motion of a viscoelastic fluid past rigid spheres and spherical bubbles", J Non-Newt Fluid Mech., 10, 115 (1982).

Tonini, R.D., U. Böhm and F.M. Brea, "Fluidization with highly viscous and non-Newtonian fluids:Mass transfer from the fluidized bed to the inner wall of an annulus", Chem Eng J , 22, 51 (1981).

Tordella, J.P., "Capillary flow of molten polyethyline A photographic study of melt fracture", Trans. Soc Rheo., 1, 203 (1957).

Uchida, S., "Slow viscous flow through a mass of particles", Ind Eng. Chem., 46, 1194 (1954).

Verschoor, H., "Experimental data on the viscous force exerted by a flowing fluid on a dense swarm of particles", App. Sci. Res A2, 155 (1951)

Wakiya, S., "A spherical obstacle in the flow of a viscous fluid through a tube", J. Phys. Soc. Japan, 8, 254 (1953).

Wasserman, M.L. and J.C Slattery, "Upper and lower bounds on the drag coefficient of a sphere in a power-model fluid", A I Ch.E.J , 10, 383 (1964).

Yamamoto, K and N Iwamura, "Flow with convective acceleration through a porous medium", J Eng. Maths., 10, 41 (1976).

Yaron, I and B Gal-Or, "Convective mass or heat transfer from size distributed drops, bubbles or solid particles", Int J Heat Mass Transfer, 14, 727 (1971).

Yaron, I. and B Gal-Or, "On viscous flow and effective viscosity of concentrated suspensions and emulsions", Rheol Acta, 11, 241 (1972).

Yu, Y.H , C Y Wen and R C Baillie, "Power-law fluids flow through multi-particle systems", Can J Chem Eng , 46, 149 (1968).

Yoshioka, N and K. Adachi, "On variational principles for a non-Newtonian fluid", J Chem Eng Japan, 4, 217 (1971).

Yoshioka, N. and K Adachi, "Some deductions from the extremum principles for non-Newtonian fluids", J Chem Eng Japan, 6, 134 (1973).

Zenz, F.A and D.F. Othmer, "Fluidization and fluid-particle systems", Reinhold, New York (1960).

Zick, A.A. and G.M. Homsy, "Stokes flow through periodic arrays of spheres", J. Fluid Mech., 115 (1982).

Zimmels, Y., "A generalized approach to flow through fixed beds, fluidization and hindered sedimentation", Chem. Eng. Commun., 67, 19 (1988).

APPENDIX I

ANALYTICAL SOLUTIONS FOR CREEPING NEWTONIAN FLUID FLOW PAST AN ASSEMBLAGE OF PARTICLES - DRAG COEFFICIENTS AND SURFACE PRESSURE DISTRIBUTION

The dimensionless form of the Navier-Stokes equation for steady, viscous and axisymmetric flow of Newtonian fluids, in terms of stream function (ψ) may be expressed in spherical polar coordinates (r, θ, ϕ) as

$$\frac{Re}{2}\left[\frac{\partial\psi}{\partial r}\frac{\partial}{\partial\theta}\left(\frac{E^2\psi}{r^2\sin^2\theta}\right)-\frac{\partial\psi}{\partial\theta}\frac{\partial}{\partial r}\left(\frac{E^2\psi}{r^2\sin^2\theta}\right)\right]\sin\theta = E^2E^2\psi \tag{A-1}$$

where, $$E^2 = \frac{\partial^2}{\partial r^2}+\frac{\sin\theta}{r^2}\frac{\partial}{\partial\theta}\left(\frac{1}{\sin\theta}\frac{\partial}{\partial\theta}\right)$$

For the case of creeping motion of sphere or creeping flow past a sphere, Eqn. (A-1) reduces to

$$E^2E^2\psi = 0 \tag{A-2}$$

The radial and tangential components of velocity vector are related to streeam function as

$$V_r = -\frac{1}{r^2\sin\theta}\frac{\partial\psi}{\partial\theta} \tag{A-3}$$

$$V_\theta = \frac{1}{r\sin\theta}\frac{\partial\psi}{\partial r} \tag{A-4}$$

A general solution of Eqn. (A-2) is of the form (Happel and Brenner, 1965).

$$\psi = \left(A_1r^4+A_2r^2+A_3r+\frac{A_4}{r}\right)\sin^2\theta \tag{A-5}$$

Therefore,

$$V_r = -2 \cos\theta \left(A_1 r^2 + A_2 + \frac{A_3}{r} + \frac{A_4}{r^3}\right) \quad \text{(A-6)}$$

$$V_\theta = \sin\theta \left(4A_1 r^2 + 2A_2 + \frac{A_3}{r} + \frac{A_4}{r^3}\right) \quad \text{(A-7)}$$

The four constants (A_1, , A_4) appearing in these equations are evaluated using the following four boundary conditions of Happel cell model

$$\text{At } r = 1;\ V_r = \cos\theta \text{ and } V_\theta = -\sin\theta \quad \text{(A-8)}$$

and

$$\text{At } r = R_c \ ;\ V_r = 0,\ \tau_{r\theta} = \eta \left\{ \frac{\partial V_\theta}{\partial r} - \frac{V_\theta}{r} + \frac{1}{r}\frac{\partial V_r}{\partial \theta} \right\} = 0 \quad \text{(A-9)}$$

These boundary conditions in conjunction with equation (A-6) and (A-7) lead to following set of equations,

$$A_1 + A_2 + A_3 + A_4 = -0\ 5 \quad \text{(A-10a)}$$

$$4A_1 + 2A_2 + A_3 - A_4 = -1 \quad \text{(A-10b)}$$

$$A_1 R_c^2 + A_2 + \frac{A_3}{R_c} + \frac{A_4}{R_c^3} = 0 \quad \text{(A-10c)}$$

$$2A_1 - \frac{A_2}{R_c^2} - \frac{A_3}{R_c^3} + \frac{2A_4}{R_c^5} = 0 \quad \text{(A-10d)}$$

In equations (A-10c) and (A-10d), R_c refers to the non-dimensional cell radius. For a given voidage and hence known value of R_c, the above set of equations can be solved simultaneously to obtain the constants A_1, . A_4. In present work, these were obtained using Matrix inversion subroutines. However, these can also be obtained

explicitly as a function of non-dimensional cell radius through the following expressions

$$A_1 = \frac{-R_c\,(2R_c + 1)}{f_1 f_3} \qquad \text{(A-11)}$$

$$A_2 = \frac{1\ 5\ R_c^2 - 0.5}{f_3} + \frac{R_c\ f_2}{f_1\ f_3} \qquad \text{(A-12)}$$

$$A_3 = -0.75 - 2.5\ A_1 - 1\ 5\ A_2 \qquad \text{(A-13)}$$

$$A_4 = 1.5\ A_1 + 0.5\ A_2 + 0\ 25 \qquad \text{(A-14)}$$

where,

$$f_1 = (R_c^2 - 1)\ (4R_c^2 + 2R_c + 4) \qquad \text{(A-15)}$$

$$f_2 = (2R_c^3 + 4R_c^2 + 6R_c + 3) \qquad \text{(A-16)}$$

$$f_3 = (2\ R_c + 1)\ (R_c - 1)^2 \qquad \text{(A-17)}$$

Knowing the value of A_1, A_2, A_3 and A_4 the radial velocity (V_r) and tangential velocity (V_θ) at any point within the flow field can be evaluated

SURFACE PRESSURE DISTRIBUTION AND DRAG COEFFICIENTS

The surface pressure may be found by integrating the θ - component of the equation of motion from the front stagnation point ($\theta = 0^o$) over the particle surface i.e., r = 1. For steady flow, the θ components of equation of motion in non-dimensional form may be expressed as:

$$\frac{1}{r}\frac{\partial p}{\partial \theta} = \frac{2}{Re}\left[\frac{\partial^2 V_\theta}{\partial r^2} + \frac{2}{r}\frac{\partial V_\theta}{\partial r} + \frac{\partial^2 V_\theta}{r^2\,\partial \theta^2} + \frac{2\partial V_r}{\partial \theta} - \frac{V_\theta}{\sin^2\theta} + \frac{\cot\theta}{r^2}\frac{\partial V_\theta}{\partial \theta}\right] \qquad \text{(A-18)}$$

At particle surface r equals unity Therefore,

$$\frac{\partial p}{\partial \theta} = \frac{2}{Re}\left[\frac{\partial^2 V_\theta}{\partial r^2} + \frac{2\partial V_\theta}{\partial r} + \frac{\partial^2 V_\theta}{\partial \theta^2} + \frac{2\partial V_r}{\partial \theta} - \frac{V_\theta}{\sin^2\theta} + \cot\theta \frac{\partial V_\theta}{\partial \theta}\right] \tag{A-19}$$

Substituting for V_r and V_θ from equations (A-6) and (A-7), it can be shown that

$$\frac{\partial p}{\partial \theta} = \frac{\sin\theta}{Re}(40A_1 + 4A_3) \tag{A-20}$$

Integrating eqn. (A-20) with pressure at $\theta = 0^\circ$ as reference pressure, ($p = 0$ at $\theta = 0$), it is found that

$$P = \frac{40A_1 + 4A_3}{Re}\left\{1 - \cos\theta\right\} \tag{A-21}$$

$$C_{DP} = \int_0^\pi -4P \sin\theta \cos\theta \, d\theta = \frac{8}{3Re}(40A_1 + 4A_3) \tag{A-22}$$

Furthermore, it can be shown that

$$C_{DF} = \frac{8}{Re}\int_0^\pi \left\{\frac{2\partial V_r}{\partial r}\cos\theta - \frac{\partial V_\theta}{\partial r}\sin\theta + \frac{V_\theta}{r}\sin\theta - \frac{1}{r}\frac{\partial V_r}{\partial \theta}\right\}\sin\theta \, d\theta \tag{A-23}$$

Substituting V_r and V_θ from equation (A-6) and (A-7), it is found that

$$C_{DF} = \frac{64}{3Re}(-5A_1 + A_3) \tag{A-24}$$

Finally, the total drag coefficient is given by

$$C_D = C_{DP} + C_{DF} \tag{A-25}$$

APPENDIX II

ORDER OF MAGNITUDE ANALYSIS FOR SURFACE SHEARR STRESS

For the streamline pattern set up in the cell, the dimensionless volumetric flow rate q created by the motion of the particle inside the cell is equal to

$$q = \pi r^2 U = \pi \qquad \text{(B-1)}$$

as $r = 1$ and $U = 1$ on the particle surface.

Denoting the dimensionless radial gap between the particle and the cell boundary as δ, one can express the area for flow at any value of θ as:

$$A_\theta = \pi(1 + \delta)^2 - \pi = \pi (2 + \delta) \delta \qquad \text{(B-2)}$$

The average angular velocity (V_θ) within the gap is therefore given by

$$V_\theta = \frac{q}{A_\theta} = \frac{\pi}{\pi\delta(2+\delta)} = \frac{1}{\delta(2+\delta)} \qquad \text{(B-3)}$$

For dense assemblages (e.g $\delta = 0.4$), etc), δ would be small and thus,

$$V_\theta \sim 0(1/\delta) \qquad \text{(B-4)}$$

This can be used to deduce the surface shear rate as,

$$\dot{e}_{av} = \left[\frac{\partial V_\theta}{\partial r} - \frac{V_\theta}{r} + \frac{1}{r} \frac{\partial V_r}{\partial \theta} \right] \Big|_{r=1} = \frac{\partial V_\theta}{\partial r} \Big|_{r=1} \qquad \text{(B-5)}$$

Utilizing (B-4), $e_{av} \sim 0(1/\delta^2)$ (B-6)

For Generalised Newtonian fluids, the average dimensionless fluid

Viscosity at the particle surface is given by

$$\eta = \left(\frac{I_2}{2} \right)^{\frac{n-1}{2}} = \left(\frac{e_{av}^2}{2} \right)^{\frac{n-1}{2}} \qquad \text{(B-7)}$$

Hence,

$$\eta \sim \frac{1}{\delta^{2(n-1)}} \qquad \text{(B-8)}$$

The dimensionless average shear stress can now be estimated as

$$\tau \approx \frac{2^n}{Re} \eta \frac{\partial V_\theta}{\partial r} \sim \frac{2^n}{Re} \frac{1}{\delta^{2(n-1)}} \frac{1}{\delta^2}$$

Or, $$\tau \sim \frac{2^n}{Re\delta^{2n}} \qquad \text{(B-9)}$$

which allows C_{DF} to be written as

$$C_{DF} \sim \frac{1}{Re} \left(\frac{1}{\delta^2} \right)^n \qquad \text{(B-10)}$$

Therefore, the friction drag coefficient can be expressed in a form

$$C_{DF} \sim Ax^n$$

where $x = \frac{1}{\delta^2}$.

It is interesting to note that the velocity gradient or shear rate for the Newtonian flow situation is $O(1/\delta^2)$. Therefore,

$$C_{DF} \sim \frac{1}{Re} (\dot{e}_{av})^n_{newt.} \qquad \text{(B-11)}$$

this observation can form the basis for evaluating the friction drag coefficients for non-Newtonian fluid flow problem from the corresponding Newtonian problem at the same voldage.